NASA CR-121178
MTI 73TR4

CONTRACTOR REPORT

EFFECTS OF VIBRATION AND SHOCK ON THE PERFORMANCE OF GAS-BEARING SPACE-POWER BRAYTON CYCLE TURBOMACHINERY

PART 3: SINUSOIDAL AND RANDOM VIBRATION DATA REDUCTION AND EVALUATION, AND RANDOM VIBRATION PROBABILITY ANALYSIS

by

J. M. Tessarzik, T. Chiang, and R. H. Badgley

JANUARY 1973

MECHANICAL TECHNOLOGY INCORPORATED
Latham, New York

Prepared for

NATIONAL AERONAUTICS AND SPACE ADMINISTRATION

NASA—Lewis Research Center

Contract NAS 3—15709

J. DUNN, Project Manager

NOTICE

This report was prepared as an account of Government-sponsored work. Neither the United States, nor the National Aeronautics and Space Administration (NASA), nor any person acting on behalf of NASA:

A.) Makes any warranty or representation, expressed or implied, with respect to the accuracy, completeness, or usefulness of the information contained in this report, or that the use of any information, apparatus, method, or process disclosed in this report may not infringe privately-owned rights; or

B.) Assumes any liabilities with respect to the use of, or for damages resulting from the use of, any information, apparatus, method or process disclosed in this report.

As used above, "person acting on behalf of NASA" includes any employee or contractor of NASA, or employee of such contractor, to the extent that such employee or contractor of NASA or employee of such contractor prepares, disseminates, or provides access to any information pursuant to his employment or contract with NASA, or his employment with such contractor.

Requests for copies of this report should be referred to

National Aeronautics and Space Administration
Scientific and Technical Information Facility
P.O. Box 33
College Park, Md. 20740

1. Report No.	2. Government Accession No.	3. Recipient's Catalog No.
NASA CR-121178		

4. Title and Subtitle	5. Report Date
EFFECTS OF VIBRATION AND SHOCK ON THE PERFORMANCE OF GAS-BEARING SPACE-POWER BRAYTON CYCLE TURBOMACHINERY	January 1973
	6. Performing Organization Code

7. Author(s)	8. Performing Organization Report No.
J.M. Tessarzik, T. Chiang, and R.H. Badgley	MTI 73TR4
	10. Work Unit No.

9. Performing Organization Name and Address	11. Contract or Grant No.
Mechanical Technology Incorporated 968 Albany-Shaker Road Latham, New York 12110	NAS 3-15709
	13. Type of Report and Period Covered
12. Sponsoring Agency Name and Address	Contractor Report
National Aeronautics and Space Administration Washington, D.C. 20546	14. Sponsoring Agency Code

15. Supplementary Notes

Project Manager, James H. Dunn, Brayton Cycle Branch, NASA Lewis Research Center, Cleveland, Ohio

16. Abstract

The random vibration response of a gas-bearing rotor-support system has been experimentally and analytically investigated in the amplitude and frequency domains.

The NASA Brayton Rotating Unit (BRU), a 36,000 rpm, 10 KWe turbogenerator had previously been subjected in the laboratory to external random vibrations, and the response data recorded on magnetic tape. This data has now been experimentally analyzed for amplitude distribution and frequency content. The results of the power spectral density analysis indicate strong vibration responses for the major rotor-bearing system components at frequencies which correspond closely to their resonant frequencies obtained under periodic vibration testing. The results of amplitude analysis indicate an increasing shift towards non-Gaussian distributions as the input level of external vibrations is raised.

Analysis of axial random vibration response of the BRU was performed by using a linear three-mass model. Power spectral densities, the root-mean-square value of the thrust bearing gas-film thickness variation, and the probability of thrust bearing surface contact were calculated for specified input random excitation.

17. Key Words (Suggested by Author(s))	18. Distribution Statement
	Unclassified - unlimited

19. Security Classif. (of this report)	20. Security Classif. (of this page)	21. No. of Pages	22. Price*
Unclassified	Unclassified	160	$3.00

* For sale by the National Technical Information Service, Springfield, Virginia 22151

FOREWORD

This report describes the results of work performed by Mechanical Technology Incorporated (MTI), Latham, New York, under Task I of NASA Contract NAS3-15709. Experimental data reduced under this Task was obtained and reported in NASA Contractor Report CR-2177, October 1971, under Contract NASw-1713.

The NASA Project Manager for this investigation was Mr. James Dunn of the Brayton Cycle Branch of the Lewis Research Center, Cleveland, Ohio. The MTI Project Manager was Dr. Robert H. Badgley. Mr. Juergen M. Tessarzik of MTI was responsible for the experimental portion of the investigation, while Dr. Thomas Chiang was responsible for the analytical portion.

The computer program used to calculate axial random vibration response probabilities for the BRU simulator rotor-bearing system was developed by Dr. Thomas Chiang.

The authors are especially grateful to Mr. Walter Spodnewski of MTI for his skillful assistance in performing the power spectral density and probability laboratory analyses of the experimental test data.

ABSTRACT

The random vibration response of a gas-bearing rotor-support system has been experimentally and analytically investigated in the amplitude and frequency domains.

The NASA Brayton Rotating Unit (BRU), a 36,000 rpm, 10 KWe turbogenerator had previously been subjected in the laboratory to external random vibrations, and the response data recorded on magnetic tape. This data has now been experimentally analyzed for amplitude distribution and frequency content. The results of the power spectral density analysis indicate strong vibration responses for the major rotor-bearing system components at frequencies which correspond closely to their resonant frequencies obtained under periodic vibration testing. The results of amplitude analysis indicate an increasing shift towards non-Gaussian distributions as the input level of external vibrations is raised.

Analysis of axial random vibration response of the BRU was performed by using a linear three-mass model. Power spectral densities, the root-mean-square value of the thrust bearing gas-film thickness variation, and the probability of thrust bearing surface contact were calculated for specified input random excitation.

TABLE OF CONTENTS

TABLE OF CONTENTS (Concluded)

LIST OF FIGURES

Figure

Figure

Figure

Figure

LIST OF TABLES

SUMMARY

The axial random vibration response of the NASA Brayton Rotating Unit (BRU) was analyzed with the BRU represented by a three-mass linear system. A computer program was extended to permit calculation of power spectral densities, the root-mean-square value of the thrust bearing gas-film thickness variation and the probability of thrust bearing surface contact for specified input random excitation.

Experimental analysis of the random BRU simulator response data has also been accomplished. Probability density and distribution functions have been computed for the data for all representative rotor-bearing system displacement sensors at low and high external vibration input levels. Similarly, a frequency analysis (displacement power spectral density) for the same data has been obtained.

The probability analysis has revealed a wide range of BRU system component responses to the externally-applied random vibration environment. Some components reacted with normal (Gaussian) or nearly-normal responses at all vibration test input levels, while others exhibited drastic changes towards non-Gaussian responses for increasing vibration input levels. Generally, implications about the physical behavior of bearing system parts can be drawn from the examination of their amplitude response analysis.

The frequency analysis of the BRU simulator response data to external random vibration inputs has revealed a general similarity in the response patterns obtained for random and sinusoidal vibration inputs. Major system resonances occurred in the frequency range between 60 and 400 Hz. The gain factor (ratio of vibration response level to input level) for most system components under random vibration was well under unity, with the rotor axial vibration generally exhibiting the highest relative response.

Evaluation of the BRU simulator bearing system component responses to sinusoidal vibration inputs over the frequency range 5 to 2000 Hz indicated a large number of fairly closely spaced resonances in the frequency range 60 to 400 Hz. These

appear to be due to resonant behavior of the rotor mass supported on the bearing gas films.

The major factors contributing to the multiplicity of observed resonances appear to include unequal journal bearing gas-film stiffnesses in the direction through and at right angles to the pivot of the flexure-supported pad, and unequal stiffnesses of the two journal bearings. Major lateral resonances appear to be of the rigid body type common to two-bearing rotor systems. Although the absolute displacement response level varies for individual parts (depending upon the direction of applied vibration relative to the direction of freedom of the particular part), no single resonance was found to be especially severe.

INTRODUCTION

The adaption of Brayton Cycle Space Power Systems to environments involving externally-imposed vibrations must logically begin with an evaluation of the capabilities of existing equipment.

The Brayton Rotating Unit (BRU), a gas turbine-driven alternator of approximately 10 KWe maximum output with a proven steady-state performance, had previously been subjected to sinusoidal and random vibration environmental test conditions (Reference 1). Test results appeared encouraging, but were not fully evaluated, especially in the area of random vibration.

In this report, previously recorded data from vibration tests of the BRU are summarized and evaluated for the case of sinusoidal vibration input conditions. Data obtained for random vibrational input conditions has been experimentally analyzed extensively in the frequency and amplitude domains (displacement power spectral density and probability density, respectively).

A computer program previously developed (Reference 1) for the analytical prediction of the axial rotor response in terms of acceleration power spectral density, under external random vibrations, has been extended to permit the calculation of the probabilities that thrust bearing gas-film thickness variations will be greater than specified values (probability density) for a specified design and vibration input condition.

Previously calculated acceleration power spectral density results are compared with the newly analyzed experimental data. Vibration excursion probabilities have been calculated for the rotor-thrust bearing combination under external random vibrations in the rotor-axial direction.

PROBABILITY OF THRUST BEARING SURFACE CONTACT DUE TO EXTERNAL, AXIAL RANDOM VIBRATION

Brayton-cycle turbomachinery may be subjected to externally-imposed random vibration under general usage conditions. Under random excitation, the internal machine elements, and particularly the gas bearings, will respond dynamically. An analysis of the axial dynamic response of the Brayton Rotating Unit (BRU) due to external random excitation was presented in Reference 1. For any prescribed random input, the response in terms of the power spectral density and the rms (root-mean-square) value of the thrust bearing gas-film thickness variation was obtained. In this report, the analysis is extended to include a probability analysis of the thrust bearing gas-film thickness variation.

Theoretical Formulation of Probability Analysis

Consider a random time-history record $y(t)$. The probability density function of $y(t)$ is defined as the probability that $y(t)$ will fall within a specific range at any given instant of time. In a time duration T, let T_y be the total amount of time that $y(t)$ falls within the range y and $y + \Delta y$. Then, as T approaches infinity, the ratio T_x/T will approach the probability that $y(t)$ falls inside the range $(y, y + \Delta y)$. In mathematical terms,

$$\text{Prob}[y < y(t) \leq y + \Delta y] = \lim_{T \to \infty} \left[\frac{T_y}{T} \right] \tag{1}$$

The probability density function is defined as

$$p(y) = \lim_{\Delta y \to 0} \frac{\text{Prob}[y < y(t) < y + \Delta y]}{\Delta y} = \frac{\text{Prob}[y < y(t) < y + dy]}{dy} \tag{2}$$

This probability density function is to be distinguished from the probability distribution function P(y) which is defined in the following:

$$P(y) = \text{Prob}[y(t) < y] = \int_{-\infty}^{y} p(y')dy' \tag{3}$$

Thus, the probability of y being less than $-\infty$ is zero and the probability of y being less than ∞ is unity.

$$P(-\infty) = \int_{-\infty}^{-\infty} p(y')dy' = 0$$

$$P(\infty) = \int_{-\infty}^{\infty} p(y')dy' = 1 \tag{4}$$

In the probability analysis of the BRU thrust bearing gas-film thickness variation due to random excitation, the primary interest is centered on the probability that the film thickness will be zero, which is of course the probability of bearing surface contact, P'. Let "h" be the mean gas-film thickness. Then, from Equation (3)

$$P(h) = \text{Prob}[y(t) < h] = \int_{-\infty}^{h} p(y')dy' \tag{5}$$

Thus, the probability of bearing surface contact is,

$$P' = \text{Prob}[y(t) > h] = \int_{h}^{\infty} p(y')dy'$$

$$= \int_{-\infty}^{\infty} p(y')dy' - \int_{-\infty}^{h} p(y')dy' \tag{6}$$

$$= 1 - P(h)$$

In Appendix A the analysis of the response power spectral density and rms value, which was shown in Appendix C of Reference 1, is recapitulated for ready reference.

The analytical model used to study the BRU axial random vibration problem is a linear constant-parameter system. This important assumption permitted the response analysis to be carried out in a simple manner. The linearity asumption is also essential for the probability analysis.

The input random excitation applied by the vibration system to the BRU during testing has a normal or Gaussian, distribution. The response of a linear system must, therefore, also have a Gaussian distribution. Based on this distribution, the probability of thrust bearing surface contact may be calculated. A detailed description of the probability analysis is presented in Appendix A.

Appendix B contains a complete listing of the computer program which implements the analysis of Appendix A. The values of the masses, stiffnesses, and damping coefficients are inputs to the computer program. Also included in Appendix B are instructions for preparing input data cards, sample input, and sample printed output.

Results of Probability Calculation of BRU Thrust Bearing Surface Contact Due to Random Excitation

The foregoing response and probability analyses were conducted for the case of axial random vibration applied to the Brayton Rotating Unit with shaft rotation. Before giving the results of the analysis of the probability of thrust bearing surface contact, it is appropriate to describe the input to the program. (Nomenclature refers to Figure 77.)

Inputs

m_1 = mass of the BRU housing structure = 96 lb.

m_2 = mass of the gimbal and thrust bearing = 7 lb.

m_3 = mass of the rotor = 21 lb.

k_1 = stiffness of connector between the BRU and shake table = 300,000 lb/in.

k_2 = stiffness of the gimbal support = 250,000 lb/in. (from page 79 of Reference 2)

k_3 = stiffness of the gas thrust bearing = 113,500 lb/in.

c_1 = damping coefficient of connector = 0.02 lb sec/in.

c_2 = damping coefficient of gimbal support = 0.02 lb sec/in.

c_3 = damping coefficient of gas thrust bearing = 84 lb sec/in.

The above values of the masses, stiffnesses and damping coefficients are the nominal values and are summarized in Table I.

TABLE I

Nominal Values of the Lumped Masses, Stiffnesses, and Damping Coefficients of an Axial Vibration Model of the Brayton Rotating Unit

Element	m (lb)	k (lb/in.)	c (lb sec/in.)
1	96	300,000	0.02
2	7	250,000	0.02
3	21	113,500	84.00

It should be noted that the values of k_1, k_3 and c_3 are only nominal values. With respect to the stiffness k_1, there are three connectors between the BRU and the shake table. Each is bolted down at one end to the shake table. When the unbolted end of the connector tends to move up, the connector behaves like a cantilever with a calculated stiffness of 75,000 lb/in. at the BRU mount point. But for downward motion the cantilever arm is considerably shorter and thus much stiffer. This stiffness is calculated to be about 1,200,000 lb/in. For the purpose of this analysis, a nominal value of k_1 = 300,000 lb/in. is chosen.

The stiffness and damping characteristics of the gas thrust bearing are functions of frequency and bearing clearance. They have been calculated by an existing gas-bearing computer program and tabulated in Tables II and III. It is seen that they both vary widely with frequency and bearing clearance. Since the random vibration analysis is limited to a linear, time-invariant system, the stiffness and damping coefficients must have fixed values. The nominal values of k_3 and c_3 are chosen at a frequency of 100 Hz and with a film thickness of

TABLE II

Dynamic Stiffness (lb/in.) of Double-Acting Gas Thrust Bearing

h(in.) / ω(Hz)	.0002	.0005	.00105
100	477,000	86,900	18,900
500	523,000	93,700	20,000
1,000	652,000	113,500	22,700
2,000	950,000	166,000	33,600

TABLE III

Dynamic Damping Coefficient (lb sec/in.) of Double-Acting Gas Thrust Bearing

h(in.) / ω(Hz)	.0002	.0005	.00105
100	413	92	33
500	392	90	33
1,000	338	84	33
2,000	191	66	32

0.0005 inch (the total axial clearance in the thrust bearing is 0.0021 inch).

The test objective power spectral density S_o is shown in Figure 1. During actual testing of the BRU, to be described below, it was found that frequent touching of the gas thrust bearing surfaces (possibly to the point of failure) would have occurred if the attempt had been made to subject the BRU to the full level of this vibration specification. Tests were therefore performed with reduced input PSD values (i.e., the shape of the PSD was preserved, but the magnitude of the PSD was reduced by a constant factor, α, across the whole spectrum). From the definitions of the power spectral density and the root-mean-square value, the root-mean-square value is reduced by a factor of $\sqrt{\alpha}$ when the power spectral density is reduced by a factor of α across the whole spectrum.

The root-mean-square (rms) acceleration of the power spectral density in Figure 1 is 5.4g. Testing was performed on the BRU at reduced PSD with the same shape, but with several rms acceleration levels including 0.54g. The response PSD is calculated based on this 0.54g rms acceleration. Thus, $\sqrt{\alpha} = \frac{0.54}{5.4} = 0.1$ and $\alpha = 0.01$.

With the above input values of masses, stiffnesses and damping coefficients, and input PSD of Figure 1 with $\alpha = 0.01$, the response PSD's Sy_1, Sy_2 and Sy_3 were calculated. Note that y_1, y_2 and y_3 are the relative displacements between m_1 and base, m_2 and m_1, and m_3 and m_2, respectively. The area underneath the PSD curve represents the mean square value of the respective quantity.

$E(y_1^2)$ = mean square value of $y_1 = 9.125 \times 10^{-8}$ in.^{2}

$E(y_2^2)$ = mean square value of $y_2 = 1.753 \times 10^{-8}$ in.^{2}

$E(y_3^2)$ = mean square value of $y_3 = 5.164 \times 10^{-8}$ in.^{2}

The square root of the mean square value is the root-mean-square (rms) value. Thus,

rms of $y_3 = 0.226 \times 10^{-3}$ in.

This is to be compared with the measured value of 0.35×10^{-3} inch.

The rms of y_3 is the statistical average of the thrust bearing gas-film thickness

variation. On the other hand, the mean value of y_3 is zero if the response to random excitation has already reached a steady state. Therefore, the rms of y_3 is also the standard deviation of y_3 which is denoted by σ_{y_3}.

If the input random excitation is low, the system remains linear. As stated earlier, the random input from the shake table to the BRU has a normal or Gaussian distribution, and for a linear system, the response to an input with Gaussian distribution also has a Gaussian distribution. Thus, knowing the rms value of y_3, (which in this case is also the standard deviation of y_3) and that y_3 has a Gaussian distribution, the probability of thrust bearing surface contact may be calculated and tabulated as a function of mean gas-film thickness.

Mean Gas-Film Thickness (in.)	Probability of Thrust Bearing Surface Contact
0.0005	0.0139
0.0006	0.0042
0.0007	0.0011

INSTRUMENTATION FOR EXPERIMENTAL ANALYSIS OF RANDOM VIBRATION TEST DATA

Introduction

The BRU simulator had previously been subjected to external sinusoidal and random vibrations which were applied in the rotor axial direction and in a direction perpendicular to the rotor axis. The response of the rotor and of many bearing system components was recorded on magnetic tape for later analysis (Reference 1). The experimental analysis presented in this report draws upon the data obtained and cataloged in Reference 1. A complete description of the Test Apparatus (BRU simulator), the test instrumentation and a description of vibration tests performed may also be found in Reference 1. For convenience, an abbreviated description of the test apparatus and the instrumentation is repeated here.

Test Apparatus

A schematic of the BRU simulator with the rotor in the vertical orientation is shown in Figure 2. The rotor, from the top down, consists of the following components:

1. The (simulated) compressor wheel, containing the cold gas simulator drive turbine.
2. The thrust runner.
3. The compressor end journal.
4. A center section (homopolar generator rotor).
5. The turbine end journal.
6. The (simulated) gas turbine wheel.

The three-pad configuration of the gas film journal bearings is shown in cross-section in Figure 2. The pads are individually supported by pivots, with one of the pivots in each bearing assembly mounted on a mechanical flexure. The flexure, which has a radial stiffness of approximately 2000 pounds per inch, permits the bearing to accommodate radial centrifugal growth of the journal and differential, radial, thermal expansion between the various bearing parts.

The double-acting thrust bearing is supported by a gimbal assembly with two sets of gimbals 90° apart. These permit the thrust bearing to align itself with the thrust runner of the rotor. The surface geometry of the thrust plates consists of nine equal sectors of 39° each with narrow radial grooves separating the sectors. Each sector in turn consists of a slightly depressed sector of 15° arc followed by the raised part in the direction of rotor rotation. Design details for the complete journal and thrust bearing assemblies are given in Reference 2.

The journal bearings, as well as both thrust bearing plates, have hydrodynamic and hydrostatic operating capabilities. For hydrostatic operation, each journal bearing pad and each raised thrust plate sector is equipped with a small gas supply hole, connected to an outside gas source. Hydrostatic bearing operation is normally employed to separate the bearing and rotor surfaces at start-up until rotor speed is high enough to produce a sufficiently large gas film for safe bearing operation. At the design speed of 36,000 rpm and above, the rotor operates hydrodynamically. The BRU design also requires hydrostatic bearing operation at shutdown to prevent rubbing contact between the rotor and the bearing surfaces at speeds too low to provide hydrodynamic film separation of the bearing surfaces. Prior to the vibration tests described in this report, all bearing and corresponding rotor surfaces had been coated by MTI with chrome oxide and refinished to the original dimensional specifications. This was done to improve the tolerance of the bearing surfaces against accidental rubs which might occur in the course of the vibration tests.

Figure 3 is a photograph of the BRU simulator in the vertical support fixture mounted on the vibration table ready for testing. The simulator is held in the support fixture without isolators by three mounting brackets extending radially outward from the simulator casing and resting on the rim of the vertical support fixture. The flexible air hoses visable in Figure 3 serve to pressurize separately each of the journal bearings, the thrust bearing plates, the bearing cavity, the thrust loader chamber and the cold gas drive turbine. Nitrogen at room temperature was used for hydrostatic bearing operation and to provide the ambient gas atmosphere during all hydrodynamic tests.

Figure 4 is a photograph of the BRU simulator in the transverse test fixture

which is attached to the shake table surface. The shake table has been rotated into a horizontal position so that the direction of vibration is perpendicular to the vertically oriented axis of rotation of the BRU. The same three mounting brackets without isolators are used for connecting the BRU simulator to the transverse test fixture as were used on the vertical fixture.

A small-scale schematic of the BRU simulator in the transverse test fixture is shown on all data graphs obtained for this arrangement. As the schematic indicates, the direction of applied vibration is in line with the instrumentation turret and thus passes also through the pivot of the flexibly-mounted pad in each journal bearing.

Test Instrumentation

The dynamic response measurements on the rotor-bearing system were made with capacitance probes. These probes may be divided for convenience into two categories: those measuring displacements of the rotor or some bearing component relative to the simulator casing, and those measuring gas-film thickness variations between the rotor and the thrust bearing or between the rotor and any of the journal bearing pads. From a total of four probes measuring thrust bearing film thickness variations, only two data signals from two probes 90^{o} apart circumferentially have generally been recorded. These two probes were axially in line with probes recording motions of the gimbaled thrust bearing relative to the casing.

Gas-film thickness variations between the rotor and individual journal bearing pads were measured with capacitance probes built into each pad. These probes, which were installed by MTI prior to tests, were located next to the pivot on the inboard side of each bearing pad (a total of six).

Two sets of two probes were used to measure rotor displacement relative to the simulator casing at two locations inboard of the journal bearings. (The angular orientation of these capacitance probes is indicated in Figure 5.) The radial motions of the two flexures supporting each one of the three pads of each journal bearing were measured near the pivot location relative to the casing. Pad motions at the pad leading edge were recorded for one solid-mounted and one

flexure-mounted pad. A schematic of the probe locations in relation to the rotor is shown in Figure 5.

Temperatures from nine locations, including both flexure-mounted journal pads, one solid-mounted pad at the compressor-end journal, and one thrust plate were recorded by automatic print-out throughout the tests.

Analyzers

The random vibration response amplitudes, which had been recorded on magnetic tape during earlier tests, were analyzed in three steps, each employing a distinctly different type of analyzer.

The root-mean-square values of the random displacement signals were extracted through application of a true rms reading voltmeter. The model used was a Hewlett-Packard 7562A log voltmeter-converter. (Many of the simpler commercial voltmeters take advantage of the fixed relationship between peak or mean absolute values to the instantaneous values of a sine signal — which normally represents an a-c voltage. These instruments are much less expensive than true rms detection circuits, but will produce inaccurate readings if they are used to measure random signals.)

The probability analyzer used on the amplitude analysis of the tape recorded BRU simulator response data was an instrument of the latest development. (Signal Analysis Industries Corporation, Model SAICOR 43-A.) The all-digital high-speed processing instrument provided on-line, real-time computation which did not require the use of tape loops for data processing. The probability functions are determined at 400 points with the horizontal axis of the display representing voltage and the range and sensitivity being determined by the setting of the input attenuators. The averaging process can be accomplished linearly or in the digital exponential mode at a minimum sampling rate of $\Delta t = 0.2$ microsecond. The computed functions are displayed on an oscilloscope screen and may be plotted from instrument memory after completion of the computation. A typical photo of the oscilloscope display and the corresponding plot produced on an x-y plotter are shown in Figure 35.

The tape recorded BRU random data was further analyzed with the aid of a real-time frequency analyzer and its companion instrument, an ensemble averager. (Spectral Dynamics Corporation, SD 301 Real-Time Analyzer and SD 302 Ensemble Averager.) This powerful and highly efficient combination permitted the averaging of up to 256 real-time spectra of BRU data for frequency analysis with bandwidth resolutions between 0.3 and 6 Hz over frequency ranges between 100 and 2000 Hz. (These values are not the performance limits of the instrument, they rather represent the range of parameters used in the BRU data analysis and were largely dictated by the length of the available tape recorded random data. The application of bandwidth variation to the BRU data analysis is further explained and demonstrated at a later section of this report, titled "Frequency Analysis — Displacement Power Spectral Density,")

The analysis results obtained by the Real-Time Analyzer are plotted on paper from instrument memory.

RESULTS OF EXPERIMENTAL ANALYSIS OF RANDOM VIBRATION TEST DATA

Amplitude Versus Time Records

Under random vibration conditions, visual inspection of the 'raw' displacement response data will yield only a limited amount of quantitative information. The amplitude limits may thus be determined, provided a long enough sample of data is being examined. A long data record is required to ensure that no gradual shift in the general signal amplitude level is taking place, even though the vibration input level is held constant. If such a change were detected, the data would be termed nonstationary and the experimental analysis methods used to obtain statistical data as presented here would not be applicable.

Visual inspection of the raw data generated for the BRU simulator reveals that, within the maximum amplitude limits of the data the ratio of very large excursions to what appears to be the average signal level, varies from one data signal to the next. In fact, this ratio appears to vary drastically for the same signal when the level of the externally-applied vibration is changed. Some of these signals appear to be distributed so unevenly in level that it is quite safe to guess that their probability density function will be skewed — in other words, the occurrence of small and large amplitudes will not follow the bell-shaped "normal" or Gaussian distribution curve.

An example of data of this type is shown in Figure 6. Both photographs represent the displacement response (relative to machine casing) of one of the flexibly-mounted pivoted journal bearing pads. For the upper photograph the random vibration input level was 0.54g (rms); and for the lower, the input level was 1.54g (rms). For the low level input, the response was very nearly Gaussian, as indicated by the amplitude probability density curve shown next to it. (The probability curves shown in this figure are scale drawings obtained by experimental analysis from random data of which short segments are shown in the oscilloscope photographs.) When the vibration input level was raised (lower photo) the amplitude distribution shifted, with most amplitudes then occurring at a higher value and a few, very substantial excursions, at the low-value region. (Physically, the low value excursions could either mean that the leading edge of

the pivoting pad came very close to hitting the rotating shaft, or conversely, that the shaft had moved far away — in the direction of the solid-mounted pad — and the flex-mounted pad was making a severe follow-up motion. In either case, the information from the photographs could be very valuable if vibration-induced pad instabilities were detected through shaft failure.)

In some instances, only inspection of the time history of the displacement data will reveal otherwise unavailable system response information. A good example of this appears in the upper photograph in Figure 7, which shows the film thickness variations between the rotor and each of the flexibly-mounted bearing pads in each of the two journal bearings. The photo indicates that both pads behave in nearly identical fashion, executing motions that are comparatively smooth and do not change randomly in amplitude. It may also be noted that the amplitudes are out of phase, indicating apparently a "conical" vibration of the rotor. (To obtain the latter information, it was almost imperative to record both traces simultaneously. Due to the lack of periodicity in the signals, they must be recorded with phase and time integrity.) The second photo in Figure 7 records the much more typical response to random vibration of the film thicknesses between the rotor and one of each of the two solid-mounted pivoted pads in each of the two journal bearings.

In studies of rotating shafts, it is common to measure and display rotor motion in a plane perpendicular to the rotor centerline. While such motions are usually steady (not necessarily small) in a nonvibrating environment, they will be very unsteady (but not necessarily unstable) under random vibration conditions. In the left column in Figure 8 the unsteady or random nature of rotor motions is demonstrated through a series of photographs taken with identical film exposure times, which show the rotor moving through vastly different distances in identical time spans. The right column in Figure 8 demonstrates, through photographs with increasingly longer exposure times, that it may be possible to observe the rotor vibrating relatively little during short and judiciously selected time periods. Longer and continuous observations will, however, show some of the very large excursions which, on a statistical basis, must be expected if they are not physically prevented in the system under test.

An excellent example of distorted vibration response of a machine member due to limitations imposed upon its physical movement may be seen in Figure 9. Both photos show the gas film thickness variation between the thrust runner and the upper plate of the thrust bearing stator. Total thrust bearing clearance and the equilibrium operating position of the rotor is indicated to the left of each photo. (Differential gas pressures in the BRU simulator housing cause the thrust runner to assume an operating position which is above the axial centerline of the bearing, see Figure 10.) At low vibration input levels, the thrust runner vibrates essentially against the rather stiff gas film spring of the upper thrust plate without actually making metal-to-metal contact. At the increased vibration level, the thrust runner moves the full distance between stator plates making frequent contact at both ends of its travel. (While thrust runner-to-stator contacts can only be inferred in Figure 9 from the fact that the thrust runner moves through a distance which equals as closely as can be determined the full thrust bearing clearance, temperature measurements in Figure 11 clearly prove that actual contact and intermittent rubbing was taking place.)

Amplitude Analysis: Root-Mean-Square (rms) Values

Calculation of the square root of the mean square (rms) values is the simplest form of data reduction on random signals. The procedure is well known (the rms value is equal to the standard deviation for quantities with a mean value of zero) and the value is readily determined for a random signal with a "true" rms reading voltmeter. Two sample plots (Figures 12 and 13) of random vibration amplitude rms values for vibration input values of 0.54, 0.75 and 1.52 g (rms) are reproduced here from Figures 83 and 86 of Reference 1. Similar plots were obtained for all measuring probes that were mounted inside the BRU simulator. The principal information that may be derived from the rms amplitude plots is the relationship between vibration input level (g-rms) and the amplitude response level (inch-rms). Table IVa provides a summary of amplitude rms values at two vibration input levels [(0.54g (rms) and 1.52g (rms)] for all measurement probes with external vibrations applied to the BRU in the axial direction. The last column in Table IVa shows the ratio of rms amplitudes for the minimum (0.54g (rms)) and maximum (1.52g (rms)) vibration input levels. The amplitude response change is remarkably uniform, with the majority of the response ratios within 20 percent of the input level ratio of 2.81. There are two exceptions for which

TABLE IV

Root-Mean-Square Amplitudes at Two Random Vibration Input Levels

(a) Axial Direction

Probe Number	Random Vibration Input Level: 0	0.52g (rms)	1.52g (rms)		
		A	B	$\frac{B}{A}$	
	in. x 10^4	in. x 10^4	in. x 10^4		
A	0.2	0.375	0.75	2.0	
D	0.25	0.375	0.85	2.2	
C	0.3	0.75	2.5	3.3	
F	0.3	1.25	3.0	2.4	
22	0.6	1.2	3.0	2.4	
21	0.43	1.1	3.1	2.8	
13	0.68	0.95	2.3	2.4	
2	0.61	1.1	2.6	2.4	
4	0.42	1.1	3.2	2.9	
20	0.47	3.6	7.0	1.9	
24	1.0	2.0	6.3	3.1	
17	0.4	3.25	6.5	2.0	
23	0.77	2.0	6.6	3.3	

(b) Transverse Direction

Probe Number	Random Vibration Input Level: 0	0.54g (rms)	1.35g (rms)		1.52g (rms)	
		A	B	$\frac{B}{A}$	C	$\frac{C}{A}$
	in. x 10^4	in. x 10^4	in. x 10^4		in. x 10^4	
A	0.2	1.1	2.5	2.3	2.8	2.5
D	0.29	0.42	0.8	1.9	N.A.	N.A.
C	0.3	0.75	2.2	2.9	2.75	3.8
F	0.34	2.0	4.8	2.4	N.A.	N.A.
22	0.72	3.1	9.0	2.9	11.0	3.5
21	0.52	2.3	7.5	3.3	8.5	3.7
13	0.8	0.85	1.8	2.1	2.1	2.5
2	0.75	3.0	8.0	2.7	9.0	3.0
4	1.2	3.5	12.0	3.4	N.A.	N.A.
20	0.21	1.9	5.5	2.9	5.5	2.9
24	0.61	1.65	3.45	2.1	N.A.	N.A.
17	0.31	1.5	4.75	2.3	N.A.	N.A.
23	1.05	1.7	3.75	2.2	N.A.	N.A.

the increase in the vibration response is less than that of the input change: the thrust bearing probes (No. 17 and 20) and the probes in the two flexibly-mounted pivoted pads (A and D). Both exceptions can be explained from known physical characteristics of the BRU, and from the respective amplitude time records (oscilloscope photographs, Figures 7 and 9). The flexibly-mounted pads have the capability to "track" the rotor to some extent, thereby sharing some of the rotor-induced vibrations with their respective support flexures. The distorted thrust bearing film thickness variations at higher vibration input levels were discussed earlier. Additional evidence for the view that at increased random vibration input levels the thrust runner will essentially bounce back and forth between the rotor plates (vibrate across the full thrust bearing clearance) is given in Table IV(b). Table IV(b) contains data similar to that in Table IV(a) except that it was obtained for the transverse direction of input vibrations. Since vibration response readings at the 1.54g (rms) input level were available for only a limited number of probes, additional values for the 1.35g (rms) vibration input have been included in this table. From this additional data, it is apparent that thrust runner rms amplitudes (probe 20) did not increase above the value reached at the input level of 1.35g (rms). The rms amplitude graph (Figure 139 of Reference 1) which includes test results for random vibration input levels as high as 1.70g (rms) confirms this observation.

Table IV(b) also confirms the expectation that vibration inputs in the lateral direction will ellicit more severe gas film thickness variations in the solid-mounted journal bearings and larger vibrations of the flexure supporting the flexibly-supported pads than axial vibration inputs.

Root-mean-square amplitude plots, as shown in Figures 12 and 13 have a very "noisy" appearance, because generally the damping built into the circuit of the measurement instrument is not large enough to eliminate the instantaneous fluctuations in the rms value. This could be considered as an advantage because the noisy looking rms curve also permits some quick, though superficial, assessment of changes in the nature of the random data signal. If the rms amplitude swings are small, the random vibration amplitude record could be expected to be rather uniform, which comparison of the records for 1.54g (rms) vibration input in Figures 13 and 9 will confirm. Small rms variations are, of course, not at all

synonymous with small random vibration levels, as Figures 12 and 13 will show. Neither are the fluctuations of the rms amplitude curve an indication of the ratio between the random signal maximum amplitude envelope and the rms value.

Theoretically, the random vibration maximum envelope should extend from $-\infty$ to $+\infty$ (Gaussian distribution), but shake table limitations (excursions are limited to $\pm 3\sigma$ about the mean) and physical restraints in the tested mechanism (BRU) do not allow a response that significantly exceeds $\pm 3\sigma$. Once these restraints and the statistical uncertainty from observation of relatively short time records have been accepted, it is reasonable to question what the approximate ratio is between rms amplitude values and the random signal maximum envelope (amplitude-time record) for the set of response measurements at hand. Table V gives a listing of such values for the test case where external random vibrations were applied to BRU simulator in the axial direction. The average ratio of rms amplitude value to maximum envelope in Table V is found to be five, or $\pm 2.5\sigma$. There are two very low values (of approximately $\pm 1.5\sigma$) which were obtained for the two thrust bearing film thickness probes at the higher (1.52g (rms)) vibration input level. Of the four highest values, three were recorded for the hydrostatically pressurized compressor-end journal bearing at the higher vibration input level and one, the highest of all ($\pm 4\sigma$), was obtained for the turbine-end flexible pad-to-shaft film thickness variation.

Amplitude Probability Analysis

Determination of the probability density and distribution functions for a random signal is an important and necessary step in the data analysis progression. Knowledge of the type of amplitude distribution (normal or not normal) which flows from the analysis of the random data permits certain conclusions to be drawn relative to the physical phenomena underlying the recorded data. Moreover, this knowledge can be used to determine some of the basic characteristics of the random data, which in turn may strongly influence the selection of procedures to be used for further analyses and interpretation of test results.

The three most important basic characteristics of random data are the stationarity, the presence of periodicities and the normality. Stationarity is of concern because the analysis procedures used for stationary data are much simpler than those for nonstationary data, and do not apply at all to the latter.

TABLE V

Root-Mean-Square Amplitudes and Maximum Envelope Values

Probe Number	Random Vibration Input Level					
	0.54g (rms)			1.52g (rms)		
	A	B		A'	B'	
	Voltmeter Reading (inch-rms)	Photo Reading (in.-envelope)	$\frac{B}{A}$	Voltmeter Reading (inch-rms)	Photo Reading (in.-envelope)	$\frac{B}{A}$
A	.000038	.00018	4.7	.000075	.00038	5.1
D	.000038	.00030	8.0	.000085	.00050	5.9
C	.000065	.00034	5.2	.00025	.00171	6.9
F	.000125	.00078	6.2	.00030	.00140	4.7
22	.00012	.00056	4.7	.00030	.00150	5.0
21	.00011	.00052	4.7	.00031	.00136	4.4
13	.000095	.00045	4.7	.00023	.00176	7.6
2	.00011	.00057	5.2	.00026	.00172	6.6
4	.00011	.00066	5.1	.00032	.00140	4.4
20	.00036	.00175	4.9	.00070	.00210	3.0
24	.00020	.00126	6.3	.00063	.00308	4.9
17	.000325	.00148	4.5	.00065	.00234	3.6
23	.00019	.00084	4.7	.00066	.00372	5.6

-22-

Testing of random data stationarity should precede the amplitude probability analysis. For the case of the BRU simulator random data stationarity is conveniently determined from the rms amplitude value plots discussed and referenced in the previous section. In general, the degree of stationarity as indicated by those plots, is quite satisfactory. For the vast majority of all recorded tests the rms response level remained constant at each external vibration input setting. Sample records were judged of sufficient length to permit differentiation of any nonstationary trends from random fluctuations of the true history. (For purposes of the reported investigation, data segmentation into frequency ranges and test for time invariance of the sample mean square values in each frequency internal was not considered necessary.)

Amplitude probability analysis may now conveniently be used to evaluate the second and third basic characteristics of random data: the presence or absence of periodic components, and the normality of the random data. (Power spectral density analysis and autocorrelation may additionally be employed for confirmation of conclusions pertaining to the periodicity reached on the basis of amplitude distribution, or may be used (perhaps less effectively) alone. For the BRU simulator, displacement power spectral density analyses were made for all random signals at two vibration input levels, as discussed in the next section.

The results of the probability analysis conducted on the BRU simulator are presented in Figures 14 through 23 for the case where external random vibrations were applied in the rotor axial direction, and in Figures 24 through 34 for the case where external random vibrations were applied in a direction perpendicular to the rotor axis. The probability analyses as shown in the above listed figures was obtained from the recorded data for which the rms amplitude values had already been presented in the series of Figures 77 through 89 and 130 through 142 in Reference 1.

Each of the probability analysis figures is composed of four graphs. Two were obtained at the lowest external random vibration input test level of 0.54g (rms) and the other two at the highest available test level, which was 1.52g (rms) for most plots, but only 1.35g (rms) for a few under transverse external vibration input. For each test level, the upper plot depicts the probability density function and the lower graph the probability distribution function. The probability

density curve may be interpreted in the following way: A selected amplitude range equal to one two-hundredth (0.02) of half of the total amplitude distribution range (corresponding to one window width or bin of the probability analyzer) had a probability of occurrence as indicated by the ordinate. The probability analysis does not produce a smooth curve because the amount of random data analyzed is not infinite. For the case of the BRU data presented, either 328 or 164 measurements were collected in each of the 400 bins of the analyzer. When displayed on an oscilloscope screen (see Figure 35), the 400 probability values associated with each of the 400 bins can be individually distinguished. However, plotting by an x-y recorder generally produces 'noisy' looking probability density curves, from which only estimated probabilities can be determined. This is not as much of a deficiency as it may at first appear, because the main value of the probability density curve may be seen in its visual presentation of symmetry about the mean amplitude value. Symmetry about the mean is a necessary but not sufficient condition for a 'normal' or Gaussian distribution. The nonsymmetrically shaped curve is not qualified for simpler statistical treatment, but it still may provide some information which immediately relates to the behavior of the physical part for which it was recorded. For the data presented in this report, moving toward the right-hand side of the probability density curve along the abscissa means an increasing signal (voltage) magnitude, which in turn is indicative of an increasing gap at the location of the capacitance probe in which the signal was generated.

Keeping this physical relationship in mind, examination of the probability density curves generated for the rotor-bearing system parts of the BRU simulator indicates the following:

1. Response amplitude distributions are less distorted (more nearly normal) at lower external vibration input levels.

2. Response amplitudes are higher when external vibrations are applied in-line with the direction of motion of the particular part (free axis) than perpendicular to it. For example: (a) at the low vibration input level, the thrust bearing film thickness variations (Figures 22 and 32) are higher when the direction of vibration coincides with the rotor axis, than for vibrations applied

transversely to it. At the high vibration input level, the difference in thrust bearing film thickness variations has been masked by the fact that in either case the thrust bearing runner had already started to move back and forth across the full thrust bearing clearance before the highest vibration input level had been reached. The gimbal motions, however, are higher for both low and high vertical vibration input levels applied in the rotor axial direction; (b) when external vibrations were applied in the transverse direction, the journal bearing pad to shaft film thickness variations as well as the rotor motion relative to the casing were larger than for the test case of axially-applied external vibrations. Since the maximum amplitude spread of both pad flexures (flexure probe 22 for compressor-end pad A and flexure probe 21 for turbine-end pad D, Figures 28 and 29 respectively) increased by more than the increases for their respective pads plus that of the opposing solidly-mounted pads, it must be concluded that all pivots experienced momentary unloading and possible pivot-seat separation. (This apparently was not the case at any test input level when external vibrations were applied axially.)

3. The distortion (skew) of the amplitude response distribution can generally be related to the applicable gas film nonlinearity and the physical boundaries that inhibit the free motion of the vibrating pars. For example: (a) the thrust runner (Figure 22) vibrated at low external vibration input levels initially about its steady-state operating position, which is approximately 0.0005 in. away from the compressor-end thrust plate (see Figure 10 for a schematic of the steady-state thrust bearing operating condition). The nonsymmetrical thrust bearing gas film stiffness about the operating point permits the rotor to make some very large excursions in the direction of the turbine end thrust plate. The number of such excursions is small, however, and the result is a highly unsymmetrical distribution in the occurrence of amplitudes. At higher vibration input levels, the thrust bearing film thickness distribution curve loses all resemblence to the

Gaussian distribution, and bears close resemblence instead to the probability distribution for a sine function. As already recognized from the time-amplitude records, this is indicative of the thrust runner bouncing back and forth between the two stator plates. Figure 22 shows, however, that the probability of the rotor being nearer the compressor-end thrust plate is higher than being nearer the turbine-end thrust plate; (b) another example of highly skewed amplitude distribution curve at higher vibration levels is given by the film thickness variations between the solid-mounted turbine-end journal bearing pad and the rotor. Figures 16 and 27 clearly show that the pad is vibrating about a mean position which is approximately 0.00035 inch away from the point beyond which no amplitudes occur (the rotor surface). The solid-mounted compressor journal bearing pad (Figure 26), which was operated with hydrostatic pressurization during the vibration tests, and thus had a higher film thickness, does not exhibit similar behavior. For the compressor journal pad, the amplitude distribution curve is much more symmetrical, apparently because the pad has more room to vibrate (larger steady-state film thickness). Interestingly, its range of vibration amplitude is smaller than that of the solid-mounted turbine journal pad. However, for the flexibly mounted compressor journal pad (which was operated hydrostatically), the range of vibration was larger than that of the hydrodynamically operating flexibly-mounted turbine-end journal bearing pad. Since both flexures vibrated with nearly equal amplitudes, the 'harder' hydrodynamic gas film stiffness of the solid-mounted turbine journal pad seems to have provided more 'bounce' to the shaft, throwing it back further towards the flex-mounted pad; (c) the skew of the amplitude distributions for the two flexures (Figures 28 and 29) with high vibration input levels in the rotor transverse direction indicates vibration which may include rotor conical motions. This is because at the compressor end, the flexure vibrates predominately away from the probe while at the turbine end most of the vibration occurs closer to the probe. This

observation seems to tie in with the previously noted out-of-phase vibration of the two flexibly-mounted pads under hydrostatic operating conditions, as shown in Figure 7, top photograph.

The probability distribution function, sometimes also called the cummulative probability distribution, is the integral of the density function. The probability density analyzer which was used to compute the density function employed a bin-by-bin summation process to arrive at the probability distribution. Consequently, the summation is exact and a smooth curve was produced. Since the ordinate of the distribution function is always normalized for 100 percent probability, it is very convenient to compare the experimental data curve with a superimposed nominal Gaussian distribution function. The closeness of agreement between these two curves should give a good visual indication of the normality of the data. For easy reference, the 16, 50 and 84 percent points have been shown on the ordinate. These correspond to $-\sigma$, 0, and $+\sigma$ points on the abscissa for the Gaussian distribution. The marks on the abscissa which divide the distribution into plus and minus three times the standard deviation ($\pm 3\sigma$) do apply, of course, only to the Gaussian distribution. For most of the data, the amplitude distribution will not equal $\pm 3\sigma$. This was already anticipated from comparison of the rms values with the amplitude envelope values as obtained from oscilloscope screen photographs, and tabulated for the BRU response data to axially-applied external vibrations in Table V. For a number of density and distribution graphs, the discrepancy in the abscissa (deviation from $\pm 3\sigma$) has been enlarged through the plotting process, particularly for very drawn out tail ends and unsymmetrical distributions. In those cases the tail ends were cut off and a somewhat magnified plot produced in the interest of maintaining a suitable ordinate resolution. Nevertheless, comparison between the amplitude values given as plus-minus figures in the probability plots, and those obtained from amplitude envelope photographs, generally gives agreement within 20 percent. The only significant exception was found in the amplitude distribution for the flex-mounted turbine journal bearing pad, for which the rms-to-photo comparison had indicated an amplitude spread of $\pm 4\sigma$ at low external vibration level input (see Table V). The amplitude distribution plot indicates a value much closer to what had been obtained for all other probes and it is in itself also fairly close to normal (Gaussian). The photograph from which the $\pm 4\sigma$ value had been obtained would probably have

contained a rare, excessively large excursion, which by itself was not enough to show up on the probability plots. Alternatively, it may not have been included in the particular stretch of data that was analyzed for the probability distributions. (This incident, which would have been termed 'out-of-range data' or 'stray-point' in the analysis of steady-state periodic data, is well within the range of possibilities — even if only a very small probability is assigned to it — that must be accepted for random data.)

The probability plots indicate in a few cases that symmetry in the density distribution is no guarantee for complete data normality. (See, for example, Figure 25.) These plots, however, generally show only slight deviations from the Gaussian. Those for which the density function shows significant skew or asymmetry cannot be treated by Gaussian statistics. The amplitude analysis test results give good indication that for certain types of moving components of a film-type bearing system, Gaussian response amplitude distribution cannot be expected for any but very small external vibration inputs.

The following table classifies the various BRU bearing system part responses as nearly Gaussian, approximately Gaussian and non-Gaussian. These classifications are arbitrary and are included only to serve the purpose of categorizing the data.

Inspection of Table VI clearly indicates a shift towards non-Gaussian distributions with the external vibration inputs applied in the transverse direction. Such a conclusion does not come as a surprise, however, because as has already been observed, transverse vibration inputs elicit much stronger responses from the journal bearing pads than do axial vibration inputs. Since the reduction of axial vibrations under transverse inputs is not sufficient to make the film thickness variation between thrust runner and thrust plates behave in a Gaussian distribution, the addition of the non-Gaussian distribution from the journal pads and flexures (vibrating more severely with this direction of input) makes the total number of non-Gaussian distributions go up.

TABLE VI

Classification Of Probability Data For Normality

Probe Designation	Direction Of Externally-Applied Vibration					
	Axial			Transverse		
	Nearly Gaussian	Approx. Gaussian	Non-Gaussian	Nearly Gaussian	Approx. Gaussian	Non-Gaussian
A Flex-Mounted Compressor Journal Pad		a,b			a,b	
D Flex-Mounted Turbine Journal Pad	a		b		a	b'
F Solid-Mounted Turbine Journal Pad		a	b			a,b'
22 Compressor Journal Flexure	a	b			a	b
21 Turbine Journal Flexure	a		b		a	b
13 Leading Edge Flex-Mounted Turbine Journal Pad	a		b		a	b
2 Rotor-To-Casing Compressor Journal		a	b			a,b
4 Rotor-To-Casing Turbine Journal		a	b	a		b'
17 Thrust Bearing						a,b'
20 Thrust Bearing			a,b			
23 Thrust Bearing Gimbal		a,b		a		b'

a – low vibration input (0.54g (rms))

b – high vibration input (1.52g (rms))

b' – high vibration input (1.35g (rms))

Frequency Analysis – Displacement Power Spectral Density

Perhaps the most important single descriptive characteristic of stationary random data is the power spectral density function (PSD), which defines the frequency composition of the data. Under random vibration conditions, the occurrence of any particular frequency at which an object moves at any given point in time follows a random variation. In this respect it may be compared to the amplitude variation, which also follows a random pattern. The significant difference is, however, that the distribution of frequencies cannot be estimated or even guessed by visual inspection of time-amplitude data only. For constant parameter linear physical systems, the output power spectrum is equal to the input power spectrum multiplied by the square of the gain factor of the system. For a unity gain factor the expected response should therefore equal the frequency distribution of the external vibration input. In the case of bandwidth-limited input at constant acceleration, the system response should show equal accelerations at all input frequencies, in effect producing a rectangular acceleration distribution over the input signal bandwidth (frequency range).

For the BRU, the specified external vibration input acceleration is not constant over the specified frequency range from 20 to 2000 Hz, but increases logaritmically from 20 to 100 Hz and then remains constant for the remainder of the spectrum (see Figure 1). Figure 36 shows the same specification test power spectral density converted from acceleration power spectral density to displacement power spectral density, (double amplitude displacement). The displacement power spectral density response data from all bearing system components in the BRU simulator should at least resemble Figure 36 if their responses were linear, which essentially means being resonance-free.

Information relative to the dynamic characteristics of the system is the primary result of the power spectral density analysis. A secondary application includes its use for the detection of periodicities. A highly resolved spectrum will reveal periodic components as sharp peaks, even when the periodicities are of relatively small intensity. Since a sharp peak in the power spectrum of the sample data may also represent narrow-band random data (resonances), attempts must be made to distinguish these two cases from one another through repetition of the power spectral density measurement with finer resolution (narrower filter

bandwidth). If the measured spectral peak represents a sine wave, the indicated bandwidth of the peak will always be equal to the bandwidth of the analyzer filter, no matter how narrow the filter. Furthermore, the indicated spectral density will always increase in direct proportion to the reduction in filter bandwidth. (This method of detection will clearly not work unless the resolution bandwidth of the analyzer filter is smaller than the bandwidth of possible narrow-band random data. It is also necessary that the available sample record be sufficiently long to make the product of filter bandwidth and analysis time (in seconds) much larger than unity. Otherwise, uncertainties in the spectral density measurements of the random portions of the data will produce spurious peaks which may obscure the peak caused by the sine wave.)

Examination of the BRU displacement power spectral density plots does not reveal any major periodicities in the intermediate test frequency range where most of the system resonances occurred. This was ascertained through multiple data analysis runs of typical stretches of random data with reduced filter bandwidth settings on the real-time analyzer. For example, in Figure 37(c) the same basic random data was used for analysis as for Figure 37(a), but the filter bandwidth was reduced from 6 Hz in Figure 37(a) to 1.5 Hz in Figure 37(c). The result is a much more finely structured analysis in the frequency domain, which, however, is limited to the total range extending from 5 to 500 Hz. (Basic instrument limitations cause the upper analysis range to shrink from 2000 Hz at 6 Hz filter bandwidth to 500 Hz at 1.5 Hz filter bandwidth and finally to 100 Hz at 0.3 Hz filter bandwidth.) Further reduction in the filter bandwidth to 0.3 Hz (Figure 37(d)) does not reveal any major deviations from the essentially flat response as already indicated in Figure 37(a). There is, however, a fairly weak peak around 60 Hz, which may indicate a sinusoidal component in the BRU system response (possibly caused by line frequency shaker stray input). Alternatively, it may only signify a small line frequency voltage superposition in one of the measurement circuits. The results shown in Figure 37 were obtained for one of the solid-mounted pads in the compressor journal bearing. They seem to be typical for system components in BRU simulator, with the possible exception of the thrust bearing gimbal and the flexibly-mounted journal bearing pad and flexure responses. Narrower filter bandwidth resolution analysis for these parts indicates the presence of previously hidden peaks and around 60 and 180 Hz (Figures 59, 61 and 75).

There is one secondary application of the frequency analyses that arises from the inherent capability of the real-time analysis instrument: the estimate of data stationarity. Data stationarity has already been examined as a prerequisite step to amplitude analysis. The stationarity was deduced from the available rms plots (Figures 12 and 13, and also from Reference 1). During frequency analysis, data stationarity may also be estimated by the following process: With the analyzer set for a maximum frequency of 2000 Hz and the sampling of one ensemble, the instrument will collect one data point from the random input that falls into each of the 500 'bins.' (For the 2000 Hz range setting, each bin is normally 4 Hz wide.) After having accepted just one point into each of the 4 Hz wide bins, the instrument memory is full and hence rejects all further inputs. The analyzer is now ready to plot the power spectral density versus frequency curve from its memory. The above process may then be repeated from the same random data but with increasingly higher numbers of data points collected into each analyzer bin. The analyzer is capable of accepting a maximum of 4096 data points per bin (4096 ensembles) for which a stretch of random input data 17 minutes long would be required. For the BRU simulator, enough test data was taken at constant vibration input levels for a maximum of 256 ensembles. Power spectral density plots for various parts of the BRU simulator were therefore obtained for 1, 8, 64, 128 and (if possible) 256 ensembles. These plots show clearly that the composition of the recorded BRU random response data does not noticeably differ for very short stretches of data from those obtained for much longer segments. A typical series of power spectral density plots obtained from the same data record, but with increasingly higher ensemble rates is presented in Figure 37(b) (8 ensembles), Figure 37(a) (64 ensembles), and Figure 41 (256 ensembles).

For the BRU simulator, the power spectral density analysis (Figures 38 through 67) give the following main results:

1. For external vibrations applied in the rotor axial direction, the thrust bearing film thickness variation indicates a nearly unity gain over the frequency range of approximately 100 to 1000 Hz. (See Figures 54 and 55.) This represents the highest 'base line' response measured (excluding the resonance peaks) in either direction of applied vibrations and for any recorded response.

2. Other bearing-system components with high response-to-input ratios (which actually amounts to low attenuation, because the gain factor is less than one) for the frequency range 100 to 1000 Hz are the thrust bearing gimbal motions (vibration applied in the rotor axial direction) and the film thickness variation between the solid-mounted pads and the rotor (with vibrations applied in the rotor transverse direction).

3. In the frequency range between 20 and approximately 60 Hz, the response of all bearing system components is either at almost constant displacement power spectral density level or exhibits slightly increasing levels with frequency. Considerable attenuation of the response vibrations relative to the shake table input vibration in this frequency region must be noted. However, the vibration response level extends into the low frequency region (5-20 Hz) for which no nominal excitation was present. The level of vibration response in the region up to 60 Hz shows a definite, positive, statistical correlation to the input level.

4. Significant power spectral density response peaks (which exceed the input power spectral density for any of the parts investigated) occurred between 100 and 800 Hz. Except for the response peaks at 600 Hz, the general distribution of resonances matches previously obtained results for sinusoidal vibration input scanning. The very narrow resonance peak at 600 Hz obviously corresponds to the running frequency of the BRU simulator and most probably represents the sinusoidal vibration due to residual rotor unbalance. (Sinusoidal vibration testing did not reveal any resonance at 600 Hz beyond the once-per-revolution rotor unbalance response.) From evaluations of the sinuosidal vibration response results obtained from the BRU simulator, it may also be concluded that the response peak amplitudes at 800 Hz are too small in absolute values to be of concern.

5. The available experimental data does not yield positive identification of the gas-film resonance frequencies associated with the

bearing system. There are at least five such frequencies, some of which are located very close together. The broad based peaks observed in the power spectral density analyses are probably due to these resonances. (The five resonance frequencies originate from the thrust bearing gas film and from the journal bearing gas film in the in-line direction with the flexibly-mounted pad (direction of minimum gas film stiffness) and at 90 degrees to it (direction of maximum journal bearing stiffness). Since the compressor journal was operated hydrostatically and the turbine journal was operated hydrodynamically during the random vibration tests, their stiffnesses are different. Consequently, each condition will produce a set of resonances at slightly different frequencies.)

ANALYSIS OF VIBRATION RESPONSE WITH SINUSOIDAL INPUTS

A considerable amount of sinusoidal vibration response data has been recorded for the BRU simulator (Ref. 1). Since complete sets of data were acquired under various BRU operating conditions, comparison between sets may be used to draw important conclusions as to the behavior of the BRU's internal components. This section describes the expected effects of actual test operating conditions upon this behavior and formulates preliminary explanations of the observed results.

Vibration data is available for the following BRU operating conditions:

Externally Applied Vibration Level (g)	Direction of Applied Vibration: Along Rotor Axis	Direction of Applied Vibration: Across Rotor Axis	Operating Mode of BRU Bearings: Compressor Journal Bearing	Operating Mode of BRU Bearings: Turbine Journal Bearing	Operating Mode of BRU Bearings: Thrust Bearing	Figure Numbers in Reference 1
.25	x		Hydro-static	Hydro-static	Hydro-static	42-52
.12		x	Hydro-static	Hydro-static	Hydro-static	105-116
.12	x		Hydro-dynamic	Hydro-dynamic	Hydro-dynamic	53-71
.12		x	Hydro-static	Hydro-dynamic	Hydro-dynamic	117-129

The two different bearing operating modes are important to the interpretation of the vibration response data in that the bearing gas film spring stiffnesses are different for each mode. For hydrostatic bearing operation, the journal bearing gas film thickness is usually larger than that for hydrodynamic operation. Therefore, the bearing usually has lower stiffness in the hydrostatic operating condition. This may be expected to produce rotor bearing system critical speeds at lower frequencies for hydrostatic operation than for hydrodynamic operation. For gas-lubricated thrust bearings, the opposite may be true. Since total thrust bearing clearance is fixed (in contrast to

the spring-loaded journal bearings), the relatively high gas supply pressure for hydrostatic operation tends to produce a fairly high thrust bearing gas film stiffness. The manner in which the thrust bearing was operated hydrodynamically during the vibration tests makes its gas film stiffness somewhat different than that expected during normal operation: the rotor was supported against gravity by the differential upward pressure in the simulator housing, to the extent that the net runner loading was against the compressor (upper) thrust plate (see Reference 1, page 24-25). The gas film thickness between the compressor-side thrust plate and the runner was approximately 0.0004 to 0.0005 inch, and thus, this side contributed the majority of the axial stiffness. The stiffness of the turbine side (lower) thrust bearing gas film was probably considerably lower than that of the upper film, because of the much higher film on the lower side. Moreover, the end of the rotor was exposed to the large-volume, low-pressure gas cushion in the circulator cavity, an element which contributes very little stiffness.

A partial structural failure of the compressor-end journal bearing early in the test series made it necessary to operate that bearing hydrostatically for the majority of the tests. For the case of laterally-applied vibration (Figures 117-129 in Reference 1), the combined operation of the hydrostatically-pressurized compressor-end journal bearing with the hydrodynamically-operating turbine-end journal bearing and thrust bearing makes it rather likely that actual resonance frequencies of the BRU simulator components will be different from those which would be expected during hydrodynamic operation of all bearings.

While the actual resonance frequencies (and mode shapes) are affected by the necessity of operating one journal bearing hydrostatically, the rotor may still be expected to exhibit some evidence of resonance (probably of low amplitude since the rotor is well balanced) at two distinct speeds.

The mode shapes at these speeds will be essentially either cylindrical or conical in nature. The order of occurrence of these modes will, of course, depend upon relationships between rotor mass, bearing span, polar amount of inertia, and moment of inertia about the rotor center of gravity. For the

BRU rotor with fully hydrodynamic bearings, the first mode has been calculated as conical at 5,270 rpm (88 Hz) and the second mode as essentially translatory at 5,680 rpm (94 Hz). The frequency ratio between the conical and the translatory modes is thus 1.07 for the fully-hydrodynamic case (see Reference 2, page 97).

The tilting-pad gas-lubricated journal bearing, in the three-pad configuration found in the BRU, has distinctly different radial spring stiffnesses in the direction of the pivot axis of the flexure-supported pad (referred to as the y-direction) compared to that in the direction perpendicular to it (referred to as the x-direction). Ratios between 2.5 and 6 for the stiffness in the x-direction to that of the y-direction seem to be typical for this type of bearing at commonly-operated gas film thicknesses. (Reference 3, page 4-14, lists calculated spring stiffness ratios of 2.8 for a number of operating conditions. Calculations performed at MTI for a journal bearing with dimensions and test operating conditions identical to those in the BRU show ratios from 3.4 at 0.00025 inch minimum film thickness to 6 at 0.0005 inch film thickness. Other, unpublished test results obtained by the senior author for a very similar gas journal bearing indicated a similar bearing stiffness component ratio of 2.5) Since the frequencies of both modes of rigid body vibration are proportional to the square root of the bearing stiffness, the frequency ratio between vibration in the x- and y-directions reduces to values between 1.58 and 2.45 for either mode. A typical mean value might be 2.2.

The foregoing discussion has identified the existence of four lateral vibration natural frequencies for the nominal BRU rotor bearing system: conical mode y-direction, translatory mode y-direction, conical mode x-direction, and translatory mode x-direction. The calculated frequency ratios are for fully-hydrodynamic BRU operation: conical y to translatory y, 1:1.07 (88:94 Hz); conical y to conical x, 1:1.58 to 1:2.45 (88:139 to 88:216 Hz); and conical x to translatory x, 1:1.07 (139:145 to 216:232 Hz).

Examination of the recorded lateral rotor motion vibration response, with external vibration applied in the rotor axial direction and full hydrodynamic

bearing operation, indicates a resonance pattern resembling the one described above. (See Figures 55 through 61 in Reference 1 for lateral rotor motions and associated pad-to-shaft film thickness variations.) The lowest of the four resonance frequencies occurs at approximately 100 Hz, with the three next lowest occurring at approximately 130, 150 and 185 Hz.

The fact that the lowest resonance frequency is observed at 100 Hz, instead of at 88 Hz as predicted, may well be due to the lower journal bearing operating film thickness (and thus higher stiffness) in the N_2 atmosphere during the vibration tests as compared to the helium-xenon atmosphere for which the resonance frequencies were predicted in Reference 2. The observed ratio of approximately 1.3 for conical to translatory resonances indicates a journal bearing stiffness ratio of approximately 1.7 for the x and y directions. This value is well within the values of 1.58 to 2.45 observed for similar bearing-rotor systems as described above.

The weak resonance peak at approximately 70 Hz in the cited reference figures is apparently caused by the thrust bearing resonance. This resonance, as exhibited in Figure 62 of Reference 1, is of a somewhat unusual type: a fairly gradual buildup of rotor amplitudes (in the vertical direction) followed by a very steep and sudden decline. The same behavior is observed for the thrust bearing gimbal (Figure 63, Reference 1). Since a distinct phase shift of nearly 180^{o} has been found to accompany the drop in thrust runner-to-stator gas film variations, it is concluded that the thrust bearing resonance does occur at approximately 70 Hz. (Figures 62 and 63 in Reference 1 show this resonance at 60 Hz. Careful reexamination of the tape-recorded data indicates, however, that the resonance actually occurred between 69 and 70 Hz. The deviation in these two figures in Reference 1, appears to be the result of nonlinearities in the x-y plotter, which was calibrated at the end-points of the horizontal scale for these particular plots.)

Since appreciable gimbal motion was found to be associated with the thrust runner-to-stator resonance, is apparent that rotor wobble was present. This offers at least a partial small peak just above 70 Hz in the plots of lateral rotor response.

The interpretation of the resonance pattern of rotor motion due to lateral external vibration inputs is considerably more difficult. The thrust bearing resonance was not expected to have shifted appreciably in frequency. This seems to be borne out by Figure 128 in Reference 1, which indicates the major peak to lie between 70 and 80 Hz. However, the bearing response now also indicates several smaller peaks, which may be the result of lateral rotor motions about the rotor center of gravity, induced by the nonsymmetrical mounting of the BRU simulator the the shaker. The lateral rotor vibration response pattern is less structured than that observed for the case of axially-applied external vibrations. Strong resonances now occur just below and just above 100 Hz, and a definite downward shift in frequency is noted. This could well be the result of reduced stiffness in the compressor journal bearing, which was operated hydrostatically during these tests.

A distinct resonance peak which occurs quite persistently between 300 and 400 Hz in most of the response plots obtained under lateral external vibration inputs, is believed to be caused by a structural resonance which either originates in the support fixture or in the interaction between the fixture and some structural component of the BRU simulator.

CONCLUSIONS

Analysis of Response of Linear System to Externally-Imposed Random Vibration

The extended analysis of the linear three-mass axial response model permits the calculation of thrust bearing surface contact probabilities for given (or assumed) mean thrust bearing gas-film thicknesses. These calculations are based, however, upon the assumption of a normal (or Gaussian) distribution of thrust runner-to-thrust plate gas-film thickness variations.

Experimental Test Evaluation*

Experimental analysis of the BRU simulator response data in the frequency domain (displacement power spectral density) has indicated a considerable degree of similarity between the rotor-bearing system responses to externally-applied sinusoidal and random vibration inputs. This seems to indicate the absence of vibrating subsystems having different resonance frequencies which, if excited simultaneously, might tend to reinforce each other to produce severe vibrations in the random vibration environment.

Comparison of the vibration response and input levels (gain factor) indicates considerable attenuation for most rotor-bearing system components. Least attenuation was noted for the rotor-thrust bearing vibrations with external excitations in the rotor-axial direction.

Amplitude analysis (probability distribution) of the BRU simulator rotor-bearing system responses has yielded a very clear picture of the physical behavior of the BRU rotor-bearing system components at different levels and directions of externally-applied vibration inputs. The experimental probability analysis has further shown that the response of most of the gas film supported rotor system

---

*The conclusions presented in this report are based upon an analysis and experimental evaluation of vibration data presented and tentatively discussed in Reference 1. They should be considered in conjunction with the conclusions presented in Reference 1.

components tends to shift toward non-Gaussian distributions as the external vibration input level is increased. This appears to be caused by the increasingly nonlinear spring stiffness characteristics of the gas films at decreasing thicknesses. The thrust bearing film thickness variations under rotor axial vibration inputs (Figure 22) is a particularly vivid example of this behavior, and underscores the need for a practical design tool to predict this phenomenon. Further development of the theoretical probability analysis, to include the nonlinear nature of the gas films, should significantly improve the prediction of the liklihood of bearing surface contacts under high levels of externally-imposed random vibration. Such development should be included in future investigations in this area.

A detailed examination of the BRU simulator response data obtained under sinusoidal vibration inputs indicates that the relatively large number of vibrating subsystems (rotor mass - gas bearing film combinations) all have the potential to produce severe resonances. For this reason, efforts to suppress the general vibration response of the BRU bearing system will have to be broadly based to treat the worst condition.

Finally, it should be noted that the thrust bearing has not had a complete evaluation under random vibration due to the nonsimilarity of dynamic gas forces on the impellers and cavities in the simulator, compared to the complete BRU. In the simulator the rotor was partially supported by gas forces in the cavity, which led to a rather low and unrepresentative stiffness of the thrust bearing gas film. The results obtained to date for the thrust bearing have, however, yielded much of the information needed to assess its dynamic behavior under random vibration, including the conclusion that some method of axial vibration attenuation must be found. Experimental evaluation of such methods in future programs should include close simulation of the actual thrust bearing properties.

LIST OF REFERENCES

1. Tessarzik, J.M., Chiang, T. and Badgley, R.H., "Effects of Vibration and Shock on the Performance of Gas-Bearing Space-Power Brayton Cycle Turbomachinery, PART 2: Sinusoidal and Random Vibration." Report No. MTI-71TR66, prepared for NASA by Mechanical Technology Incorporated, October 1971.

2. Davis, J.E., "The Design and Fabrication of the Brayton Rotating Unit (BRU)." Report No. APS-5334-R, prepared by AiResearch Manufacturing Company of Arizona for NASA-Lewis Research Center under Contract NAS3-9427, March 15, 1971.

3. McCabe, J.T., Chu, T.Y. and Colsher, R., "Gas Bearing Parametric Analysis for Nuclear Brayton Turbine Alternator Compressor (TAC)." Technical Report No. F-C3164, prepared by Franklin Institute Research Laboratories for AiResearch Manufacturing, April 1972.

4. Crandall, S.H. and Mark, W.D., RANDOM VIBRATION IN MECHANICAL SYSTEMS, Academic Press, New York, London, 1963.

5. Kozin, F., "A Brief Introduction to Some Basic Ideas on the Topic of Random Functions," published in Stochastic Processes in Dynamical Problems. Presented at the 1969 Winter Annual Meeting of the American Society of Mechanical Engineers.

6. Bendat, J.S., PRINCIPLES AND APPLICATIONS OF RANDOM NOISE THEORY, John Wiley and Sons, New York, 1968.

7. Bendat, J.S. and Piersol, A.G., RANDOM DATA: ANALYSIS AND MEASUREMENT PROCEDURES, Wiley Interscience, New York, 1971.

MATHEMATICAL SYMBOLS

c	damping coefficient, lb-sec/in.
$E(\ )$	mean square value of ( )
f	frequency, Hz
h	mean gas-film thickness, in.
H	transfer function
k	spring stiffness, lb/in.
m	mass, lb-sec^2/in.
p	probability density function
P'	probability of thrust bearing surface contact
S	power spectral density
S_o	input power spectral density
x_1, x_2, x_3, x_b	coordinates defined in Figure 77
y_1, y_2, y_3	relative coordinates defined in Equation (A-4)
Z	defined in Equation (A-20)
μ_{y_3}	mean value of y_3
σ_{y_3}	standard deviation of y_3
ψ_{y_3}	root-mean-square value of y_3
ω	frequency, rad/sec

APPENDIX A

PROBABILITY ANALYSIS OF DYNAMIC RESPONSE OF BRAYTON ROTATING UNIT TO AXIAL RANDOM EXCITATIONS

The dynamic response of the BRU thrust bearing due to axial random excitation was analyzed in Appendix C of Reference 1. For easy reference, the analysis is recapitualted herein, together with the thrust bearing gas film thickness variation probability analysis.

The Brayton rotating unit was modeled as a three-mass system, as shown in Figure 77. A sketch of the BRU is shown in Figure 78, in which the various masses and springs are identified with the model shown in Figure 77. The base of the three-mass system is the shake table, by which random excitations are transmitted to the BRU. The quantities k_1 and c_1 are, respectively, the stiffness and damping of the connectors which provide the joint between the BRU and the shake table; m_1 is the mass of the BRU housing structure; k_2 and c_2 are the thrust bearing gas-film stiffness and damping, respectively; and finally, m_3 is the rotor mass. The equations of motion of the three-mass system shown in Figure 77 are:

$$m_1\ddot{x}_1 + c_1(\dot{x}_1-\dot{x}_b) + c_2(\dot{x}_1-\dot{x}_2) + k_1(x_1-x_b) + k_2(x_1-x_2) = 0 \qquad \text{(A-1)}$$

$$m_2\ddot{x}_2 + c_2(\dot{x}_2-\dot{x}_1) + c_3(\dot{x}_2-\dot{x}_3) + k_2(x_2-x_1) + k_3(x_2-x_3) = 0 \qquad \text{(A-2)}$$

$$m_3\ddot{x}_3 + c_3(\dot{x}_3-\dot{x}_2) + k_3(x_3-x_2) = 0 \qquad \text{(A-3)}$$

Introducing relative coordinates between mass points,

$$y_1 = x_1 - x_b$$

$$y_2 = x_2 - x_1 \qquad \text{(A-4)}$$

$$y_3 = x_3 - x_2$$

Equations (A-1) and (A-3) become

$$m_1\ddot{y}_1 + c_1\dot{y}_1 - c_2\dot{y}_2 + k_1y_1 - k_2y_2 = -m_1\ddot{x}_b \quad \text{(A-5)}$$

$$m_2(\ddot{y}_1 + \ddot{y}_2) + c_2\dot{y}_2 - c_3\dot{y}_3 + k_2y_2 - k_3y_3 = -m_2\ddot{x}_b \quad \text{(A-6)}$$

$$m_3(\ddot{y}_1 + \ddot{y}_2 + \ddot{y}_3) + c_3\dot{y}_3 + k_3y_3 = -m_3\ddot{x}_b \quad \text{(A-7)}$$

Dividing Equations (A-5), A-6) and (A-7) by m_1, m_2 and m_3 respectively,

$$\ddot{y}_1 + \frac{c_1}{m_1}\dot{y}_1 - \frac{c_2}{m_1}\dot{y}_2 + \frac{k_1}{m_1}y_1 - \frac{k_2}{m_1}y_2 = -\ddot{x}_b \quad \text{(A-8)}$$

$$\ddot{y}_1 + \ddot{y}_2 + \frac{c_2}{m_2}\dot{y}_2 - \frac{c_3}{m_2}\dot{y}_3 + \frac{k_2}{m_2}y_2 - \frac{k_3}{m_2}y_3 = -\ddot{x}_b \quad \text{(A-9)}$$

$$\ddot{y}_1 + \ddot{y}_2 + \ddot{y}_3 + \frac{c_3}{m_3}\dot{y}_3 + \frac{k_3}{m_3}y_3 = -\ddot{x}_b \quad \text{(A-10)}$$

Subtracting Equation (A-8) from Equation (A-9),

$$\ddot{y}_2 - \frac{c_1}{m_1}\dot{y}_1 + \left[\frac{c_2}{m_1} + \frac{c_2}{m_2}\right]\dot{y}_2 - \frac{c_3}{m_2}\dot{y}_3 - \frac{k_1}{m_1}y_1 + \left[\frac{k_2}{m_1} + \frac{k_2}{m_2}\right]y_2 - \frac{k_3}{m_2}y_3 = 0 \quad \text{(A-11)}$$

Subtracting Equation (A-9) from Equation (A-10),

$$\ddot{y}_3 - \frac{c_2}{m_2}\dot{y}_2 + \left[\frac{c_3}{m_2} + \frac{c_3}{m_3}\right]\dot{y}_3 - \frac{k_2}{m_2}y_2 + \left[\frac{k_3}{m_2} + \frac{k_3}{m_3}\right]y_3 = 0 \quad \text{(A-12)}$$

Equations (A-8), (A-11) and (A-12) can be written in the matrix form as follows:

$$\begin{bmatrix} 1 & 0 & 0 \\ 0 & 1 & 0 \\ 0 & 0 & 1 \end{bmatrix} \cdot \begin{bmatrix} \ddot{y}_1 \\ \ddot{y}_2 \\ \ddot{y}_3 \end{bmatrix} + \begin{bmatrix} \frac{c_1}{m_1} & -\frac{c_2}{m_1} & 0 \\ -\frac{c_1}{m_1} & \frac{c_2}{m_1}+\frac{c_2}{m_2} & -\frac{c_3}{m_2} \\ 0 & -\frac{c_2}{m_2} & \frac{c_3}{m_2}+\frac{c_3}{m_3} \end{bmatrix} \cdot \begin{bmatrix} \dot{y}_1 \\ \dot{y}_2 \\ \dot{y}_3 \end{bmatrix} + \begin{bmatrix} \frac{k_1}{m_1} & -\frac{k_2}{m_1} & 0 \\ -\frac{k_1}{m_1} & \frac{k_2}{m_1}+\frac{k_2}{m_2} & -\frac{k_2}{m_2} \\ 0 & -\frac{k_2}{m_2} & \frac{k_3}{m_2}+\frac{k_3}{m_3} \end{bmatrix} \cdot \begin{bmatrix} y_1 \\ y_2 \\ y_3 \end{bmatrix} = \begin{bmatrix} -\ddot{x}_b \end{bmatrix} \cdot \begin{bmatrix} 1 \\ 0 \\ 0 \end{bmatrix} \quad \text{(A-13)}$$

To obtain the complex frequency response, assume

$$x_b = e^{i\omega t} \tag{A-14}$$

$$\begin{bmatrix} y_1 \\ y_2 \\ y_3 \end{bmatrix} = \begin{bmatrix} H_{y_1}(\omega) \\ H_{y_2}(\omega) \\ H_{y_3}(\omega) \end{bmatrix} \cdot e^{i\omega t} \tag{A-15}$$

and substitute into Equation (A-13):

$$-\omega^2 [I] \begin{bmatrix} H_{y_1}(\omega) \\ H_{y_2}(\omega) \\ H_{y_3}(\omega) \end{bmatrix} + i\omega[C] \begin{bmatrix} H_{y_1}(\omega) \\ H_{y_2}(\omega) \\ H_{y_3}(\omega) \end{bmatrix} + [K] \begin{bmatrix} H_{y_1}(\omega) \\ H_{y_2}(\omega) \\ H_{y_3}(\omega) \end{bmatrix} = \omega^2 \begin{bmatrix} 1 \\ 0 \\ 0 \end{bmatrix} \tag{A-16}$$

where

$$[I] = \begin{bmatrix} 1 & 0 & 0 \\ 0 & 1 & 0 \\ 0 & 0 & 1 \end{bmatrix} \tag{A-17}$$

$$[C] = \begin{bmatrix} \frac{c_1}{m_1} & -\frac{c_2}{m_1} & 0 \\ -\frac{c_1}{m_1} & \frac{c_2}{m_1} + \frac{c_2}{m_2} & -\frac{c_3}{m_2} \\ 0 & -\frac{c_2}{m_2} & \frac{c_3}{m_2} + \frac{c_3}{m_3} \end{bmatrix} \tag{A-18}$$

$$[K] = \begin{bmatrix} \frac{k_1}{m_1} & -\frac{k_2}{m_1} & 0 \\ -\frac{k_1}{m_1} & \frac{k_2}{m_1}+\frac{k_2}{m_2} & -\frac{k_3}{m_2} \\ 0 & -\frac{k_2}{m_2} & \frac{k_3}{m_2}+\frac{k_3}{m_3} \end{bmatrix} \tag{A-19}$$

Define a matrix Z:

$$[Z] \equiv -[I] + i\frac{1}{\omega}[C] + \frac{1}{\omega^2}[K] \tag{A-20}$$

Equation (A-16) can be written as

$$[Z] \begin{bmatrix} H_{y_1}(\omega) \\ H_{y_2}(\omega) \\ H_{y_3}(\omega) \end{bmatrix} = \omega^2 \begin{bmatrix} 1 \\ 0 \\ 0 \end{bmatrix}$$

Thus,

$$\begin{bmatrix} H_{y_1}(\omega) \\ H_{y_2}(\omega) \\ H_{y_3}(\omega) \end{bmatrix} = \omega^2 [Z]^{-1} \begin{bmatrix} 1 \\ 0 \\ 0 \end{bmatrix} \tag{A-21}$$

The complex frequency responses, $H_{y_1}(\omega)$, $H_{y_2}(\omega)$ and $H_{y_3}(\omega)$ can be readily calculated from Equation (A-21). The complex frequency response functions are sometimes called transfer functions. They give the response at one point due to a unit input excitation at some other point.

It was shown, for example, in References 4 and 5 that the input and output power spectral densities of a random process are also related by the transfer functions in the following manner.

$$S_{y_i}(\omega) = |H_{y_i}(\omega)|^2 \quad S_0(\omega) \qquad (i=1, 2, 3) \tag{A-22}$$

where

$S_{y_i}(\omega)$ = PSD of the system output y_i (i=1, 2, 3).

$S_0(\omega)$ = PSD of the system input.

$H_{y_i}(\omega)$ = magnitude of transfer function as calculated from (A-21).

Of particular interest is $S_{y_3}(\omega)$ which is the power spectral density of the thrust bearing gas-film thickness variation. The mean square value can be obtained by integrating the power spectral density throughout the whole spectrum.

$$\psi^2_{y_3} = \int_{\omega_1}^{\omega_2} S_{y_3}(\omega)\, d\omega \tag{A-23}$$

where $\psi^2_{y_3}$ = mean square value of y_3

ω_1, ω_2 = lower and upper limits of the spectrum

The mean square value is related to the variance σ^2 and the mean value μ by the following:

$$\sigma^2_{y_3} = \psi^2_{y_3} - \mu^2_{y_3} \tag{A-24}$$

Since y_3 is the thrust bearing gas-film thickness variation, its mean value is zero for steady-state operation.

$$\mu_{y_3} = 0 \tag{A-25}$$

Therefore, knowing the power spectral density of y_3 we calculate from Equation (A-23) to (A-25), the standard deviation σ_{y_3} or the variance $\sigma^2_{y_3}$.

$$\sigma^2_{y_3} = \psi^2_{y_3} = \int_{\omega_1}^{\omega_2} S_{y_3}(\omega)\, d\omega \tag{A-26}$$

The random excitation output of the shake table has a normal or Gaussian distribution. The shake table is rigidly connected to the BRU base which is shown in Figure 77. Thus, the input axial random excitation of the BRU is the same as the shake table output and has a Gaussian distribution.

Now, the model of the BRU rotor-bearing system, as shown in Figure 77, is a linear constant-parameter system. For such a system, a random input with Gaussian distribution would yield a random response with the same distribution (References 6 and 7).

Thus, the Gaussian probability density function of y_3 can be expressed as

$$p(y_3) = \frac{1}{\sigma_{y_3}\sqrt{2\pi}} \exp\left(-\frac{y_3^2}{2\,\sigma^2_{y_3}}\right) \tag{A-27}$$

Let h be the mean gas-film thickness. Then, whenever y_3 is greater than or equal to h, there is solid contact or rubbing between bearing surfaces. The probability that $y_3 \geq h$ or the probability of bearing surface contact, is given by:

$$P' = \int_{h}^{\infty} p(y_3)\, dy_3 = \int_{h}^{\infty} \frac{1}{\sqrt{2\pi}} \frac{1}{\sigma_{y_3}} \exp\left(-\frac{y_3^2}{2\sigma_{y_3}^2}\right) dy_3 \qquad \text{(A-28)}$$

$$= \int_{\bar{h}}^{\infty} \frac{1}{\sqrt{2\pi}} \exp\left(-\frac{1}{y}\ \bar{y}_3^2\right)\ d\bar{y}_3$$

where $y_3 = y_3/\sigma_{y_3}$

$\bar{h} = h/\sigma_{y_3}$

The values of integral in (A-28) have been tabulated versus $\bar{h}$, for example on page 387 of Reference 7.

APPENDIX B

COMPUTER PROGRAM FOR PREDICTING THE DYNAMIC RESPONSE OF THE BRAYTON ROTATING UNIT TO AXIAL RANDOM EXCITATIONS AND PROBABILITY OF THRUST BEARING SURFACE CONTACT

This Appendix presents a complete listing of the computer program MTI-492, which calculates the axial response of the Brayton Rotating Unit under random excitation and the probability of thrust bearing surface contact. Also included in this Appendix are instructions for preparing input data cards, sample input and sample computer output.

PROGRAM INPUT CARDS

Card 1 FORMAT (I5)

This card reads in NCASE which is the number of cases.

Card 2 FORMAT (80H)

This card contains the descriptive identification for the case being computed.

Card 3 FORMAT (8E10.3)

This card reads in FAC.

FAC = numerical factor to be multiplied with the power spectral density specifications to permit calculations at various levels without requiring the entire specification to be modified and resubmitted as input.

Card 4 FORMAT (8E10.3)

This card contains ENGM(1), ENGC(1) and ENGK(1).

ENGM(1) = m_1 in pounds
ENGC(1) = c_1 in lb sec/in.
ENGK(1) = k_1 in lb/in.

The quantities m_1, c_1 and k_1 are shown in Figure 77.

Card 5 FORMAT (8E10.3)

This card contains ENGM(2), ENGC(2) and ENGK(2).

ENGM(2) = m_2 in pounds
ENGC(2) = c_2 in lb sec/in.
ENGK(2) = k_2 in lb/in.

The quantities m_2, c_2 and k_2 are shown in Figure 77.

Card 6 FORMAT (8E10.3)

This card contains ENGM(3), ENGC(3) and ENGK(3).

ENGM(3) = m_3 in pounds
ENGC(3) = c_3 in lb sec/in.

ENGK(3) = k_3 in lb/in.

The quantities m_3, c_3 and k_3 are shown in Figure 77.

Card 7 FORMAT (5I5)

This card contains NRANG, SPEC, NFILMT.

NRANG = number of frequency ranges. Each frequency range will be defined in Card 8 by an initial frequency, a final frequency and an incremental frequency.

SPEC = 1: PSD of Figure 1 will be read in.

2: a white noise displacement PSD of 1 in^2/Hz will be read in.

3: a white noise acceleration PSD of 0.01 g^2/Hz will be read in.

NOTE: The PSD values read in will be multiplied by FAC specified in Card 3.

NFILMT = Number of film thicknesses (up to a maximum of 10).

Card 8 FORMAT (8E10.3)

This set of cards specifies the frequencies at which the response PSD will be calculated. The number of cards in this set is equal to NRANG of Card 7. Each card containing, WINIT, WFIN and WDELT represents a frequency range.

WINIT = initial frequency in Hz.

WFIN = final frequency in Hz.

WDELT = incremental frequency in Hz.

Card 9 FORMAT (8E10.3)

This card contains FLMTH(I), which is the film thicknesses in inches. A total of I = NFILMT values is to be read in.

NOTE: Card 2 through Card 8 represent one case. The whole sequence can be repeated as many times as the number of cases specified in Card 1.

```
C                                                                       FEB173    1
C                    MECHANICAL TECHNOLOGY INCORPORATED                 FEB173    2
C                          968 ALBANY-SHAKER ROAD                       FEB173    3
C                          LATHAM, NEW YORK 12110                       FEB173    4
C                              518-785-2211                             FEB173    5
C                                                                       FEB173    6
C                    AXIAL RESPONSE OF TURBOMACHINERY TO                FEB173    7
C                  STATIONARY RANDOM EXCITATION - OCTOBER, 1972         FEB173    8
      DIMENSION TITLE(10),M(3,3),C(3,3),K(3,3)                          VIBRAN    3
      DIMENSION WNAT(3),ZETA(3),MU(3),ENGM(3),ENGC(3),ENGK(3)           VIBRAN    4
      DIMENSION WINIT(5),WDELT(5),WFIN(5),FINIT(5),FDELT(5),FFIN(5)     VIBRAN    5
      DIMENSION PSD(3),PSDY(3)                                          VIBRAN    6
      DIMENSION YINT(3),TOTY(3)                                         VIBRAN    7
      DIMENSION RMS(5),ZALPHA(50),PROB(50)                              AU3072    1
      COMMON/FT/ FLMTH(10),NFILMT                                       AU3072    2
      REAL M,K,MU                                                       VIBRAN    8
      INTEGER SPEC                                                      VIBRAN    9
      DATA(ZALPHA(I),I=1,42)/.0,.1,.2,.3,.4,.5,.6,.7,.8,.9,1.,1.1,1.2,  AU3072    3
     1  1.3,1.4,1.5,1.6,1.7,1.8,1.9,2.0,2.1,2.2,2.3,2.4,2.5,2.6,2.7,2.8, AU3072    4
     2  2.9,3.0,3.1,3.2,3.3,3.4,3.5,3.6,3.7,3.8,3.9,4.0,4.1/             AU3072    5
      DATA (PROB(I),I=1,42)/ .5,.4602,.4207,.3821,.3446,.3085,.2743,    AU3072    6
     1  .2420,.2119,.1841,.1587,.1357,.1151,.0968, .0808,.0668,.0548,    AU3072    7
     2  .0446,.0359,.0287,.0228,.0179,.0139,.0107,.00820,.00621,.00466,  AU3072    8
     3  .00347,.00256,.00187,.00130,.00100,.00070,.00050,.00034,.00024,  AU3072    9
     4  .00017,.00011,.00006,.00002,.00,.00/                            AU3072   10
      NALPHA=42                                                         AU3072   11
      READ(5,115)NCASE                                                  VIBRAN   10
      KCASE=0                                                           VIBRAN   11
    5 CALL READIT(TITLE,ENGM,ENGC,ENGK,NRANG,SPEC,WINIT,WFIN,WDELT,FAC) VIBRAN   12
      CALL WRITIT(TITLE,ENGM,ENGC,ENGK,NRANG,SPEC,WINIT,WFIN,WDELT,FAC) VIBRAN   13
      CALL MATRX2(M,C,K,ENGM,ENGC,ENGK)                                 VIBRAN   14
      WRITE(6,195)                                                      VIBRAN   15
      DO 2 I=1,3                                                        VIBRAN   16
      TOTY(I)=0.                                                        VIBRAN   17
    2 WRITE(6,190)(M(I,J),J=1,3),(C(I,J),J=1,3),(K(I,J),J=1,3)          VIBRAN   18
      TOTS=0.                                                           VIBRAN   19
      TOTP=0.                                                           VIBRAN   20
      DO 420 III=1,NRANG                                                VIBRAN   21
      WRITE(6,90)                                                       VIBRAN   22
      WRITE(6,100)III,WINIT(III),WFIN(III),WDELT(III)                   VIBRAN   23
      WRITE(6,110)                                                      VIBRAN   24
      W=WINIT(III)                                                      VIBRAN   25
      DEL=WDELT(III)                                                    VIBRAN   26
      W=W-DEL                                                           VIBRAN   27
      DO 650 J=1,3                                                      VIBRAN   28
  650 YINT(J)=0.                                                        VIBRAN   29
      PSINT=0.                                                          VIBRAN   30
      SCALIN=0.                                                         VIBRAN   31
      DO 400 II=1,1000                                                  VIBRAN   32
      W=W+DEL                                                           VIBRAN   33
      XW=W                                                              VIBRAN   34
      IF(W.GT.WFIN(III)) GO TO 400                                      VIBRAN   35
      ALL CALCULATIONS ARE DONE IN RADIANS/SEC                          VIBRAN   36
      W=W*2.*3.14159                                                    VIBRAN   37
        CALL CALC(M,C,K,W,PSD)                                          VIBRAN   38
      CONVERT ALL FREQUENCIES IN TO HZ BEFORE CALLING FOR SPECS         VIBRAN   39
      F=W/(2.*3.14159)                                                  VIBRAN   40
      GO TO (585,600,610,600,600 ),SPEC                                 VIBRAN   41
  585 CALL SPEC1(F,SCALE)                                               VIBRAN   42
      GO TO 645                                                         VIBRAN   43
  600 CALL SPEC2(F,SCALE)                                               VIBRAN   44
      GO TO 645                                                         VIBRAN   45
  610 CALL SPEC3(F,SCALE)                                               VIBRAN   46
```

```
645 CONTINUE                                                          VIBRAN    47
    SCALE=SCALE*FAC                                                   VIBRAN    48
    IF(W.NE.0.) PSINCH=SCALE*(386.**2/W**4)                           VIBRAN    49
    IF(W.EQ.0.) PSINCH=SCALE*(386.**2/(1.E-15)**4)                    VIBRAN    50
    IF(II.EQ.1.OR.XW.GE.(WFIN(III)-.01)) GO TO 200                    VIBRAN    51
    PSINT=PSINT+PSINCH                                                VIBRAN    52
    SCALIN=SCALIN+SCALE                                               VIBRAN    53
    GO TO 220                                                         VIBRAN    54
200 PSINT=PSINT+.5*PSINCH                                             VIBRAN    55
    SCALIN=SCALIN+.5*SCALE                                            VIBRAN    56
    IF(XW.LT.(WFIN(III)-.01)) GO TO 220                               VIBRAN    57
    PSINT=PSINT*WDELT(III)                                            VIBRAN    58
    SCALIN=SCALIN*WDELT(III)                                          VIBRAN    59
220 CONTINUE                                                          VIBRAN    60
    DO 330 J=1,3                                                      VIBRAN    61
    PSDY(J)=SCALE*PSD(J)*386.**2                                      VIBRAN    62
    IF(II.EQ.1.OR.XW.GE.(WFIN(III)-.01))GO TO 350                     VIBRAN    63
    YINT(J)=YINT(J)+PSDY(J)                                           VIBRAN    64
    GO TO 330                                                         VIBRAN    65
350 YINT(J)=YINT(J)+.5*PSDY(J)                                        VIBRAN    66
    IF(XW.GE.(WFIN(III)-.01)) YINT(J)=YINT(J)*WDELT(III)              VIBRAN    67
330 CONTINUE                                                          VIBRAN    68
    CONVERT ENGINEERING FREQUENCIES BACK INTO HZ                      VIBRAN    69
    W=W/(2.*3.14159)                                                  VIBRAN    70
    WRITE(6,120)W,(PSDY(J),J=1,3),PSINCH,SCALE                        VIBRAN    71
400 IF(II.EQ.1000) WRITE(6,160)(YINT(J),J=1,3),PSINT,SCALIN           VIBRAN    72
    DO 30 J=1,3                                                       VIBRAN    73
 30 TOTY(J)=TOTY(J)+YINT(J)                                           VIBRAN    74
    TOTP=TOTP+PSINT                                                   VIBRAN    75
    TOTS=TOTS+SCALIN                                                  VIBRAN    76
    WRITE(6,170)(TOTY(J),J=1,3),TOTP,TOTS                             VIBRAN    77
    DO 40 J=1,3                                                       AU3072    12
 40 RMS(J)=SQRT(TOTY(J))                                              AU3072    13
    RMS(4)=SQRT(TOTP)                                                 AU3072    14
    RMS(5)=SQRT(TOTS)                                                 AU3072    15
    WRITE(6,180) (RMS(J),J=1,5)                                       AU3072    16
    IF(NFILMT.EQ.0) GO TO 420                                         AU3072    17
    IF(III.NE.NRANG) GO TO 420                                        0C1872     1
    WRITE(6,125)                                                      AU3072    18
    DO 50 J=1,NFILMT                                                  AU3172     1
    ZAL=FLMTH(J)/RMS(3)                                               AU3172     2
    CALL TLU(ZAL,RPROB,ZALPHA,PROB,NALPHA)                            AU3172     3
 50 WRITE(6,130) FLMTH(J),RPROB                                       AU3172     4
420 CONTINUE                                                          VIBRAN    78
    KCASE=KCASE+1                                                     VIBRAN    79
    IF(KCASE-NCASE)5,425,425                                          VIBRAN    80
425 CALL EXIT                                                         VIBRAN    81
 90 FORMAT(1H1,//25X,80(1H*)//)                                       VIBRAN    82
100 FORMAT(25X,22HFREQUENCY RANGE NUMBER,I5/                          VIBRAN    83
   1       25X,21HCOVERS THE RANGE FROM,F9.2,3X,2HTO,F9.2/            VIBRAN    84
   2       25X,19HIN INCREMENTS OF    ,F7.2/)                         VIBRAN    85
110 FORMAT(25X,80H  FREQUENCY       PSD OF Y1     PSD OF Y2     PSD OF Y3 VIBRAN    86
   1    PSD INPUT    PSD INPUT   /                                    VIBRAN    87
   2       25X,80H     (HZ)          (IN*IN/HZ)    (IN*IN/HZ)    (IN*IN/HZ) VIBRAN    88
   3   (IN*IN/HZ)      (G*G/HZ)      /)                              VIBRAN    89
115 FORMAT(I5)                                                        VIBRAN    90
120 FORMAT(25X,F12.3,4X,5(E10.3,3X))                                  VIBRAN    91
160 FORMAT(/23X,16HINTEGRATED VALUE,2X,5(E10.3,3X))                   AU3072    23
170 FORMAT(23X,16HTOTAL INT. VALUE,2X,5(E10.3,3X))                    AU3072    24
180 FORMAT(23X,9HRMS VALUE,9X,5(E10.3,3X))                            AU3072    25
125 FORMAT(/,23X,20HMEAN FILM THICKNESS ,5X,                          0C1872     2
   1  22HPROB. OF SOLID CONTACT  ,/,31X,6H(INCH),/)                   AU3072    27
130 FORMAT(28X,F10.6,16X,E10.3)                                       AU3072    28
195 FORMAT(///5X,10HMATRIX M  ,36X,10HMATRIX C  ,36X,10HMATRIX K   )  VIBRAN    94
190 FORMAT(5X,3(E10.3,3X),7X,3(E10.3,3X),7X,3(E10.3,3X))              VIBRAN    95
    END                                                               VIBRAN    96
```

```
                                                                        FEB173    9
      SUBROUTINE READIT(TITLE,ENGM,ENGC,ENGK,NRANG,SPEC,WINIT,WFIN,WDELT READIT    2
     1,FAC              )                                               READIT    3
      INTEGER SPEC                                                      READIT    4
      DIMENSION ENGM(3),ENGC(3),ENGK(3),WINIT(5),WFIN(5),WDELT(5)       READIT    5
      DIMENSION TITLE(8)                                                READIT    6
      COMMON/FT/ FLMTH(10),NFILMT                                       AU3072   29
      READ(5,115)(TITLE(I),I=1,8)                                       READIT    7
      READ(5,100)FAC                                                    READIT    8
      DO 10 I=1,3                                                       READIT    9
   10 READ(5,100)ENGM(I),ENGC(I),ENGK(I)                                READIT   10
      READ(5,110) NRANG,SPEC,NFILMT                                     AU3072   30
      DO 20 I=1,NRANG                                                   READIT   12
   20 READ(5,100)WINIT(I),WFIN(I),WDELT(I)                              READIT   13
      IF(NFILMT.EQ.0) GO TO 500                                         AU3072   31
      READ(5,100) (FLMTH(I),I=1,NFILMT)                                 AU3072   32
  100 FORMAT(8E10.3)                                                    READIT   14
  110 FORMAT(5I5)                                                       READIT   15
  115 FORMAT(8A10)                                                      READIT   16
  500 RETURN                                                            AU3072   33
      END                                                               READIT   18


                                                                        FEB173   10
      SUBROUTINE WRITIT(TITLE,ENGM,ENGC,ENGK,NRANG,SPEC,WINIT,WFIN,WDELT WRITIT    2
     1,FAC              )                                               WRITIT    3
      INTEGER SPEC                                                      WRITIT    4
      DIMENSION ENGM(3),ENGC(3),ENGK(3),WINIT(5),WFIN(5),WDELT(5)       WRITIT    5
      DIMENSION TITLE(8)                                                WRITIT    6
      I=3                                                               WRITIT    7
      WRITE(6,100)(TITLE(I),I=1,8)                                      WRITIT    8
      WRITE(6,105)FAC                                                   WRITIT    9
      WRITE(6,110)SPEC                                                  WRITIT   10
      WRITE(6,120)                                                      WRITIT   11
      WRITE(6,130)                                                      WRITIT   12
      DO 10 J=1,I                                                       WRITIT   13
   10 WRITE(6,140)J,ENGM(J),ENGC(J),ENGK(J)                             WRITIT   14
      WRITE(6,150)NRANG                                                 WRITIT   15
      WRITE(6,160)                                                      WRITIT   16
      DO 20 I=1,NRANG                                                   WRITIT   17
   20 WRITE(6,170)I,WINIT(I),WFIN(I),WDELT(I)                           WRITIT   18
      RETURN                                                            WRITIT   19
  100 FORMAT(1H1//30X,8A10//)                                           WRITIT   20
  105 FORMAT(40X,27HMULTIPLIER FOR INPUT PSD = ,E10.3 /)                WRITIT   21
  110 FORMAT(40X,60HINPUT VIBRATION POWER SPECTRAL DENSITY SPECIFICATION WRITIT   22
     1 CODE IS,I5,1H./)                                                 WRITIT   23
  120 FORMAT(40X,65HROTOR BEARING SYSTEM PROPERTIES ARE SPECIFIED BY THE WRITIT   24
     1 FOLLOWING   /40X,   15HSETS OF VALUES /)                         WRITIT   25
  130 FORMAT(45X,50H MASS         WEIGHT         DAMPING         SPRING  / WRITIT   26
     1       45X,50HSPRING       OF MASS       (LBS*SEC       STIFFNESS / WRITIT   27
     2       45X,50H  NO          (LBS)         PER INCH)      (LBS/INCH)) WRITIT   28
  140 FORMAT(45X,I5,2(5X,F10.3),5X,E10.3)                               WRITIT   29
  150 FORMAT(//40X,   13HTHE FOLLOWING,I5,30H FREQUENCY RANGES WILL BE R WRITIT   30
     1UN /)                                                             WRITIT   31
  160 FORMAT(45X,50HRANGE        INITIAL          FINAL          FREQUENCY/ WRITIT   32
     1       45X,50H  NO        FREQUENCY       FREQUENCY       INCREMENT) WRITIT   33
  170 FORMAT(45X,I5,2(5X,F10.2),5X,F10.3)                               WRITIT   34
      END                                                               WRITIT   35
```

```
                                                                      FEB173     11
      SUBROUTINE SPEC1(F,SCALE)                                       SPEC1       2
                                                                      SPEC1       3
      SNAP8 SPEC                                                      SPEC1       4
      NASA LEWIS SPEC 417-2,REV C, 1JUNE69                            SPEC1       5
      PARAGRAPH 3.5.1.2.2                                             SPEC1       6
      EGS SYSTEM 5OPERATING)                                          SPEC1       7
                                                                      SPEC1       8
      IF(F .GT. 100. .AND. F .LT. 2000.) GO TO 5090                   SPEC1       9
      IF(F .GT.2000. .OR. F.LT. 19.) GO TO 5110                       SPEC1      10
      FX=F                                                            SPEC1      11
      F2=100.                                                         SPEC1      12
      PSD2=.015                                                       SPEC1      13
      R=3.                                                            SPEC1      14
      SCALE=PSD2*(FX/F2)**(R/3.)                                      SPEC1      15
      RETURN                                                          SPEC1      16
 5090 SCALE=.015                                                      SPEC1      17
      RETURN                                                          SPEC1      18
 5110 SCALE=0.                                                        SPEC1      19
      RETURN                                                          SPEC1      20
      END                                                             SPEC1      21


                                                                      FEB173     12
      SUBROUTINE SPEC2(F,SCALE)                                       SPEC2       2
      SCALE=(2.*3.14159*F)**4/386.**2                                 SPEC2       3
      RETURN                                                          SPEC2       4
      END                                                             SPEC2       5


                                                                      FEB173     13
      SUBROUTINE SPEC3(F,SCALE)                                       SPEC3       2
      SCALE=.01                                                       SPEC3       3
      RETURN                                                          SPEC3       4
      END                                                             SPEC3       5
```

```
                                                                      FEB173     14
      SUBROUTINE MINV(A,N,D,L,M)                                      MINV       2
      INVERT A MATRIX                                                 MINV       3
                                                                      MINV       4
      USAGE                                                           MINV       5
      CALL MINV(A,N,D,L,M)                                            MINV       6
                                                                      MINV       7
      DESCRIPTION OF PARAMETERS                                       MINV       8
      A - INPUT MATRIX, DISTROYED IN COMPUTATION AND REPLACED BY      MINV       9
      RESULTANT INVERSE.                                              MINV      10
      N - ORDER OF MATRIX A                                           MINV      11
      D - RESULTANT DETERMINANT                                       MINV      12
      L - WORK VECTOR OF LENGTH N                                     MINV      13
      M - WORK VECTOR OF LENGTH N                                     MINV      14
                                                                      MINV      15
      REMARKS                                                         MINV      16
      MATRIX A MUST BE A GENERAL MATRIX                               MINV      17
                                                                      MINV      18
      METHOD                                                          MINV      19
      THE STANDARD GAUSS-JORDAN METHOD IS USED. THE DETERMINANT       MINV      20
      IS ALSO CALCULATED. A DETERMINANT OF ZERO INDICATES THAT        MINV      21
      THE MATRIX IS SINGULAR.                                         MINV      22
                                                                      MINV      23
      DIMENSION A(3,1),L(1),M(1)                                      MINV      24
      COMPLEX A,BIGA,HOLD,D                                           MINV      25
      SEARCH FOR LARGEST ELEMENT                                      MINV      26
      D=1.0                                                           MINV      27
      NK=-N                                                           MINV      28
      DO 80 K=1,N                                                     MINV      29
      NK=NK+N                                                         MINV      30
      L(K)=K                                                          MINV      31
      M(K)=K                                                          MINV      32
      KK=NK+K                                                         MINV      33
      BIGA=A(KK)                                                      MINV      34
      DO 20 J=K,N                                                     MINV      35
      IZ=N*(J-1)                                                      MINV      36
      DO 20 I=K,N                                                     MINV      37
      IJ=IZ+I                                                         MINV      38
   10 IF(CABS(BIGA)-CABS(A(IJ))) 15,20,20                             MINV      39
   15 BIGA=A(IJ)                                                      MINV      40
      L(K)=I                                                          MINV      41
      M(K)=J                                                          MINV      42
   20 CONTINUE                                                        MINV      43
      INTERCHANGE ROWS                                                MINV      44
      J=L(K)                                                          MINV      45
      IF(J-K) 35,35,25                                                MINV      46
   25 KI=K-N                                                          MINV      47
      DO 30 I=1,N                                                     MINV      48
      KI=KI+N                                                         MINV      49
      HOLD=-A(KI)                                                     MINV      50
      JI=KI-K+J                                                       MINV      51
      A(KI)=A(JI)                                                     MINV      52
   30 A(JI) =HOLD                                                     MINV      53
      INTERCHANGE COLUMNS                                             MINV      54
   35 I=M(K)                                                          MINV      55
      IF(I-K) 45,45,38                                                MINV      56
   38 JP=N*(I-1)                                                      MINV      57
      DO 40 J=1,N                                                     MINV      58
      JK=NK+J                                                         MINV      59
      JI=JP+J                                                         MINV      60
      HOLD=-A(JK)                                                     MINV      61
      A(JK)=A(JI)                                                     MINV      62
```

```
 40 A(JI) =HOLD                                                          MINV   63
    DIVIDE COLUMN BY MINUS PIVOT (VALUE OF PIVOT ELEMENT IS              MINV   64
    CONTAINED IN BIGA)                                                   MINV   65
 45 IF(CABS(BIGA)) 48,46,48                                              MINV   66
 46 D=0.0                                                                MINV   67
    RETURN                                                               MINV   68
 48 DO 55 I=1,N                                                          MINV   69
    IF(I-K) 50,55,50                                                     MINV   70
 50 IK=NK+I                                                              MINV   71
    A(IK)=A(IK)/(-BIGA)                                                  MINV   72
 55 CONTINUE                                                             MINV   73
    REDUCE MATRIX                                                        MINV   74
    DO 65 I=1,N                                                          MINV   75
    IK=NK+I                                                              MINV   76
    HOLD=A(IK)                                                           MINV   77
    IJ=I-N                                                               MINV   78
    DO 65 J=1,N                                                          MINV   79
    IJ=IJ+N                                                              MINV   80
    IF(I-K) 60,65,60                                                     MINV   81
 60 IF(J-K) 62,65,62                                                     MINV   82
 62 KJ=IJ-I+K                                                            MINV   83
    A(IJ)=HOLD*A(KJ)+A(IJ)                                               MINV   84
 65 CONTINUE                                                             MINV   85
    DIVIDE ROW BY PIVOT                                                  MINV   86
    KJ=K-N                                                               MINV   87
    DO 75 J=1,N                                                          MINV   88
    KJ=KJ+N                                                              MINV   89
    IF(J-K) 70,75,70                                                     MINV   90
 70 A(KJ)=A(KJ)/BIGA                                                     MINV   91
 75 CONTINUE                                                             MINV   92
    PRODUCT OF PIVOJS                                                    MINV   93
    D=D*BIGA                                                             MINV   94
    REPLACE PIVOT BY RECIPROCAL                                          MINV   95
    A(KK)=1.0/BIGA                                                       MINV   96
 80 CONTINUE                                                             MINV   97
    FINAL ROW AND COLUMN INTERCHANGE                                     MINV   98
    K=N                                                                  MINV   99
100 K=(K-1)                                                              MINV  100
    IF(K) 150,150,105                                                    MINV  101
105 I=L(K)                                                               MINV  102
    IF(I-K) 120,120,108                                                  MINV  103
108 JQ=N*(K-1)                                                           MINV  104
    JR=N*(I-1)                                                           MINV  105
    DO 110 J=1,N                                                         MINV  106
    JK=JQ+J                                                              MINV  107
    HOLD=A(JK)                                                           MINV  108
    JI=JR+J                                                              MINV  109
    A(JK)=-A(JI)                                                         MINV  110
110 A(JI) =HOLD                                                          MINV  111
120 J=M(K)                                                               MINV  112
    IF(J-K) 100,100,125                                                  MINV  113
125 KI=K-N                                                               MINV  114
    DO 130 I=1,N                                                         MINV  115
    KI=KI+N                                                              MINV  116
    HOLD=A(KI)                                                           MINV  117
    JI=KI-K+J                                                            MINV  118
    A(KI)=-A(JI)                                                         MINV  119
130 A(JI) =HOLD                                                          MINV  120
    GO TO 100                                                            MINV  121
150 RETURN                                                               MINV  122
    END                                                                  MINV  123
```

```
                                                                        FEB173    15
      SUBROUTINE MATRX2(M,C,K,ENGM,ENGC,ENGK)                           MATRX2     2
      DIMENSION M(3,3),C(3,3),K(3,3),D(3),W(3),ZETA(3),MU(3)            MATRX2     3
      DIMENSION ENGM(3),ENGC(3),ENGK(3)                                 MATRX2     4
      REAL M,K,MU                                                       MATRX2     5
      DATA N/3/                                                         MATRX2     6
      DO 1090 I=1,N                                                     MATRX2     7
      W(I)=SQRT(ENGK(I)/(ENGM(I)/386.))                                 MATRX2     8
      ZETA(I)=.5*(ENGC(I)/(SQRT(ENGK(I)*ENGM(I)/386.)))                 MATRX2     9
 1090 CONTINUE                                                          MATRX2    10
      DO 1135 I=1,N                                                     MATRX2    11
      DO 1135 J=1,N                                                     MATRX2    12
      M(I,J)=0.                                                         MATRX2    13
      IF(I.EQ.J) M(I,J)=1.                                              MATRX2    14
 1135 CONTINUE                                                          MATRX2    15
      MU(1)=1.                                                          MATRX2    16
      MU(2)=ENGM(2)/ENGM(1)                                             MATRX2    17
      MU(3)=ENGM(3)/ENGM(2)                                             MATRX2    18
      C(1,1)=ZETA(1)*W(1)                                               MATRX2    19
      C(1,2)=-ZETA(2)*W(2)*MU(2)                                        MATRX2    20
      C(1,3)=0.                                                         MATRX2    21
      C(2,1)=-ZETA(1)*W(1)                                              MATRX2    22
      C(2,2)=(1.+MU(2))*ZETA(2)*W(2)                                    MATRX2    23
      C(2,3)=-ZETA(3)*W(3)*MU(3)                                        MATRX2    24
      C(3,1)=0.0                                                        MATRX2    25
      C(3,2)=-ZETA(2)*W(2)                                              MATRX2    26
      C(3,3)=(1.+MU(3))*ZETA(3)*W(3)                                    MATRX2    27
      K(1,1)=W(1)**2                                                    MATRX2    28
      K(1,2)=-W(2)**2*MU(2)                                             MATRX2    29
      K(1,3)=0.                                                         MATRX2    30
      K(2,1)=-W(1)**2                                                   MATRX2    31
      K(2,2)=W(2)**2*(1.+MU(2))                                         MATRX2    32
      K(2,3)=-W(3)**2*MU(3)                                             MATRX2    33
      K(3,1)=0.0                                                        MATRX2    34
      K(3,2)=-W(2)**2                                                   MATRX2    35
      K(3,3)=W(3)**2*(1.+MU(3))                                         MATRX2    36
      RETURN                                                            MATRX2    37
      END                                                               MATRX2    38
```

```
                                                                      FEB173    16
      SUBROUTINE CALC(M,C,K,W,PSD)                                    CALC      2
      DIMENSION M(3,3),C(3,3),K(3,3),PSD(3),Z(3,3),H(3,3),DUMY1(3),   CALC      3
     1          DUMY2(3)                                             CALC      4
      COMPLEX EYE,Z,DUMY1,DUMY2,H,DETZ                                CALC      5
      REAL M,K                                                        CALC      6
      DATA N/3/                                                       CALC      7
      EYE=CMPLX(0.,1.)                                                CALC      8
      DO 60 J=1,N                                                     CALC      9
      DO 60 I=1,N                                                     CALC     10
   60 Z(I,J)=(-W*W*M(I,J)+K(I,J))+EYE*W*C(I,J)                        CALC     11
      CALL MINV(Z,N,DETZ,DUMY1,DUMY2)                                 CALC     12
      DO 110 I=1,N                                                    CALC     13
      DO 110 J=1,N                                                    CALC     14
      H(I,J)=Z(I,J)                                                   CALC     15
      PSD(I)=(CABS(H(I,1)))**2                                        CALC     16
  110 CONTINUE                                                        CALC     17
      RETURN                                                          CALC     18
      END                                                             CALC     19


                                                                      FEB173    17
      SUBROUTINE TLU(A,B,C,D,N)                                       AU3072    34
      DIMENSION C(1),D(1)                                             AU3072    35
      IF(N-1)1,2,3                                                    AU3072    36
    1 B=0.                                                            AU3072    37
      GO TO 100                                                       AU3072    38
    2 B=D(1)                                                          AU3072    39
      GO TO 100                                                       AU3072    40
    3 ML=1                                                            AU3072    41
      MU=N                                                            AU3072    42
    8 IF(MU-ML-1) 15,15,9                                             AU3072    43
    9 M=(MU+ML)/2                                                     AU3072    44
      IF(C(1)-C(2))11,2,10                                            AU3072    45
   10 IF(C(M)-A)13,12,14                                              AU3072    46
   11 IF(A-C(M))13,12,14                                              AU3072    47
   12 B=D(M)                                                          AU3072    48
      GO TO 100                                                       AU3072    49
   13 MU=M                                                            AU3072    50
      GO TO 8                                                         AU3072    51
   14 ML=M                                                            AU3072    52
      GO TO 8                                                         AU3072    53
   15 B=D(ML)+(D(MU)-D(ML))*((A-C(ML))/(C(MU)-C(ML)))                 AU3072    54
  100 RETURN                                                          AU3072    55
      END                                                             AU3072    56
```

SAMPLE TEST CASE INPUT

```
  1
AXIAL RANDOM VIBRATION RESPONSE - NOMINAL CASE  10-10-72
 0.01
 96.       0.02      300000.
  7.       0.02      250000.
 21.       84.       113500.
   3    1     5
 20.      200.        2.
200.      400.        5.
400.     2000.       20.
.0004     .0005      .0006      .0007      .0008
```

SAMPLE TEST CASE OUTPUT

AXIAL RANDOM VIBRATION RESPONSE - NOMINAL CASE 10-10-72

MULTIPLIER FOR INPUT PSD = 1.000E-02

INPUT VIBRATION POWER SPECTRAL DENSITY SPECIFICATION CODE IS 1.

ROTOR BEARING SYSTEM PROPERTIES ARE SPECIFIED BY THE FOLLOWING SETS OF VALUES

MASS SPRING NO	WEIGHT OF MASS (LBS)	DAMPING (LBS*SEC PER INCH)	SPRING STIFFNESS (LBS/INCH)
1	96.000	.020	3.000E+05
2	7.000	.020	2.500E+05
3	21.000	84.000	1.135E+05

THE FOLLOWING 3 FREQUENCY RANGES WILL BE RUN

RANGE NO	INITIAL FREQUENCY	FINAL FREQUENCY	FREQUENCY INCREMENT
1	20.00	200.00	2.000
2	200.00	400.00	5.000
3	400.00	2000.00	20.000

MATRIX M

1.000E+00	0.	0.
0.	1.000E+00	0.
0.	0.	1.000E+00

MATRIX C

4.021E-02	-4.021E-02	0.
-4.021E-02	5.916E-01	-2.316E+03
0.	-5.514E-01	3.088E+03

MATRIX K

1.206E+06	-1.005E+06	0.
-1.206E+06	1.479E+07	-6.259E+06
0.	-1.379E+07	8.345E+06

FREQUENCY RANGE NUMBER 1
COVERS THE RANGE FROM 20.00 TO 200.00
IN INCREMENTS OF 2.00

FREQUENCY (HZ)	PSD OF Y1 (IN*IN/HZ)	PSD OF Y2 (IN*IN/HZ)	PSD OF Y3 (IN*IN/HZ)	PSD INPUT (IN*IN/HZ)	PSD INPUT (G*G/HZ)
20.000	5.328E-12	3.975E-13	1.087E-12	1.792E-08	3.000E-05
22.000	5.910E-12	4.424E-13	1.210E-12	1.347E-08	3.300E-05
24.000	6.506E-12	4.888E-13	1.337E-12	1.037E-08	3.600E-05
26.000	7.119E-12	5.370E-13	1.470E-12	8.159E-09	3.900E-05
28.000	7.750E-12	5.871E-13	1.607E-12	6.532E-09	4.200E-05
30.000	8.401E-12	6.394E-13	1.751E-12	5.311E-09	4.500E-05
32.000	9.074E-12	6.942E-13	1.902E-12	4.376E-09	4.800E-05
34.000	9.772E-12	7.516E-13	2.061E-12	3.648E-09	5.100E-05
36.000	1.050E-11	8.119E-13	2.227E-12	3.074E-09	5.400E-05
38.000	1.125E-11	8.755E-13	2.403E-12	2.613E-09	5.700E-05
40.000	1.204E-11	9.427E-13	2.589E-12	2.241E-09	6.000E-05
42.000	1.286E-11	1.014E-12	2.787E-12	1.936E-09	6.300E-05
44.000	1.372E-11	1.090E-12	2.997E-12	1.683E-09	6.600E-05
46.000	1.463E-11	1.170E-12	3.220E-12	1.473E-09	6.900E-05
48.000	1.558E-11	1.256E-12	3.459E-12	1.297E-09	7.200E-05
50.000	1.658E-11	1.348E-12	3.715E-12	1.147E-09	7.500E-05
52.000	1.764E-11	1.446E-12	3.990E-12	1.020E-09	7.800E-05
54.000	1.876E-11	1.552E-12	4.285E-12	9.107E-10	8.100E-05
56.000	1.995E-11	1.666E-12	4.603E-12	8.166E-10	8.400E-05
58.000	2.122E-11	1.789E-12	4.947E-12	7.350E-10	8.700E-05
60.000	2.257E-11	1.921E-12	5.320E-12	6.639E-10	9.000E-05
62.000	2.401E-11	2.066E-12	5.725E-12	6.017E-10	9.300E-05
64.000	2.556E-11	2.223E-12	6.166E-12	5.470E-10	9.600E-05
66.000	2.722E-11	2.394E-12	6.647E-12	4.988E-10	9.900E-05
68.000	2.900E-11	2.581E-12	7.174E-12	4.561E-10	1.020E-04
70.000	3.093E-11	2.786E-12	7.752E-12	4.181E-10	1.050E-04
72.000	3.302E-11	3.011E-12	8.388E-12	3.842E-10	1.080E-04
74.000	3.529E-11	3.259E-12	9.090E-12	3.539E-10	1.110E-04
76.000	3.776E-11	3.534E-12	9.868E-12	3.267E-10	1.140E-04
78.000	4.045E-11	3.839E-12	1.073E-11	3.022E-10	1.170E-04
80.000	4.341E-11	4.178E-12	1.170E-11	2.801E-10	1.200E-04
82.000	4.666E-11	4.557E-12	1.277E-11	2.601E-10	1.230E-04
84.000	5.025E-11	4.983E-12	1.398E-11	2.419E-10	1.260E-04
86.000	5.423E-11	5.461E-12	1.535E-11	2.255E-10	1.290E-04
88.000	5.865E-11	6.003E-12	1.689E-11	2.104E-10	1.320E-04
90.000	6.360E-11	6.618E-12	1.865E-11	1.967E-10	1.350E-04
92.000	6.916E-11	7.320E-12	2.065E-11	1.842E-10	1.380E-04
94.000	7.544E-11	8.126E-12	2.296E-11	1.726E-10	1.410E-04
96.000	8.257E-11	9.056E-12	2.562E-11	1.621E-10	1.440E-04
98.000	9.072E-11	1.014E-11	2.872E-11	1.524E-10	1.470E-04
100.000	1.001E-10	1.140E-11	3.235E-11	1.434E-10	1.500E-04
102.000	1.088E-10	1.263E-11	3.591E-11	1.325E-10	1.500E-04
104.000	1.189E-10	1.409E-11	4.010E-11	1.226E-10	1.500E-04
106.000	1.307E-10	1.582E-11	4.510E-11	1.136E-10	1.500E-04
108.000	1.447E-10	1.790E-11	5.110E-11	1.054E-10	1.500E-04
110.000	1.615E-10	2.042E-11	5.840E-11	9.794E-11	1.500E-04
112.000	1.819E-10	2.352E-11	6.737E-11	9.113E-11	1.500E-04
114.000	2.069E-10	2.738E-11	7.857E-11	8.490E-11	1.500E-04
116.000	2.382E-10	3.228E-11	9.278E-11	7.920E-11	1.500E-04
118.000	2.780E-10	3.860E-11	1.111E-10	7.396E-11	1.500E-04
120.000	3.297E-10	4.695E-11	1.354E-10	6.915E-11	1.500E-04
122.000	3.986E-10	5.826E-11	1.683E-10	6.473E-11	1.500E-04
124.000	4.935E-10	7.407E-11	2.144E-10	6.065E-11	1.500E-04
126.000	6.289E-10	9.701E-11	2.813E-10	5.689E-11	1.500E-04
128.000	8.313E-10	1.319E-10	3.830E-10	5.342E-11	1.500E-04
130.000	1.151E-09	1.879E-10	5.469E-10	5.021E-11	1.500E-04
132.000	1.692E-09	2.845E-10	8.293E-10	4.723E-11	1.500E-04
134.000	2.674E-09	4.634E-10	1.353E-09	4.448E-11	1.500E-04
136.000	4.513E-09	8.068E-10	2.361E-09	4.192E-11	1.500E-04
138.000	7.241E-09	1.336E-09	3.918E-09	3.954E-11	1.500E-04
140.000	7.807E-09	1.489E-09	4.373E-09	3.733E-11	1.500E-04
142.000	5.096E-09	1.005E-09	2.957E-09	3.527E-11	1.500E-04
144.000	2.877E-09	5.873E-10	1.732E-09	3.335E-11	1.500E-04
146.000	1.703E-09	3.601E-10	1.064E-09	3.156E-11	1.500E-04
148.000	1.086E-09	2.382E-10	7.050E-10	2.989E-11	1.500E-04
150.000	7.391E-10	1.681E-10	4.986E-10	2.833E-11	1.500E-04
152.000	5.289E-10	1.249E-10	3.713E-10	2.686E-11	1.500E-04
154.000	3.937E-10	9.669E-11	2.879E-10	2.550E-11	1.500E-04
156.000	3.024E-10	7.727E-11	2.306E-10	2.421E-11	1.500E-04
158.000	2.383E-10	6.339E-11	1.896E-10	2.301E-11	1.500E-04
160.000	1.916E-10	5.314E-11	1.592E-10	2.188E-11	1.500E-04
162.000	1.568E-10	4.537E-11	1.362E-10	2.082E-11	1.500E-04
164.000	1.302E-10	3.933E-11	1.183E-10	1.982E-11	1.500E-04
166.000	1.095E-10	3.456E-11	1.042E-10	1.888E-11	1.500E-04
168.000	9.311E-11	3.073E-11	9.282E-11	1.800E-11	1.500E-04
170.000	7.994E-11	2.760E-11	8.355E-11	1.717E-11	1.500E-04
172.000	6.922E-11	2.502E-11	7.591E-11	1.638E-11	1.500E-04
174.000	6.041E-11	2.288E-11	6.954E-11	1.564E-11	1.500E-04
176.000	5.309E-11	2.107E-11	6.419E-11	1.495E-11	1.500E-04
178.000	4.698E-11	1.954E-11	5.966E-11	1.428E-11	1.500E-04
180.000	4.182E-11	1.824E-11	5.580E-11	1.366E-11	1.500E-04
182.000	3.746E-11	1.713E-11	5.250E-11	1.307E-11	1.500E-04
184.000	3.374E-11	1.617E-11	4.966E-11	1.251E-11	1.500E-04
186.000	3.056E-11	1.534E-11	4.721E-11	1.198E-11	1.500E-04
188.000	2.784E-11	1.462E-11	4.510E-11	1.148E-11	1.500E-04
190.000	2.551E-11	1.400E-11	4.327E-11	1.100E-11	1.500E-04
192.000	2.350E-11	1.345E-11	4.168E-11	1.055E-11	1.500E-04
194.000	2.178E-11	1.298E-11	4.030E-11	1.012E-11	1.500E-04
196.000	2.031E-11	1.257E-11	3.911E-11	9.717E-12	1.500E-04
198.000	1.906E-11	1.221E-11	3.808E-11	9.330E-12	1.500E-04
200.000	1.801E-11	1.190E-11	3.719E-11	8.962E-12	1.500E-04
INTEGRATED VALUE	8.972E-08	1.699E-08	4.993E-08	1.772E-07	2.220E-02
TOTAL INT. VALUE	8.972E-08	1.699E-08	4.993E-08	1.772E-07	2.220E-02
RMS VALUE	2.995E-04	1.304E-04	2.235E-04	4.209E-04	1.490E-01

****

FREQUENCY RANGE NUMBER 2
COVERS THE RANGE FROM 200.00 TO 400.00
IN INCREMENTS OF 5.00

FREQUENCY (HZ)	PSD OF Y1 (IN*IN/HZ)	PSD OF Y2 (IN*IN/HZ)	PSD OF Y3 (IN*IN/HZ)	PSD INPUT (IN*IN/HZ)	PSD INPUT (G*G/HZ)
200.000	1.801E-11	1.190E-11	3.719E-11	8.962E-12	1.500E-04
205.000	1.611E-11	1.128E-11	3.543E-11	8.120E-12	1.500E-04
210.000	1.507E-11	1.082E-11	3.416E-11	7.373E-12	1.500E-04
215.000	1.473E-11	1.043E-11	3.309E-11	6.711E-12	1.500E-04
220.000	1.493E-11	1.002E-11	3.194E-11	6.121E-12	1.500E-04
225.000	1.547E-11	9.493E-12	3.041E-11	5.595E-12	1.500E-04
230.000	1.608E-11	8.768E-12	2.821E-11	5.124E-12	1.500E-04
235.000	1.646E-11	7.816E-12	2.527E-11	4.702E-12	1.500E-04
240.000	1.639E-11	6.689E-12	2.172E-11	4.322E-12	1.500E-04
245.000	1.579E-11	5.501E-12	1.793E-11	3.980E-12	1.500E-04
250.000	1.473E-11	4.375E-12	1.432E-11	3.671E-12	1.500E-04
255.000	1.340E-11	3.398E-12	1.116E-11	3.391E-12	1.500E-04
260.000	1.199E-11	2.604E-12	8.582E-12	3.138E-12	1.500E-04
265.000	1.062E-11	1.985E-12	6.562E-12	2.908E-12	1.500E-04
270.000	9.357E-12	1.514E-12	5.020E-12	2.698E-12	1.500E-04
275.000	8.240E-12	1.161E-12	3.857E-12	2.507E-12	1.500E-04
280.000	7.265E-12	8.960E-13	2.983E-12	2.333E-12	1.500E-04
285.000	6.423E-12	6.975E-13	2.327E-12	2.174E-12	1.500E-04
290.000	5.698E-12	5.480E-13	1.830E-12	2.027E-12	1.500E-04
295.000	5.075E-12	4.345E-13	1.452E-12	1.893E-12	1.500E-04
300.000	4.537E-12	3.477E-13	1.163E-12	1.770E-12	1.500E-04
305.000	4.072E-12	2.807E-13	9.384E-13	1.657E-12	1.500E-04
310.000	3.668E-12	2.286E-13	7.635E-13	1.553E-12	1.500E-04
315.000	3.317E-12	1.876E-13	6.260E-13	1.456E-12	1.500E-04
320.000	3.009E-12	1.552E-13	5.169E-13	1.368E-12	1.500E-04
325.000	2.738E-12	1.293E-13	4.297E-13	1.285E-12	1.500E-04
330.000	2.499E-12	1.085E-13	3.595E-13	1.209E-12	1.500E-04
335.000	2.288E-12	9.164E-14	3.025E-13	1.139E-12	1.500E-04
340.000	2.099E-12	7.789E-14	2.560E-13	1.073E-12	1.500E-04
345.000	1.931E-12	6.659E-14	2.178E-13	1.012E-12	1.500E-04
350.000	1.781E-12	5.726E-14	1.863E-13	9.556E-13	1.500E-04
355.000	1.646E-12	4.951E-14	1.600E-13	9.029E-13	1.500E-04
360.000	1.524E-12	4.302E-14	1.381E-13	8.538E-13	1.500E-04
365.000	1.414E-12	3.757E-14	1.197E-13	8.079E-13	1.500E-04
370.000	1.314E-12	3.297E-14	1.041E-13	7.651E-13	1.500E-04
375.000	1.224E-12	2.906E-14	9.093E-14	7.251E-13	1.500E-04
380.000	1.141E-12	2.573E-14	7.970E-14	6.877E-13	1.500E-04
385.000	1.066E-12	2.288E-14	7.010E-14	6.527E-13	1.500E-04
390.000	9.972E-13	2.042E-14	6.186E-14	6.199E-13	1.500E-04
395.000	9.341E-13	1.830E-14	5.476E-14	5.891E-13	1.500E-04
400.000	8.762E-13	1.646E-14	4.862E-14	5.602E-13	1.500E-04
INTEGRATED VALUE	1.432E-09	5.320E-10	1.708E-09	5.232E-10	3.000E-02
TOTAL INT. VALUE	9.115E-08	1.752E-08	5.164E-08	1.777E-07	5.220E-02
RMS VALUE	3.019E-04	1.324E-04	2.272E-04	4.215E-04	2.285E-01

FREQUENCY RANGE NUMBER 3
COVERS THE RANGE FROM 400.00 TO 2000.00
IN INCREMENTS OF 20.00

FREQUENCY (HZ)	PSD OF Y1 (IN*IN/HZ)	PSD OF Y2 (IN*IN/HZ)	PSD OF Y3 (IN*IN/HZ)	PSD INPUT (IN*IN/HZ)	PSD INPUT (G*G/HZ)
400.000	8.762E-13	1.646E-14	4.862E-14	5.602E-13	1.500E-04
420.000	6.866E-13	1.116E-14	3.104E-14	4.608E-13	1.500E-04
440.000	5.474E-13	7.954E-15	2.060E-14	3.826E-13	1.500E-04
460.000	4.428E-13	5.920E-15	1.412E-14	3.203E-13	1.500E-04
480.000	3.627E-13	4.573E-15	9.956E-15	2.701E-13	1.500E-04
500.000	3.004E-13	3.646E-15	7.185E-15	2.294E-13	1.500E-04
520.000	2.513E-13	2.984E-15	5.289E-15	1.961E-13	1.500E-04
540.000	2.120E-13	2.493E-15	3.955E-15	1.686E-13	1.500E-04
560.000	1.803E-13	2.117E-15	2.995E-15	1.458E-13	1.500E-04
580.000	1.544E-13	1.817E-15	2.287E-15	1.267E-13	1.500E-04
600.000	1.331E-13	1.570E-15	1.755E-15	1.106E-13	1.500E-04
620.000	1.154E-13	1.358E-15	1.349E-15	9.705E-14	1.500E-04
640.000	1.005E-13	1.172E-15	1.034E-15	8.547E-14	1.500E-04
660.000	8.806E-14	1.006E-15	7.887E-16	7.557E-14	1.500E-04
680.000	7.747E-14	8.554E-16	5.971E-16	6.707E-14	1.500E-04
700.000	6.844E-14	7.201E-16	4.480E-16	5.972E-14	1.500E-04
720.000	6.069E-14	5.997E-16	3.332E-16	5.336E-14	1.500E-04
740.000	5.402E-14	4.943E-16	2.457E-16	4.782E-14	1.500E-04
760.000	4.824E-14	4.038E-16	1.800E-16	4.298E-14	1.500E-04
780.000	4.322E-14	3.276E-16	1.311E-16	3.874E-14	1.500E-04
800.000	3.884E-14	2.644E-16	9.529E-17	3.501E-14	1.500E-04
820.000	3.500E-14	2.127E-16	6.918E-17	3.172E-14	1.500E-04
840.000	3.163E-14	1.709E-16	5.026E-17	2.880E-14	1.500E-04
860.000	2.865E-14	1.374E-16	3.661E-17	2.622E-14	1.500E-04
880.000	2.602E-14	1.106E-16	2.676E-17	2.391E-14	1.500E-04
900.000	2.369E-14	8.927E-17	1.965E-17	2.186E-14	1.500E-04
920.000	2.162E-14	7.227E-17	1.450E-17	2.002E-14	1.500E-04
940.000	1.977E-14	5.872E-17	1.076E-17	1.837E-14	1.500E-04
960.000	1.811E-14	4.790E-17	8.035E-18	1.688E-14	1.500E-04
980.000	1.663E-14	3.924E-17	6.034E-18	1.555E-14	1.500E-04
1000.000	1.529E-14	3.229E-17	4.559E-18	1.434E-14	1.500E-04
1020.000	1.409E-14	2.668E-17	3.466E-18	1.325E-14	1.500E-04
1040.000	1.301E-14	2.214E-17	2.650E-18	1.226E-14	1.500E-04
1060.000	1.202E-14	1.845E-17	2.038E-18	1.136E-14	1.500E-04
1080.000	1.113E-14	1.543E-17	1.576E-18	1.054E-14	1.500E-04
1100.000	1.032E-14	1.297E-17	1.226E-18	9.794E-15	1.500E-04
1120.000	9.587E-15	1.094E-17	9.587E-19	9.113E-15	1.500E-04
1140.000	8.916E-15	9.257E-18	7.535E-19	8.490E-15	1.500E-04
1160.000	8.302E-15	7.865E-18	5.951E-19	7.920E-15	1.500E-04
1180.000	7.740E-15	6.706E-18	4.723E-19	7.396E-15	1.500E-04
1200.000	7.226E-15	5.736E-18	3.766E-19	6.915E-15	1.500E-04
1220.000	6.754E-15	4.923E-18	3.016E-19	6.473E-15	1.500E-04
1240.000	6.319E-15	4.238E-18	2.426E-19	6.065E-15	1.500E-04
1260.000	5.920E-15	3.660E-18	1.960E-19	5.689E-15	1.500E-04
1280.000	5.551E-15	3.169E-18	1.589E-19	5.342E-15	1.500E-04
1300.000	5.211E-15	2.752E-18	1.294E-19	5.021E-15	1.500E-04
1320.000	4.897E-15	2.396E-18	1.057E-19	4.723E-15	1.500E-04
1340.000	4.606E-15	2.092E-18	8.667E-20	4.448E-15	1.500E-04
1360.000	4.336E-15	1.831E-18	7.131E-20	4.192E-15	1.500E-04
1380.000	4.086E-15	1.606E-18	5.888E-20	3.954E-15	1.500E-04
1400.000	3.854E-15	1.412E-18	4.876E-20	3.733E-15	1.500E-04
1420.000	3.638E-15	1.244E-18	4.052E-20	3.527E-15	1.500E-04
1440.000	3.437E-15	1.099E-18	3.376E-20	3.335E-15	1.500E-04
1460.000	3.250E-15	9.724E-19	2.822E-20	3.156E-15	1.500E-04
1480.000	3.075E-15	8.623E-19	2.365E-20	2.989E-15	1.500E-04
1500.000	2.912E-15	7.660E-19	1.988E-20	2.833E-15	1.500E-04
1520.000	2.760E-15	6.818E-19	1.675E-20	2.686E-15	1.500E-04
1540.000	2.617E-15	6.080E-19	1.415E-20	2.550E-15	1.500E-04
1560.000	2.484E-15	5.431E-19	1.198E-20	2.421E-15	1.500E-04
1580.000	2.359E-15	4.859E-19	1.017E-20	2.301E-15	1.500E-04
1600.000	2.242E-15	4.355E-19	8.657E-21	2.188E-15	1.500E-04
1620.000	2.132E-15	3.909E-19	7.383E-21	2.082E-15	1.500E-04
1640.000	2.029E-15	3.515E-19	6.311E-21	1.982E-15	1.500E-04
1660.000	1.932E-15	3.165E-19	5.406E-21	1.888E-15	1.500E-04
1680.000	1.840E-15	2.854E-19	4.640E-21	1.800E-15	1.500E-04
1700.000	1.754E-15	2.577E-19	3.991E-21	1.717E-15	1.500E-04
1720.000	1.673E-15	2.330E-19	3.439E-21	1.638E-15	1.500E-04
1740.000	1.597E-15	2.110E-19	2.970E-21	1.564E-15	1.500E-04
1760.000	1.525E-15	1.913E-19	2.569E-21	1.495E-15	1.500E-04
1780.000	1.457E-15	1.736E-19	2.226E-21	1.428E-15	1.500E-04
1800.000	1.392E-15	1.578E-19	1.933E-21	1.366E-15	1.500E-04
1820.000	1.332E-15	1.436E-19	1.681E-21	1.307E-15	1.500E-04
1840.000	1.274E-15	1.308E-19	1.464E-21	1.251E-15	1.500E-04
1860.000	1.220E-15	1.193E-19	1.278E-21	1.198E-15	1.500E-04
1880.000	1.168E-15	1.089E-19	1.117E-21	1.148E-15	1.500E-04
1900.000	1.119E-15	9.959E-20	9.775E-22	1.100E-15	1.500E-04
1920.000	1.073E-15	9.113E-20	8.570E-22	1.055E-15	1.500E-04
1940.000	1.029E-15	8.347E-20	7.524E-22	1.012E-15	1.500E-04
1960.000	9.874E-16	7.653E-20	6.616E-22	9.717E-16	1.500E-04
1980.000	9.478E-16	7.024E-20	5.825E-22	9.330E-16	1.500E-04
2000.000	9.102E-16	6.453E-20	5.136E-22	8.962E-16	1.500E-04
INTEGRATED VALUE	9.702E-11	1.216E-12	2.579E-12	7.428E-11	2.400E-01
TOTAL INT. VALUE	9.125E-08	1.753E-08	5.164E-08	1.778E-07	2.922E-01
RMS VALUE	3.021E-04	1.324E-04	2.272E-04	4.216E-04	5.406E-01

MEAN FILM THICKNESS (INCH)	PROB. OF SOLID CONTACT
.000400	3.936E-02
.000500	1.389E-02
.000600	4.180E-03
.000700	1.059E-03
.000800	2.257E-04

FIGURES

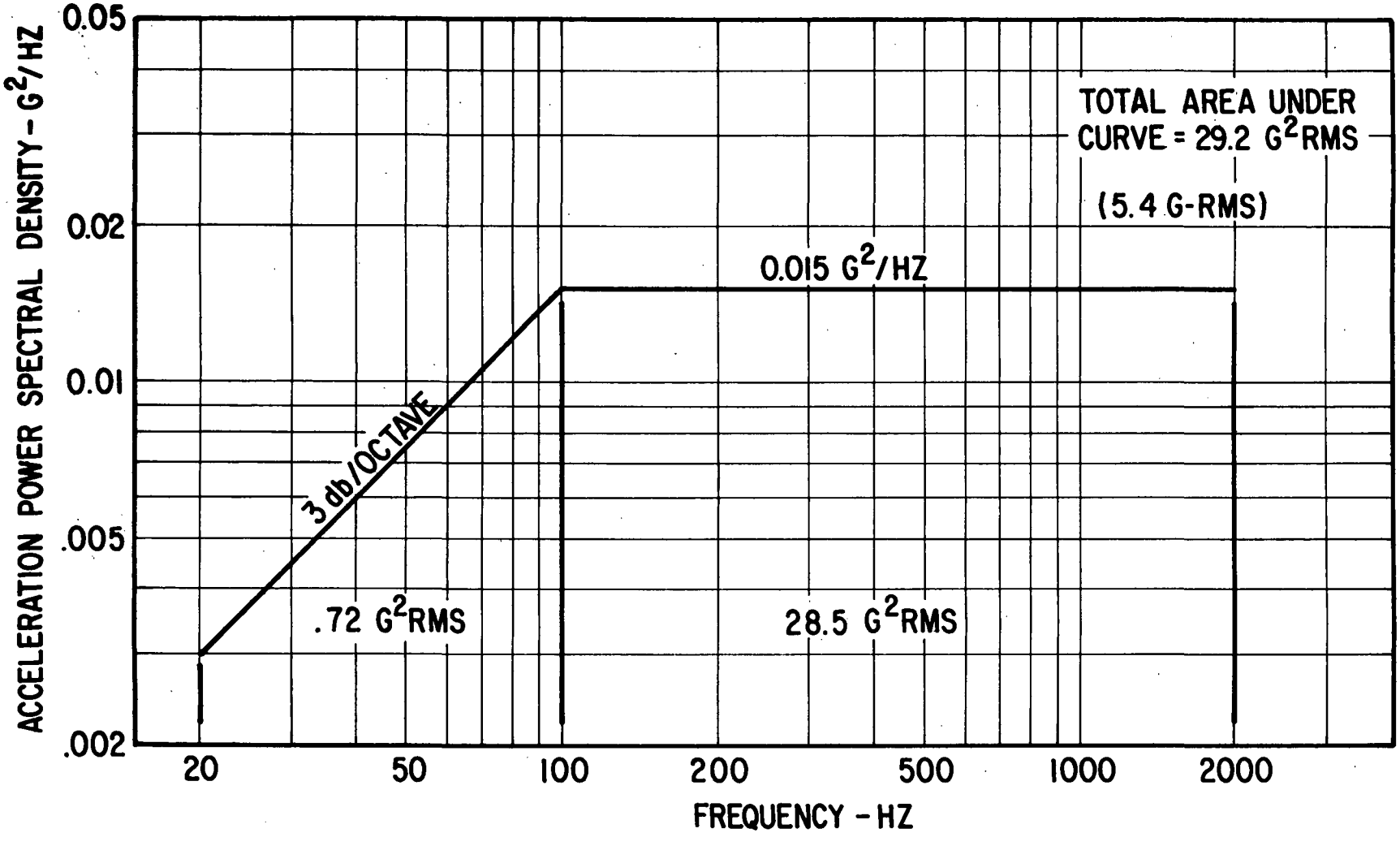

Fig. 1 Random Vibration Acceleration Power Spectral Density Test Specification 417-2 (Rev. C) For Electrical Generating System Components (Operating) During Space Flight Operation

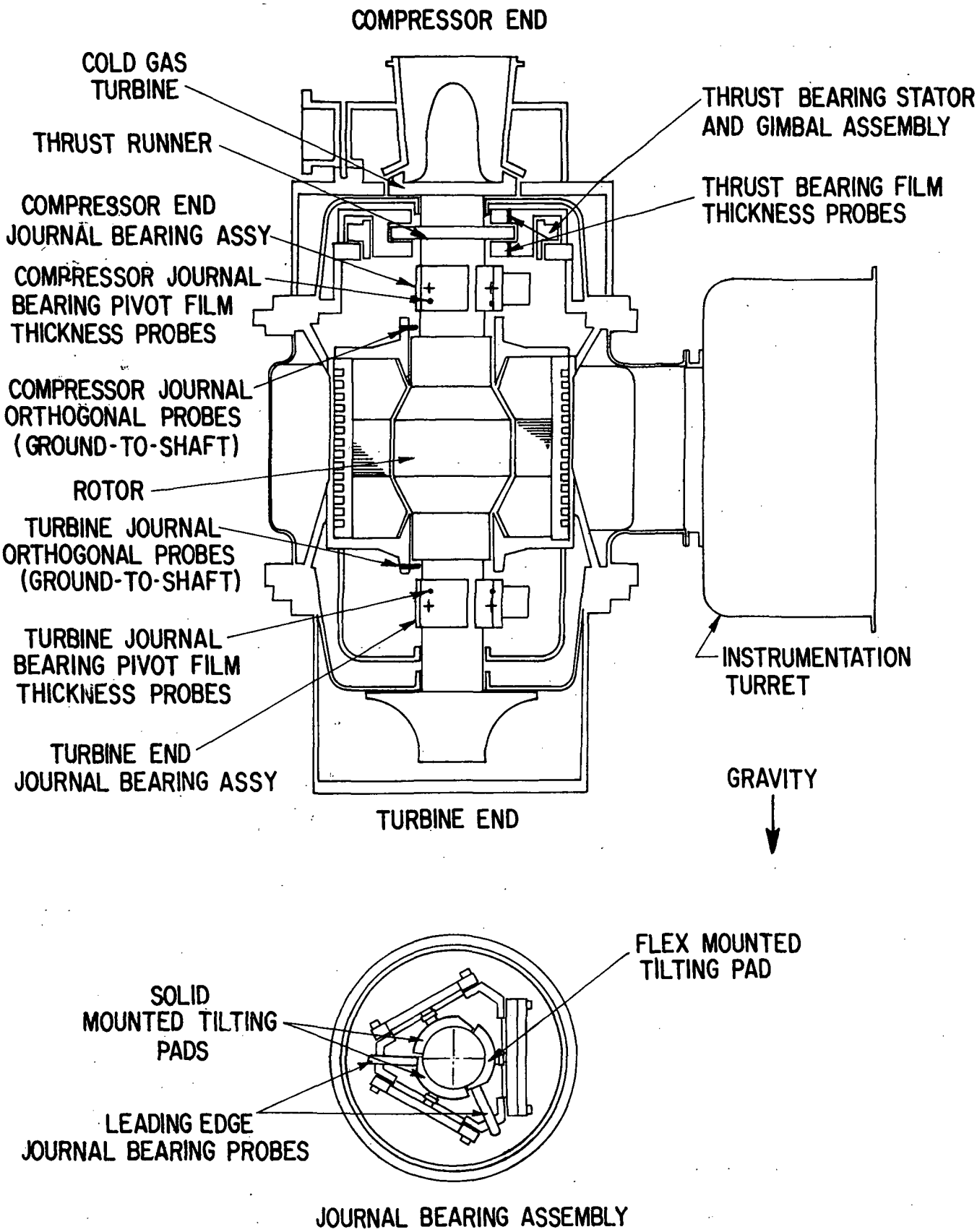

Fig. 2 Schematic of BRU Simulator

MTI-12282

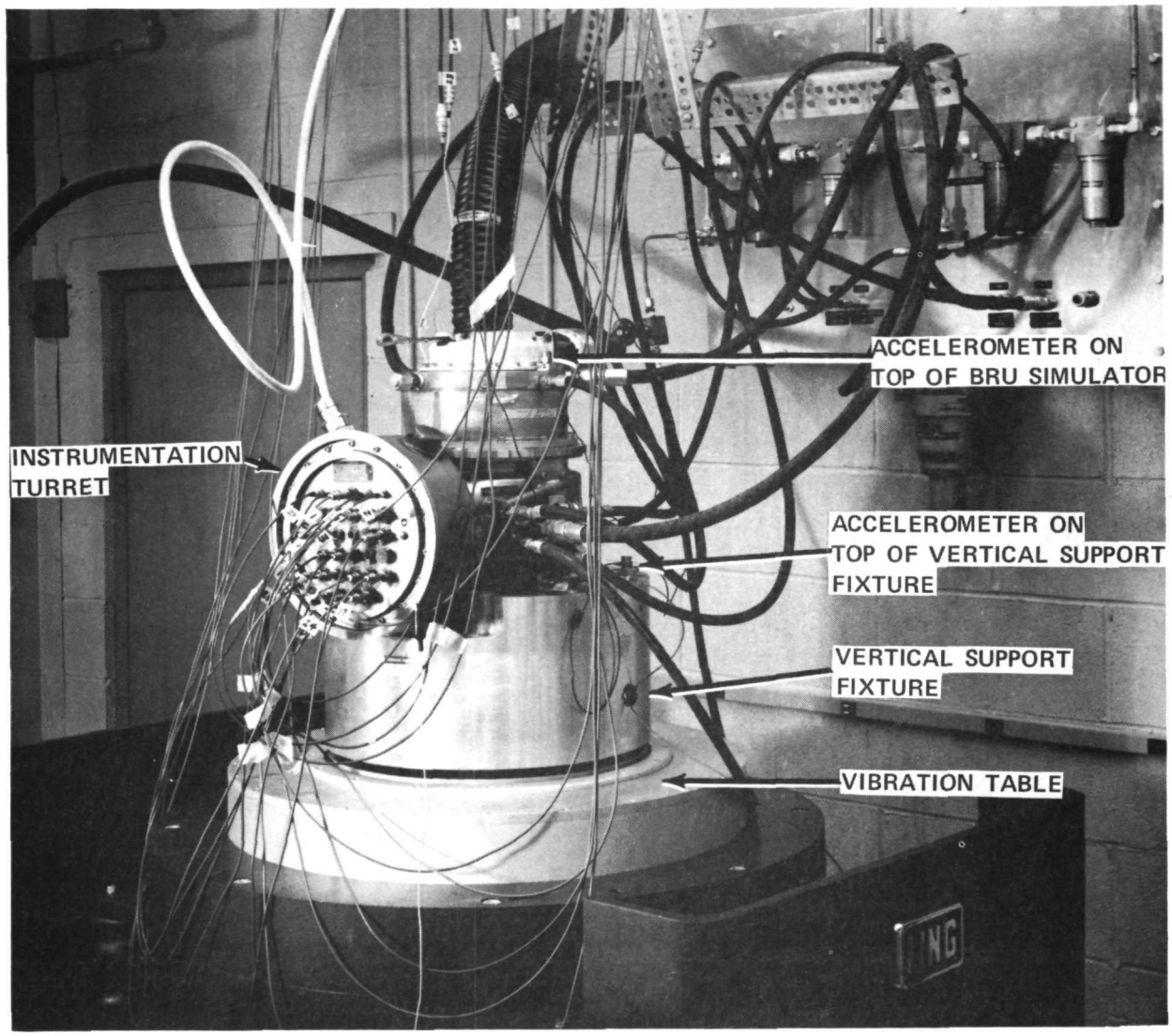

Fig. 3 BRU Simulator In Vertical Support Fixture For Vibration Testing

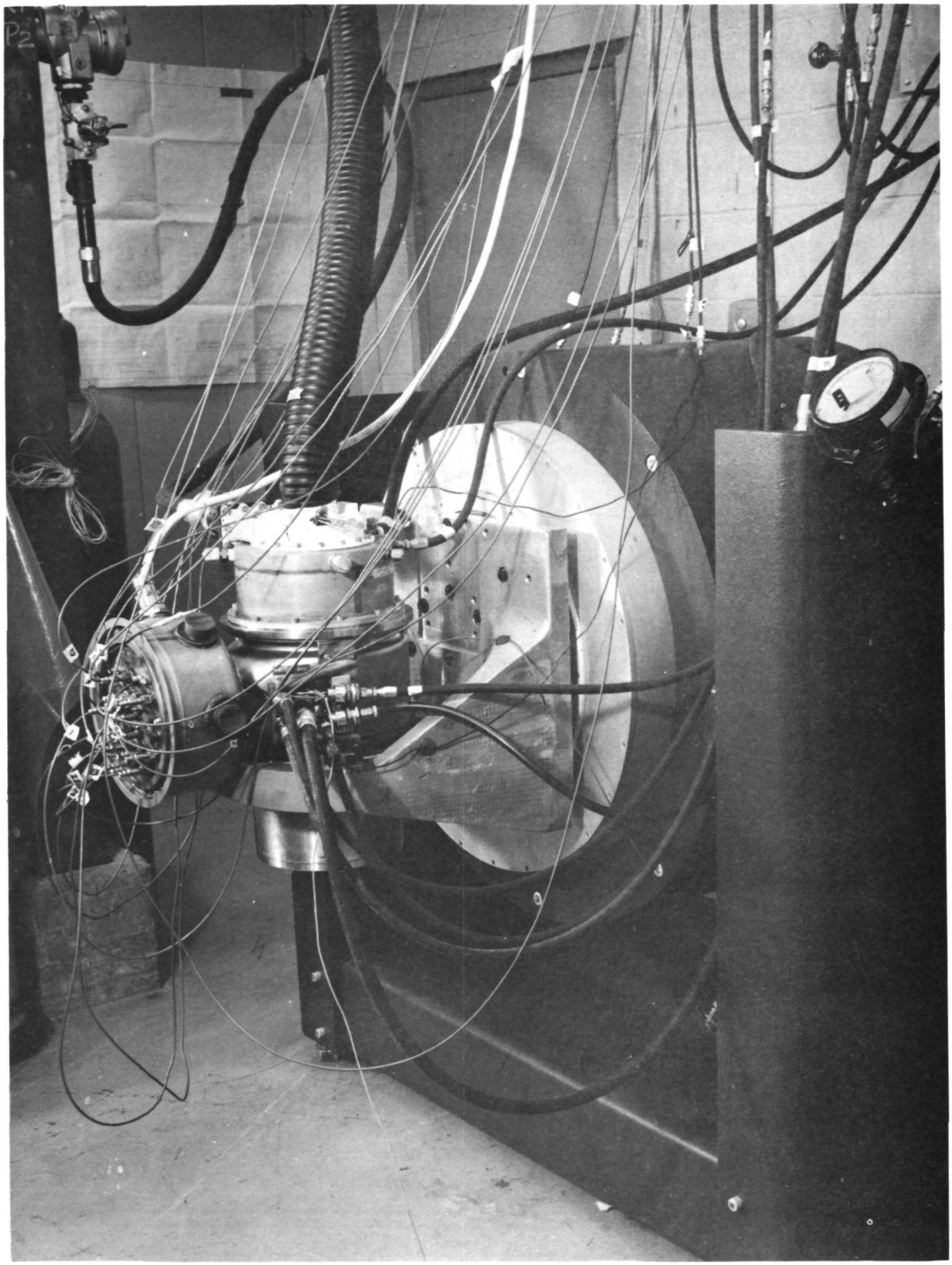

Fig. 4 BRU Simulator In Support Fixture For Transverse Vibration Testing

MTI-11265

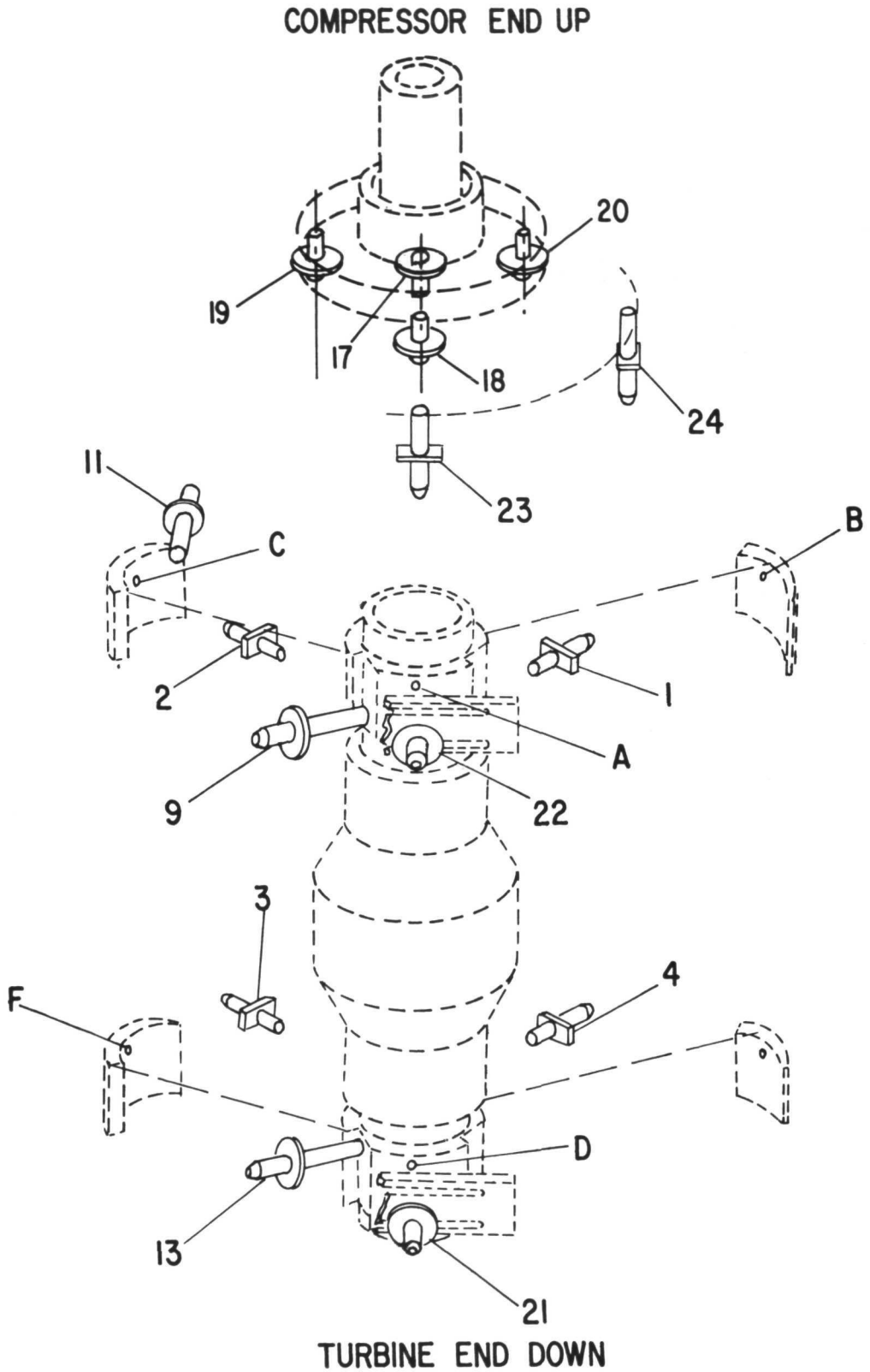

Fig. 5 Proximity Probe Locations on BRU Simulator Rotor and Bearings

MTI-12289

RANDOM VIBRATION INPUT
LEVEL : 0.54 G_{RMS}

ONE MAJOR VERTICAL
DIVISION EQUALS : 0.0002 INCH

ONE MAJOR HORIZONTAL
DIVISION EQUALS : 10 m SEC

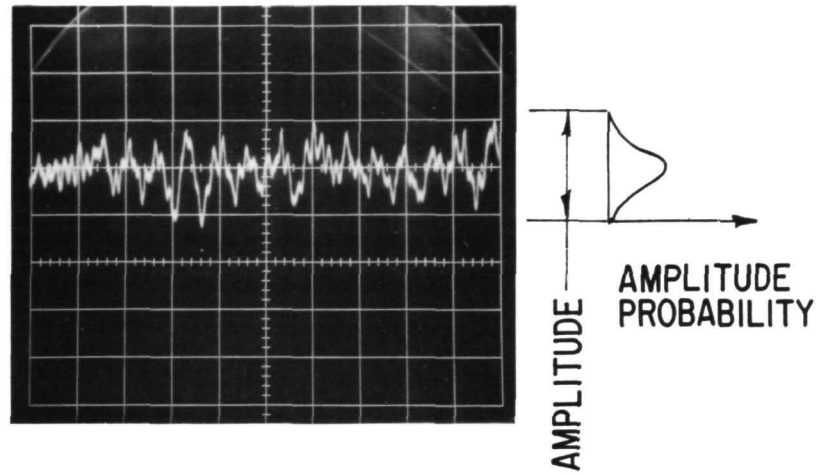

RANDOM VIBRATION INPUT
LEVEL : 1.52 G_{RMS}

ONE MAJOR VERTICAL
DIVISION EQUALS : 0.0002 INCH

ONE MAJOR HORIZONTAL
DIVISION EQUALS : 10 m SEC

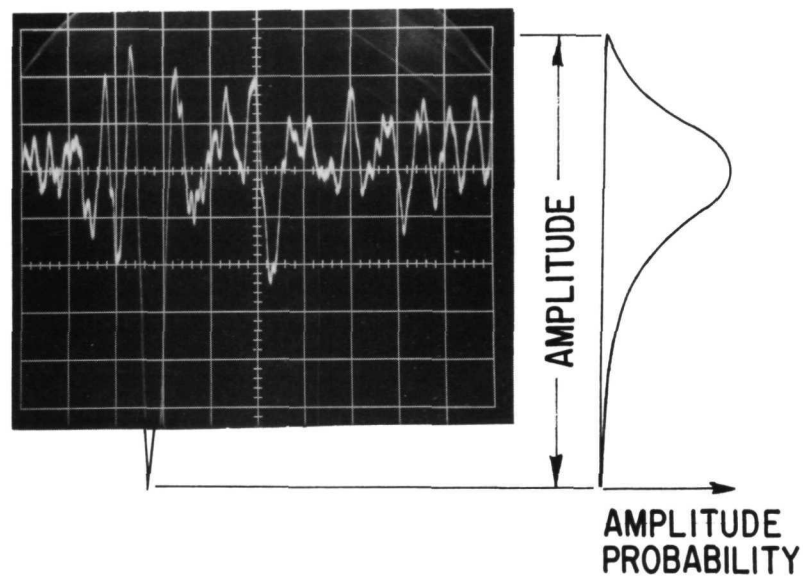

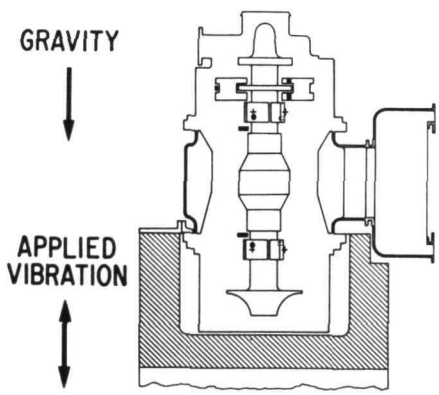

AMBIENT GAS : N_2
AMBIENT PRESSURE : 35 PSIA
ROTOR SPEED : 36,000 RPM
HYDROSTATIC SUPPLY PRESSURE :
THRUST BRG : —
TURBINE JOURNAL BRG : —
COMPRESSOR JOURNAL BEARING : 55 PSIA
DISPLACEMENT PROBE NO. 13

Fig. 6 Casing-To-Pad Leading Edge Amplitude-Time History For Flex-Mounted Turbine Journal Bearing Pad Under Externally-Imposed Shaped Random Vibrations According To NASA Spec 417-2-C-3.5

UPPER TRACE: FLEX. MOUNTED PAD (D) TURBINE JOURNAL

LOWER TRACE: FLEX. MOUNTED PAD (A) COMPRESSOR JOURNAL

VERTICAL SCALE: 0.00025 IN./DIV.

HORIZONTAL SCALE: 20 MSEC/DIV.

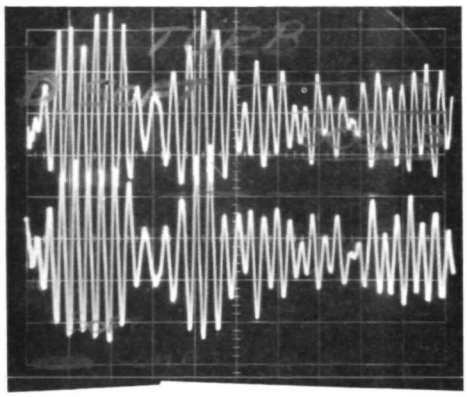

UPPER TRACE: SOLID MOUNTED PAD (F) TURBINE JOURNAL

LOWER TRACE: SOLID MOUNTED PAD (C) COMPRESSOR JOURNAL

VERTICAL SCALE: 0.00025 IN./DIV.

HORIZONTAL SCALE: 20 MSEC/DIV.

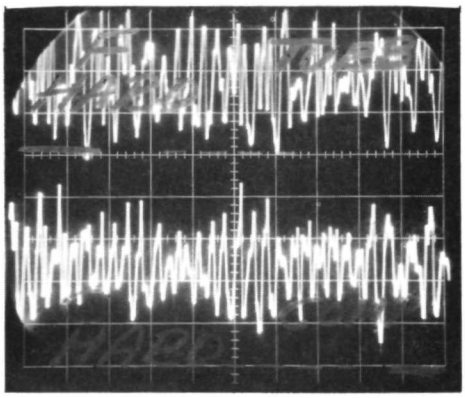

UPPER TRACE: COMPRESSOR JOURNAL FLEXURE PROBE (NO. 22)

VERTICAL SCALE: 0.0005 IN./DIV.

LOWER TRACE: THRUST BEARING GIMBAL PROBE (NO. 23)

VERTICAL SCALE: 0.00075 IN./DIV.

HORIZONTAL SCALE: 20 MSEC/DIV.

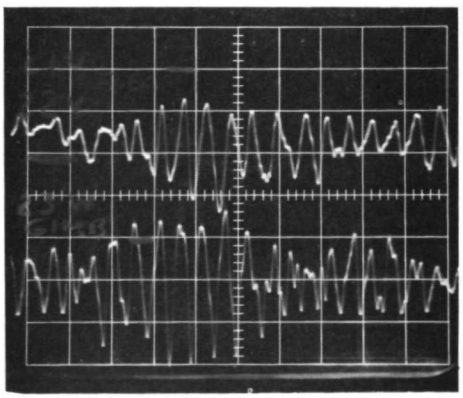

RANDOM VIBRATION INPUT LEVEL: 0.95 G_{RMS}

AMBIENT CONDITIONS: N_2 @ 14.7 PSIA

HYDROSTATIC SUPPLY PRESSURE: 150 PSIA

ROTOR SPEED: 2500 RPM

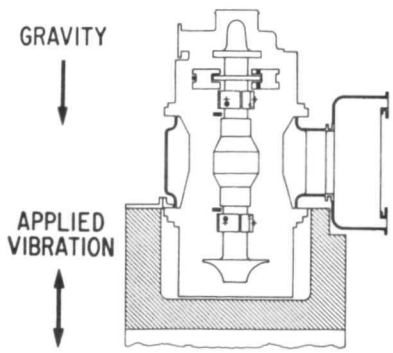

Fig. 7 Bearing Amplitudes Under Shaped Random Vibrations According To NASA Spec 417-2-C-3.5

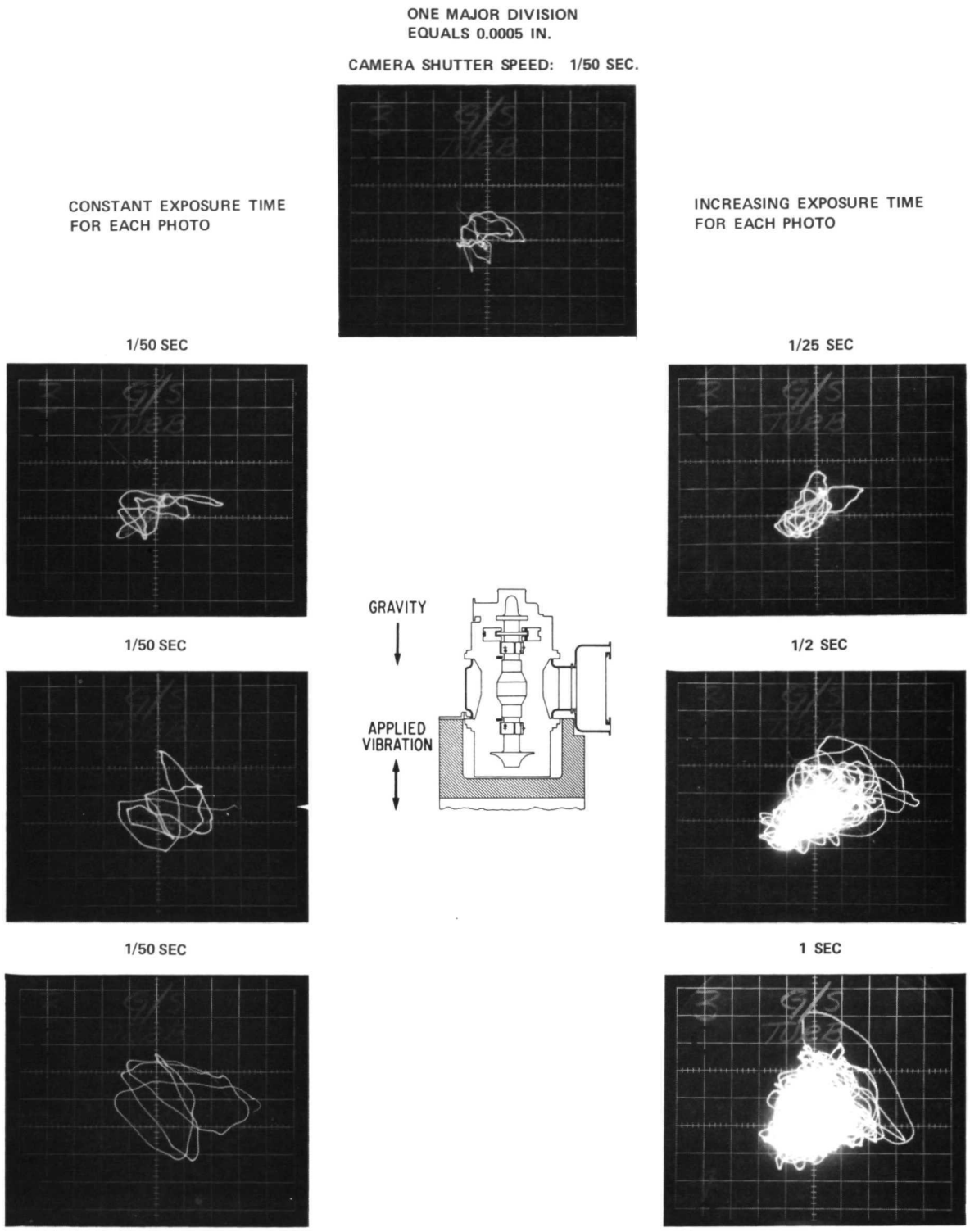

Fig. 8 Rotor Amplitudes (Casing-To-Shaft) Under Shaped Random Vibrations According to NASA Spec 417-2-C-3.5

MTI-11733

RANDOM VIBRATION INPUT
LEVEL : 0.54 G_{RMS}

ONE MAJOR VERTICAL
DIVISION EQUALS : 0.00025 INCH

ONE MAJOR HORIZONTAL
DIVISION EQUALS : 10 msec

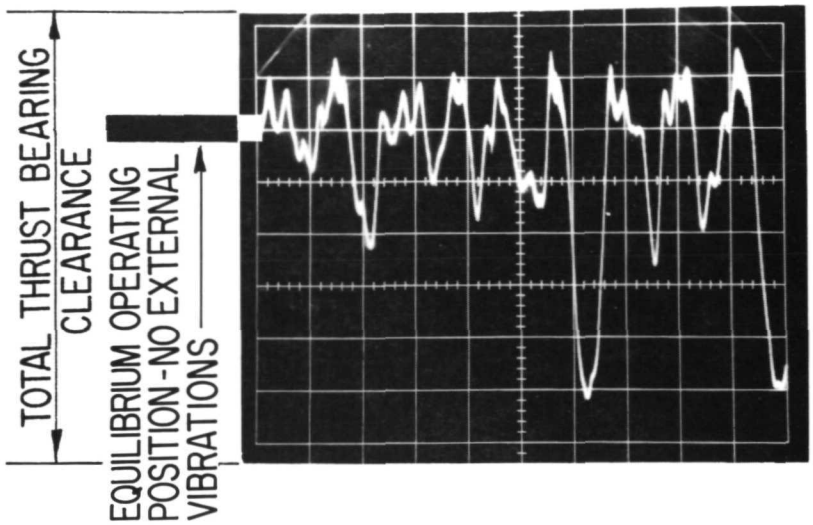

RANDOM VIBRATION INPUT
LEVEL : 1.52 G_{RMS}

ONE MAJOR VERTICAL
DIVISION EQUALS : 0.00025 INCH

ONE MAJOR HORIZONTAL
DIVISION EQUALS : 10 msec

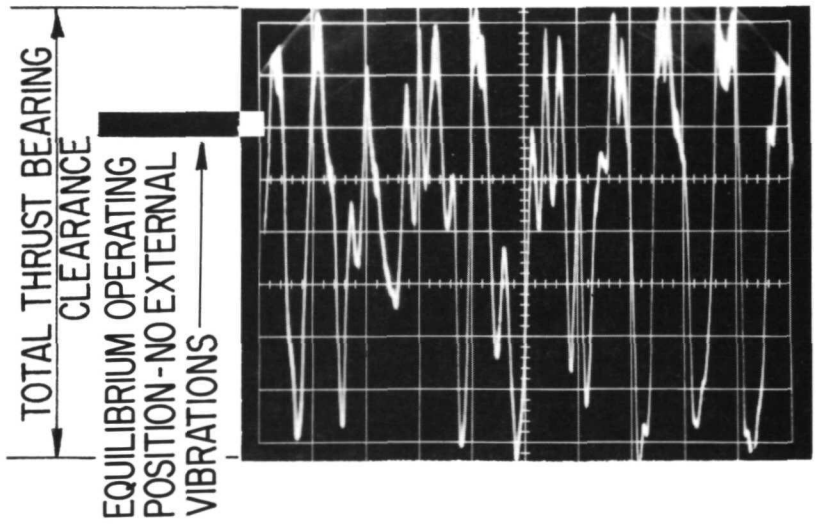

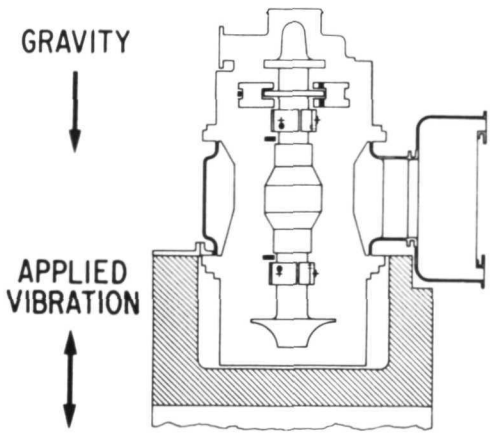

AMBIENT GAS : N_2
AMBIENT PRESSURE : 35 PSIA
ROTOR SPEED : 36,000 RPM
HYDROSTATIC SUPPLY PRESSURE :
THRUST BRG : —
TURBINE JOURNAL BRG : —
COMPRESSOR JOURNAL BEARING : 55 PSIA
DISPLACEMENT PROBE NO. 20

Fig. 9 Thrust Bearing Film Thickness Variation With Time Under Externally-Imposed Shaped Random Vibrations According To NASA Spec 417-2-C-3.5

MTI-14032

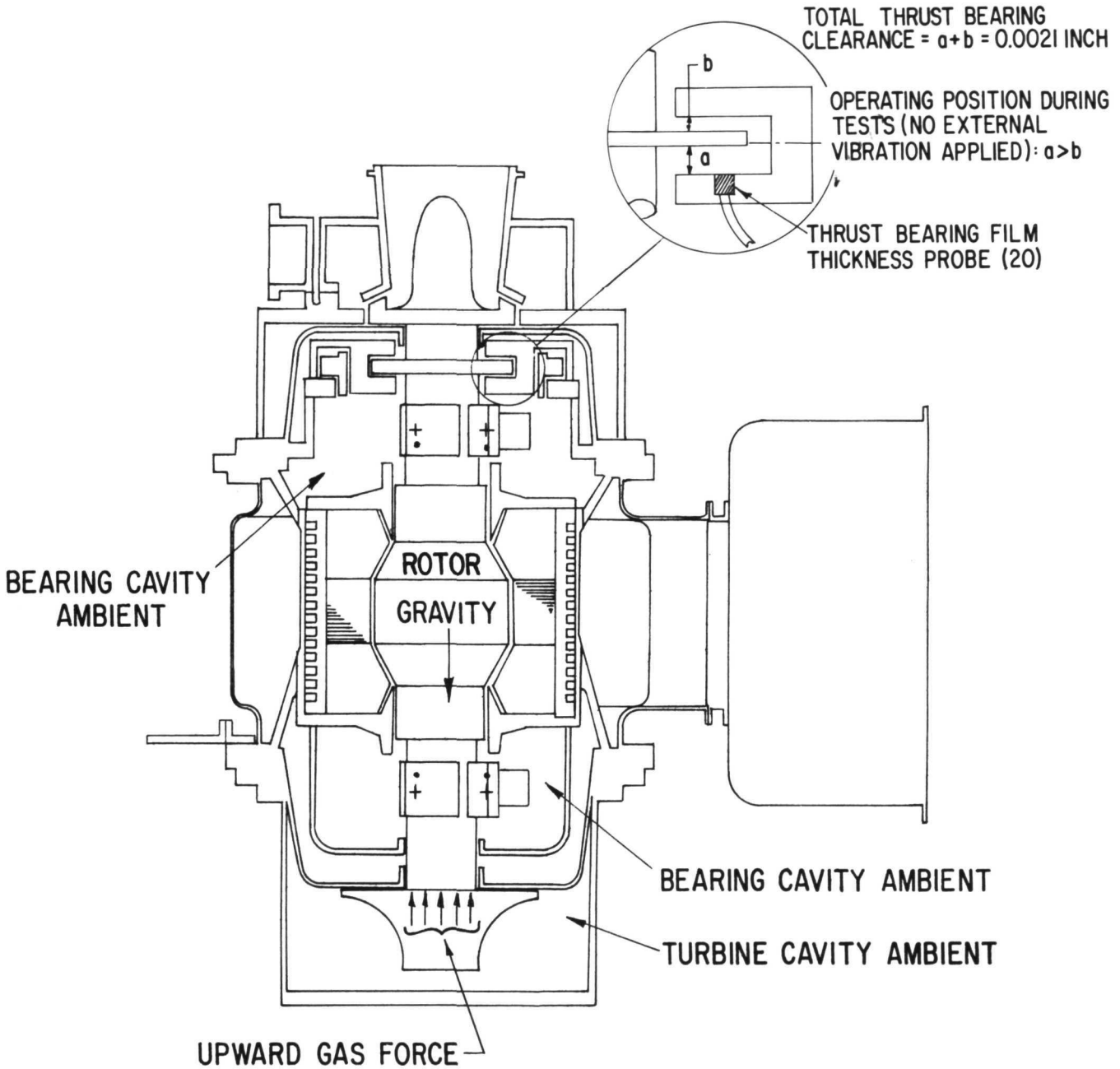

Fig. 10 Schematic Of BRU Simulator With Static Rotor Force Designation And Typical Thrust Runner Position During Vibration Tests

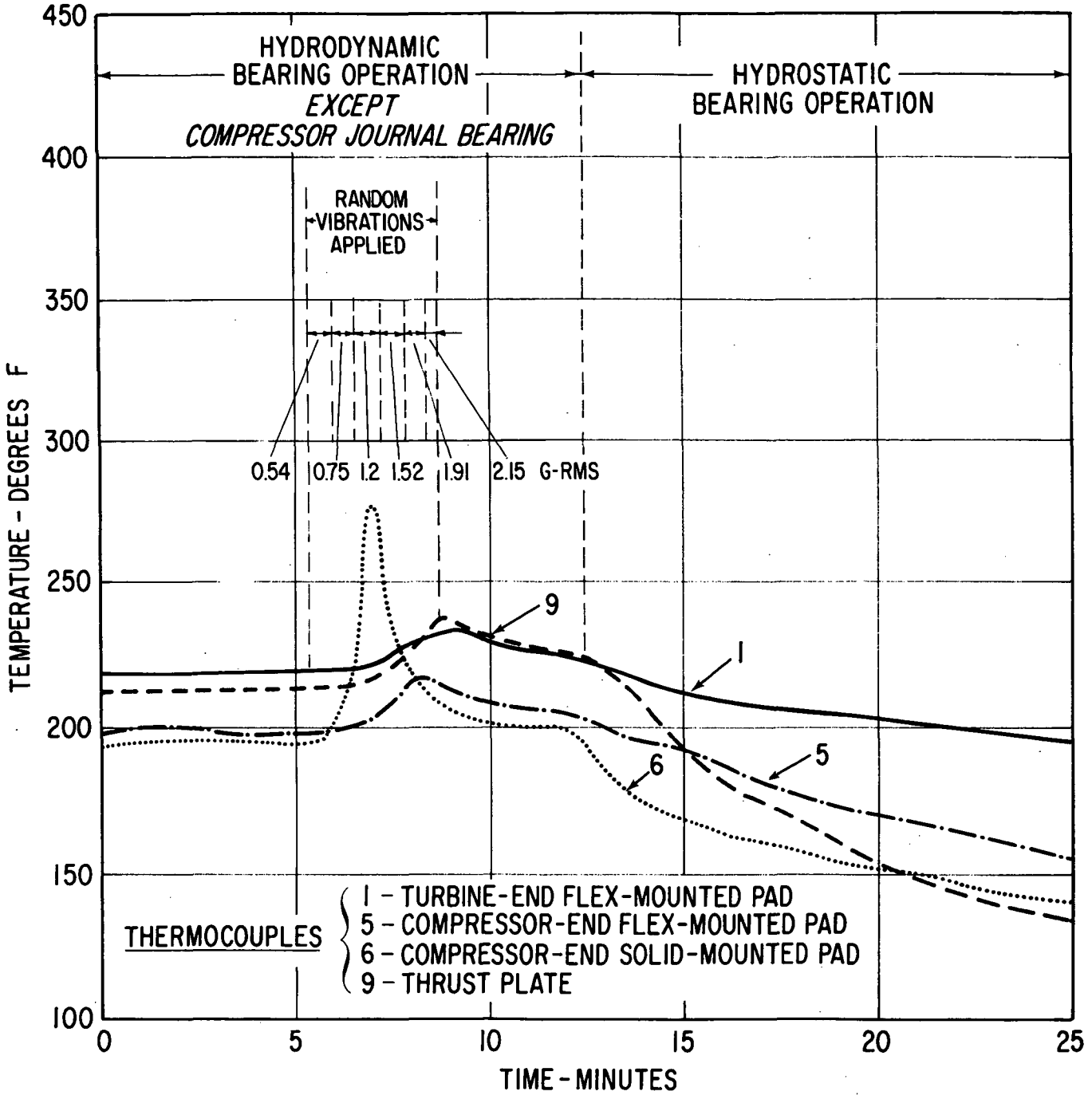

Fig. 11 Measured Temperatures In BRU Simulator Components With Axial Random Excitation (Shaft Speed 36,000 rpm)

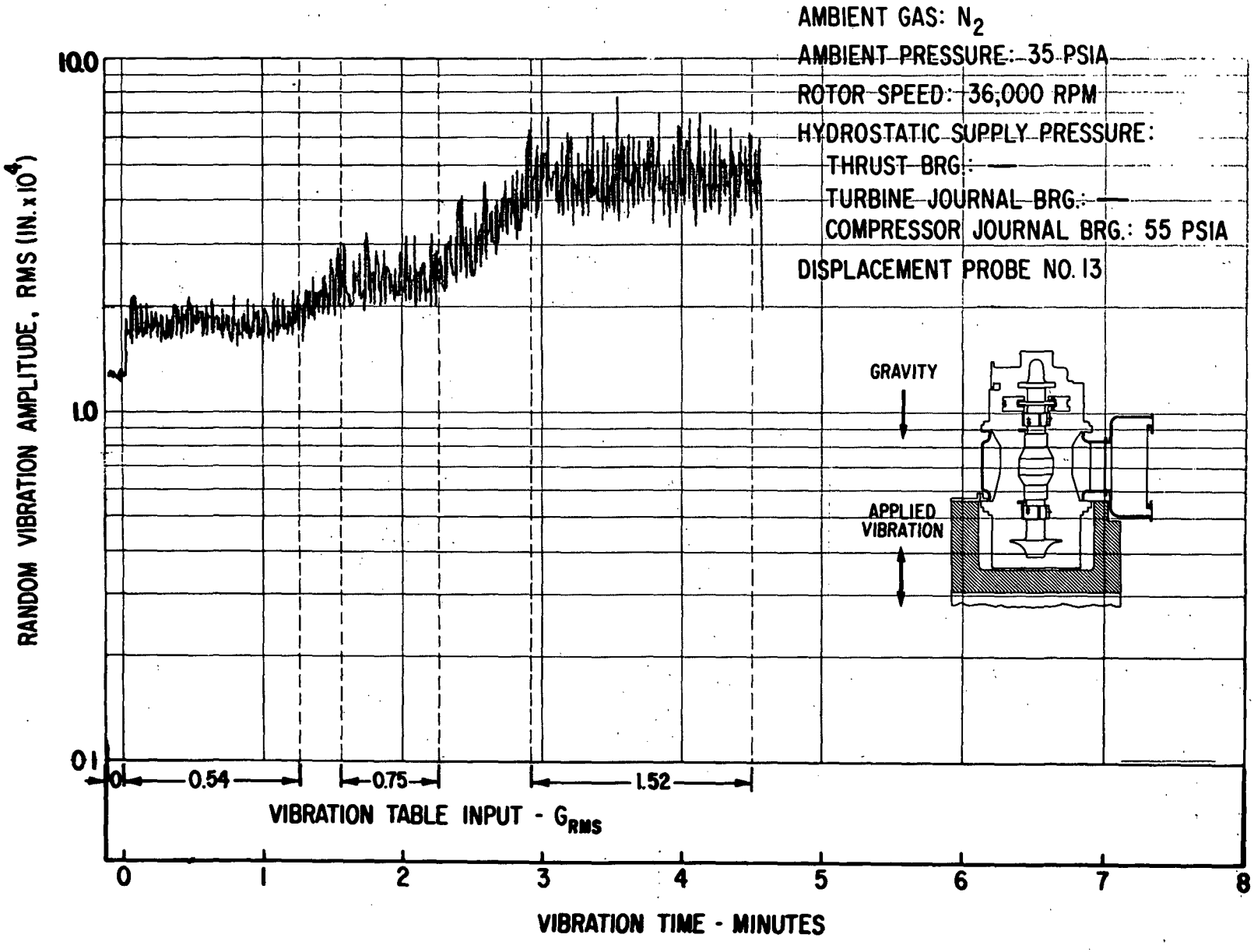

Fig. 12 Casing-To-Pad Leading Edge Amplitudes For Flex-Mounted Turbine Journal Bearing Pad Under Externally-Imposed Shaped Random Vibrations According To NASA Spec 417-2-C-3.5

MTI-14057

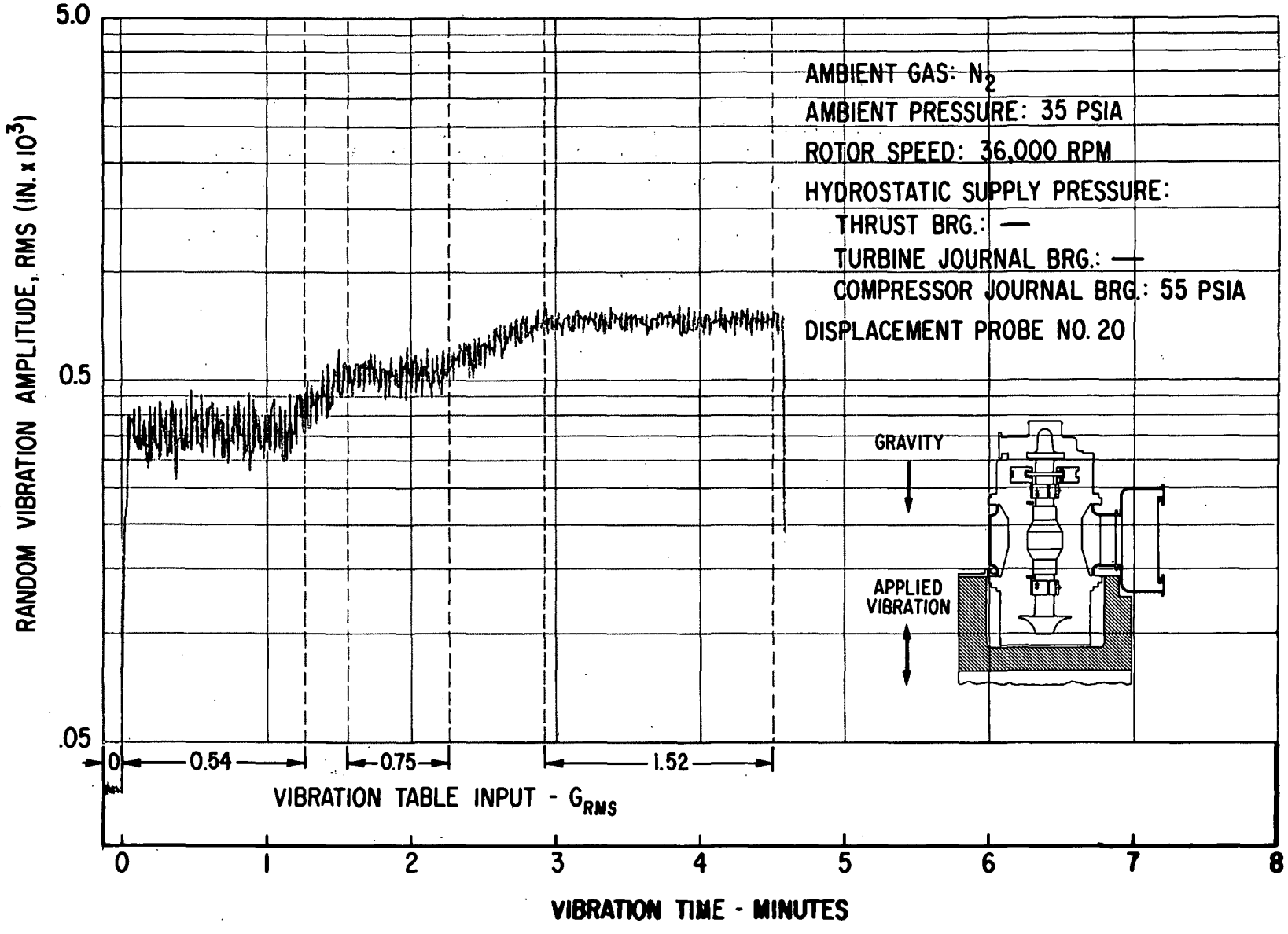

Fig. 13 Thrust Bearing Film Thickness Variation Under Externally-Imposed Shaped Random Vibrations According to NASA Spec 417-2-C-3.5

MTI-14058

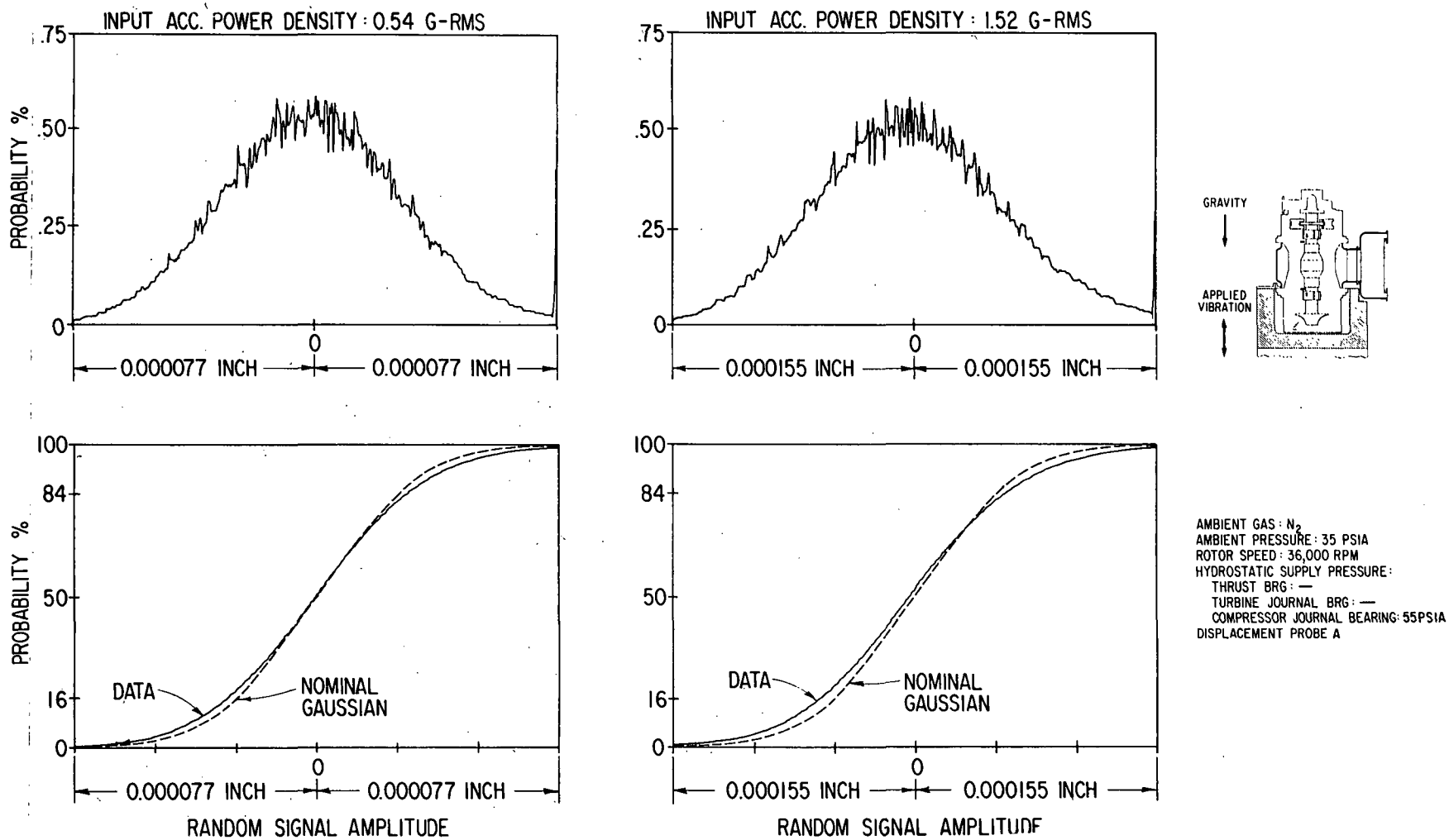

Fig. 14 Amplitude Probability Distribution Of Pad-To-Shaft Pivot Film Thickness Variation For Flex-Mounted Compressor Journal Bearing Pad Under Externally-Imposed Shaped Random Vibrations According to NASA Spec 417-2-C-3.5

MTI-14050

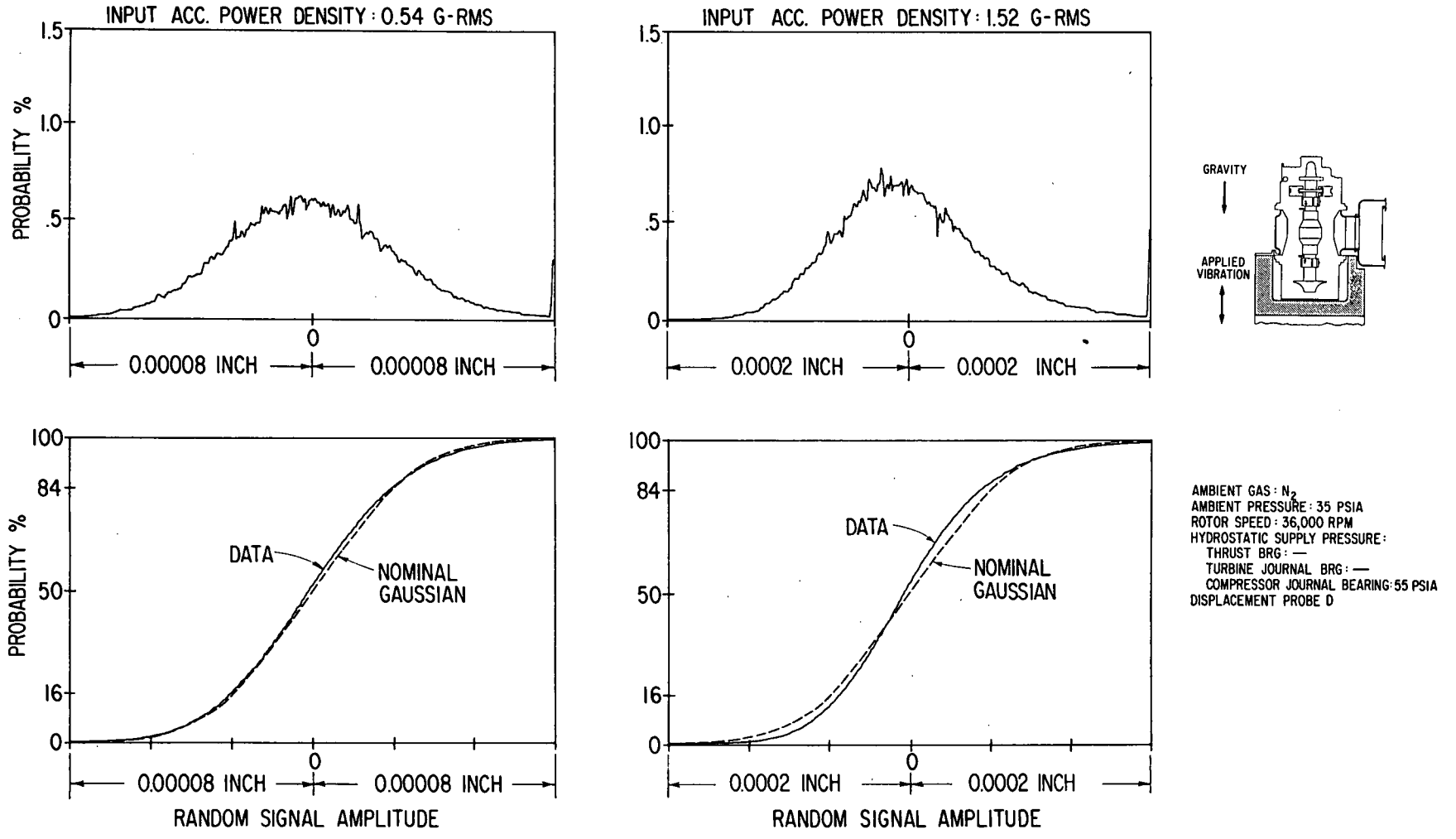

Fig. 15 Amplitude Probability Distribution Of Pad-To-Shaft Pivot Film Thickness Variation For Flex-Mounted Turbine Journal Bearing Pad Under Externally-Imposed Shaped Random Vibrations According To NASA Spec 417-2-C-3.5

MTI-14031

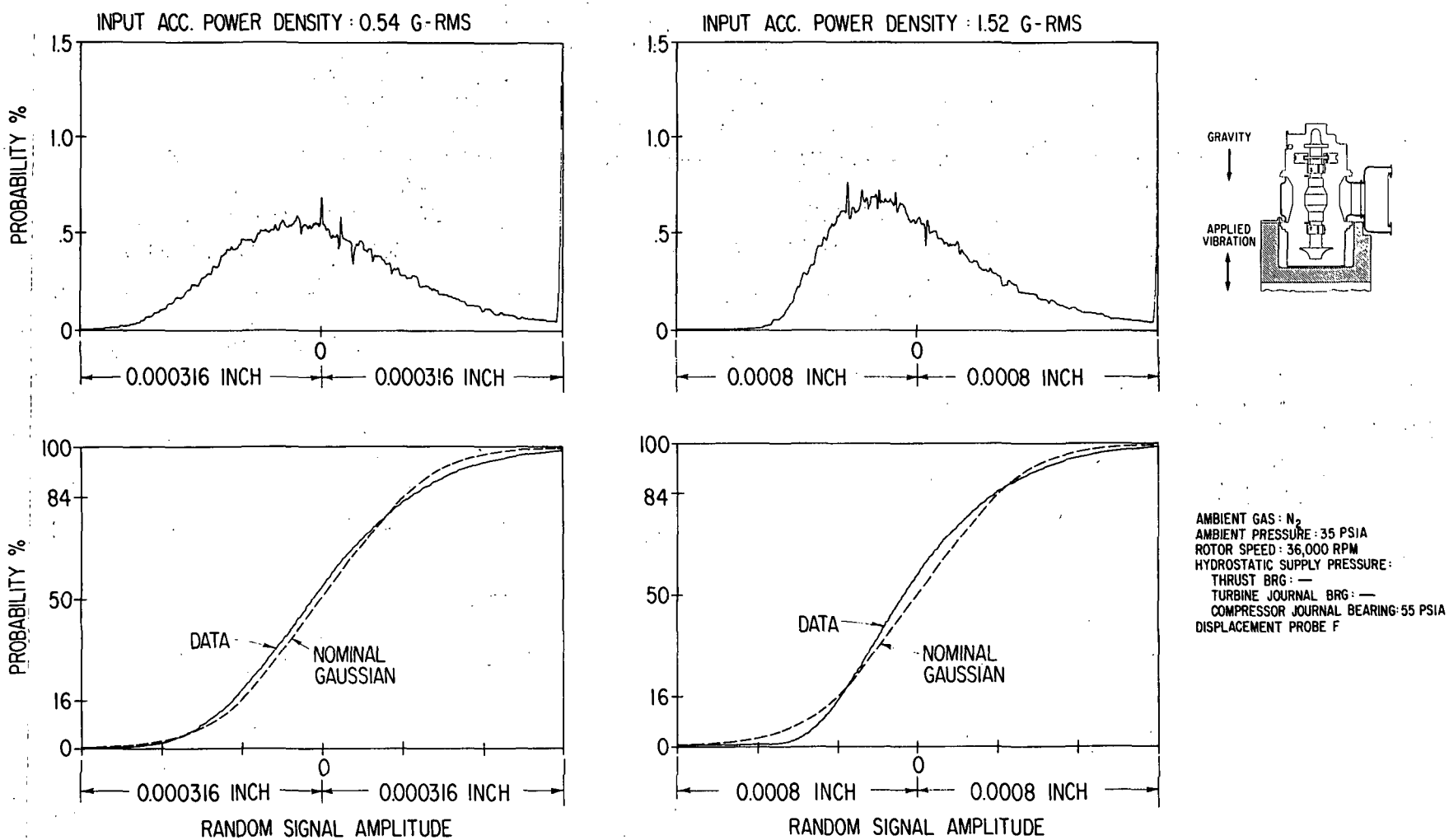

Fig. 16 Amplitude Probability Distribution Of Pad-To-Shaft Pivot Film Thickness Variation For Solid-Mounted Turbine Journal Bearing Pad Under Externally-Imposed Shaped Random Vibrations According To NASA Spec 417-2-C-3.5

MTI-14045

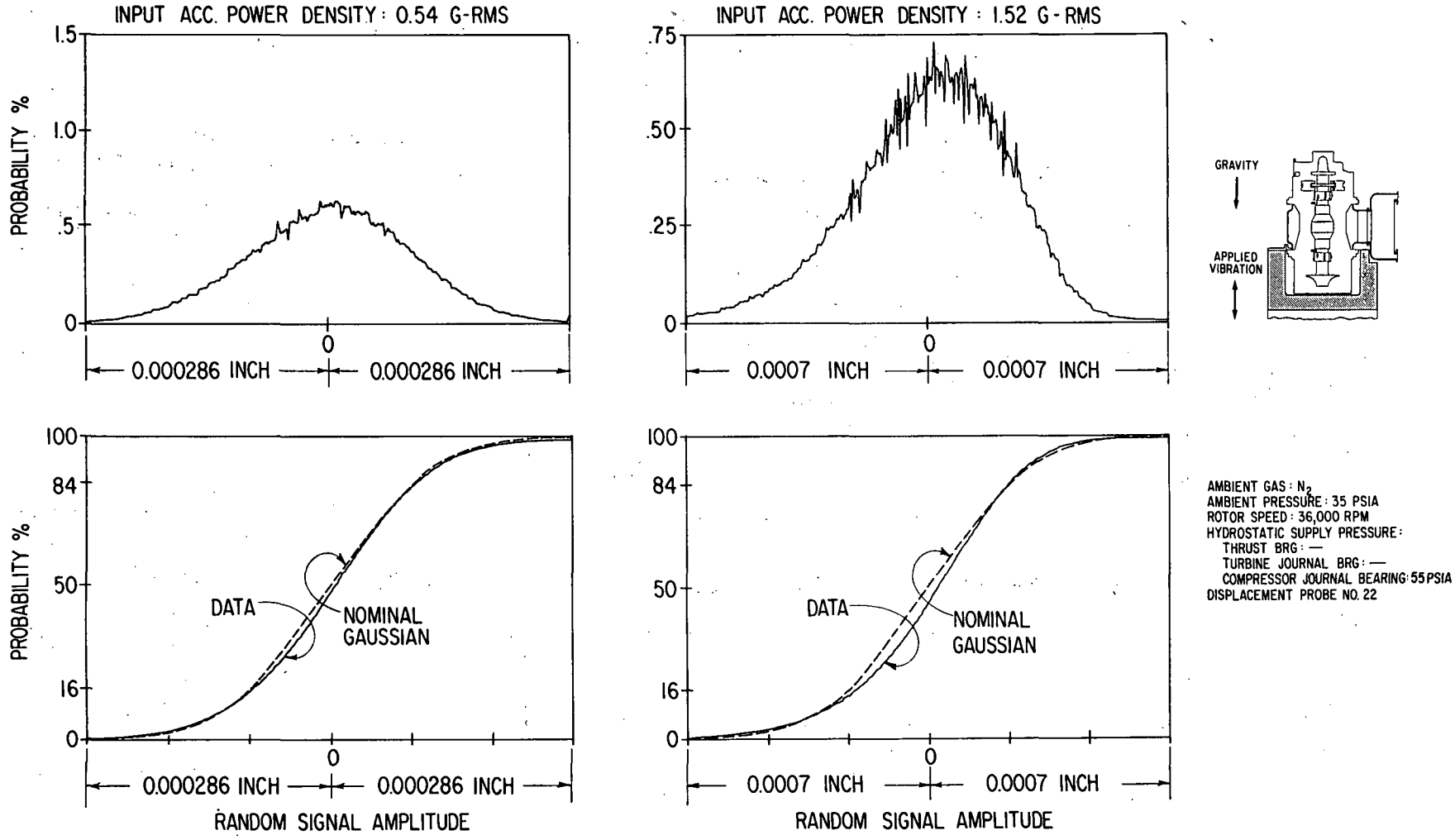

Fig. 17 Amplitude Probability Distribution Of Compressor Journal Flexure Amplitudes Under Externally-Imposed Shaped Random Vibrations According To NASA Spec 417-2-C-3.5

MTI-14046

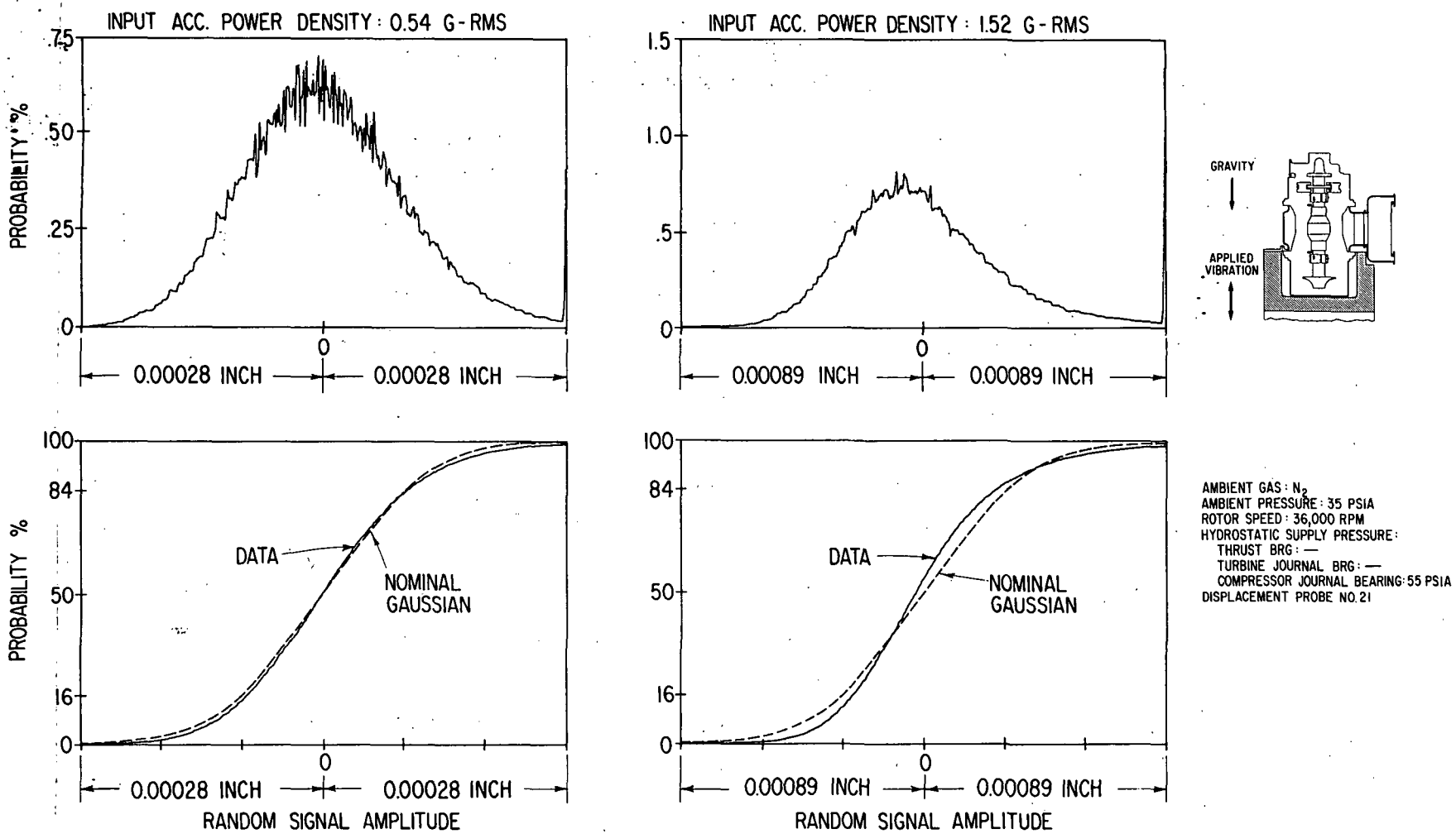

Fig. 18 Amplitude Probability Distribution Of Turbine Journal Flexure Amplitudes Under Externally-Imposed Shaped Random Vibrations According To NASA Spec 417-2-C-3.5

MTI-14047

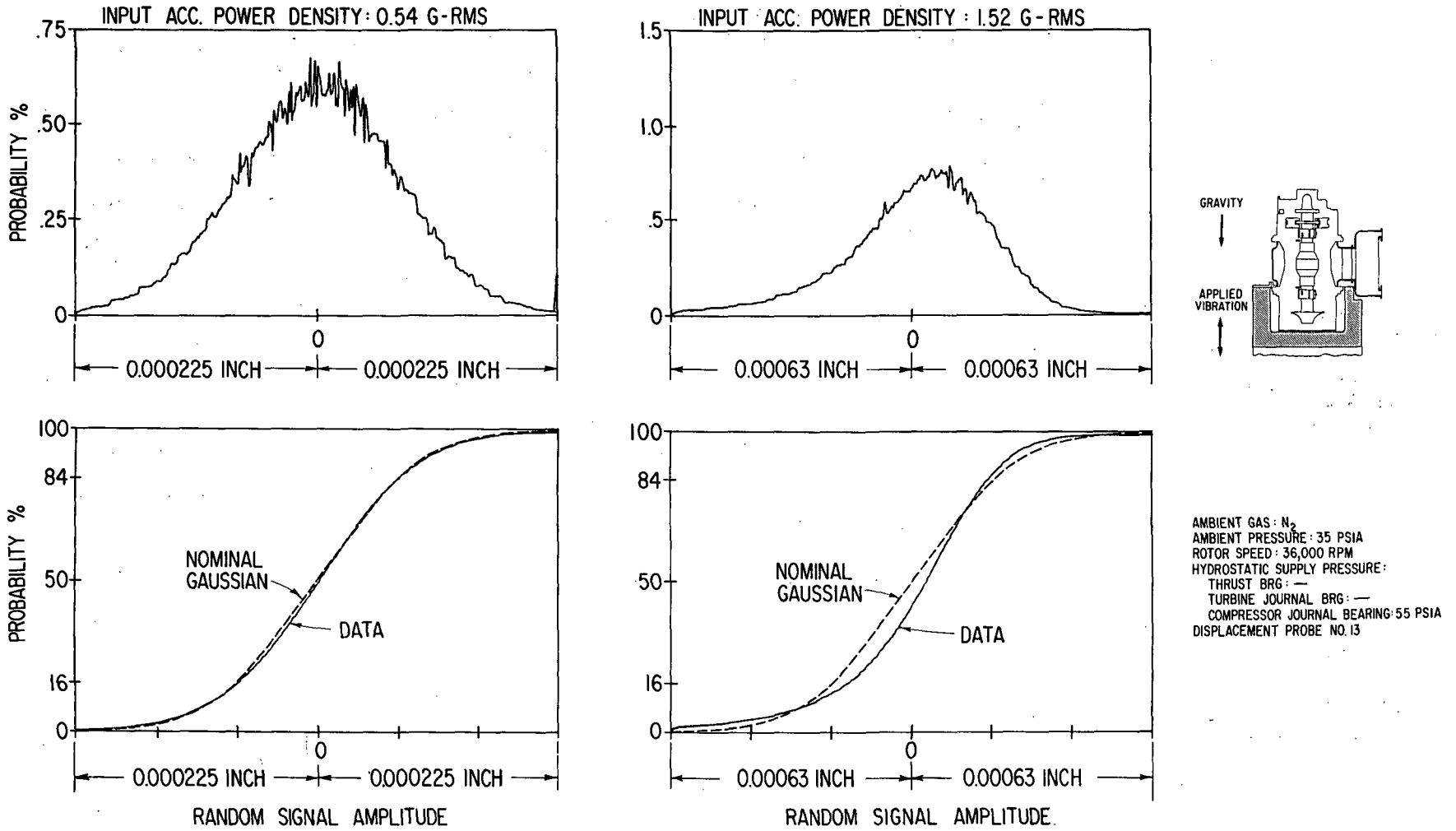

Fig. 19 Amplitude Probability Distribution Of Casing-To-Pad Leading Edge Amplitudes For Flex-Mounted Turbine Journal Bearing Pad Under Externally-Imposed Shaped Random Vibrations According To NASA Spec 417-2-C-3.5

MTI-14048

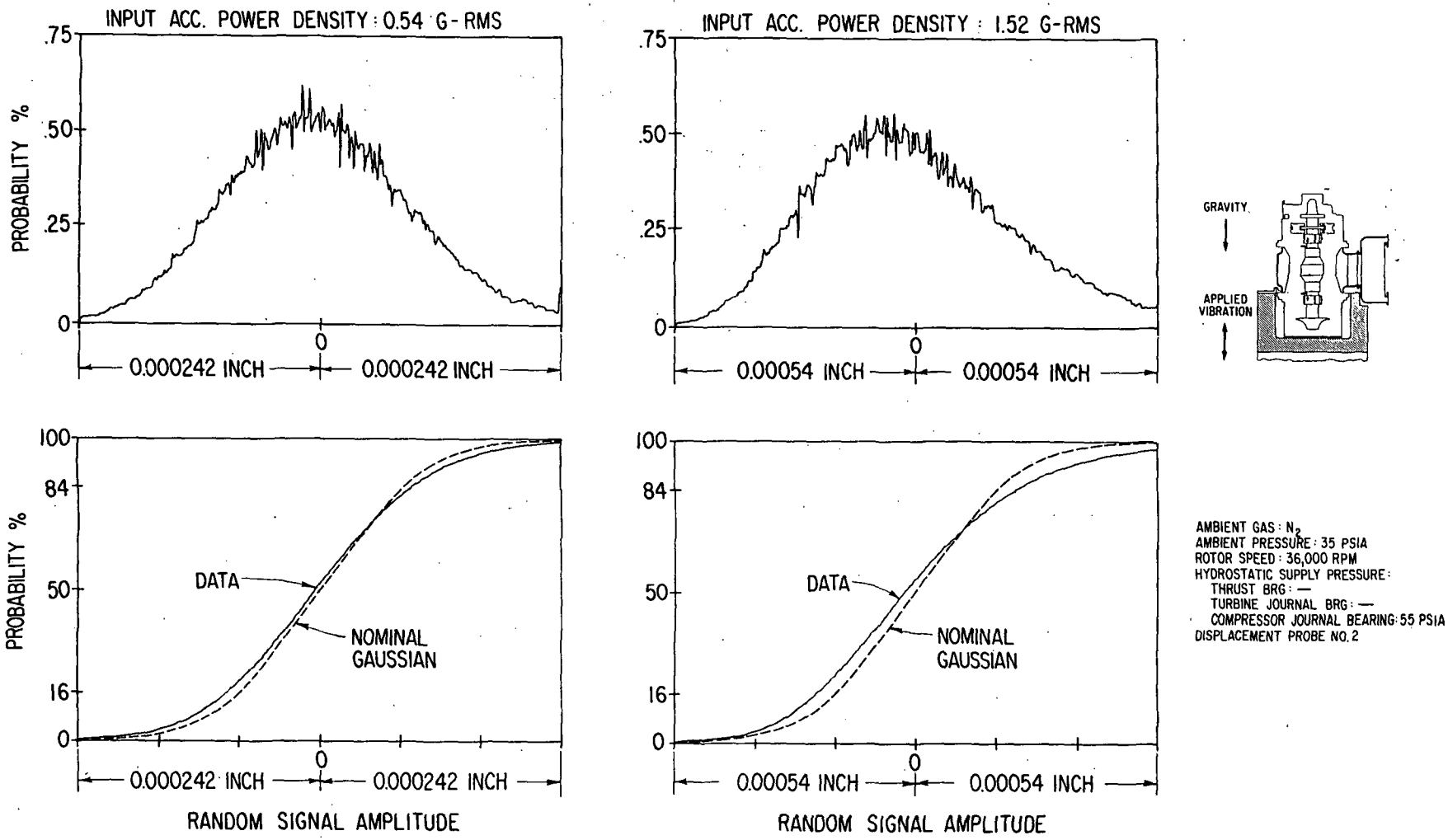

Fig. 20 Amplitude Probability Distribution Of Compressor Journal Rotor Amplitudes (Casing-To-Shaft) Under Externally-Imposed Shaped Random Vibrations According To NASA Spec 417-2-C-3.5

MTI-14049

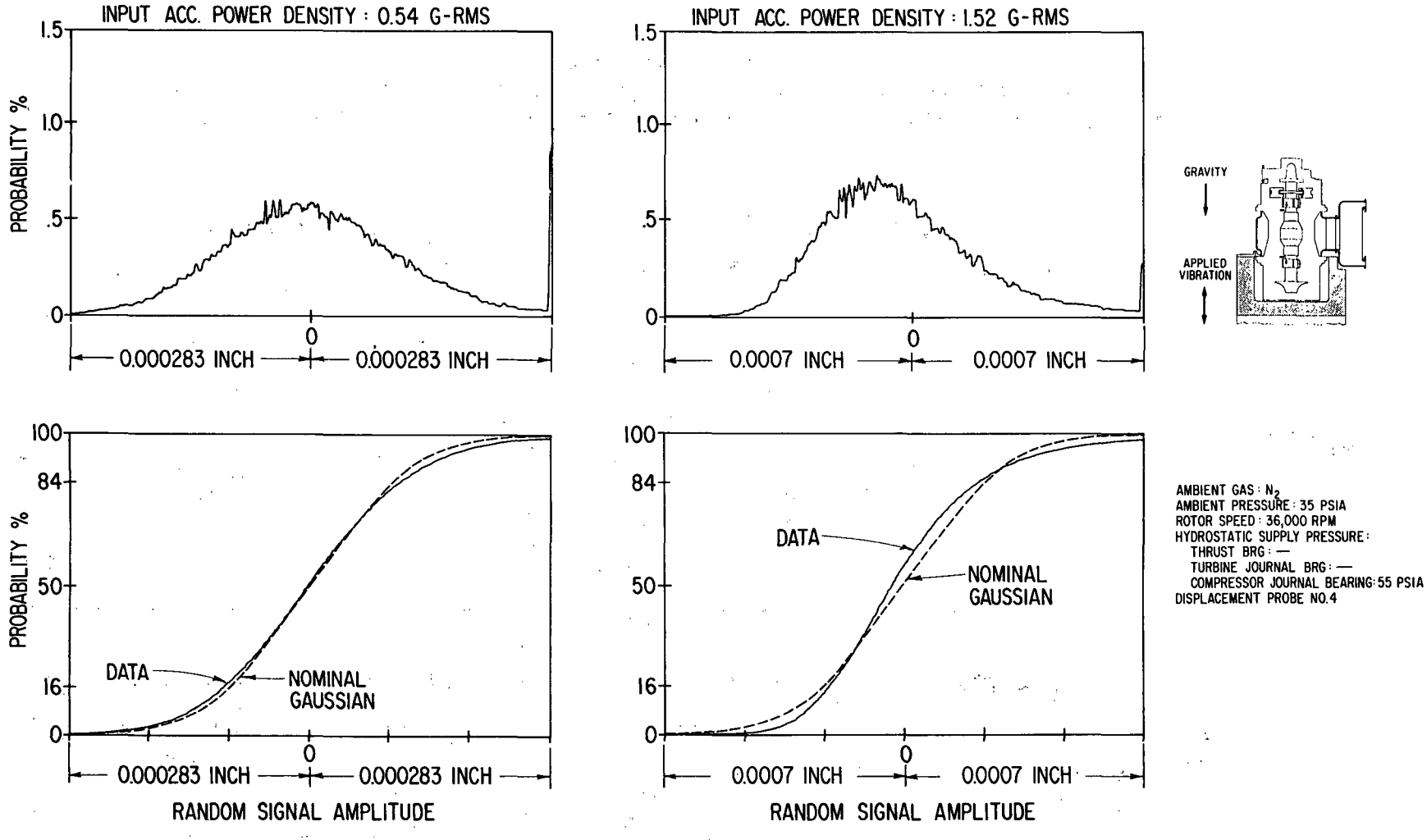

Fig. 21 Amplitude Probability Distribution Of Turbine Journal Rotor Amplitudes (Casing-To-Shaft) Under Externally-Imposed Shaped Random Vibrations According To NASA Spec 417-2-C-3.5

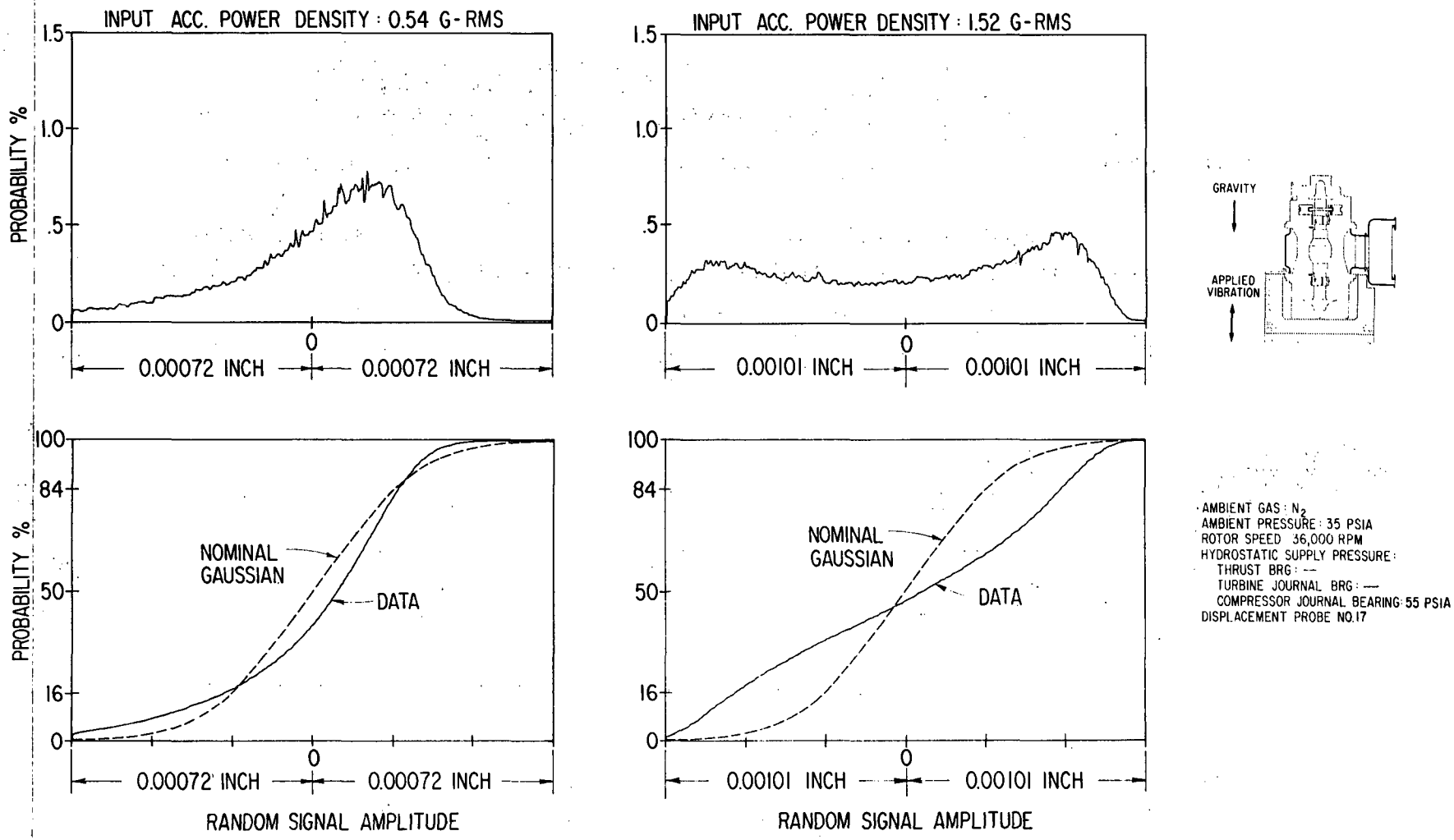

Fig. 22 Amplitude Probability Distribution Of Thrust Bearing Film Thickness Variation Under Externally-Imposed Shaped Random Vibrations According To NASA Spec 417-2-C-3.5

MTI-14029

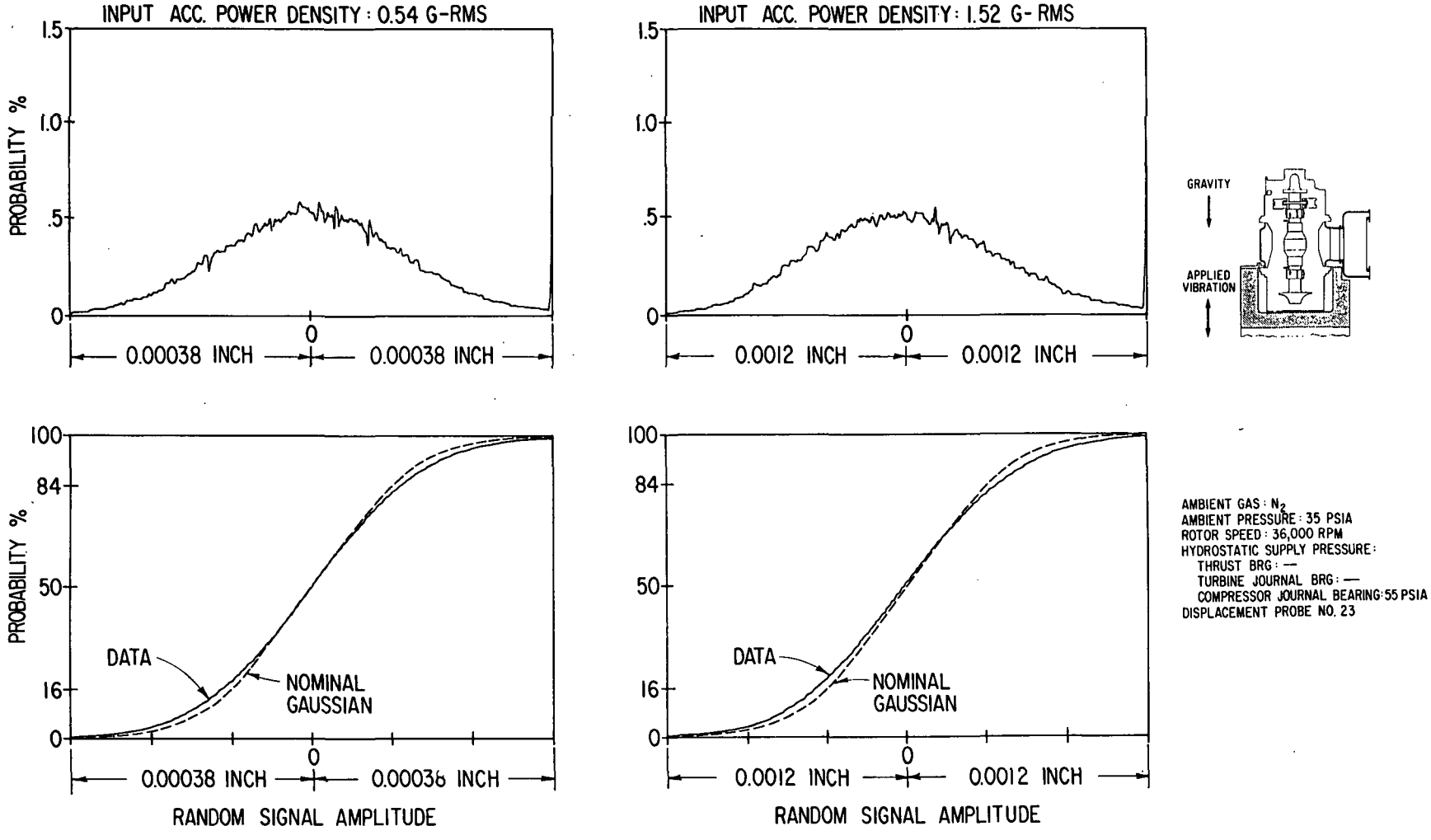

Fig. 23 Amplitude Probability Distribution Of Thrust Bearing Gimbal Amplitudes Under Externally-Imposed Shaped Random Vibrations According To NASA Spec 417-2-C-3.5

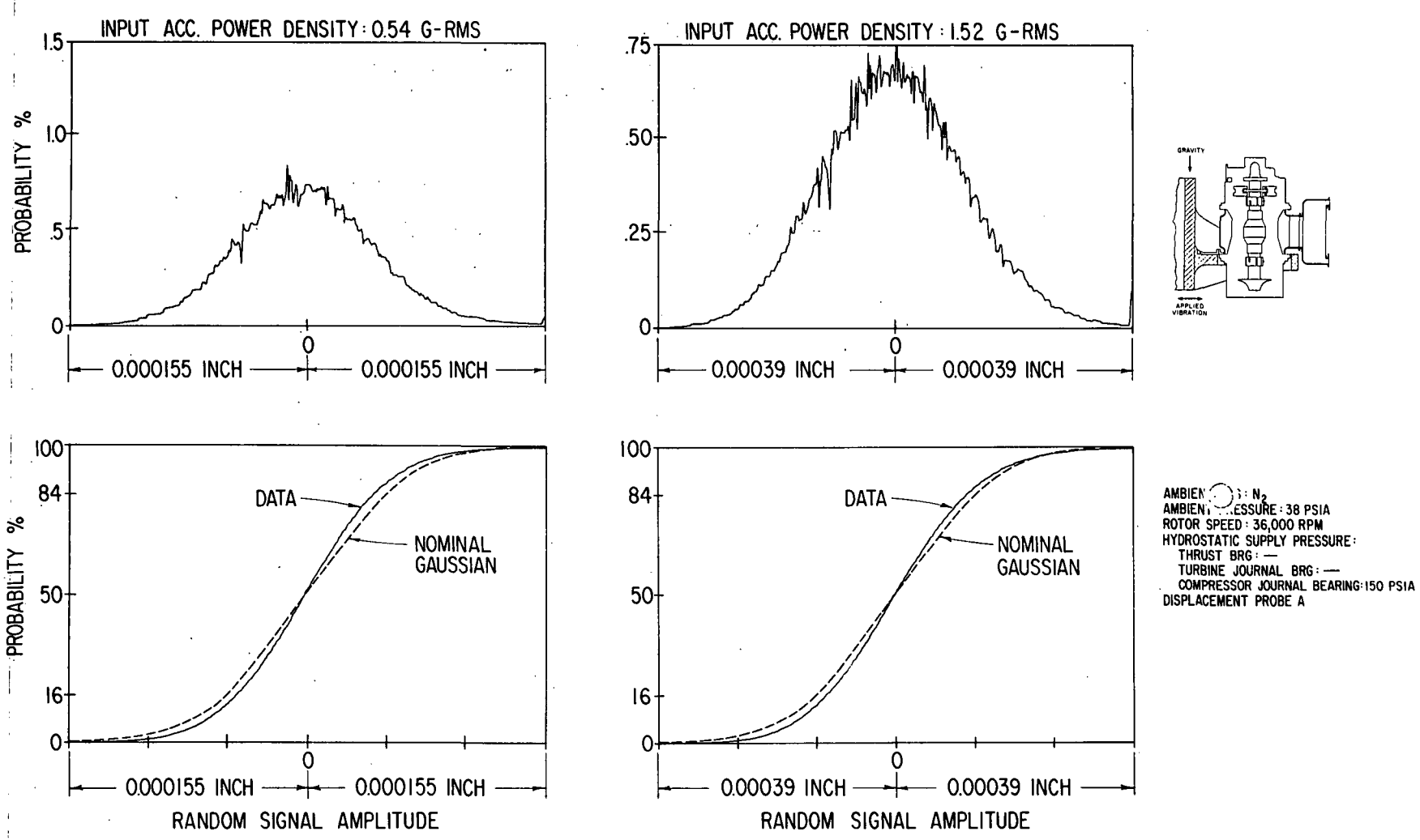

Fig. 24 Amplitude Probability Distribution Of Pad-To-Shaft Pivot Film Thickness Variation For Flex-Mounted Compressor Journal Bearing Pad Under Externally-Imposed Shaped Random Vibrations According To NASA Spec 417-2-C-3.5

MTI-14067

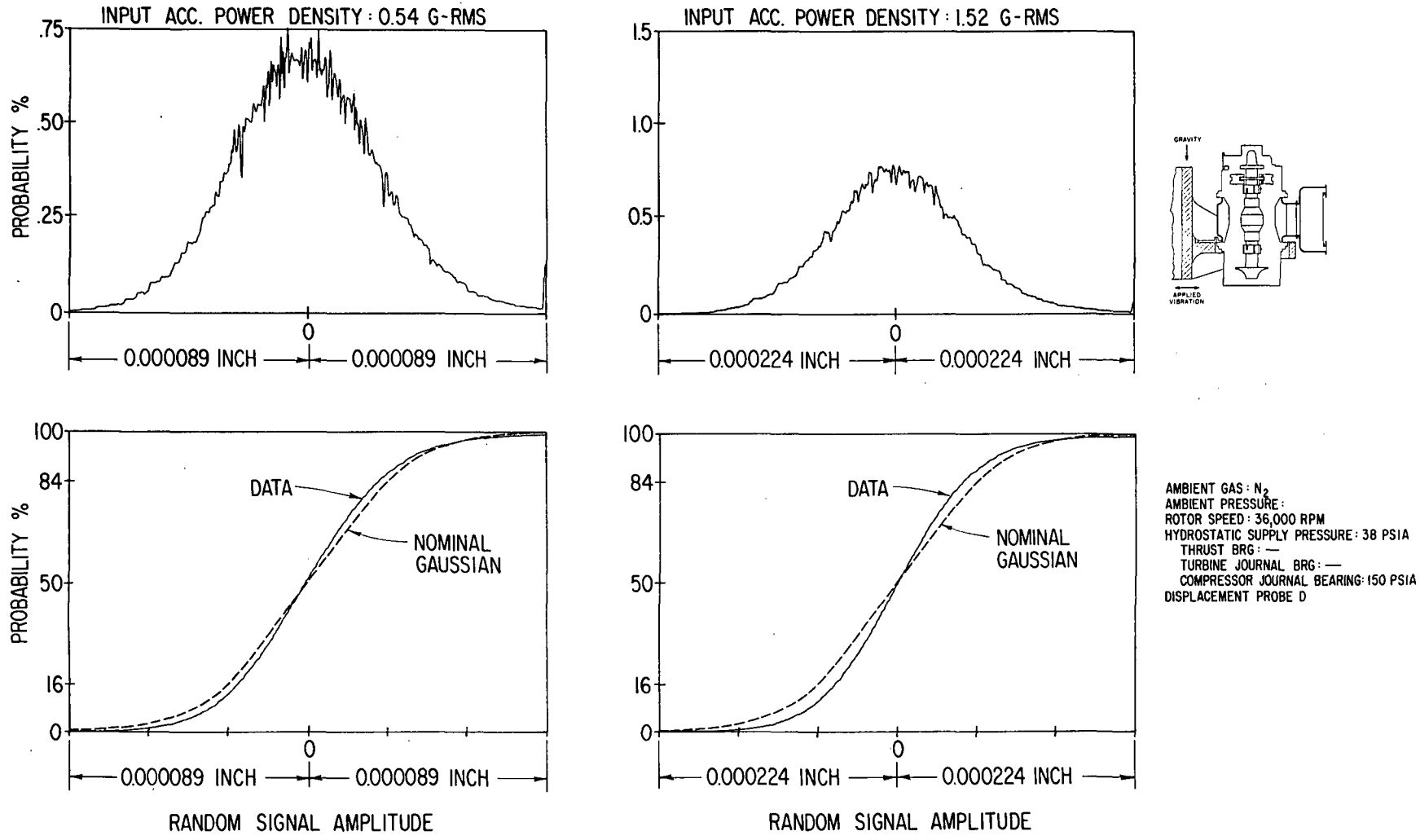

Fig. 25 Amplitude Probability Distribution Of Pad-To-Shaft Pivot Film Thickness Variation For Flex-Mounted Turbine Journal Bearing Pad Under Externally-Imposed Shaped Random Vibrations According To NASA Spec 417-2-C-3.5

MTI-13676

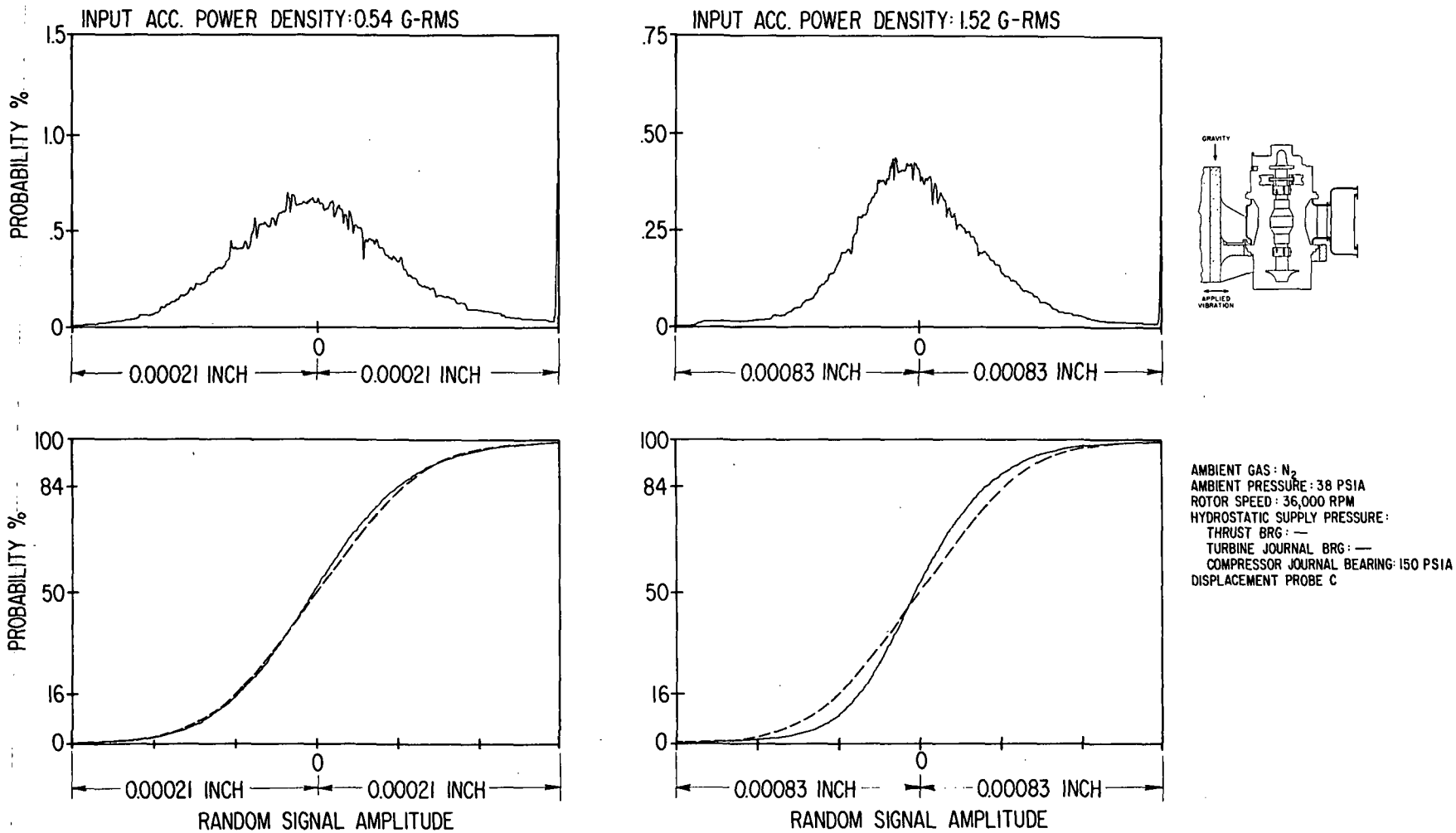

Fig. 26 Amplitude Probability Distribution Of Pad-To-Shaft Pivot Film Thickness Variation For Solid-Mounted Compressor Journal Bearing Pad Under Externally-Imposed Shaped Random Vibrations According To NASA Spec 417-2-C-3.5

MTI-14066

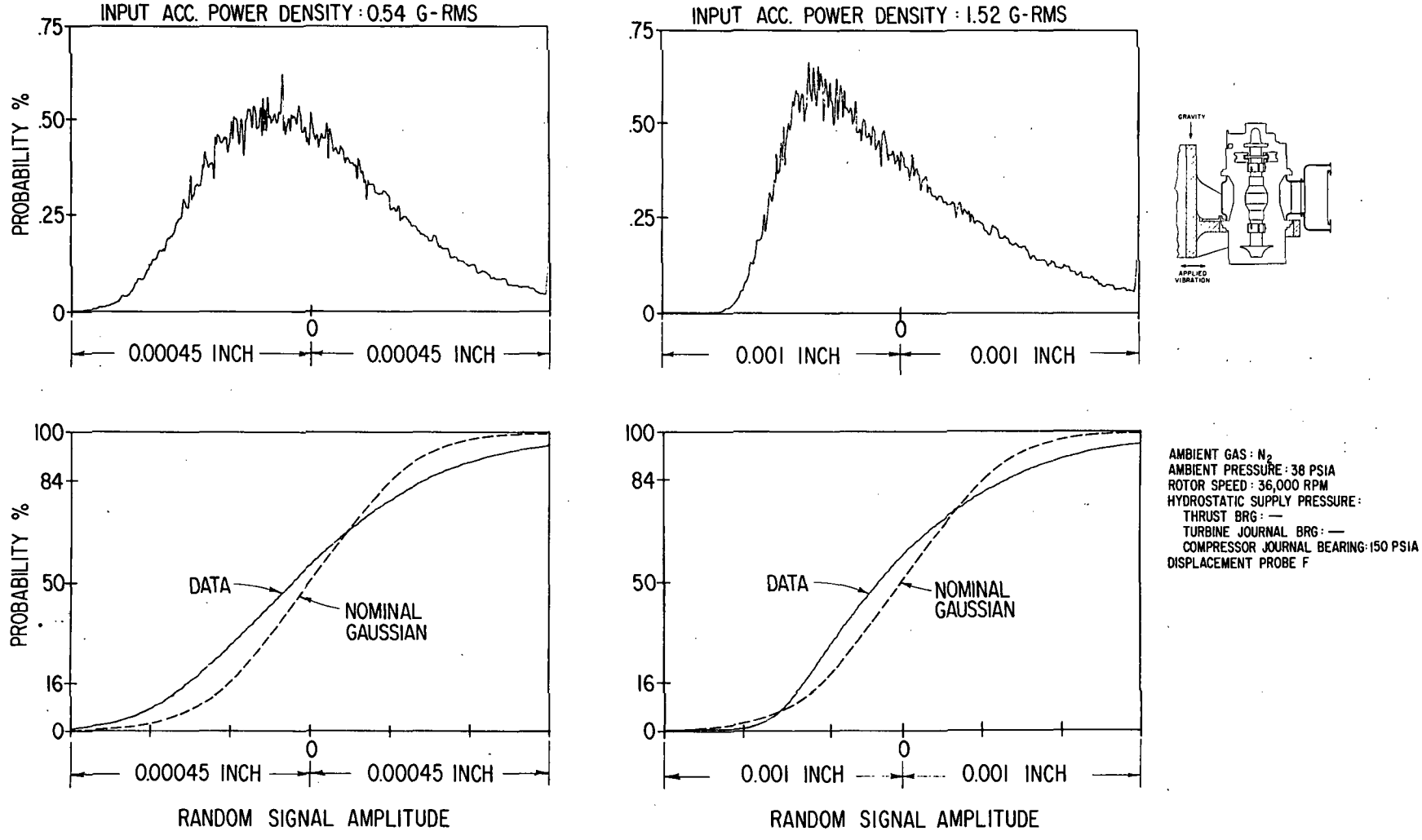

Fig. 27 Amplitude Probability Distribution Of Pad-To-Shaft Pivot Film Thickness Variation For Solid-Mounted Turbine Journal Bearing Pad Under Externally-Imposed Shaped Random Vibrations According To NASA Spec 417-2-C-3.5

MTI-14078

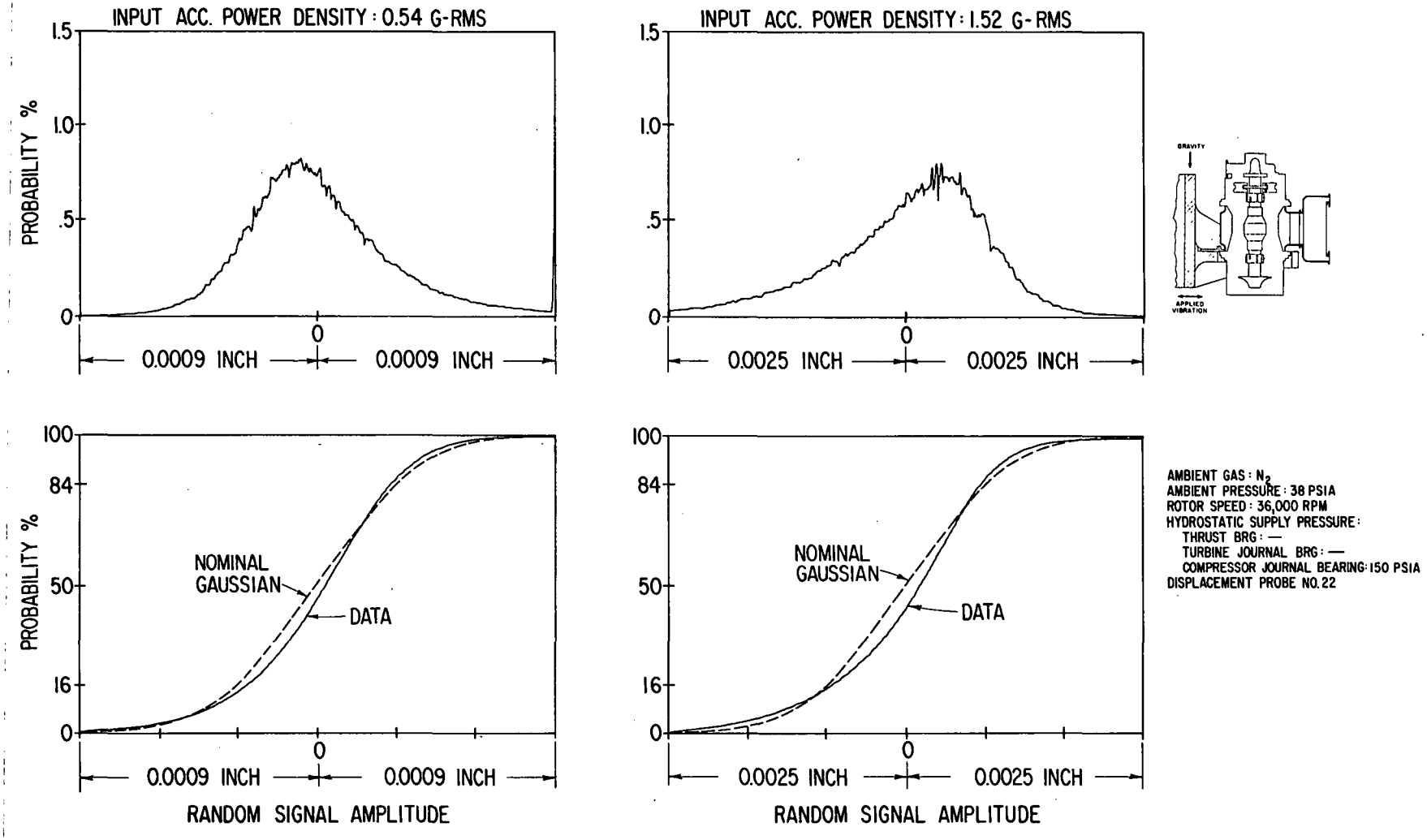

Fig. 28 Amplitude Probability Distribution Of Compressor Journal Flexure Amplitudes Under Externally-Imposed Shaped Random Vibrations According To NASA Spec 417-2-C-3.5

MTI-14040

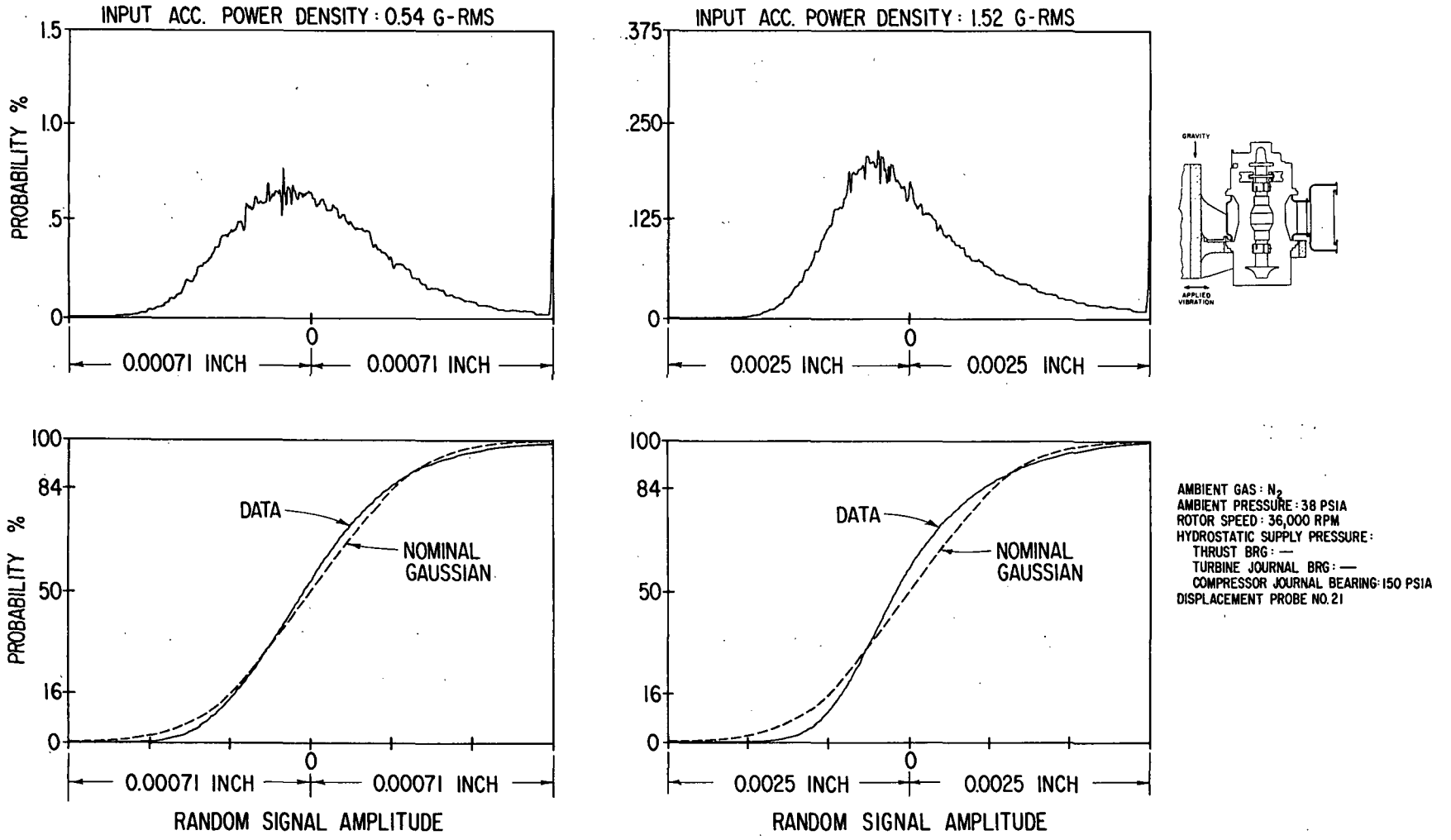

Fig. 29 Amplitude Probability Distribution Of Turbine Journal Flexure Amplitudes Under Externally-Imposed Shaped Random Vibrations According To NASA Spec 417-2-C-3.5

MTI-14041

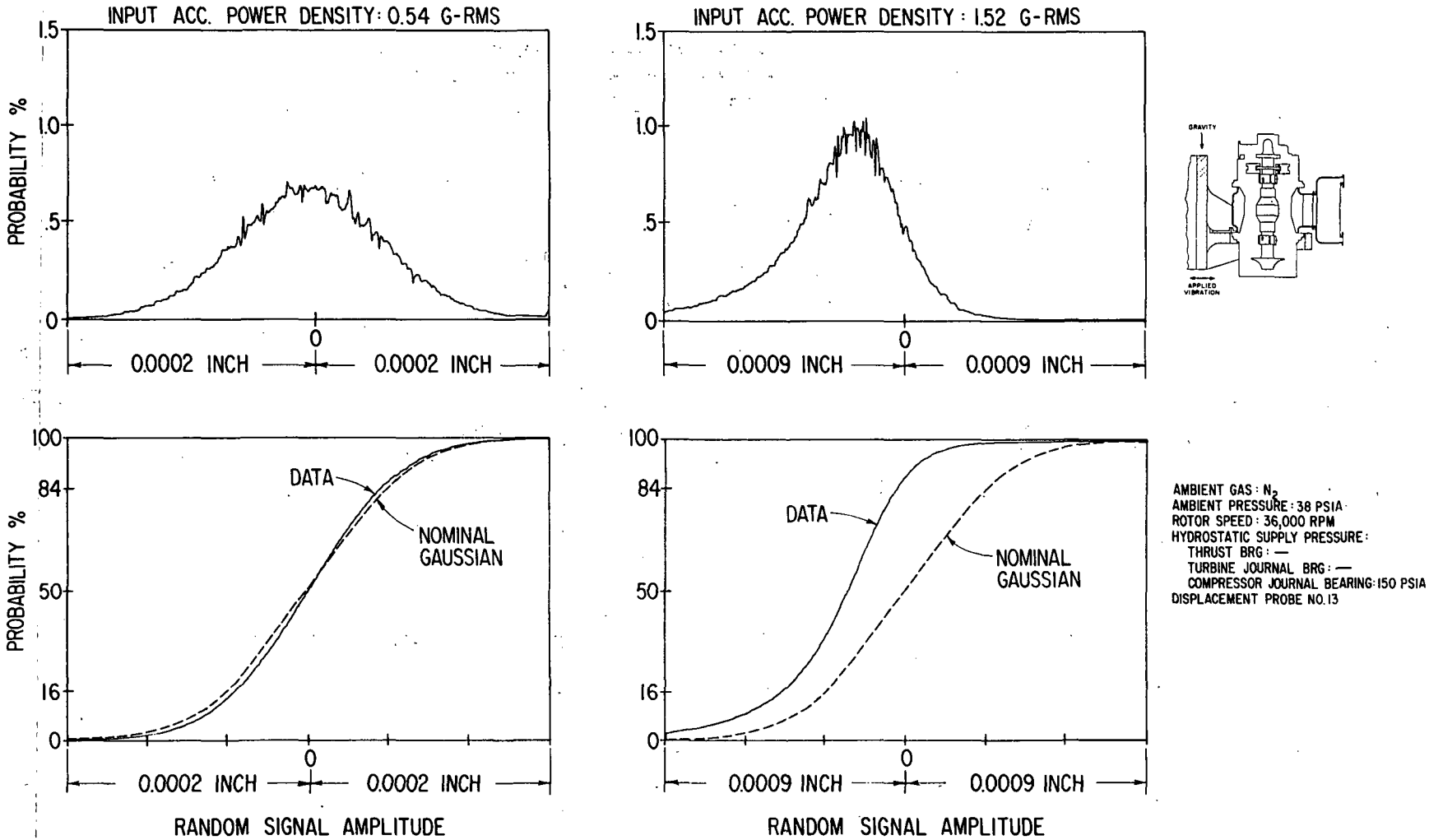

Fig. 30 Amplitude Probability Distribution Of Casing-To-Pad Leading Edge Amplitudes For Flex-Mounted Turbine Journal Bearing Pad Under Externally-Imposed Shaped Random Vibrations According To NASA Spec 417-2-C-3.5

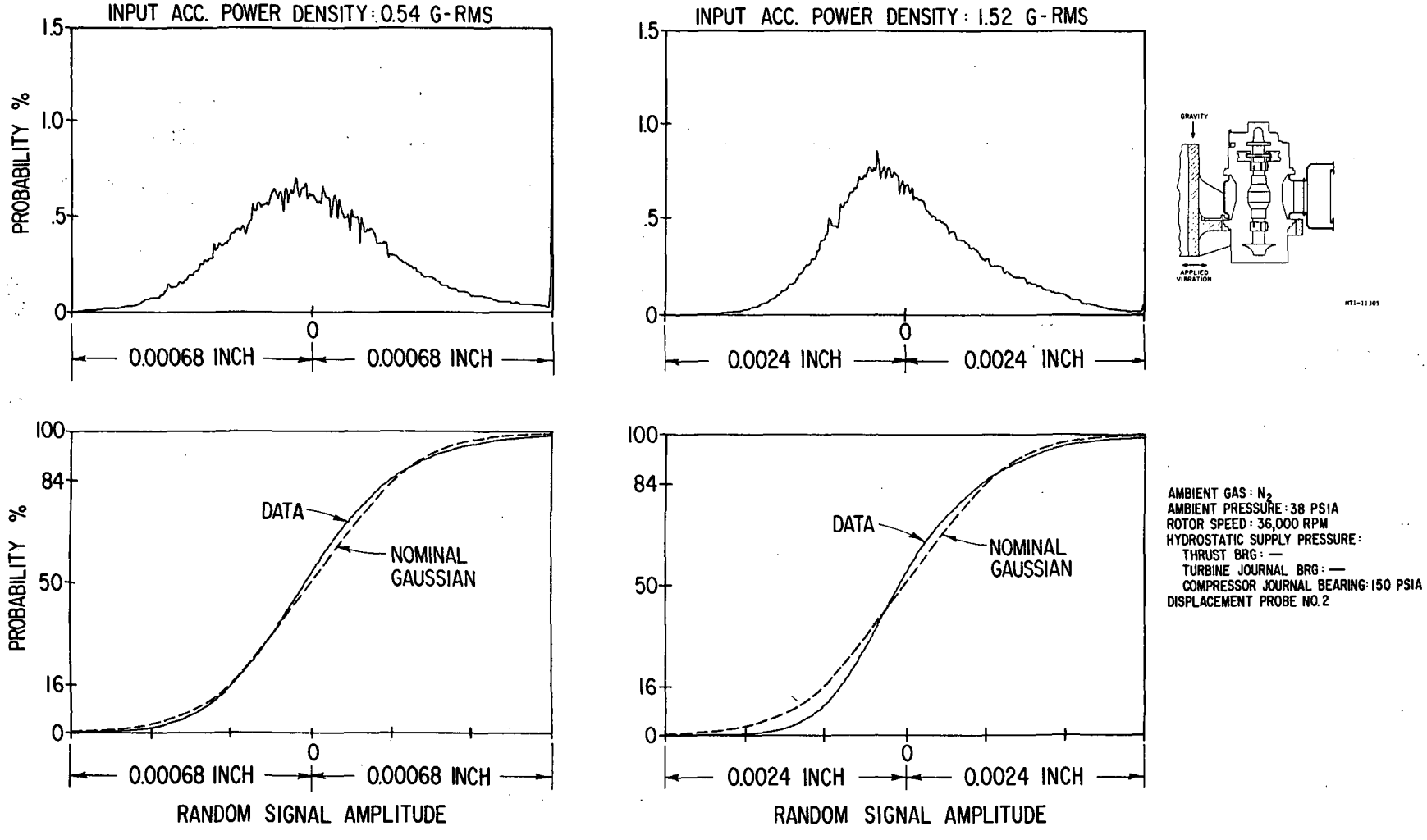

Fig. 31 Amplitude Probability Distribution Of Compressor Journal Rotor Amplitudes (Casing-To-Shaft) Under Externally-Imposed Shaped Random Vibrations According To NASA Spec 417-2-C-3.5

MTI-14043

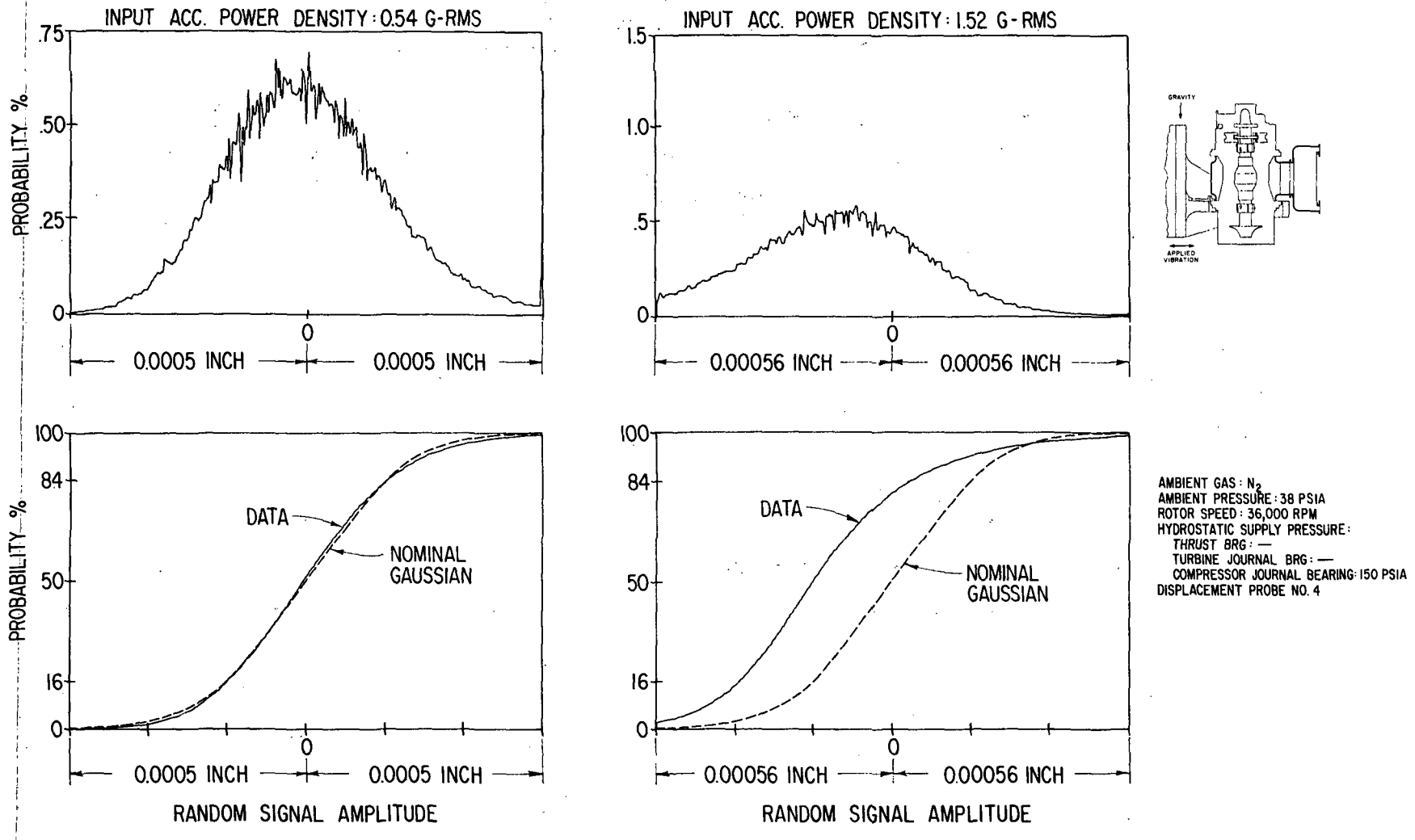

Fig. 32 Amplitude Probability Distribution Of Turbine Journal Rotor Amplitudes (Casing-To-Shaft) Under Shaped Random Vibrations *According To NASA Spec 417-2-C-3.5*

MTI-14044

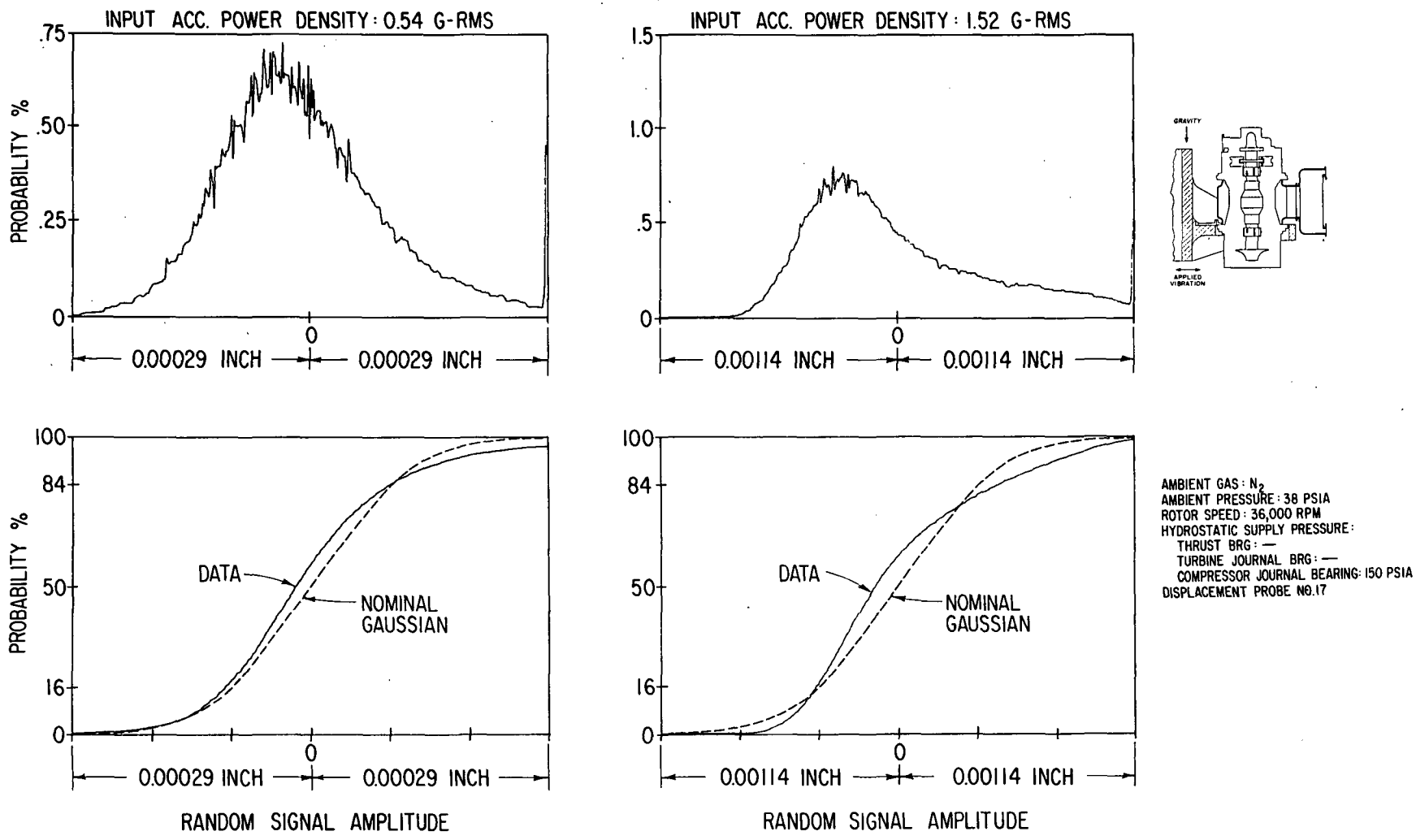

Fig. 33 Amplitude Probability Distribution Of Thrust Bearing Film Thickness Variation Under Externally-Imposed Shaped Random Vibrations According To NASA Spec 417-2-C-3.5

MTI-14079

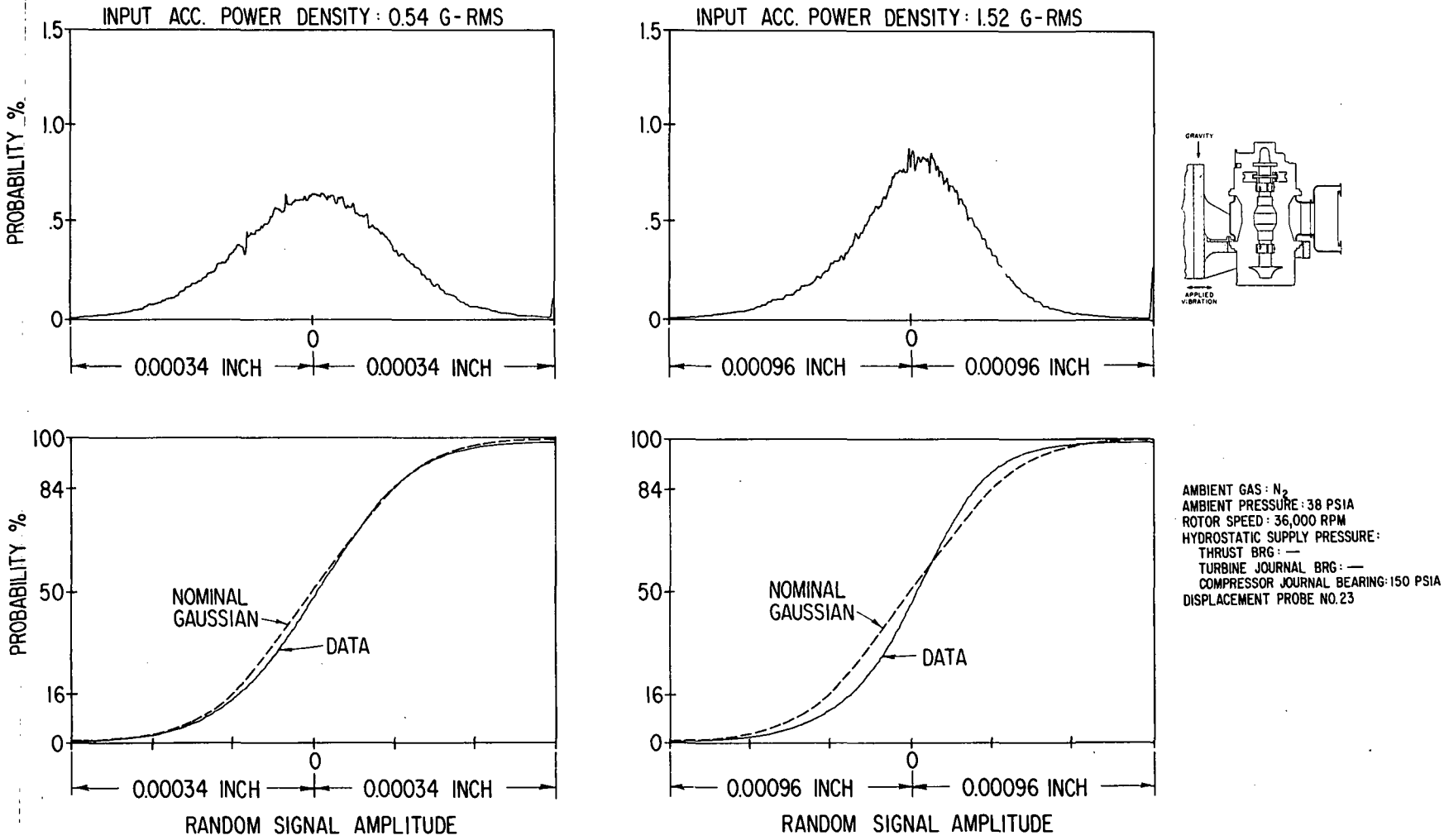

Fig. 34 Amplitude Probability Distribution Of Thrust Bearing Gimbal Amplitudes Under Externally-Imposed Shaped Random Vibrations According To NASA Spec 417-2-C-3.5

MTI-14068

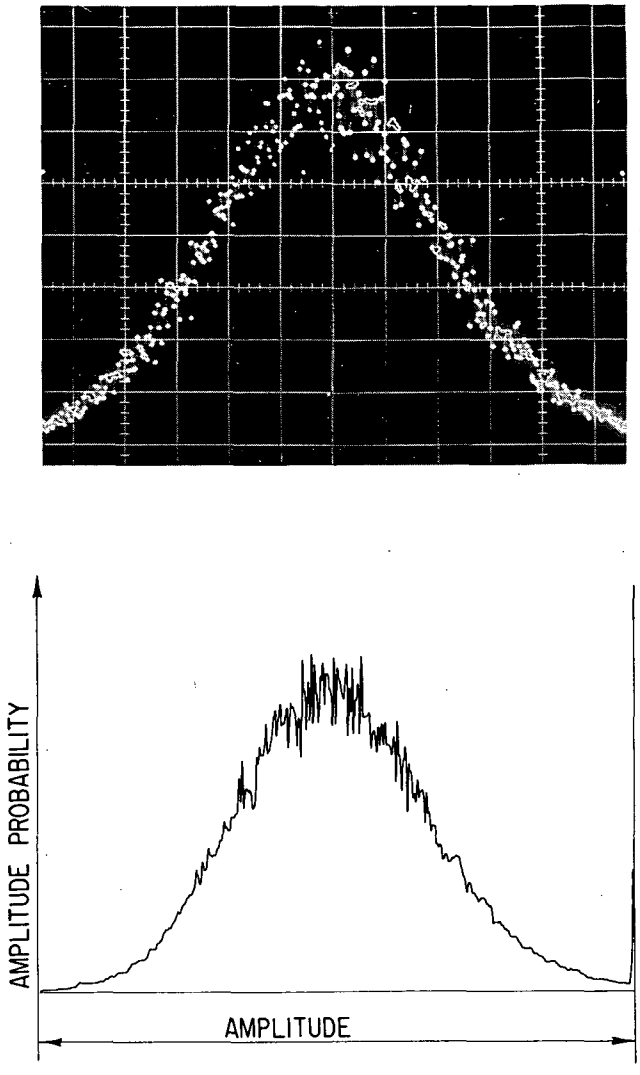

Fig. 35 Oscilloscope Display And Equivalent X-Y Recording Of A Probability Distribution (Probe C At 0.54g-rms External Vibration Input — Reference 1, Figure 79)

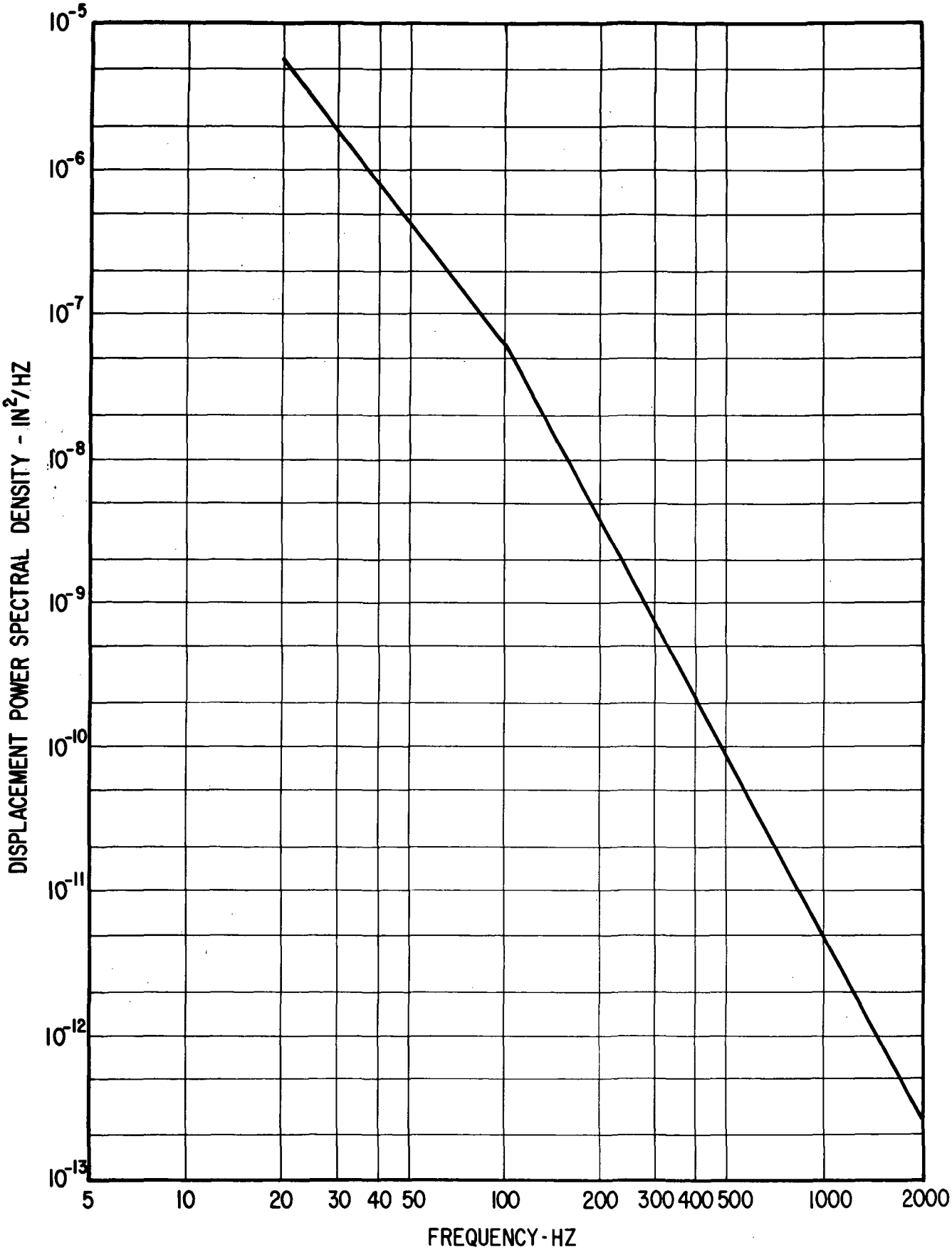

Fig. 36 Random Vibration Displacement Power Spectral Density Test Specification 417-2 (Rev. C) For Electrical Generating System Components (Operating) During Space Flight Operation

MTI-14051

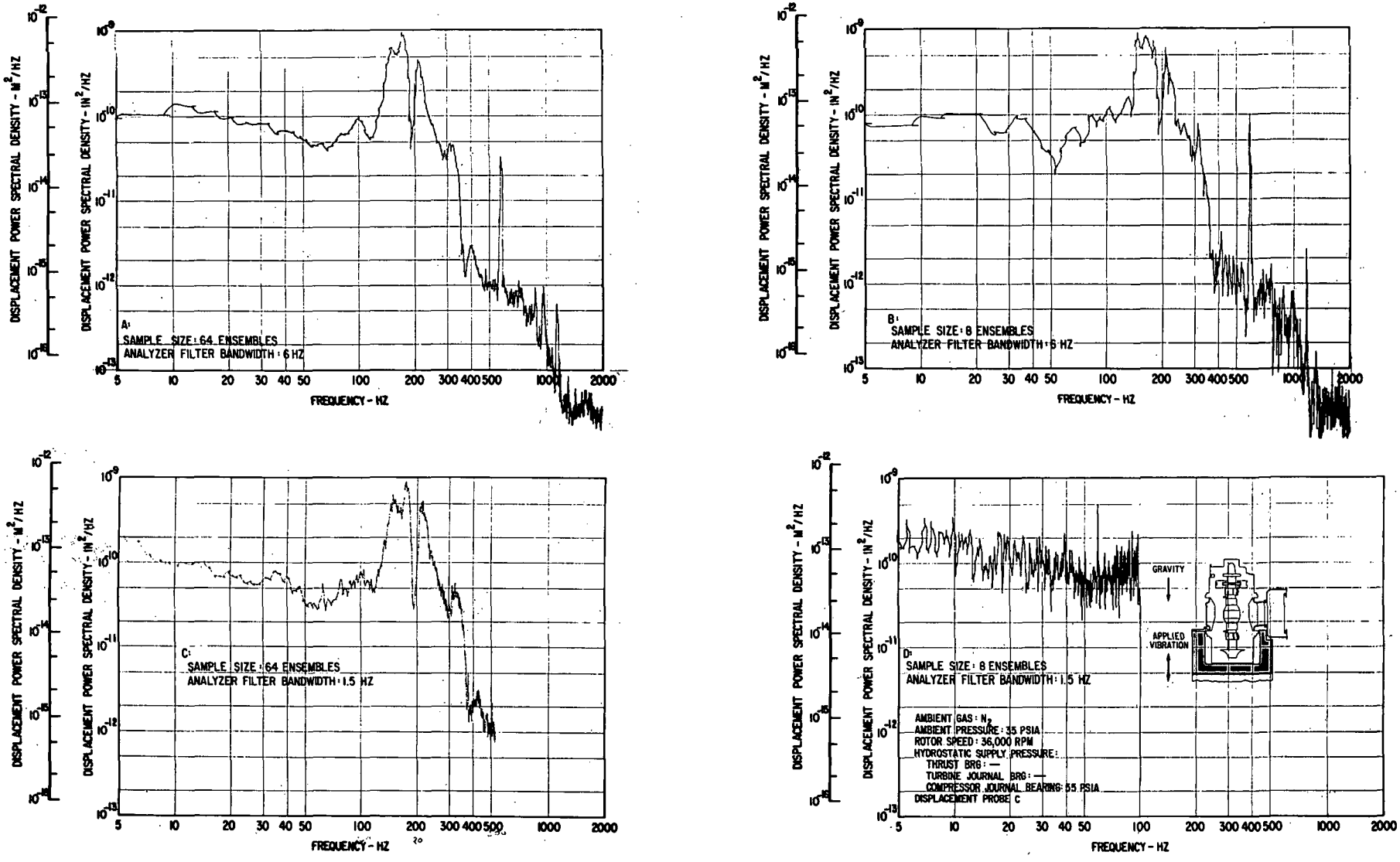

Fig. 37 Frequency Distributions Obtained With 6, 1.5 And 0.3 Hz Bandwidth For 64 And 8 Ensembles Of Pad-To-Shaft Film Thickness Variation Measurements For The Solid-Mounted Compressor Journal Bearing Pad Under Externally-Imposed Shaped Random Vibrations (1.52 g rms Input) According To NASA Spec 417-2-C-3.5

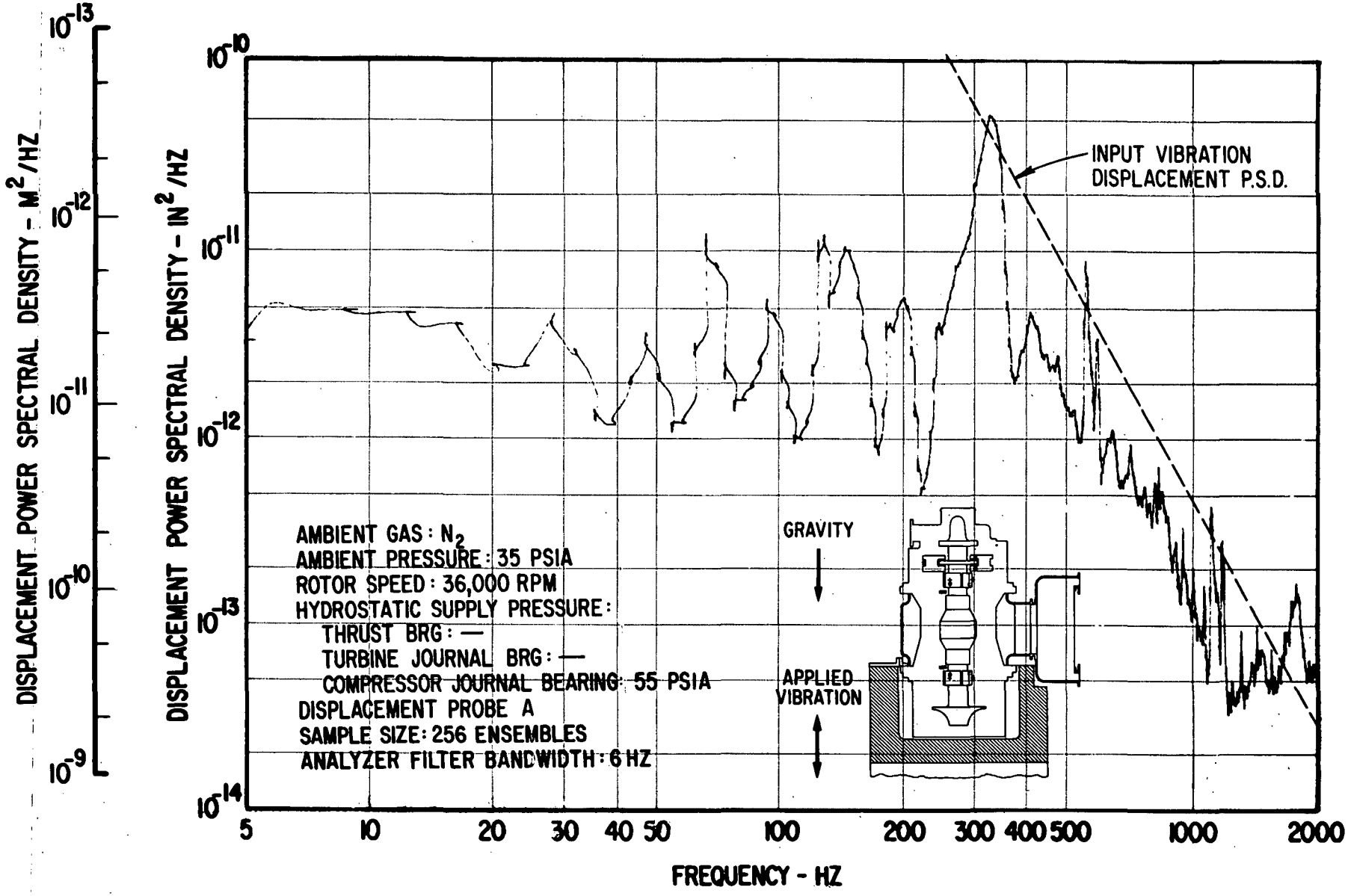

Fig. 38 Frequency Distribution (5 - 2000 Hz) Of Pad-To-Shaft Pivot Film Thickness Variation For Flex-Mounted Compressor Journal Bearing Pad Under Externally-Imposed Shaped Random Vibrations (1.52 g rms Input) According To NASA Spec 417-2-C-3.5

MTI-13680

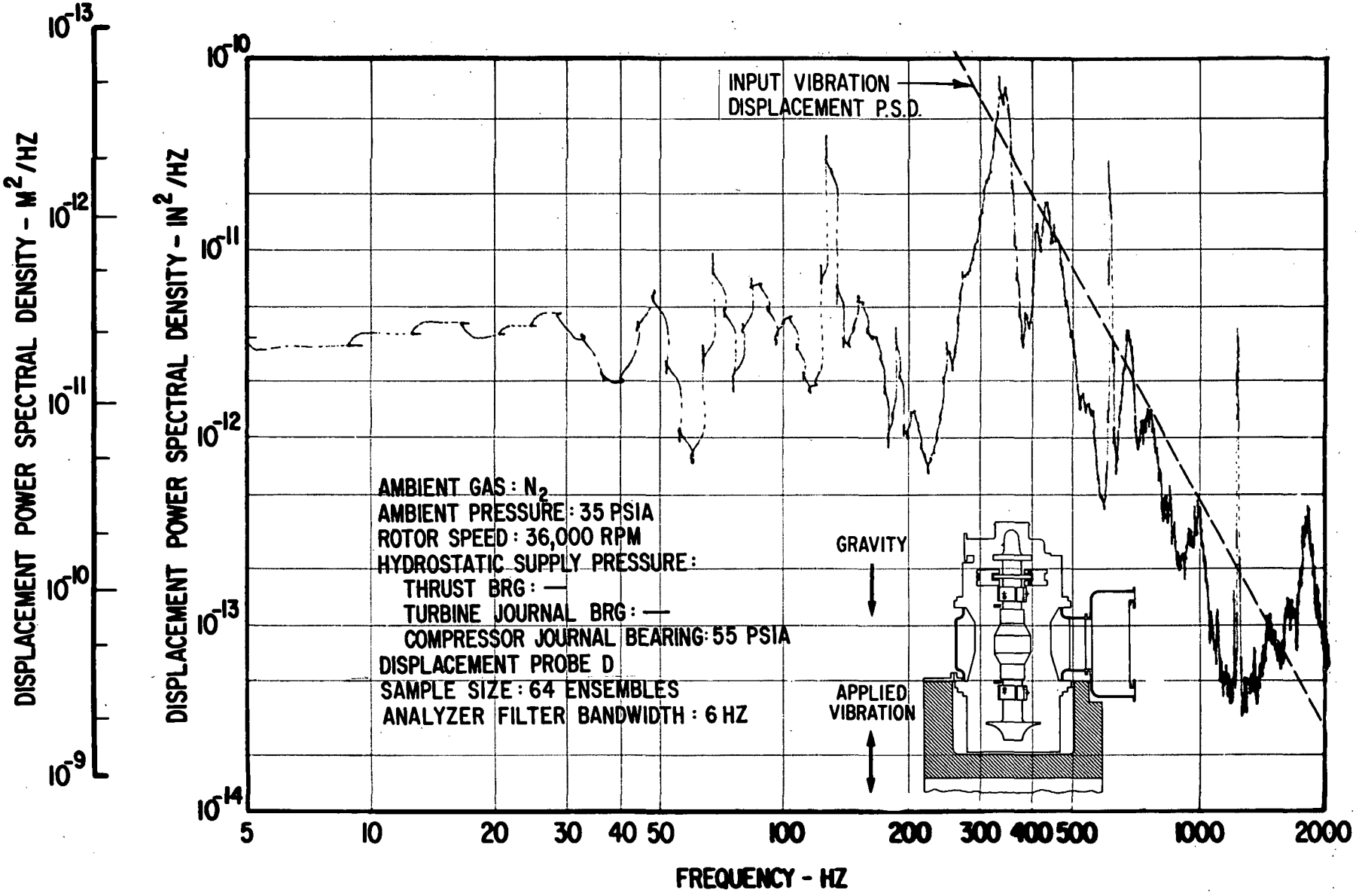

Fig. 39 Frequency Distribution (5 - 2000 Hz) Of Pad-To-Shaft Pivot Film Thickness Variation For Flex-Mounted Turbine Journal Bearing Pad Under Externally-Imposed Shaped Random Vibrations (1.52 g rms Input) According To NASA Spec 417-2-C-3.5

MTI-13681

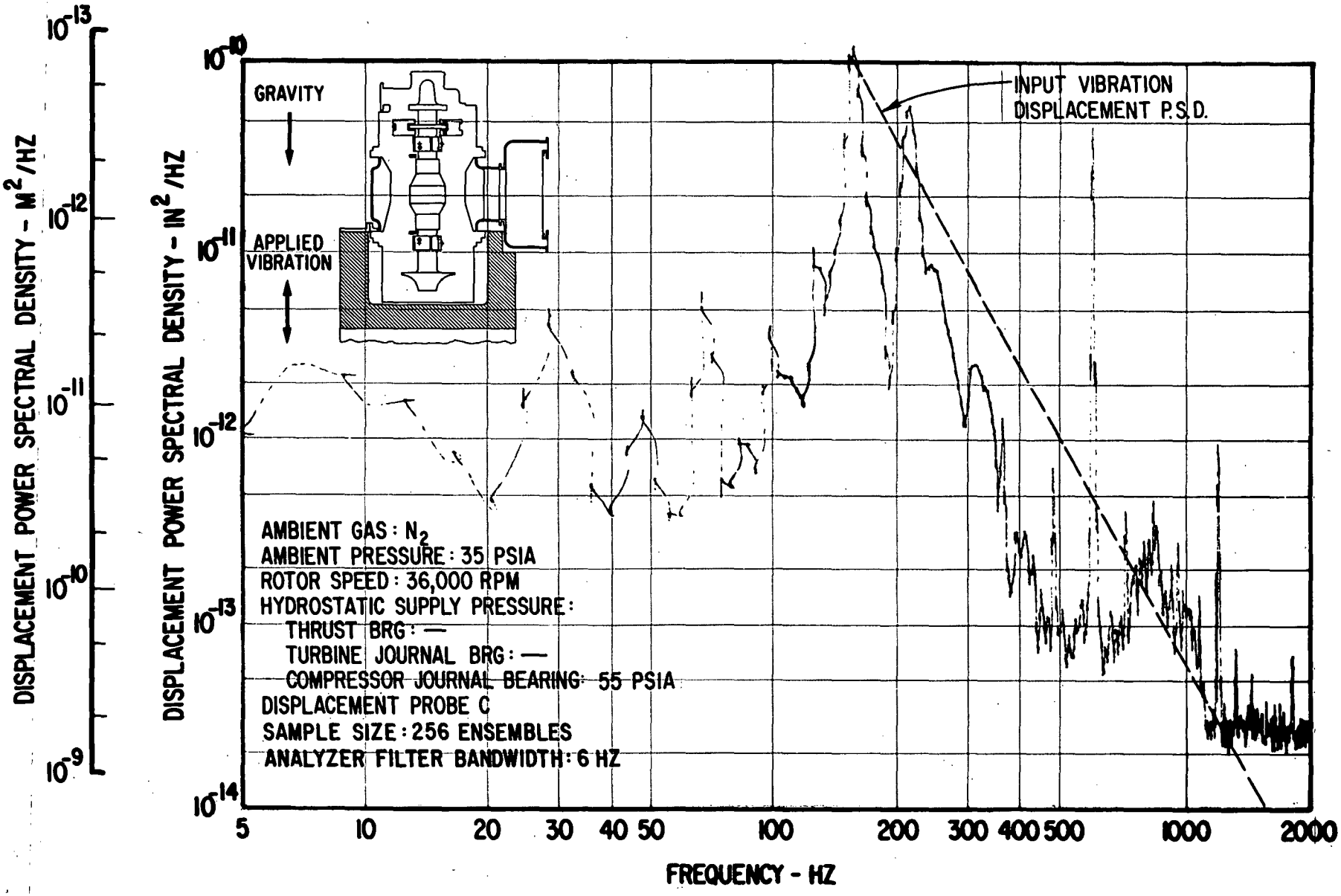

Fig. 40 Frequency Distribution (5 - 2000 Hz) Of Pad-To-Shaft Pivot Film Thickness Variation For Solid-Mounted Compressor Journal Bearing Pad Under Externally-Imposed Shaped Random Vibrations (0.54 g rms Input) According To NASA Spec 417-2-C-3.5

MTI-14054

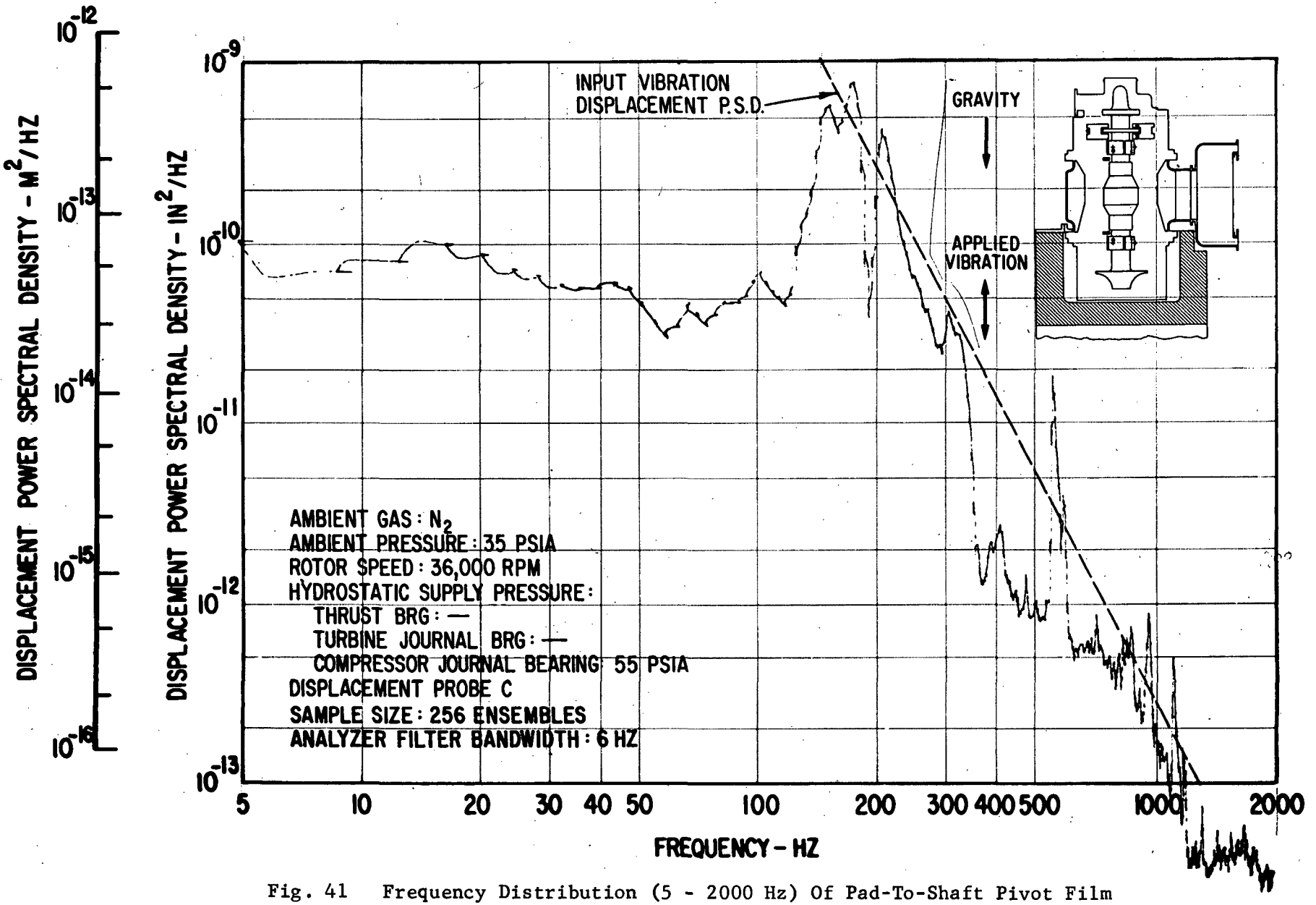

Fig. 41 Frequency Distribution (5 - 2000 Hz) Of Pad-To-Shaft Pivot Film Thickness Variation For Solid-Mounted Compressor Journal Bearing Pad Under Externally-Imposed Shaped Random Vibrations (1.52 g rms Input) According To NASA Spec 417-2-C-3.5

MTI-14037

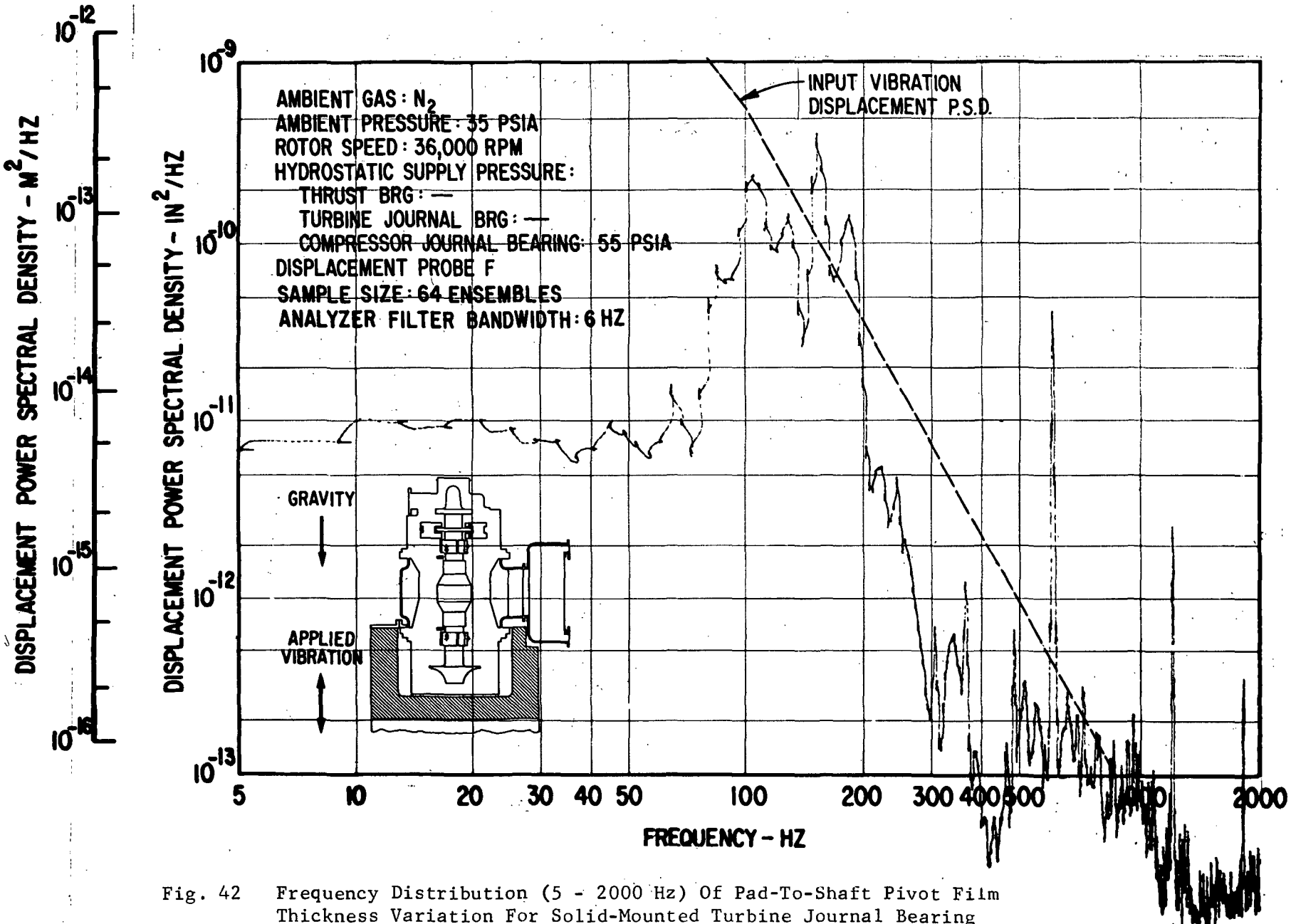

Fig. 42 Frequency Distribution (5 - 2000 Hz) Of Pad-To-Shaft Pivot Film Thickness Variation For Solid-Mounted Turbine Journal Bearing Pad Under Externally-Imposed Shaped Random Vibrations (0.54 g rms Input) According To NASA Spec 417-2-C-3.5

MTI-14074

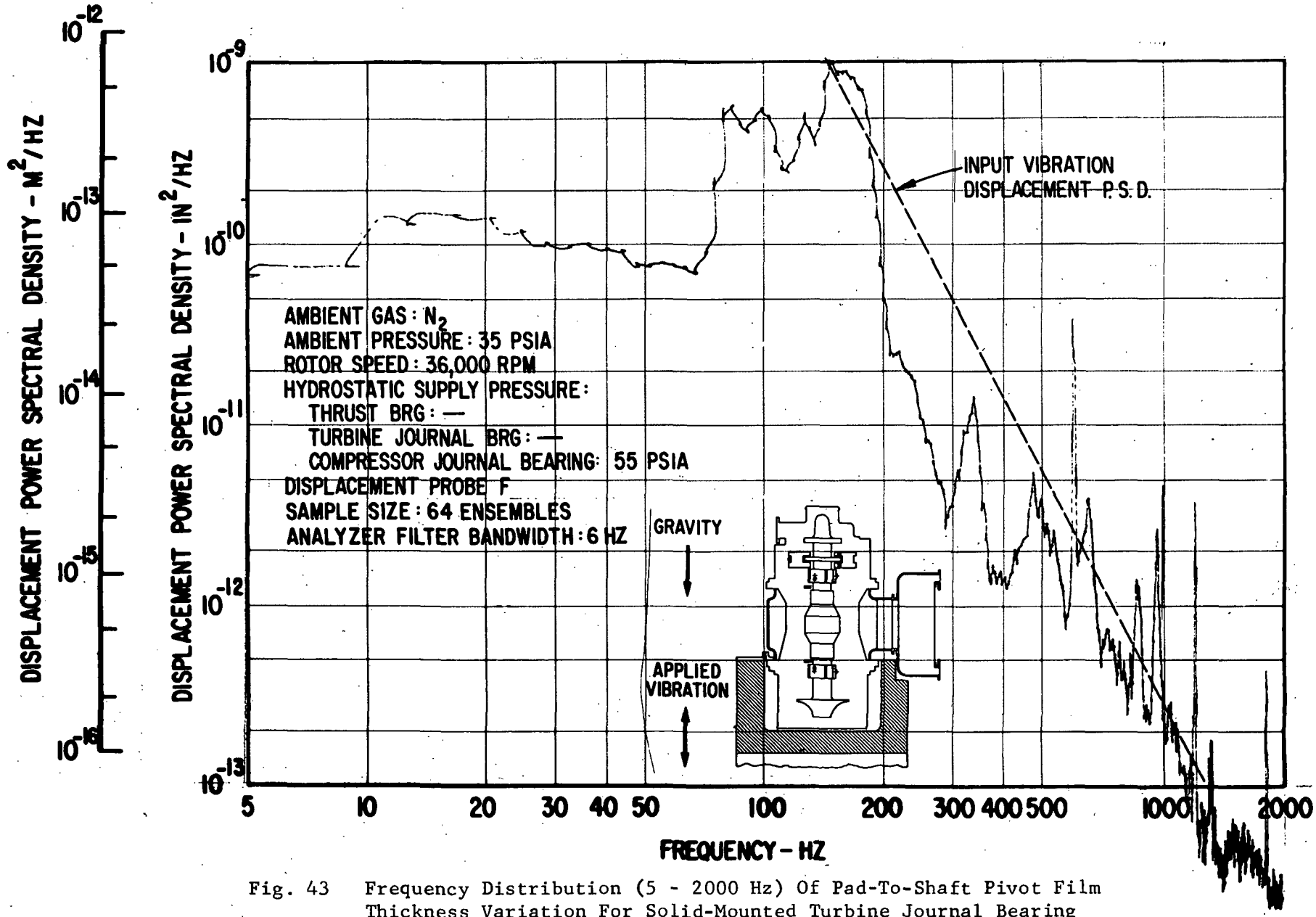

Fig. 43 Frequency Distribution (5 - 2000 Hz) Of Pad-To-Shaft Pivot Film Thickness Variation For Solid-Mounted Turbine Journal Bearing Pad Under Externally-Imposed Shaped Random Vibrations (1.52 g rms Input) According To NASA Spec 417-2-C-3.5

MTI-14039

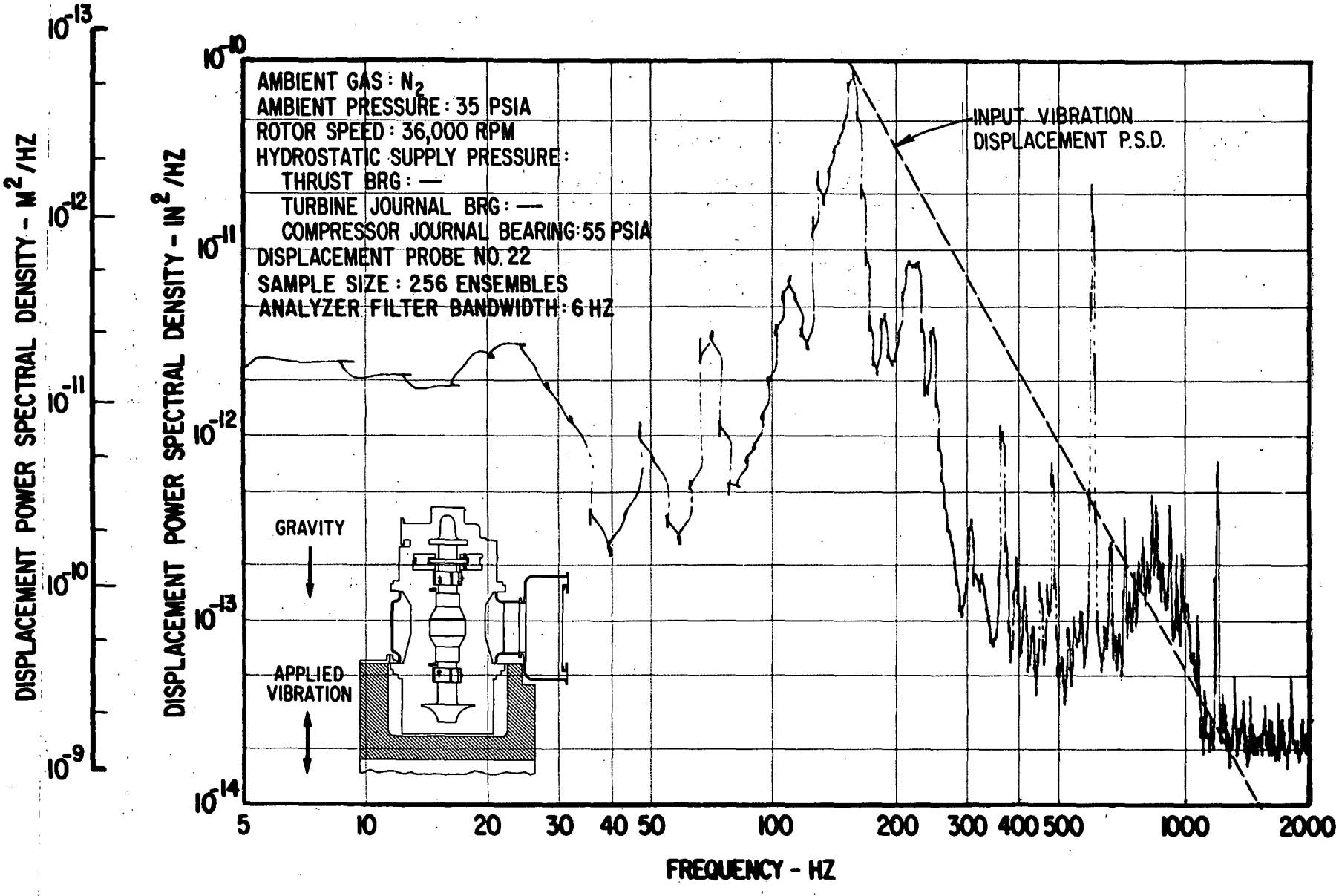

Fig. 44 Frequency Distribution (5 - 2000 Hz) Of Compressor Journal Flexure Amplitudes Under Externally-Imposed Shaped Random Vibrations (0.54 g rms Input) According To NASA Spec 417-2-C-3.5

MTI-14055

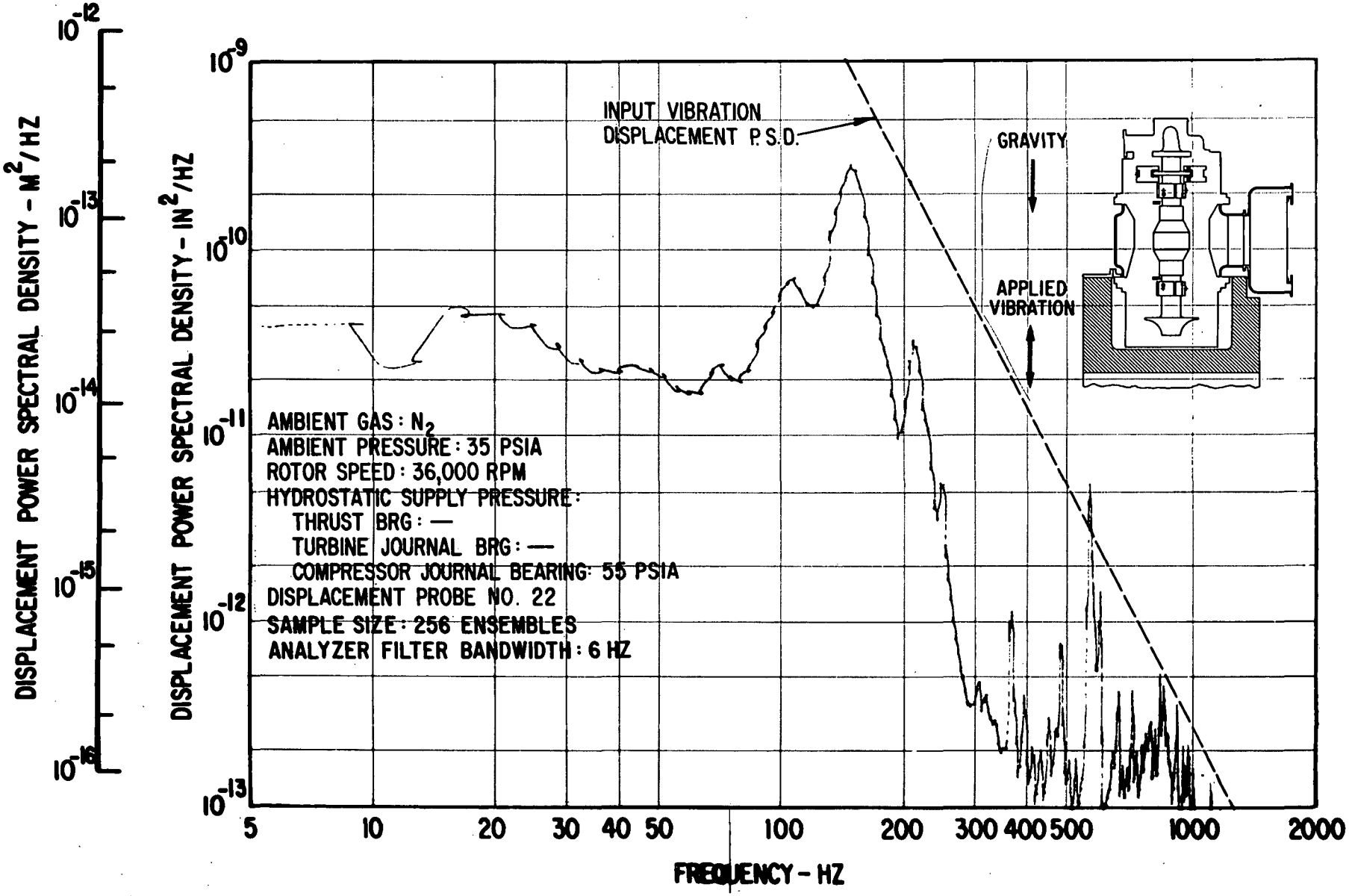

Fig. 45 Frequency Distribution (5 - 2000 Hz) Of Compressor Journal Flexure Amplitudes Under Externally-Imposed Shaped Random Vibrations (1.52 g rms Input) According To NASA Spec 417-2-C-3.5

MTI-14026

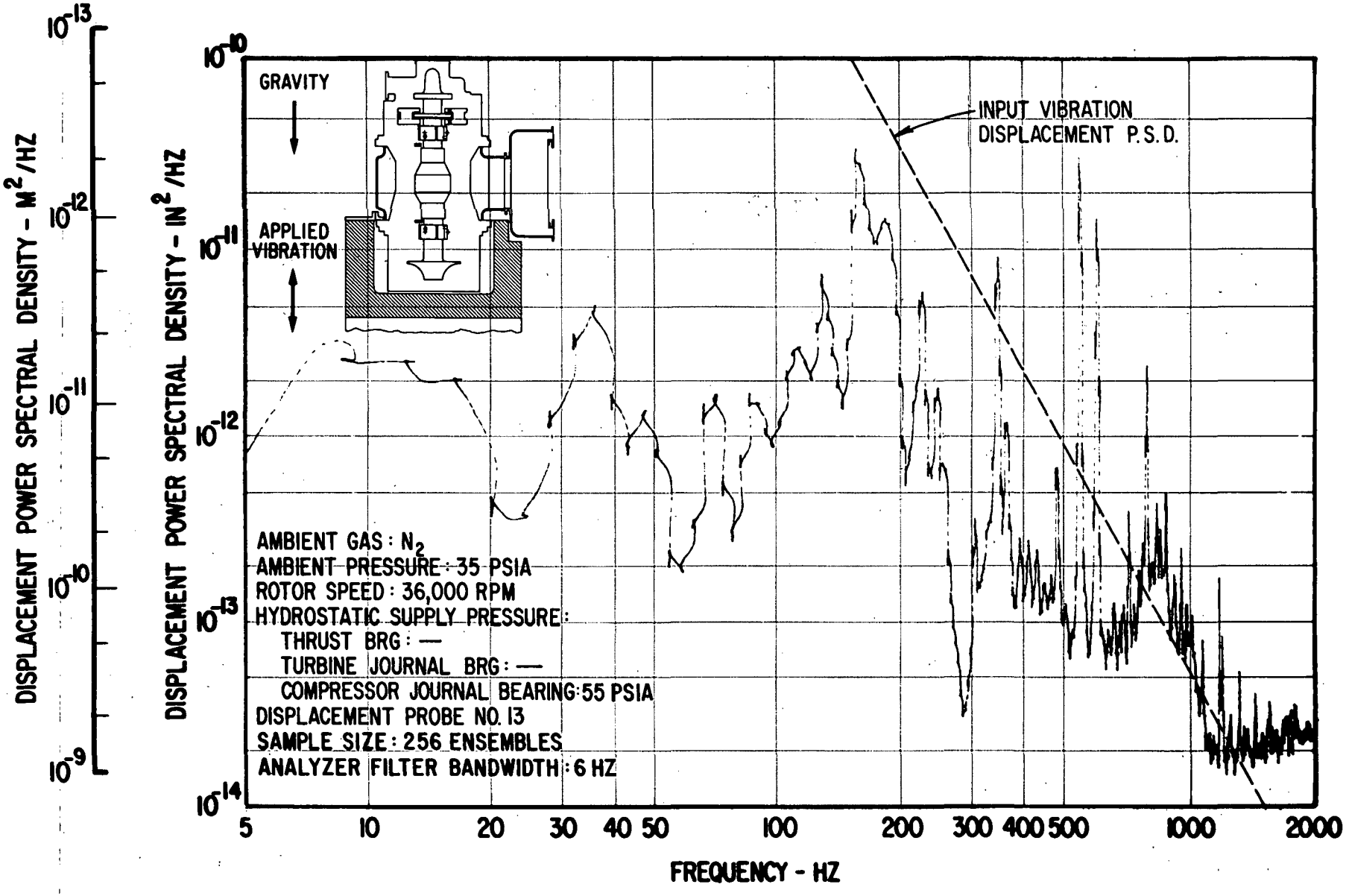

Fig. 46 Frequency Distribution (5 - 2000 Hz) Of Casing-To-Pad Leading Edge Amplitudes For Flex-Mounted Turbine Journal Bearing Pad Under Externally-Imposed Shaped Random Vibrations (0.54 g rms Input) According To NASA Spec 417-2-C-3.5

MTI-13682

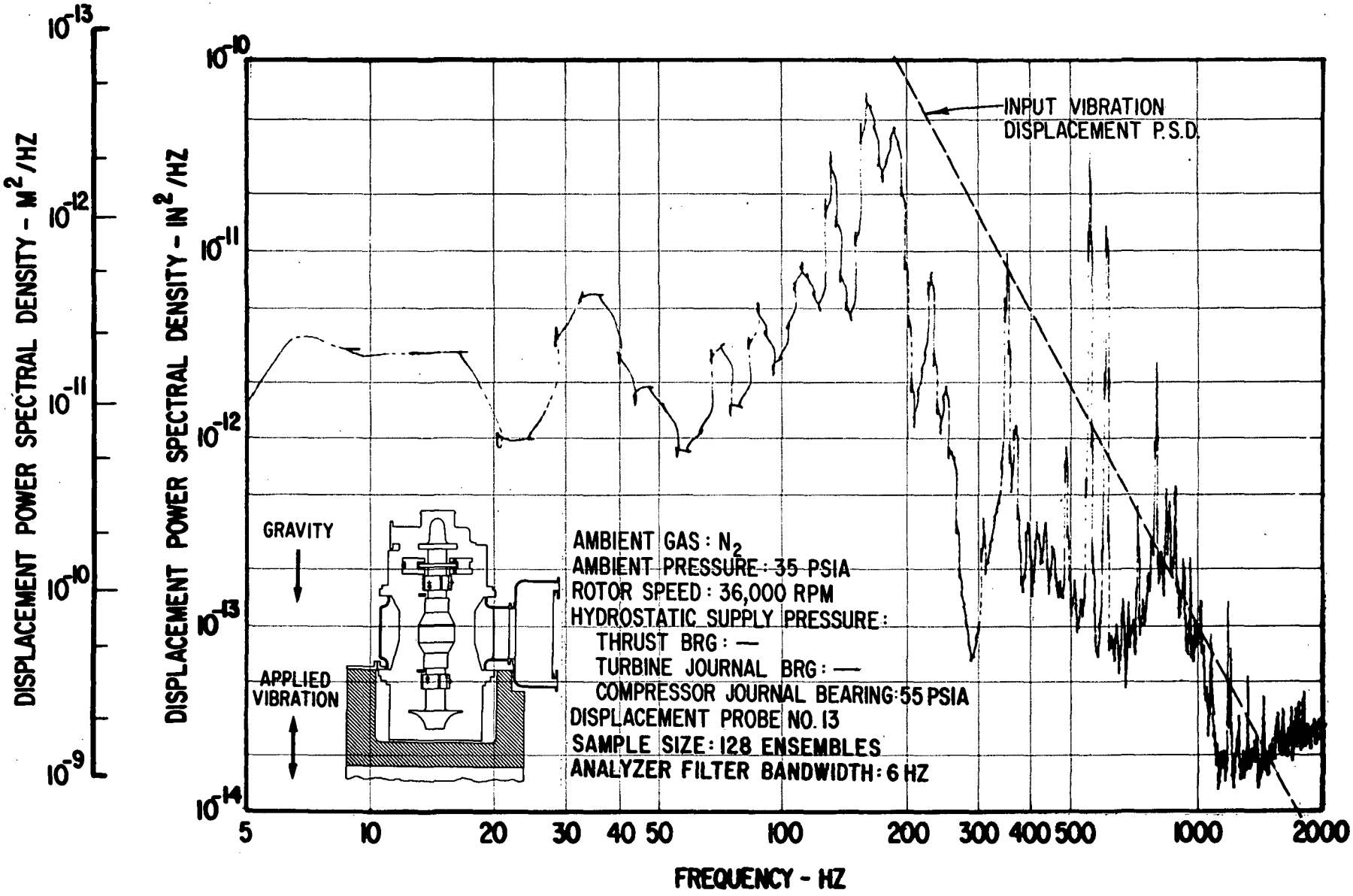

Fig. 47 Frequency Distribution (5 - 2000 Hz) Of Casing-To-Pad Leading Edge Amplitudes For Flex-Mounted Turbine Journal Bearing Pad Under Externally-Imposed Shaped Random Vibrations (0.75 g rms Input) According To NASA Spec 417-2-C-3.5

MTI-13683

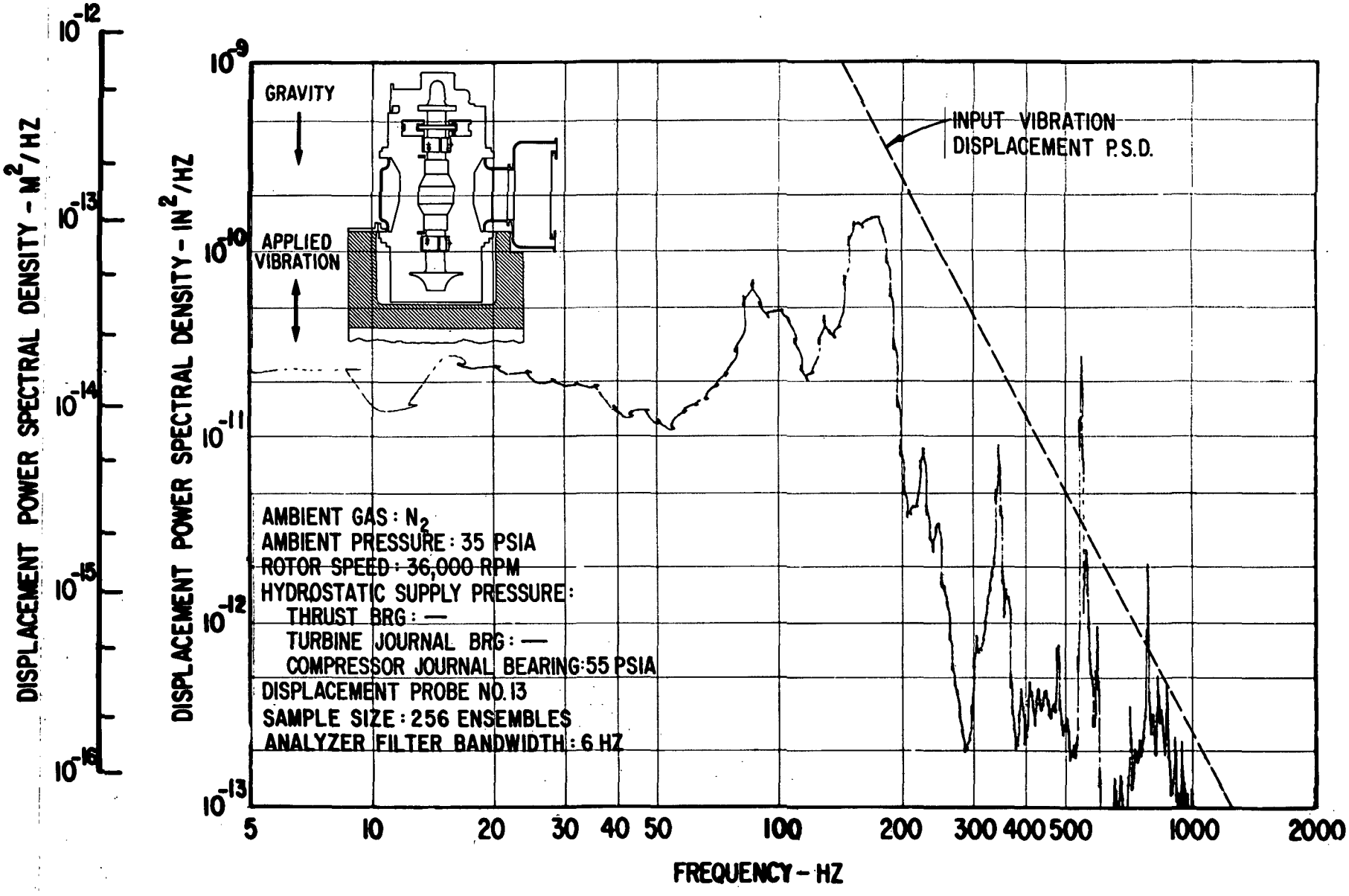

Fig. 48 Frequency Distribution (5 - 2000 Hz) Of Casing-To-Pad Leading Edge Amplitudes For Flex-Mounted Turbine Journal Bearing Pad Under Externally-Imposed Shaped Random Vibrations (1.52 g rms Input) According To NASA Spec 417-2-C-3.5

MTI-13677

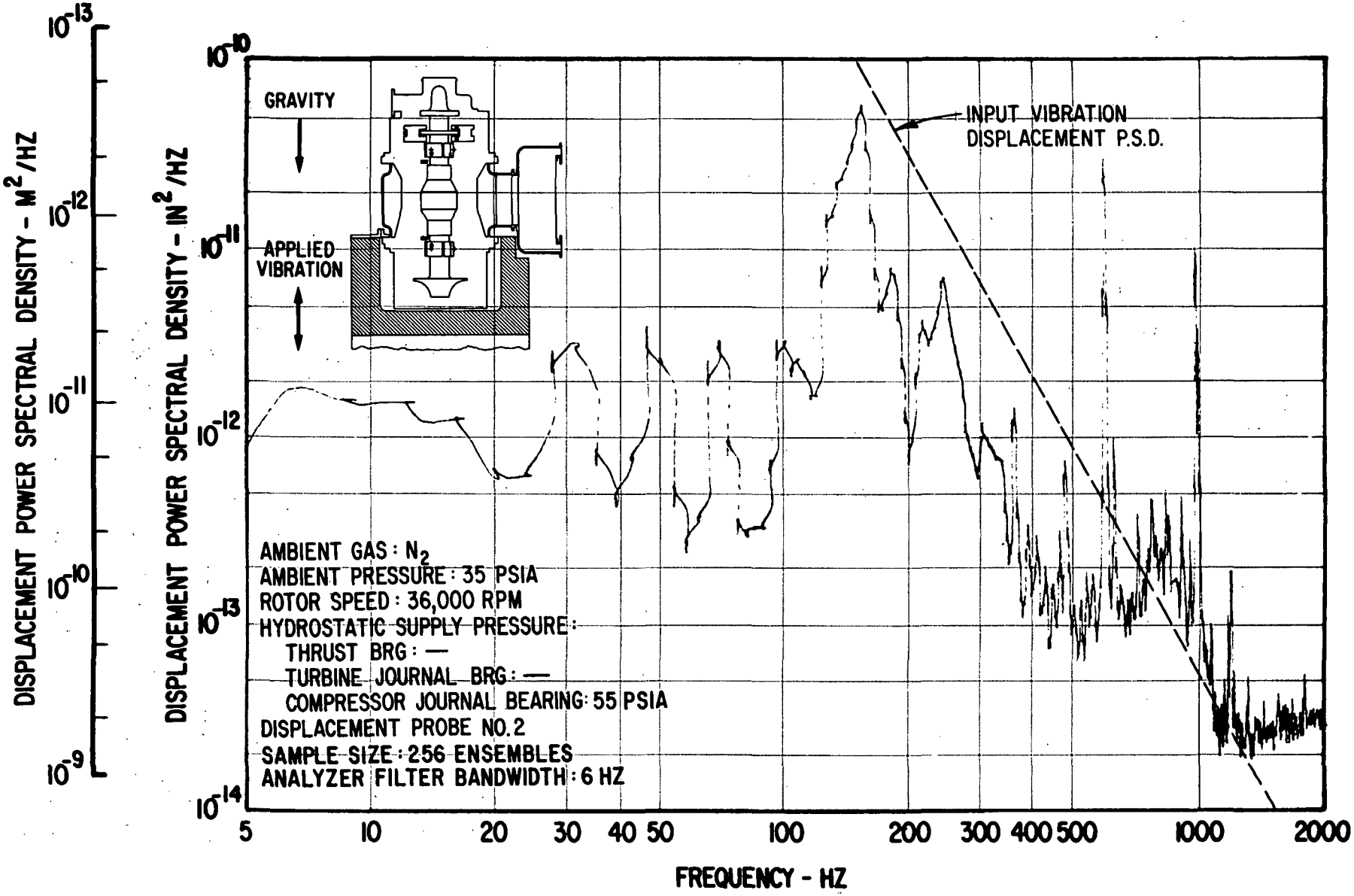

Fig. 49 Frequency Distribution (5 - 2000 Hz) Of Compressor Journal Rotor Amplitudes (Casing-To-Shaft) Under Externally-Imposed Shaped Random Vibrations (0.54 g rms Input) According To NASA Spec 417-2-C-3.5

MTI-13684

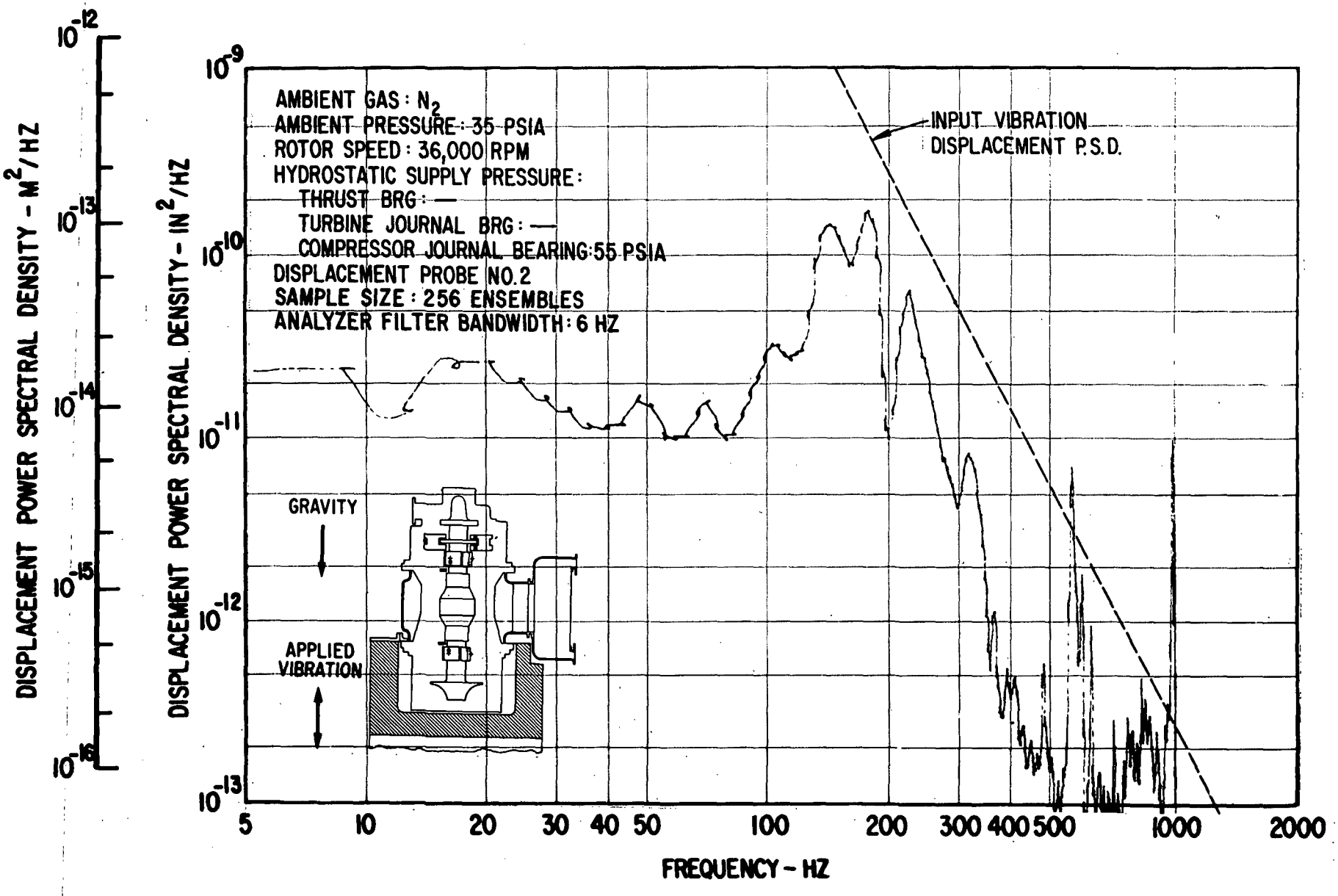

Fig. 50 Frequency Distribution (5 - 2000 Hz) Of Compressor Journal Rotor Amplitudes (Casing-To-Shaft) Under Externally-Imposed Shaped Random Vibrations (1.52 g rms Input) According To NASA Spec 417-2-C-3.5

MTI-14077

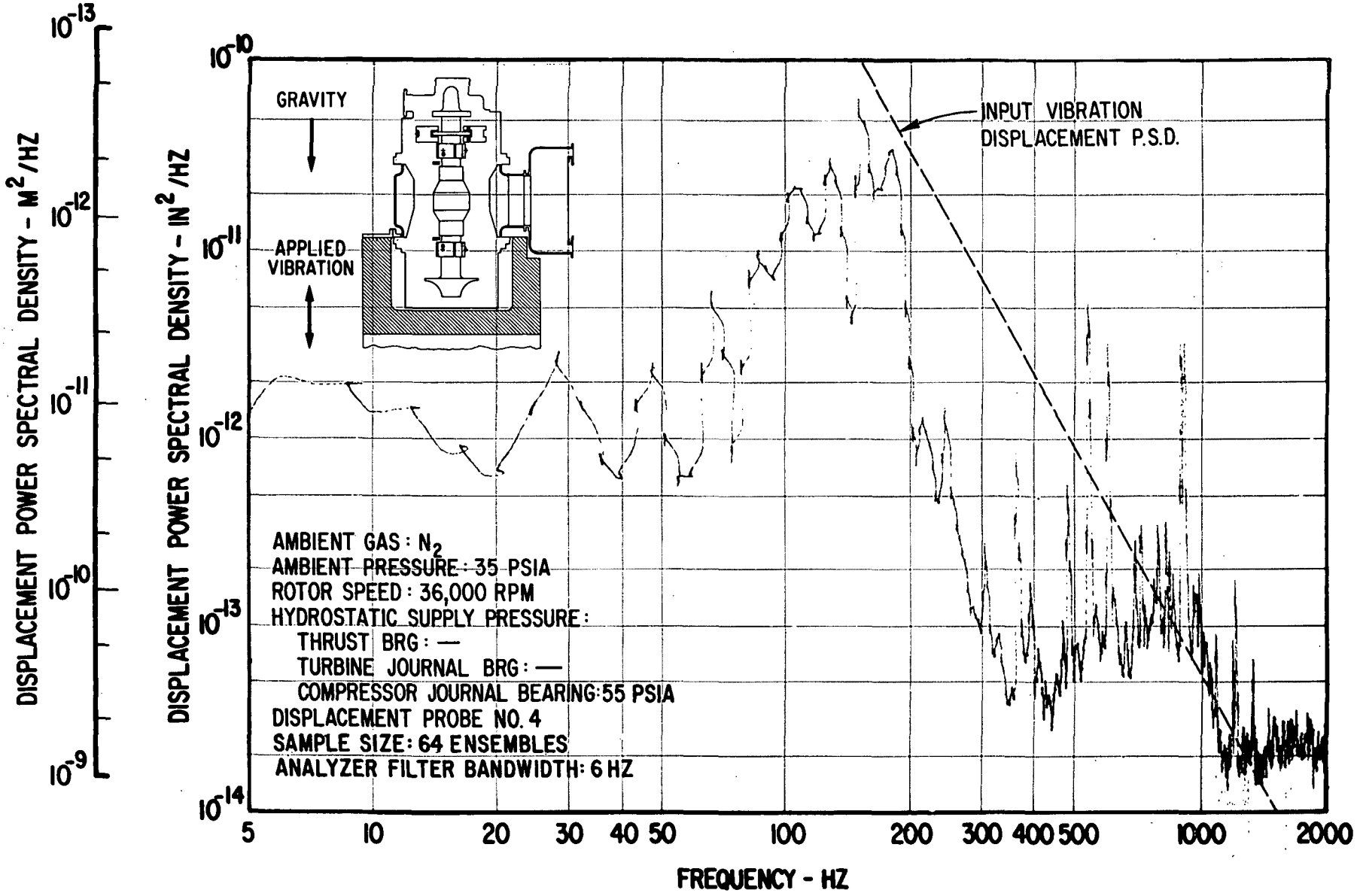

Fig. 51 Frequency Distribution (5 - 2000 Hz) Of Turbine Journal Rotor Amplitudes (Casing-To-Shaft) Under Externally-Imposed Shaped Random Vibrations (0.54 g rms Input) According To NASA Spec 417-2-C-3.5

MTI-13685

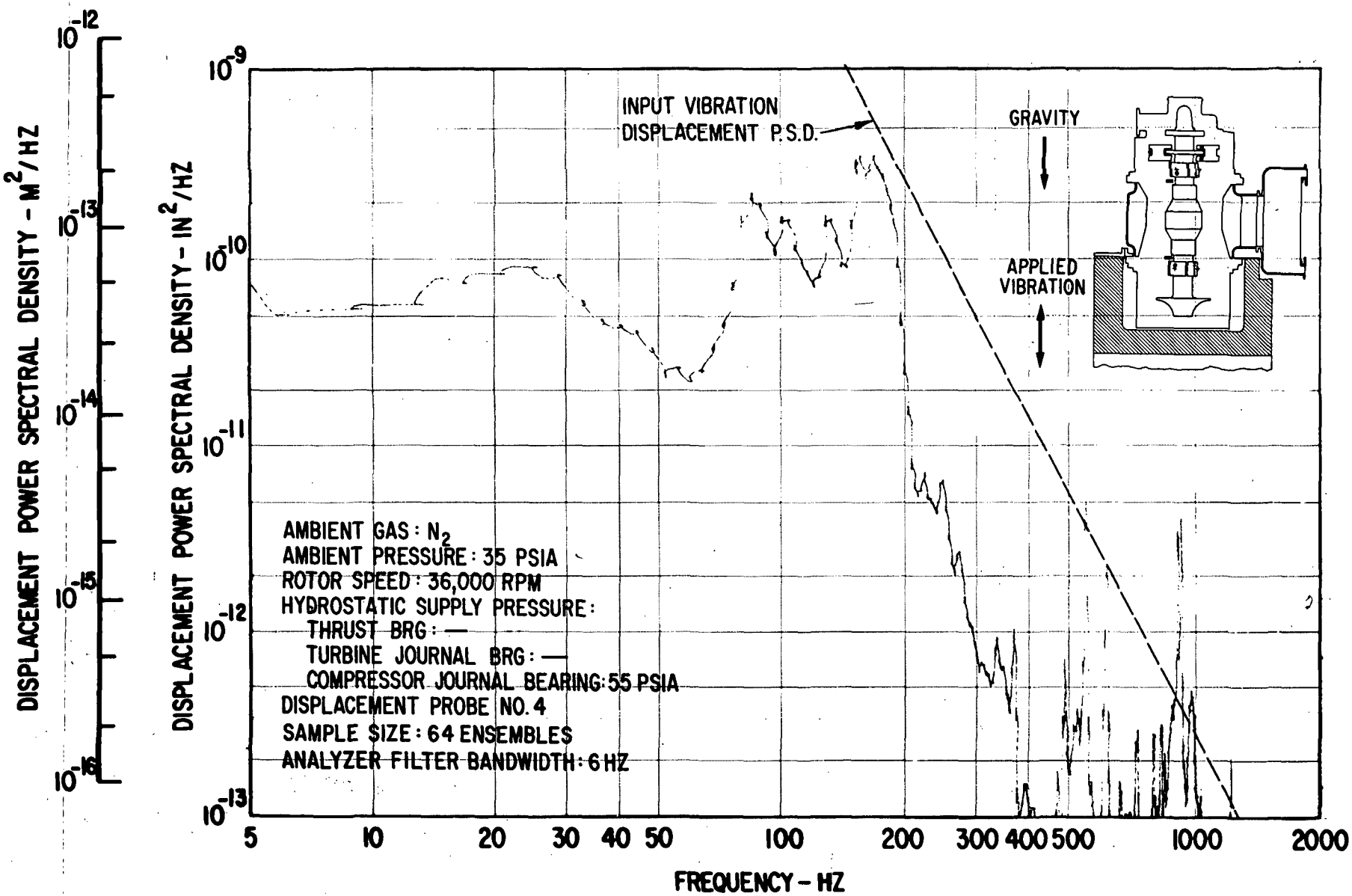

Fig. 52 Frequency Distribution (5 - 2000 Hz) Of Turbine Journal Rotor Amplitudes (Casing-To-Shaft) Under Externally-Imposed Shaped Random Vibrations (1.52 g rms Input) According To NASA Spec 417-2-C-3.5

MTI-14076

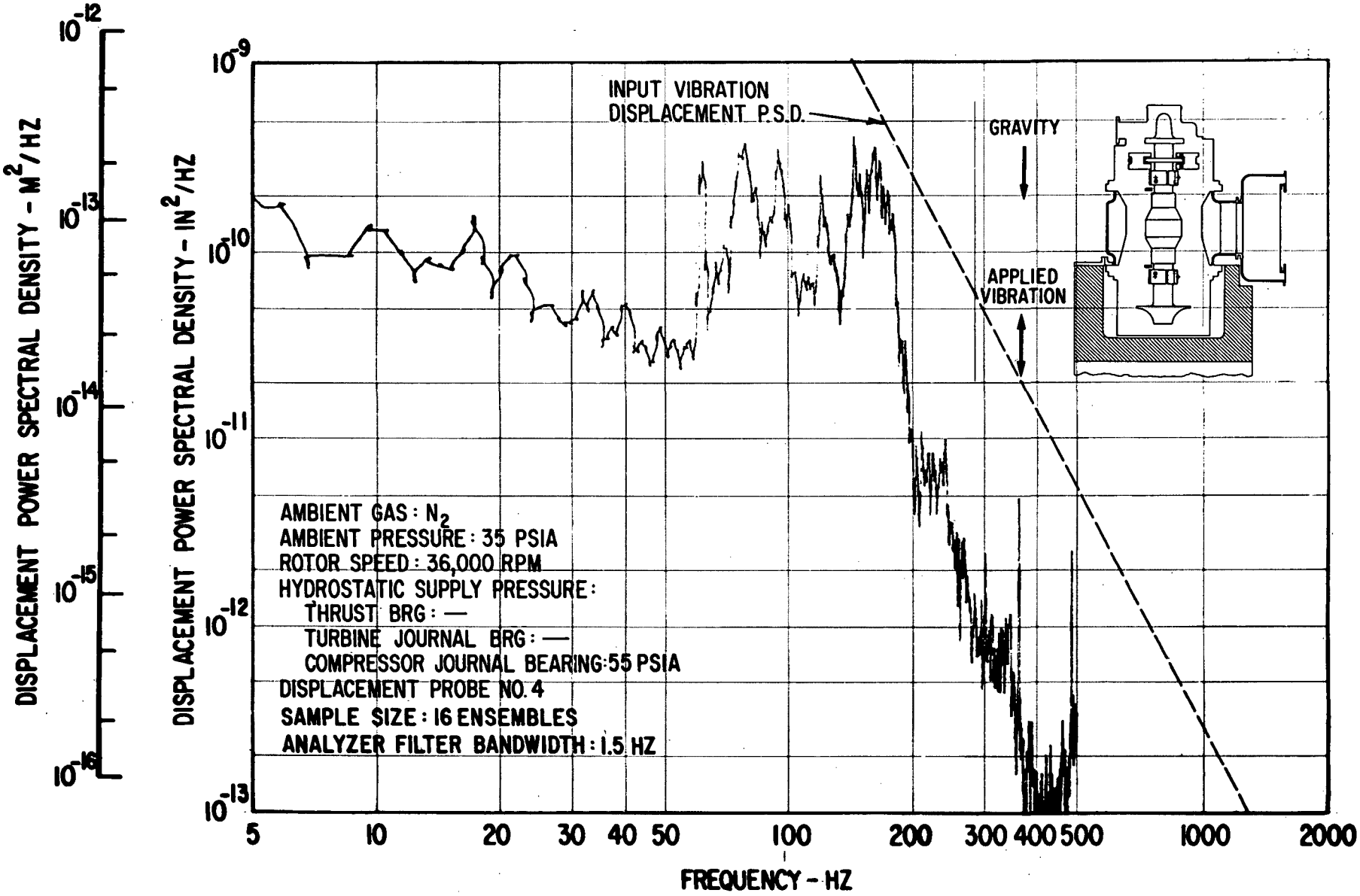

Fig. 53 Frequency Distribution (5 - 500 Hz) Of Turbine Journal Rotor Amplitudes (Casing-To-Shaft) Under Externally-Imposed Shaped Random Vibrations (1.52 g rms) According To NASA Spec 417-2-C-3.5

MTI-14038

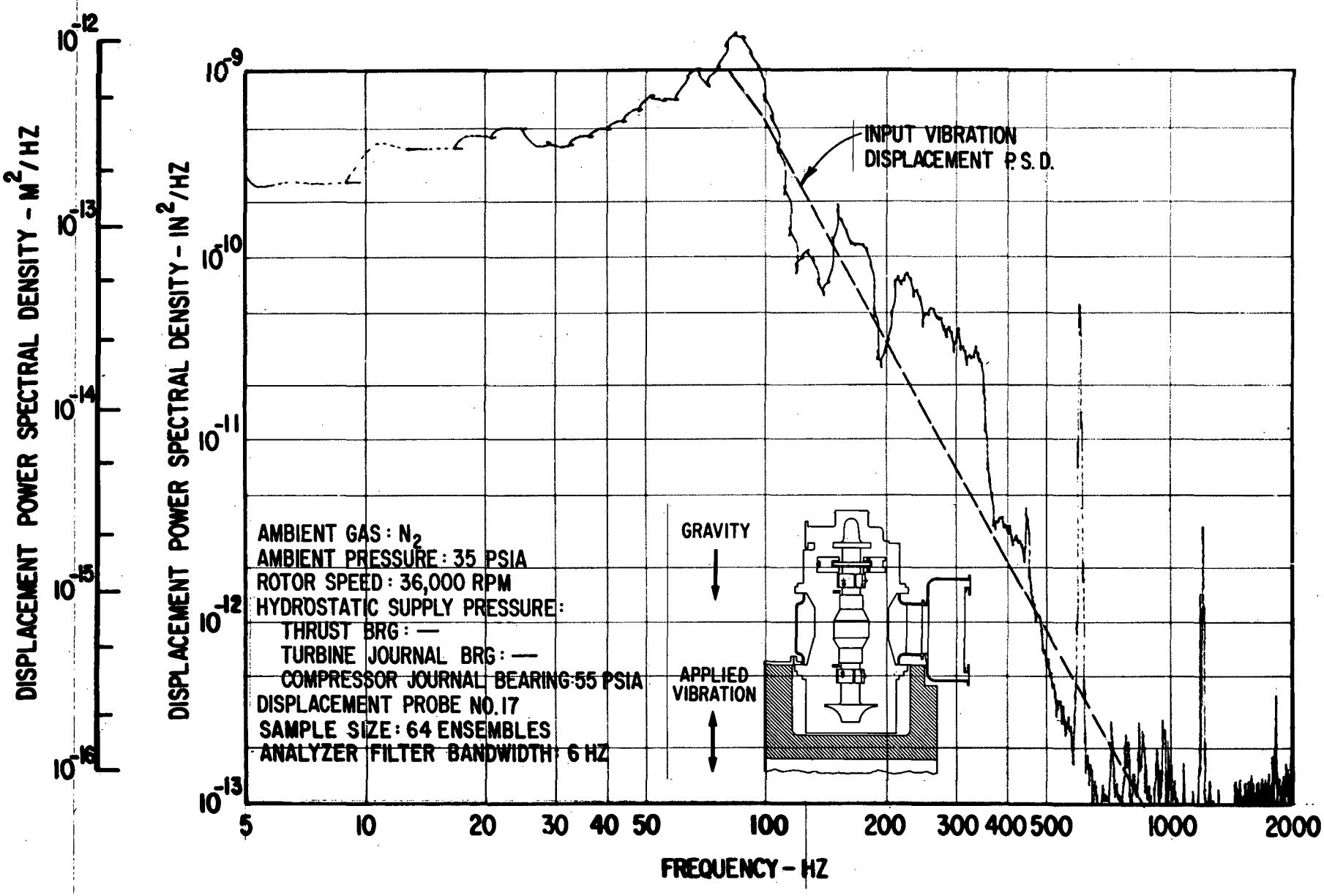

Fig. 54 Frequency Distribution (5 - 2000 Hz) Of Thrust Bearing Film Thickness Variation Under Externally-Imposed Shaped Random Vibrations (0.54 g rms Input) According To NASA Spec 417-2-C-3.5

MIT-14075

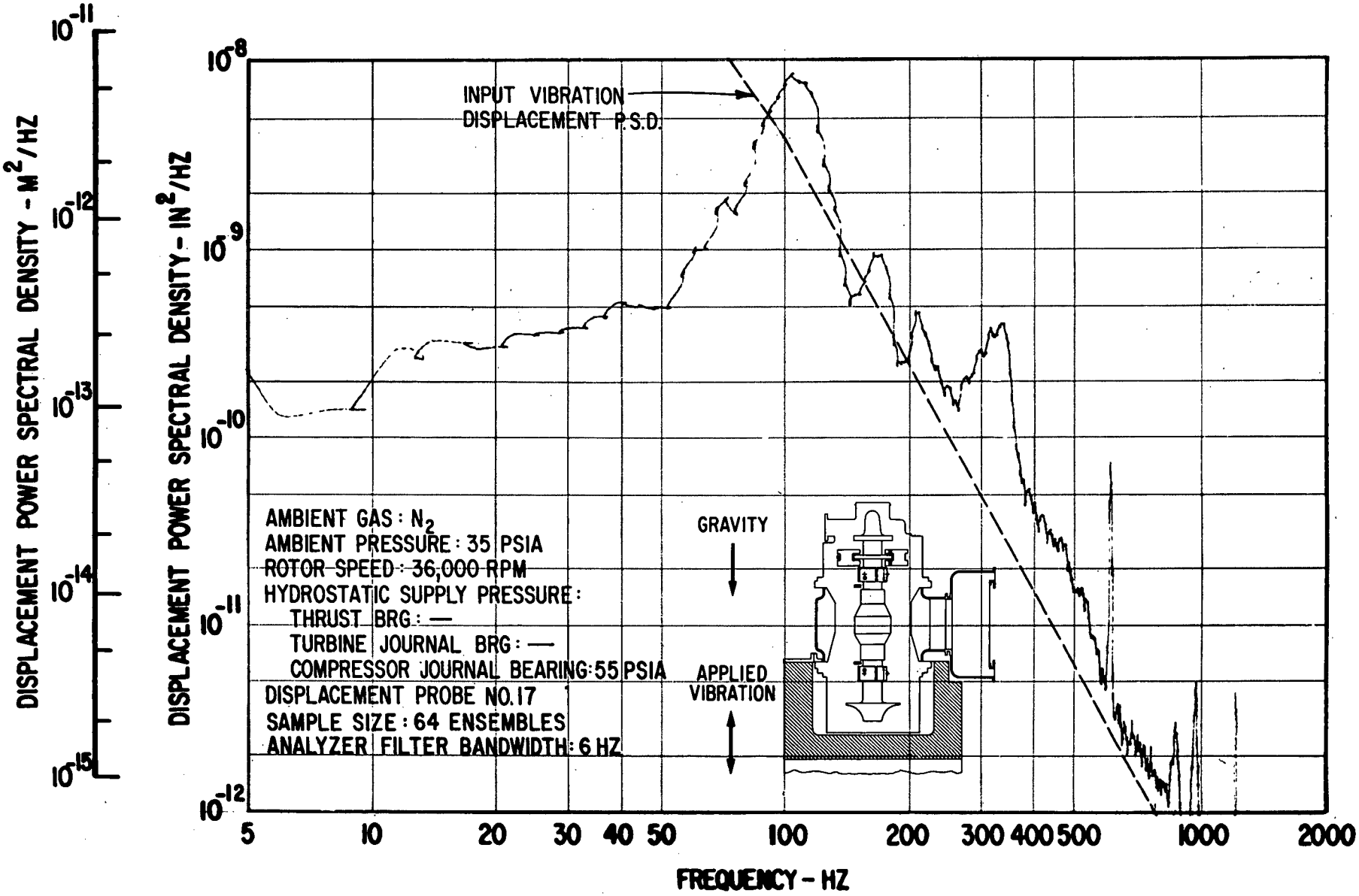

Fig. 55 Frequency Distribution (5 - 2000 Hz) Of Thrust Bearing Film Thickness Variation Under Externally-Imposed Shaped Random Vibrations (1.52 g rms Input) According To NASA Spec 417-2-C-3.5

MTI-13675

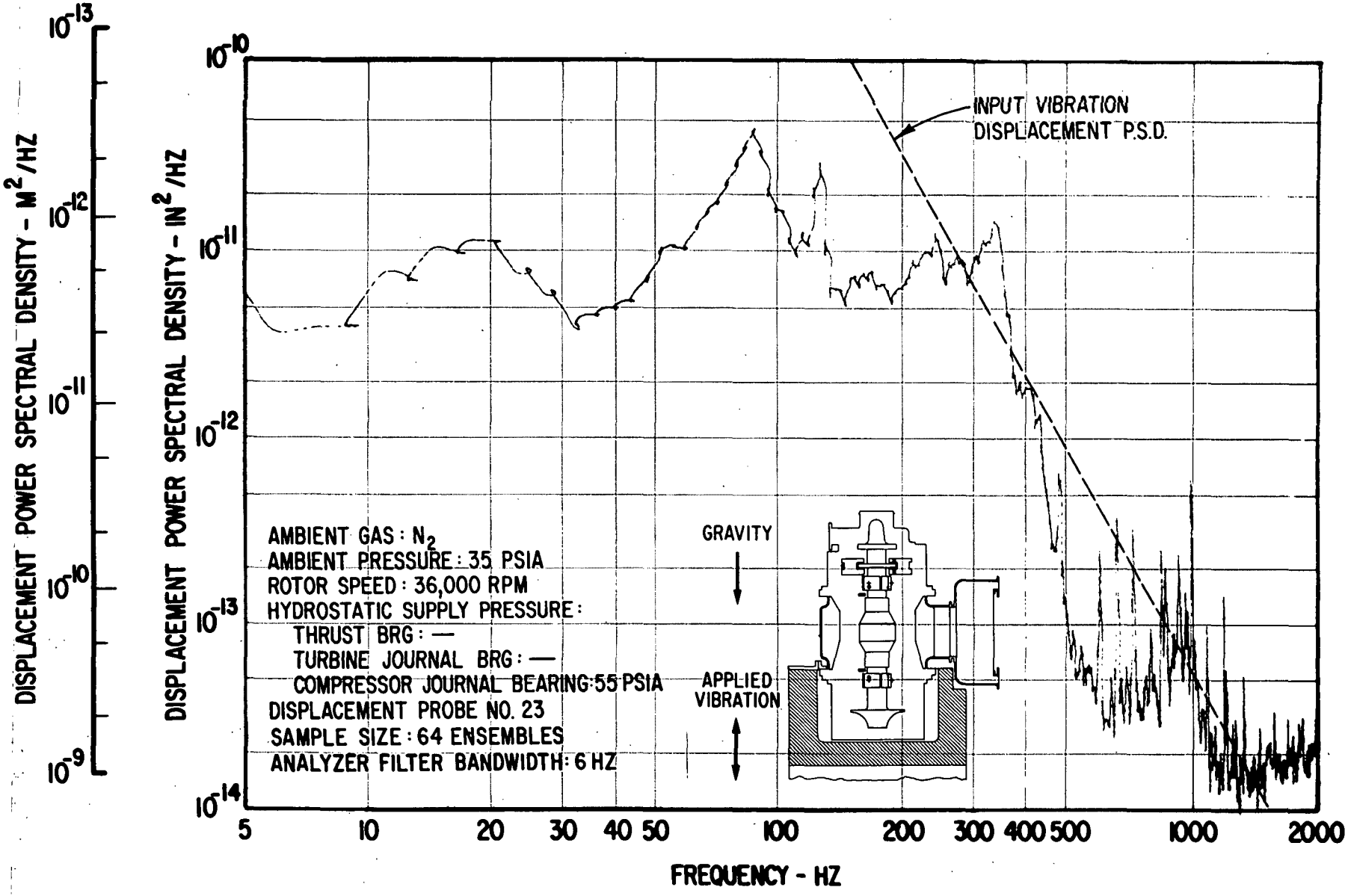

Fig. 56 Frequency Distribution (5 - 2000 Hz) Of Thrust Bearing Gimbal Amplitudes Under Externally-Imposed Shaped Random Vibrations (0.54 g rms Input) According To NASA Spec 417-2-C-3.5

MTI-13686

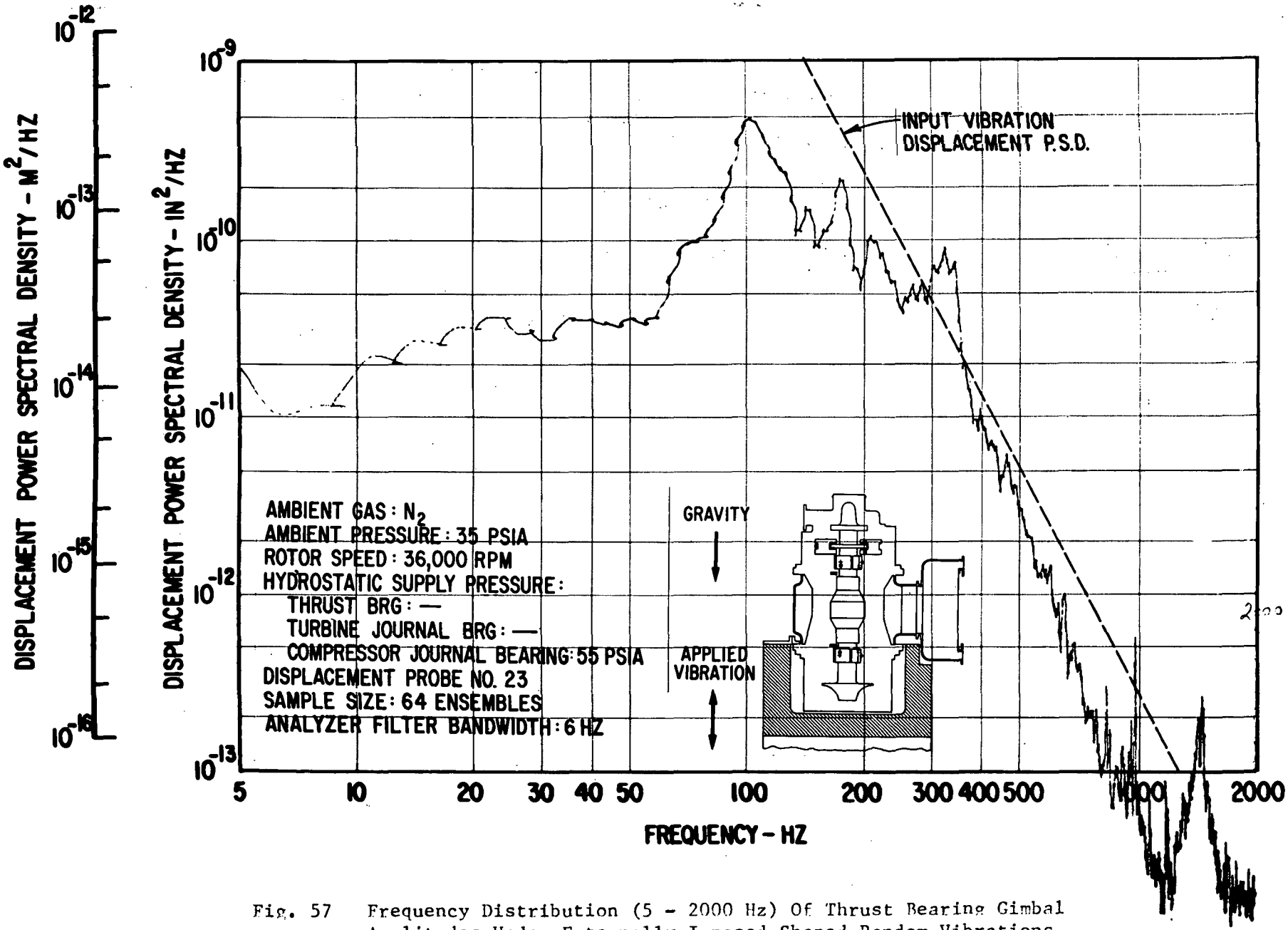

Fig. 57 Frequency Distribution (5 - 2000 Hz) Of Thrust Bearing Gimbal Amplitudes Under Externally-Imposed Shaped Random Vibrations (1.52 g rms Input) According To NASA Spec 417-2-C-3.5

MTI-14025

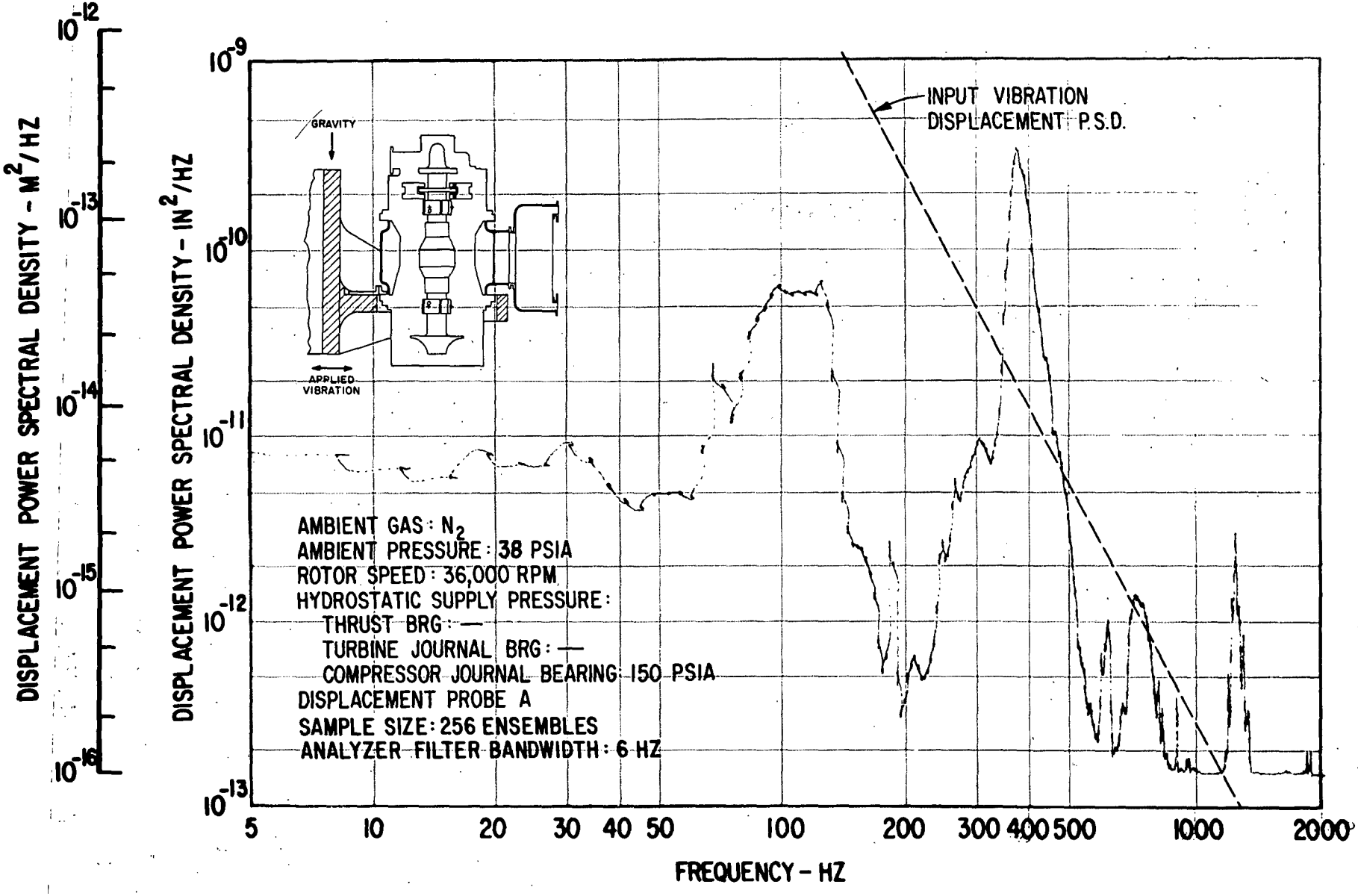

Fig. 58 Frequency Distribution (5 - 2000 Hz) Of Pad-To-Shaft Pivot Film Thickness Variation For Flex-Mounted Compressor Journal Bearing Pad Under Externally-Imposed Sinusoidal Vibrations (1.52 g rms Input) According To NASA Spec 417-2-C-3.5

MTI-14073

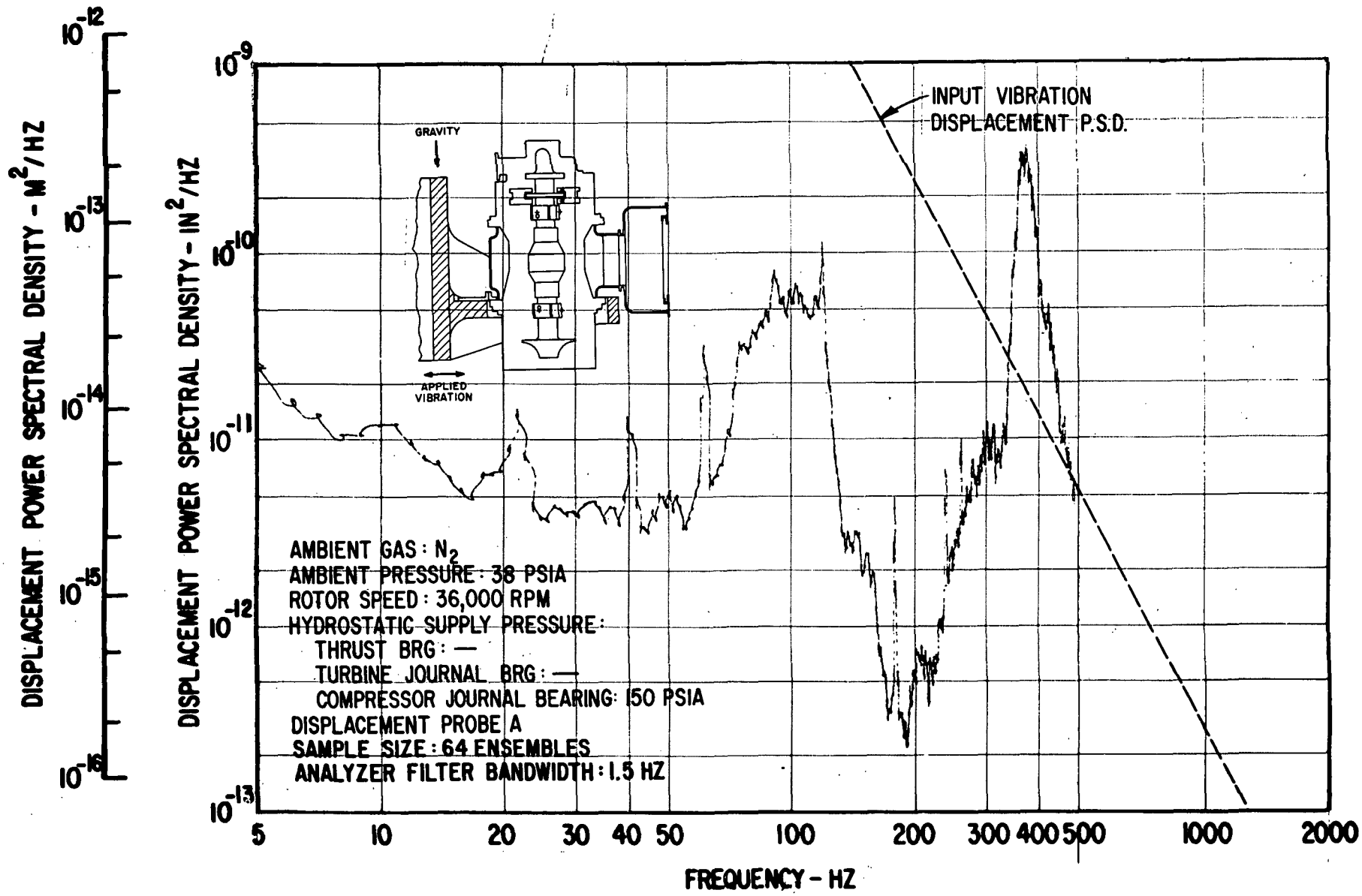

Fig. 59 Frequency Distribution (5 - 500 Hz) Of Pad-To-Shaft Pivot Film Thickness Variation For Flex-Mounted Compressor Journal Bearing Pad Under Externally-Imposed Sinusoidal Vibrations (1.52 g rms Input) According To NASA Spec 417-2-C-3.5

MTI-14036

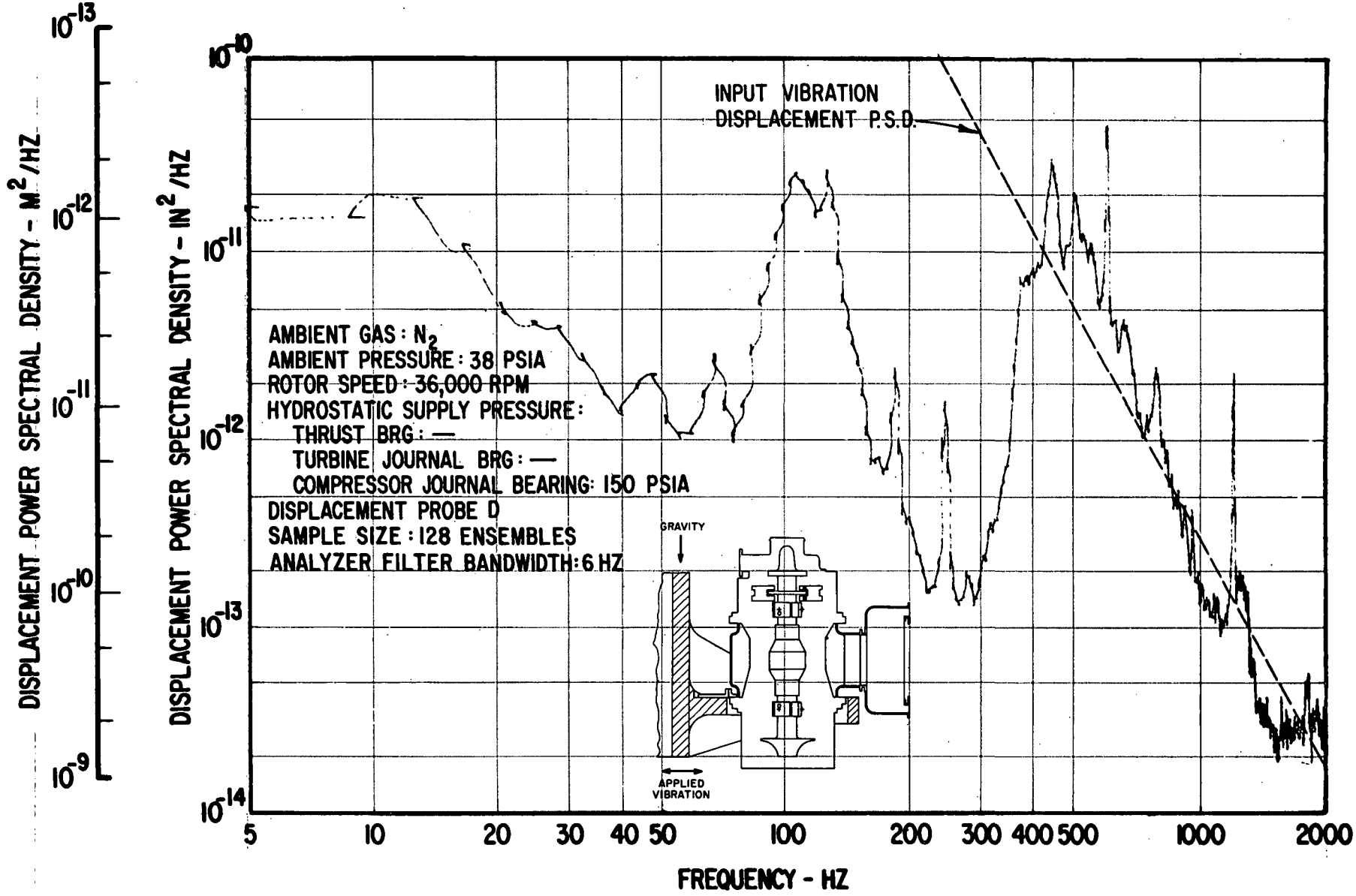

Fig. 60 Frequency Distribution (5 - 2000 Hz) Of Pad-To-Shaft Pivot Film Thickness Variation For Flex-Mounted Turbine Journal Bearing Pad Under Externally-Imposed Shaped Random Vibrations (1.35 g rms Input) According To NASA Spec 417-2-C-3.5

MTI-13687

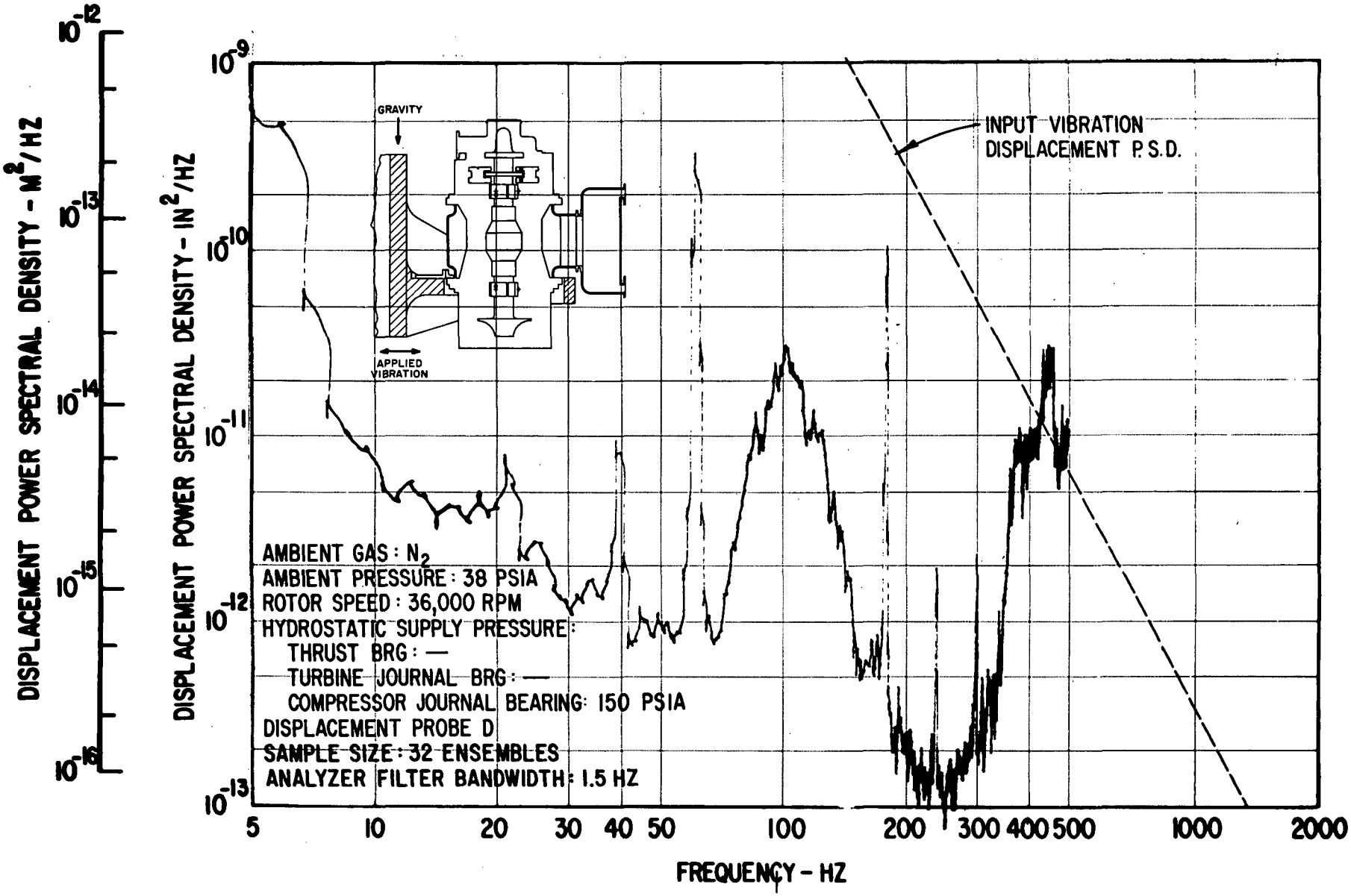

Fig. 61 Frequency Distribution (5 - 500 Hz) Of Pad-To-Shaft Pivot Film Thickness Variation For Flex-Mounted Turbine Journal Bearing Pad Under Externally-Imposed Shaped Random Vibrations (1.35 g rms Input) According To NASA Spec 417-2-C-3.5

MTI-14024

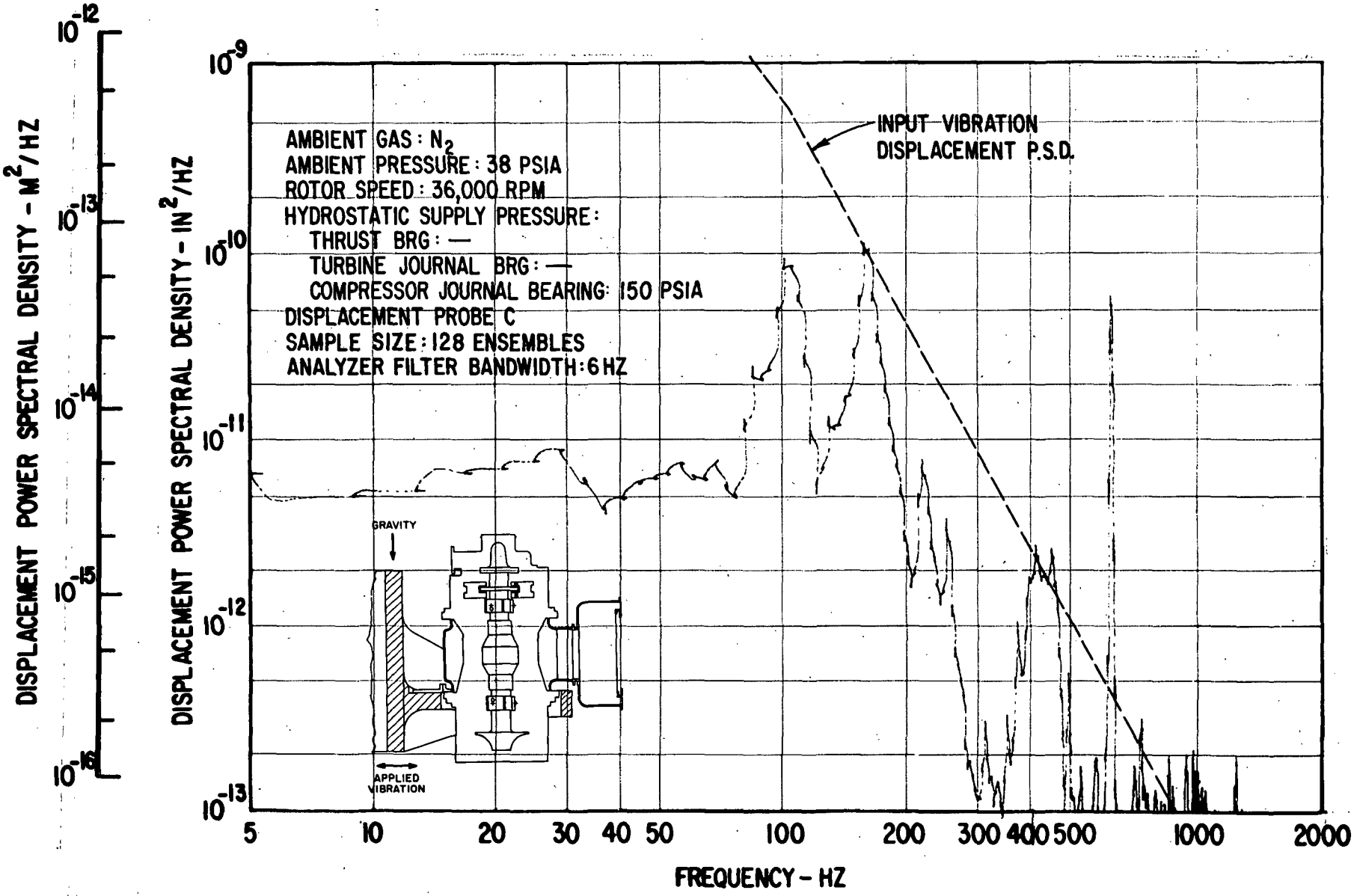

Fig. 62 Frequency Distribution (5 - 2000 Hz) Of Pad-To-Shaft Pivot Film Thickness Variation For Solid-Mounted Compressor Journal Bearing Pad Under Externally-Imposed Shaped Random Vibrations (0.54 g rms Input) According To NASA Spec 417-2-C-3.5

MTI-14072

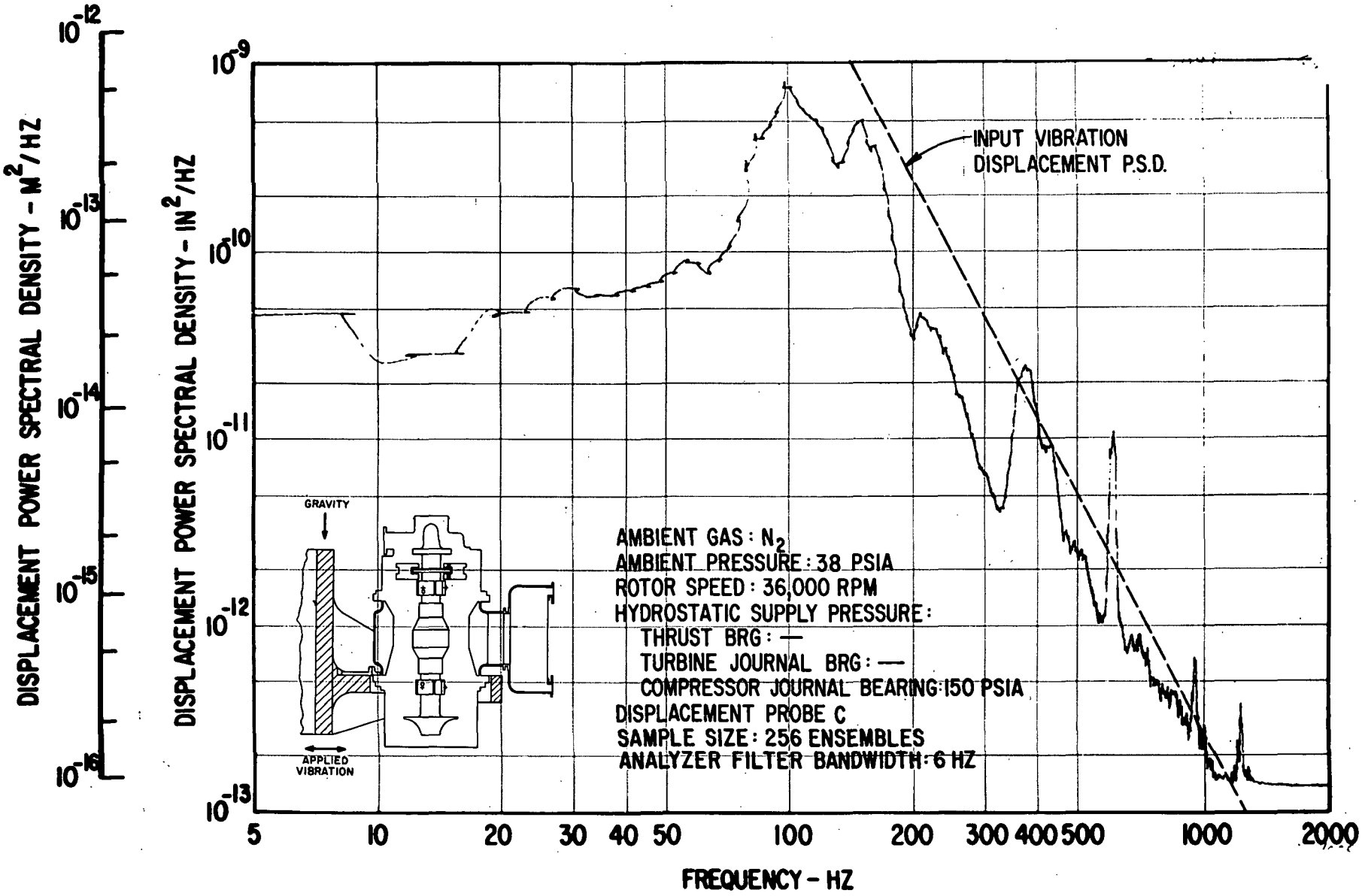

Fig. 63 Frequency Distribution (5 - 2000 Hz) Of Pad-To-Shaft Pivot Film Thickness Variation For Solid-Mounted Compressor Journal Bearing Pad Under Externally-Imposed Shaped Random Vibrations (1.52 g rms Input) According To NASA Spec 417-2-C-3.5

MTI-14035

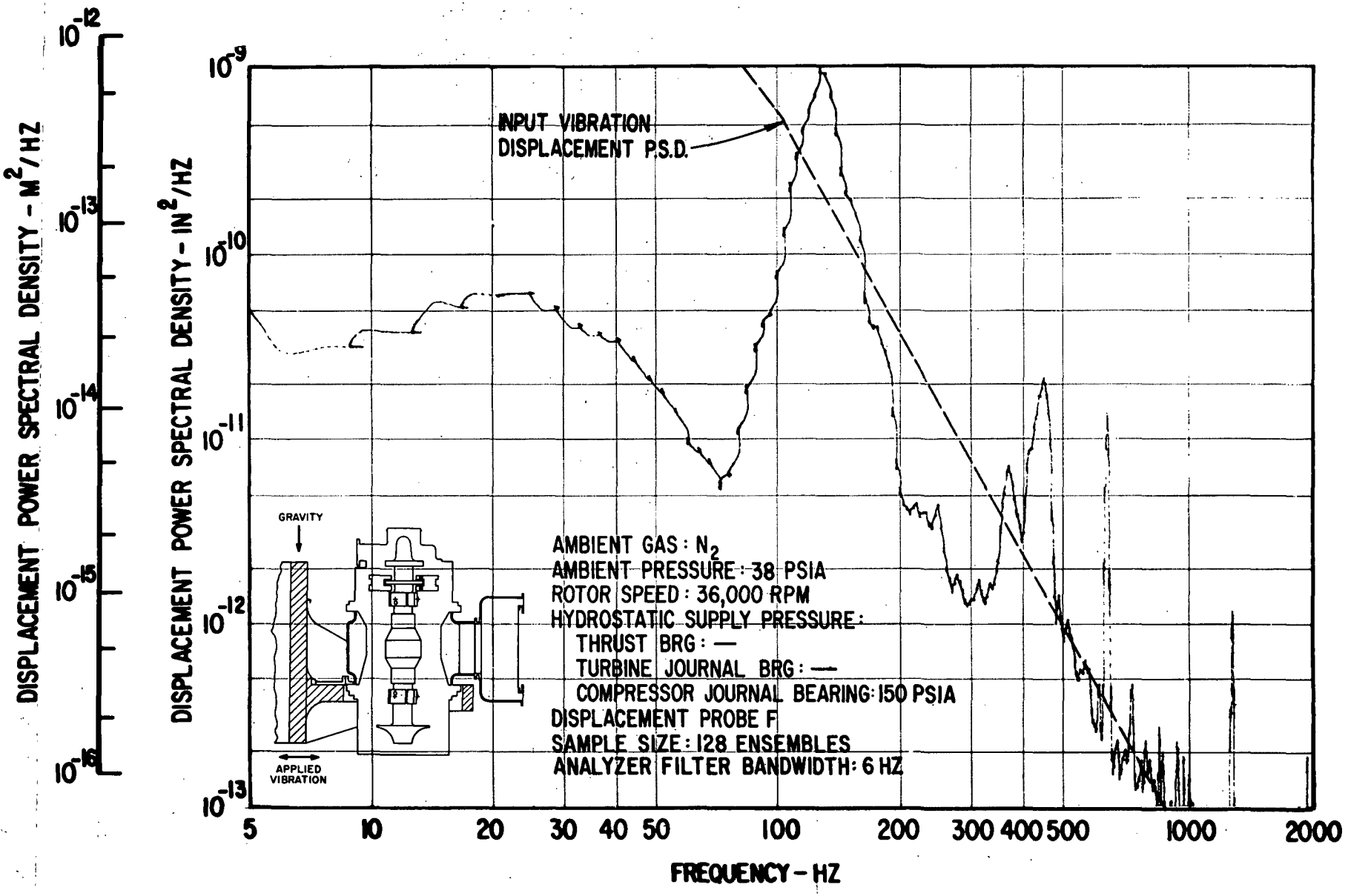

Fig. 64 Frequency Distribution (5 - 2000 Hz) Of Pad-To-Shaft Pivot Film Thickness Variation For Solid-Mounted Turbine Journal Bearing Pad Under Externally-Imposed Shaped Random Vibrations (0.54 g rms Input) According To NASA Spec 417-2-C-3.5

MTI-14071

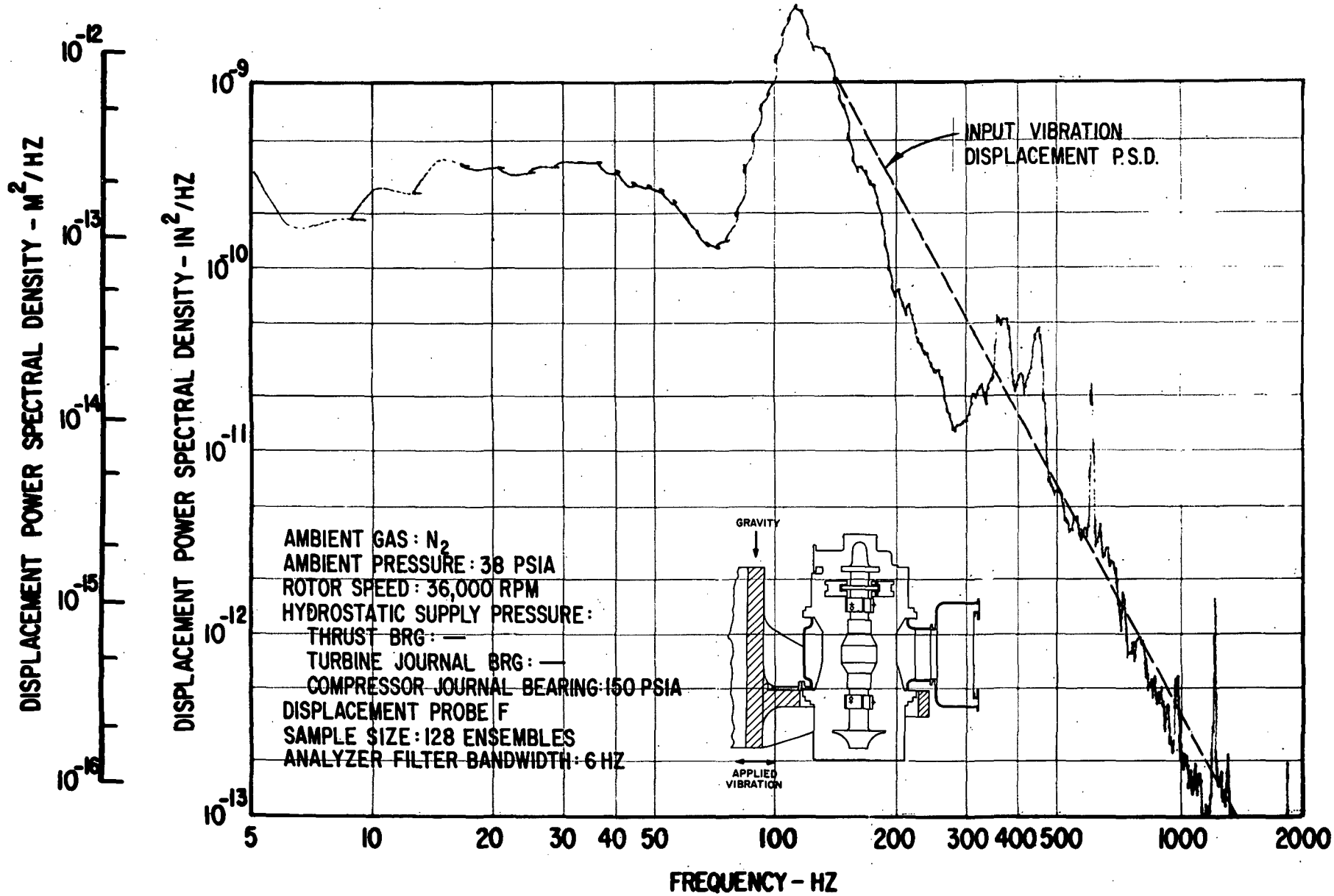

Fig. 65 Frequency Distribution (5 - 2000 Hz) Of Pad-To-Shaft Pivot Film Thickness Variation For Solid-Mounted Turbine Journal Bearing Pad Under Externally-Imposed Shaped Random Vibrations (1.35 g rms Input) According To NASA Spec 417-2-C-3.5

MTI-14083

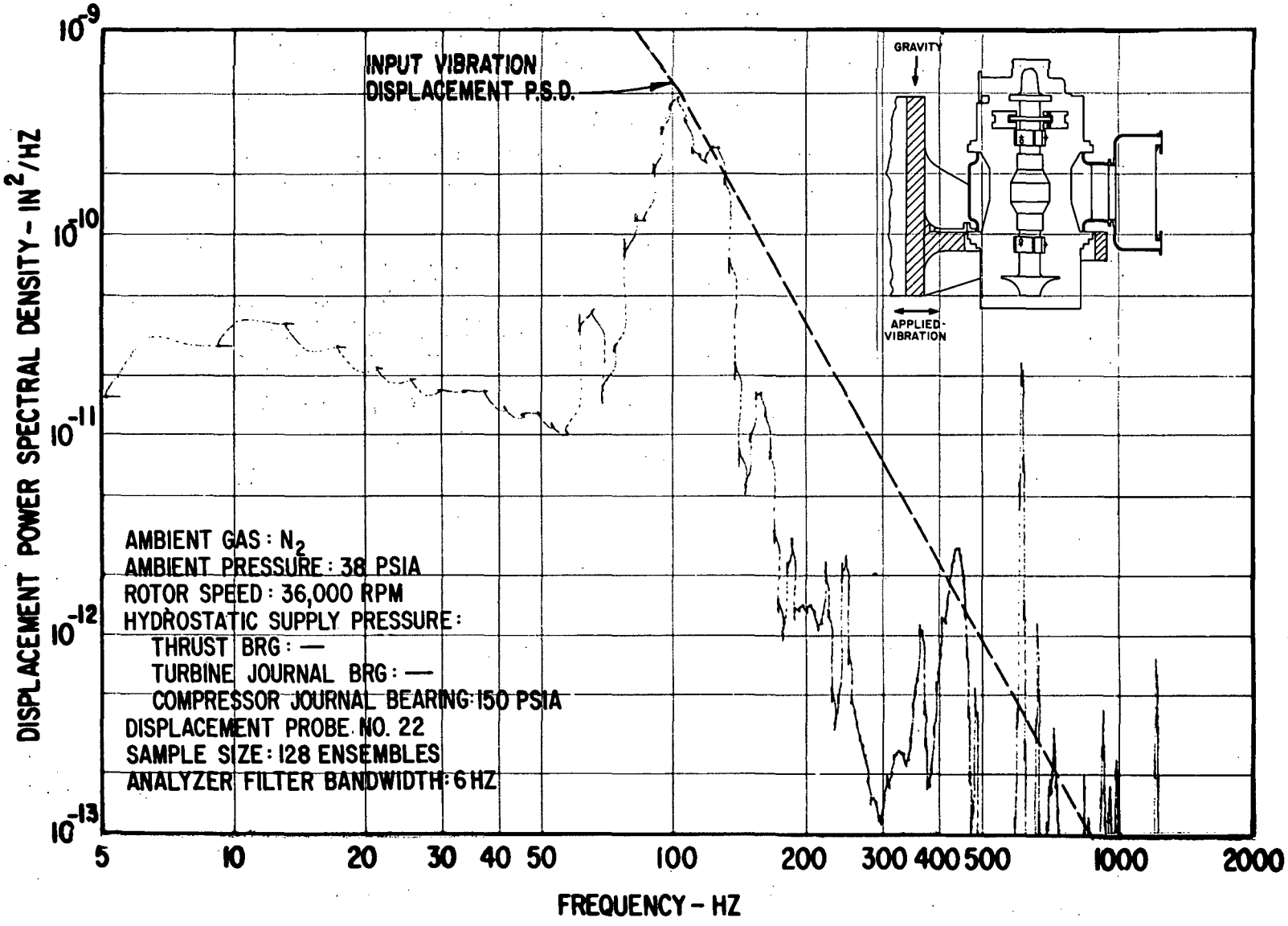

Fig. 66 Frequency Distribution (5 - 2000 Hz) Of Compressor Journal Flexure Amplitudes Under Externally-Imposed Shaped Random Vibrations (0.54 g rms Input) According To NASA Spec 417-2-C-3.5

MTI-13678

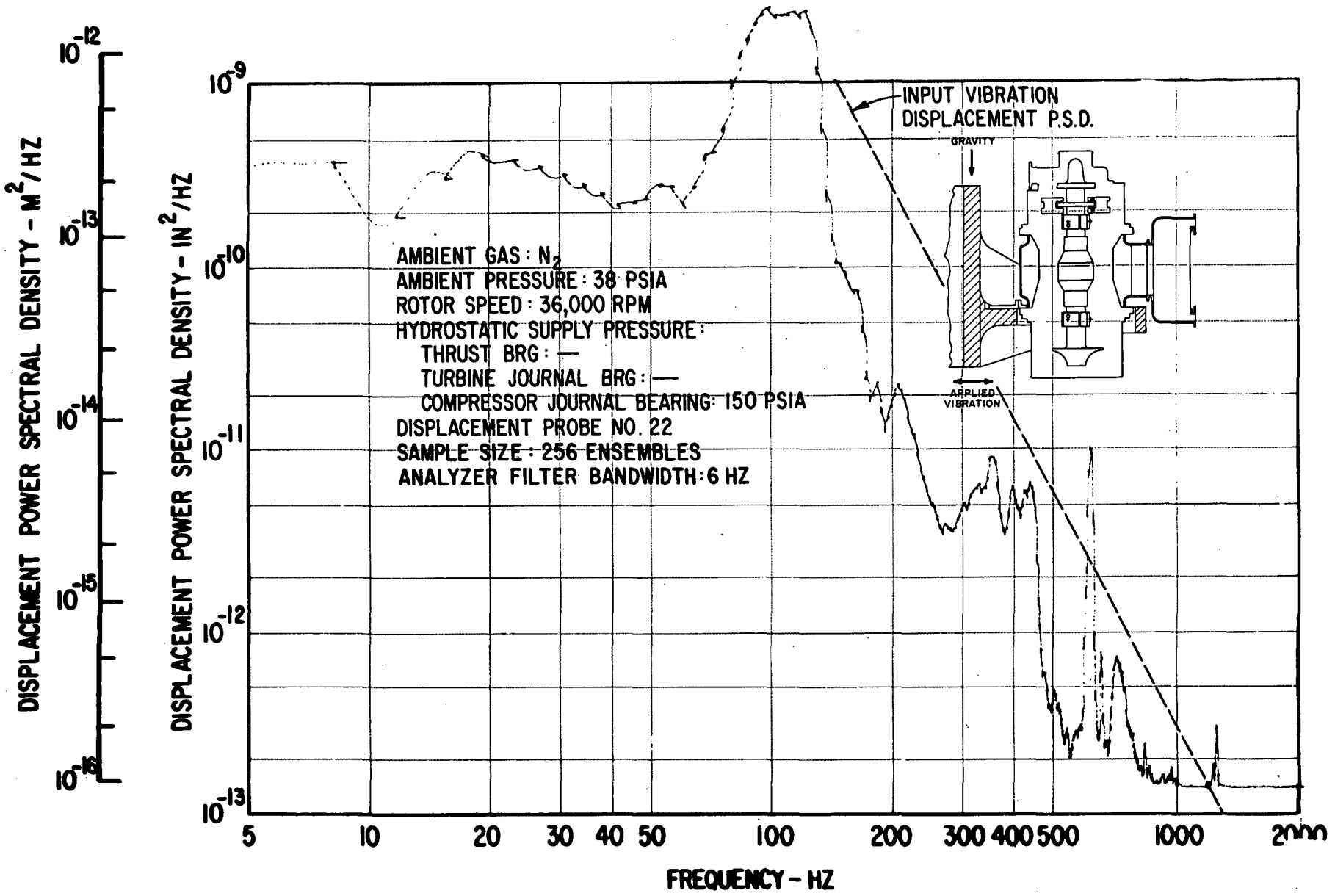

Fig. 67 Frequency Distribution (5 - 2000 Hz) Of Compressor Journal Flexure Amplitudes Under Externally-Imposed Shaped Random Vibrations (1.52 g rms Input) According To NASA Spec 417-2-C-3.5

MTI-14023

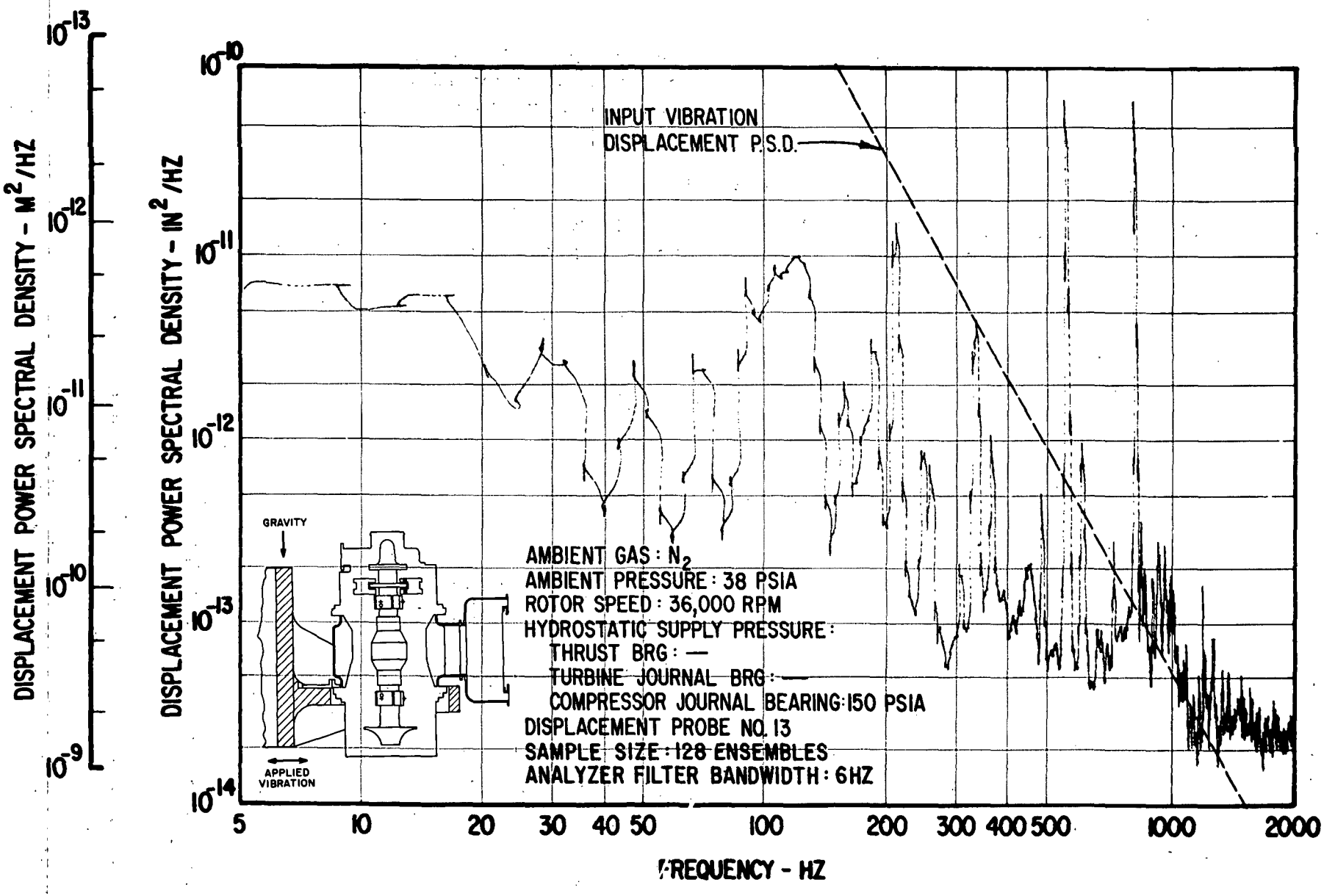

Fig. 68 Frequency Distribution (5 - 2000 Hz) Of Casing-To-Pad Leading Edge Amplitudes For Flex-Mounted Turbine Journal Bearing Pad Under Externally-Imposed Shaped Random Vibrations (0.54 g rms Input) According To NASA Spec 417-2-C-3.5

MTI-13688

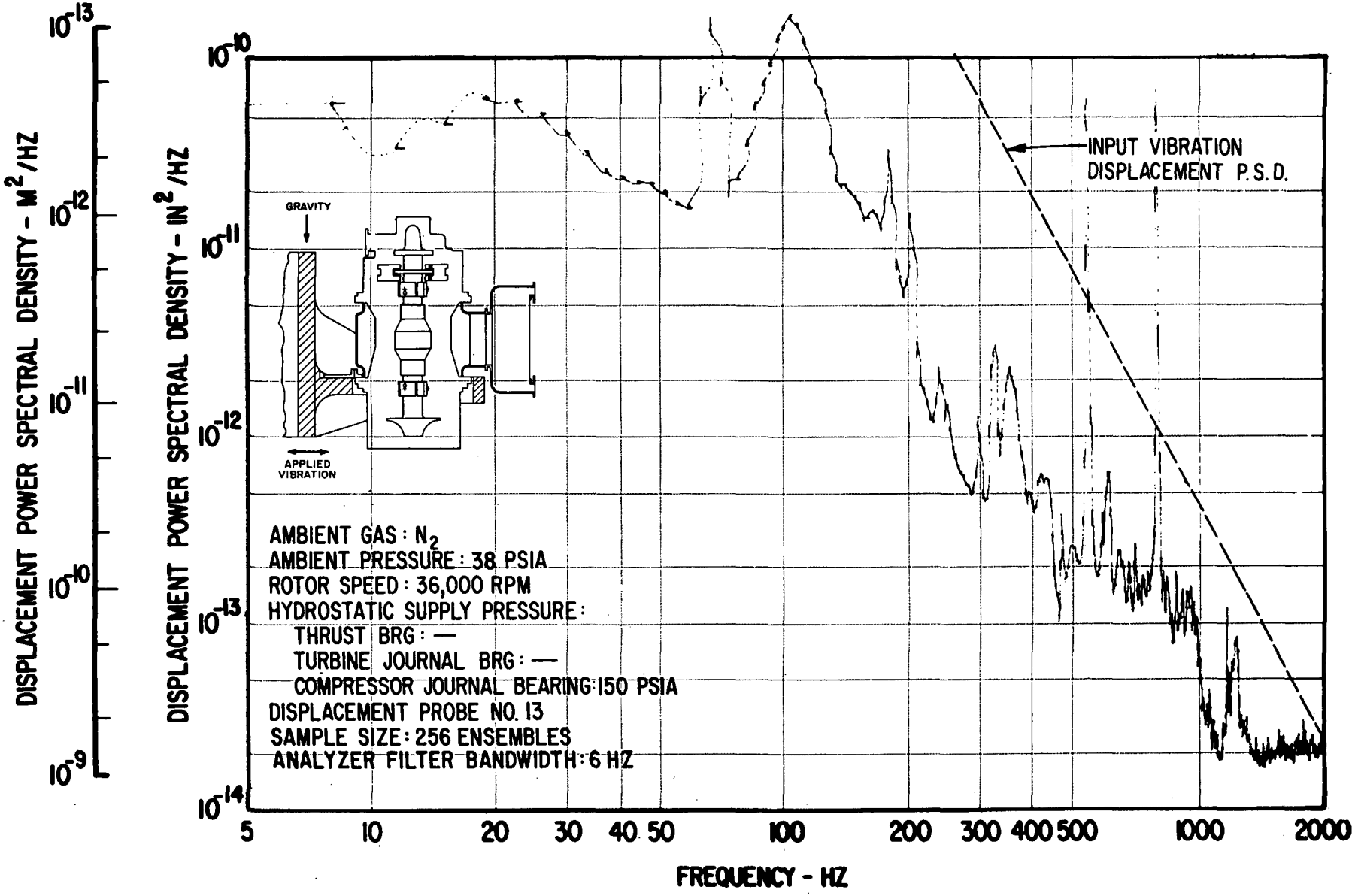

Fig. 69 Frequency Distribution (5 - 2000 Hz) Of Casing-To-Pad Leading Edge Amplitudes For Flex-Mounted Turbine Journal Bearing Pad Under Externally-Imposed Shaped Random Vibrations (1.52 g rms Input) According To NASA Spec 417-2-C-3.5

MTI-13689

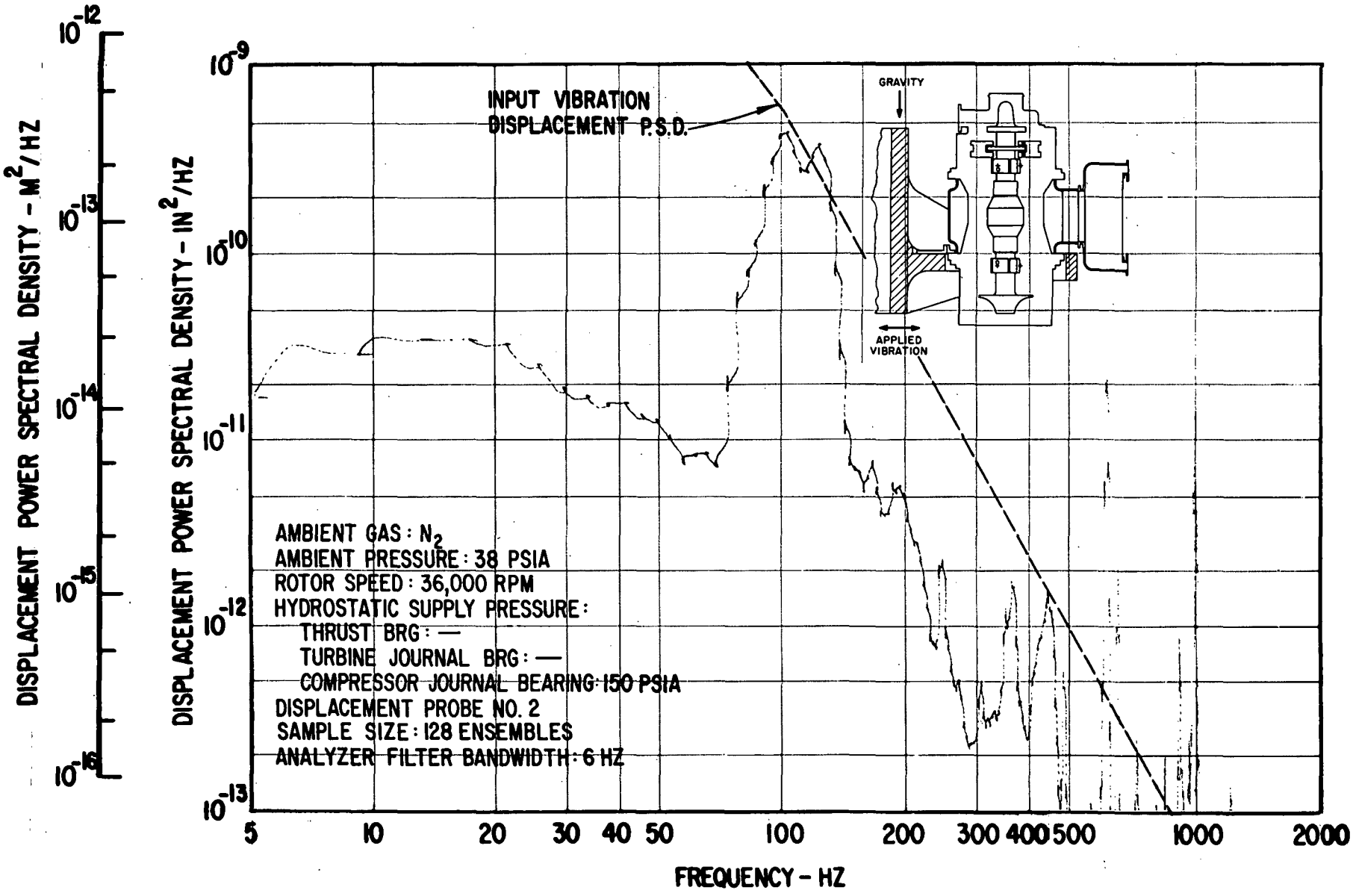

Fig. 70 Frequency Distribution (5 - 2000 Hz) Of Compressor Journal Rotor Amplitudes (Casing-To-Shaft) Under Externally-Imposed Shaped Random Vibrations (0.54 g rms Input) According To NASA Spec 417-2-C-3.5

MTI-14070

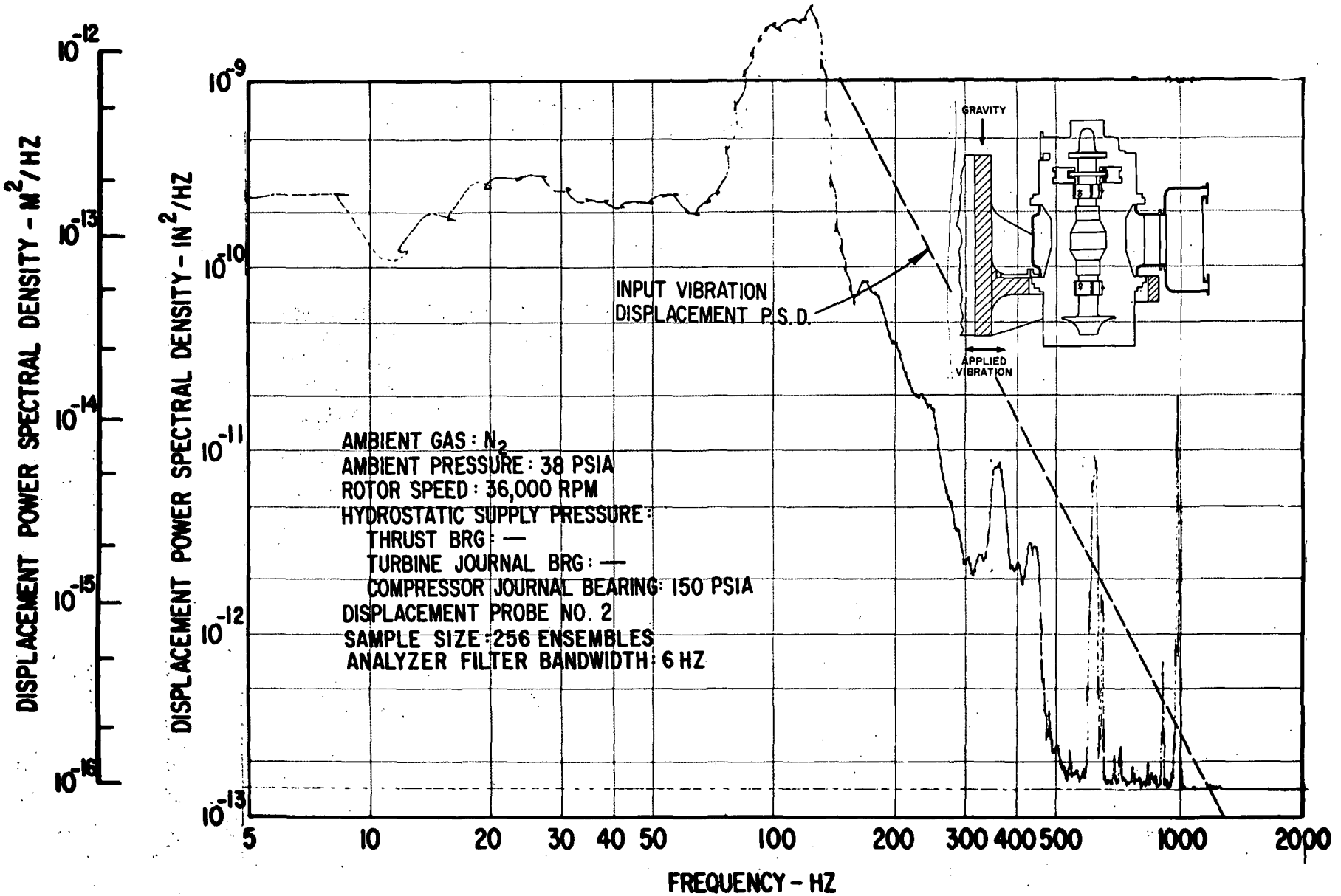

Fig. 71 Frequency Distribution (5 - 2000 Hz) Of Compressor Journal Rotor Amplitudes (Casing-To-Shaft) Under Externally-Imposed Shaped Random Vibrations (1.52 g rms Input) According To NASA Spec 417-2-C-3.5

MTI-13672

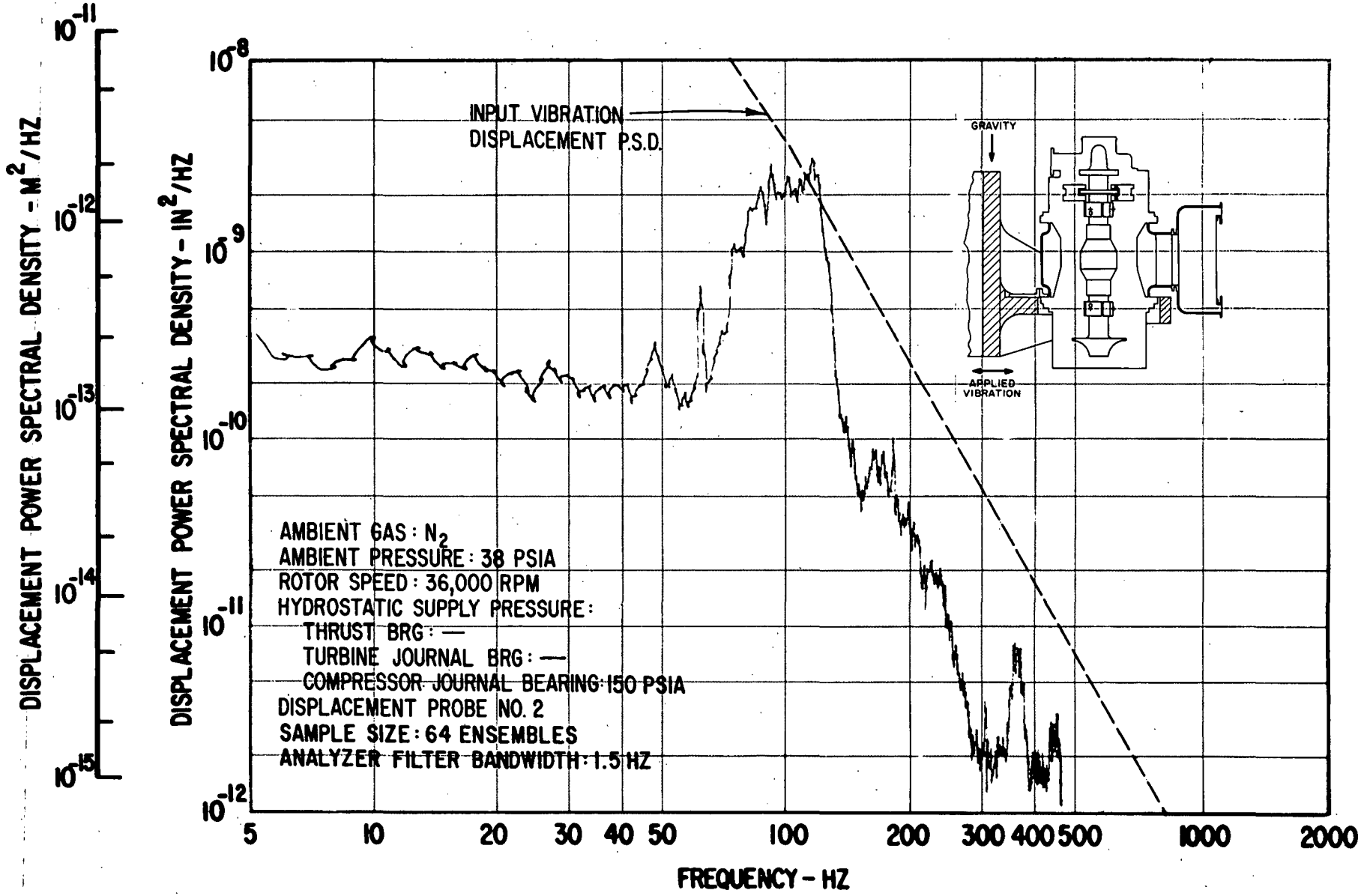

Fig. 72 Frequency Distribution (5 - 500 Hz) Of Compressor Journal Rotor Amplitudes (Casing-To-Shaft) Under Externally-Imposed Shaped Random Vibrations (1.52 g rms Input) According To NASA Spec 417-2-C-3.5

MTI-14080

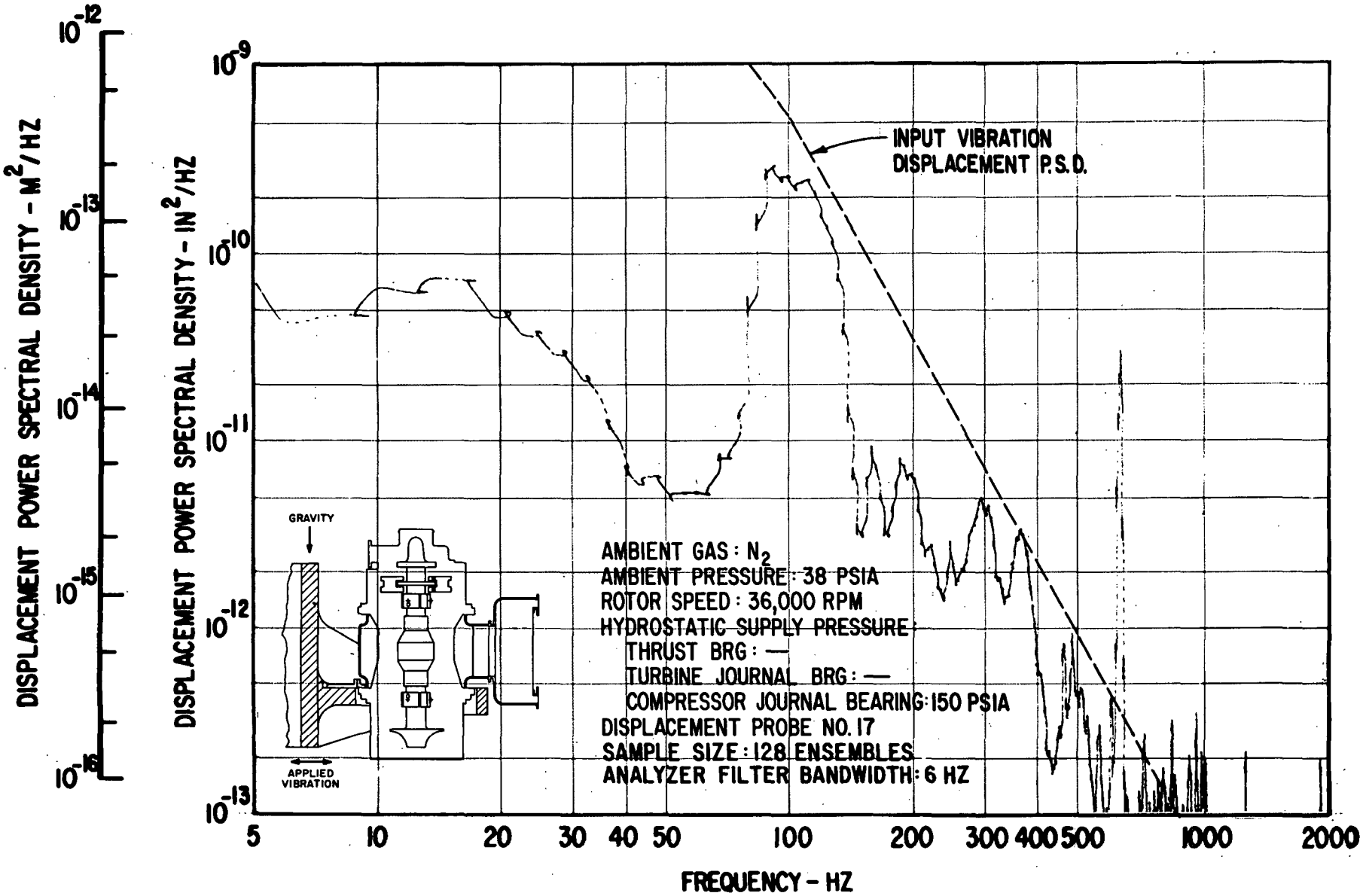

Fig. 73 Frequency Distribution (5 - 2000 Hz) Of Thrust Bearing Film Thickness Variation Under Externally-Imposed Shaped Random Vibrations (0.54 g rms Input) According To NASA Spec 417-2-C-3.5

MTI-14082

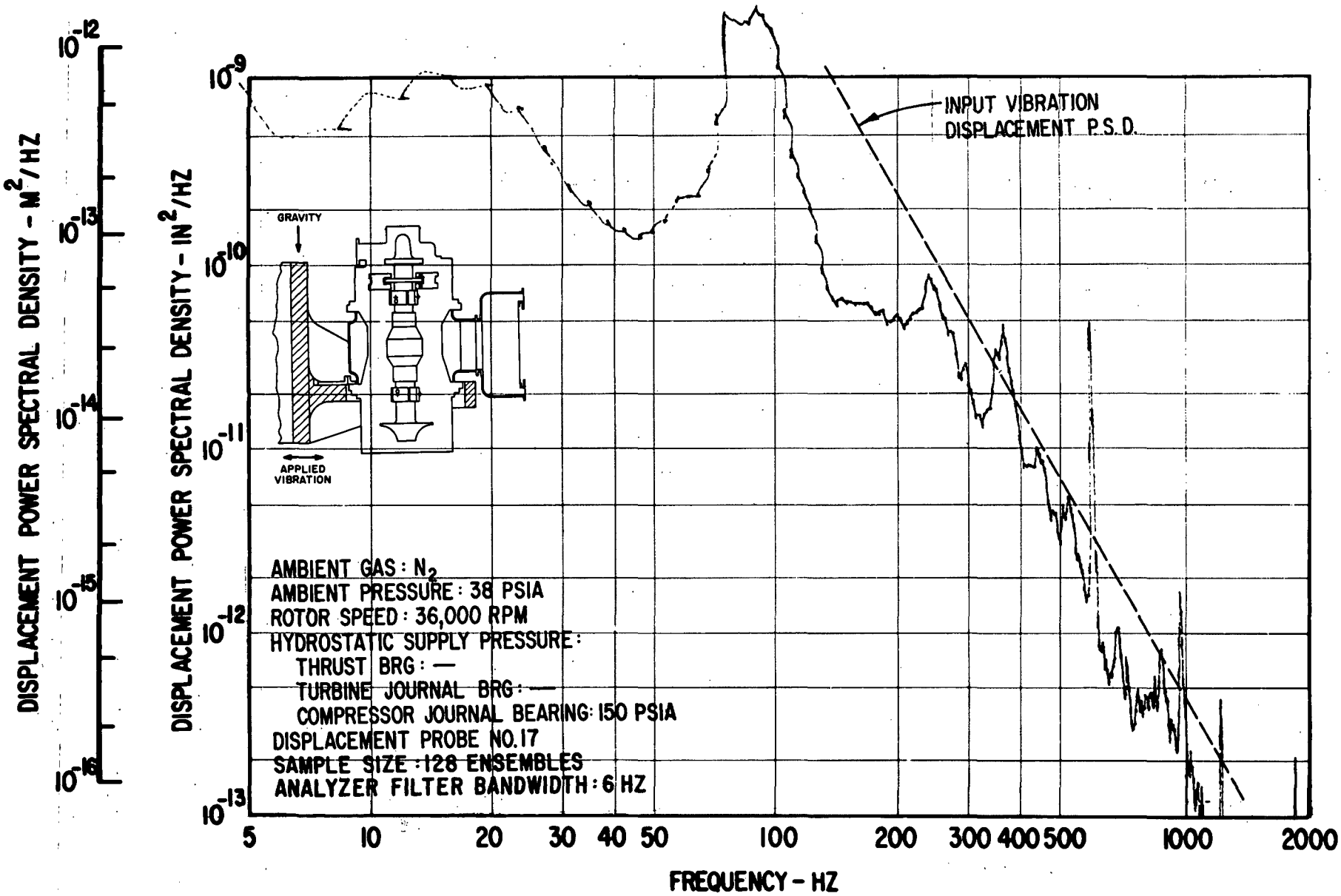

Fig. 74 Frequency Distribution (5 - 2000 Hz) Of Thrust Bearing Film Thickness Variation Under Externally-Imposed Shaped Random Vibrations (1.35 g rms Input) According To NASA Spec 417-2-C-3.5

MTI-13679

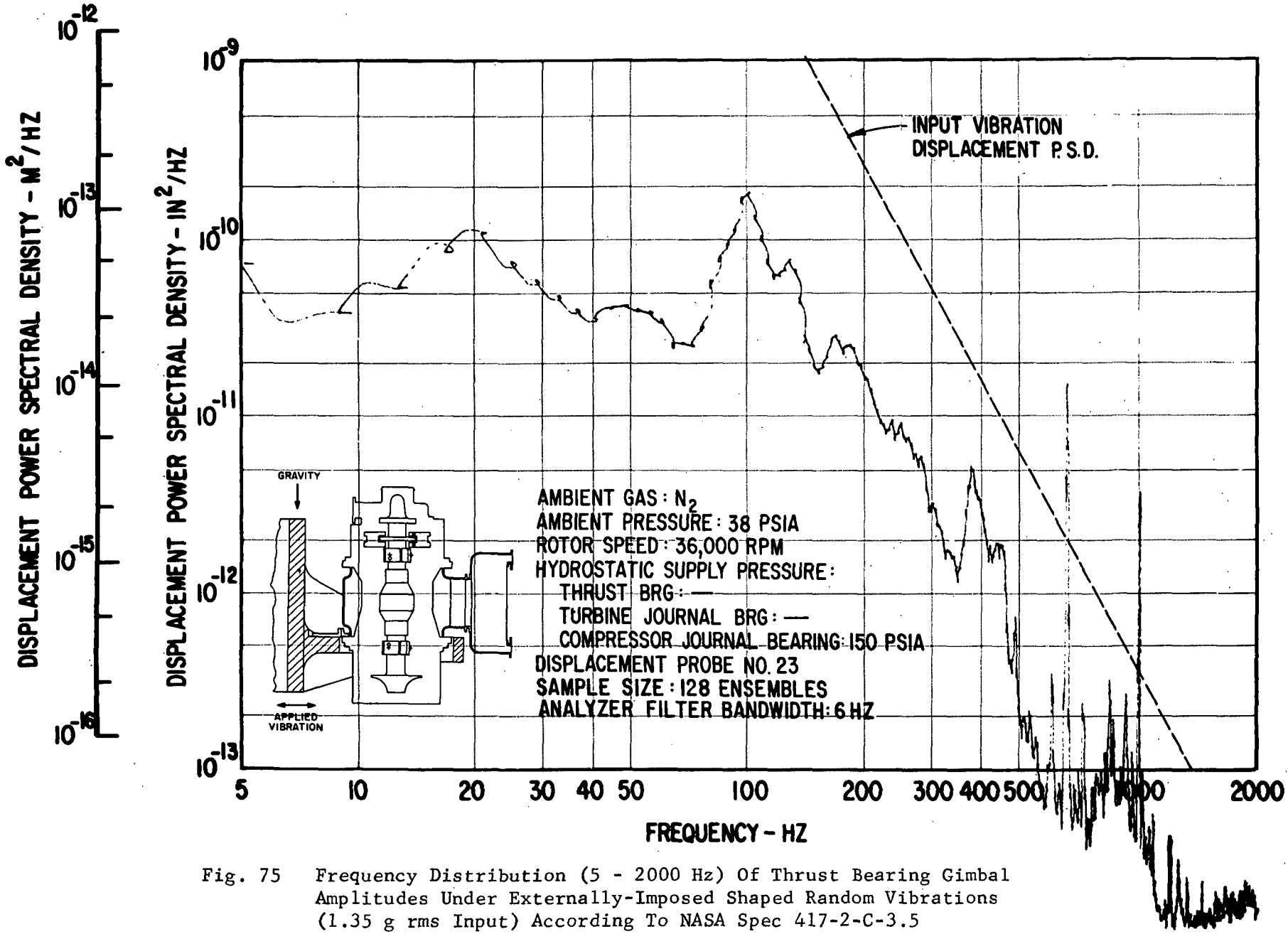

Fig. 75 Frequency Distribution (5 - 2000 Hz) Of Thrust Bearing Gimbal Amplitudes Under Externally-Imposed Shaped Random Vibrations (1.35 g rms Input) According To NASA Spec 417-2-C-3.5

MTI-14081

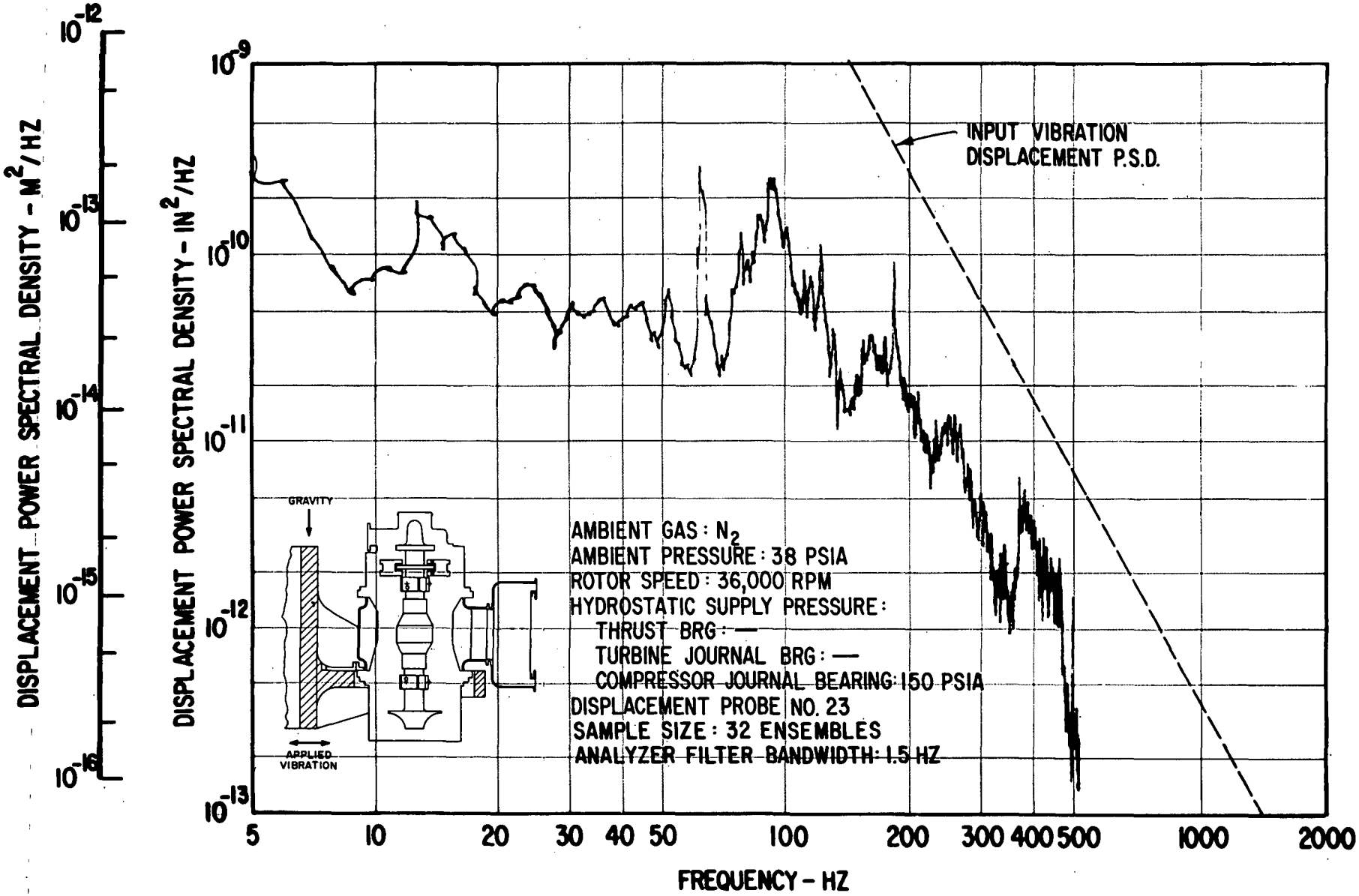

Fig. 76 Frequency Distribution (5 - 500 Hz) Of Thrust Bearing Gimbal Amplitudes Under Externally-Imposed Shaped Random Vibrations (1.35 g rms Input) According To NASA Spec 417-2-C-3.5

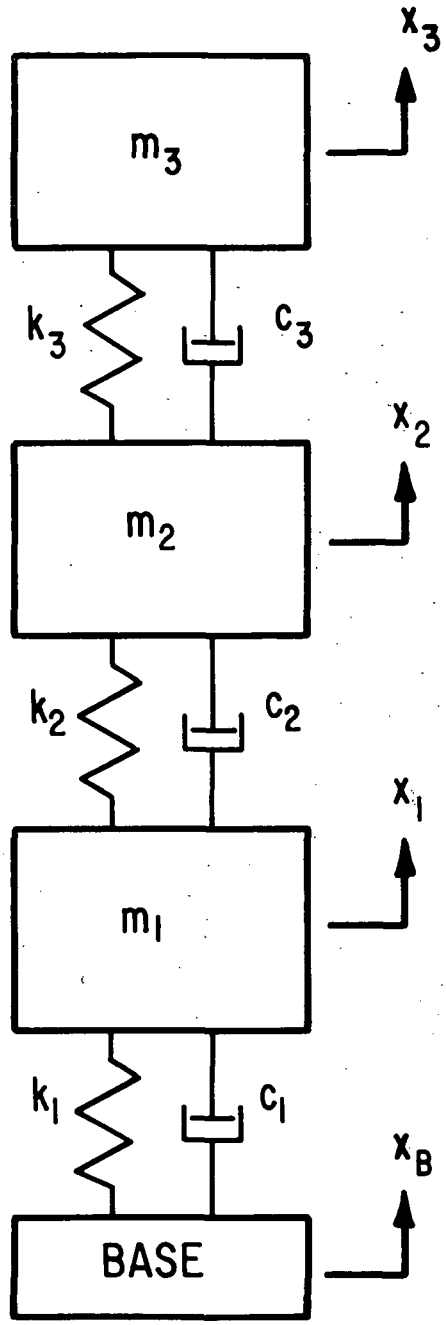

Fig. 77 Lumped-Mass Model Used For Calculation Of Axial Vibration Response Of BRU Rotor-Bearing System To Specified Random Base Excitation

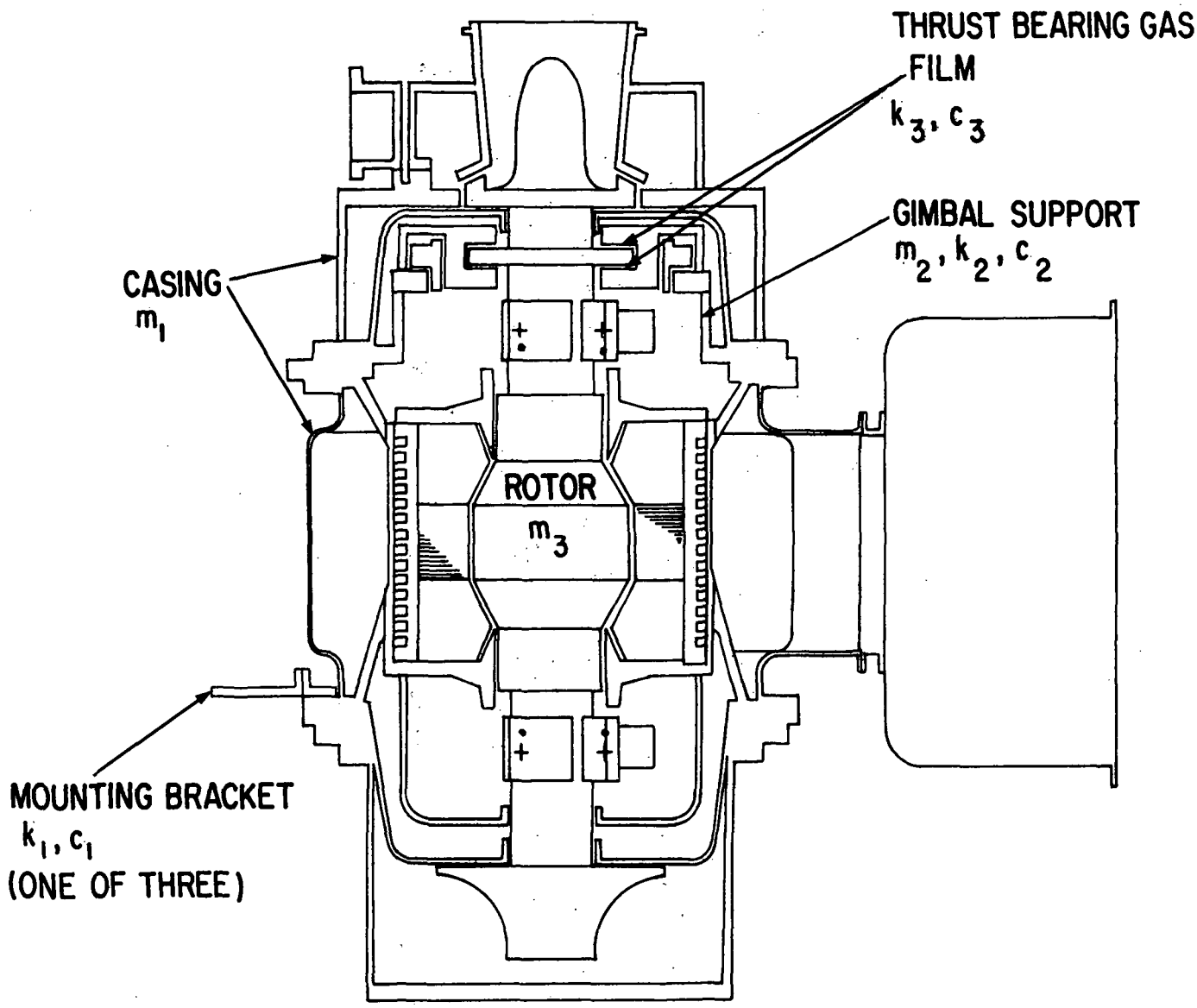

Fig. 78 Schematic Of Brayton Rotating Unit With Mass, Spring And Damper Designations

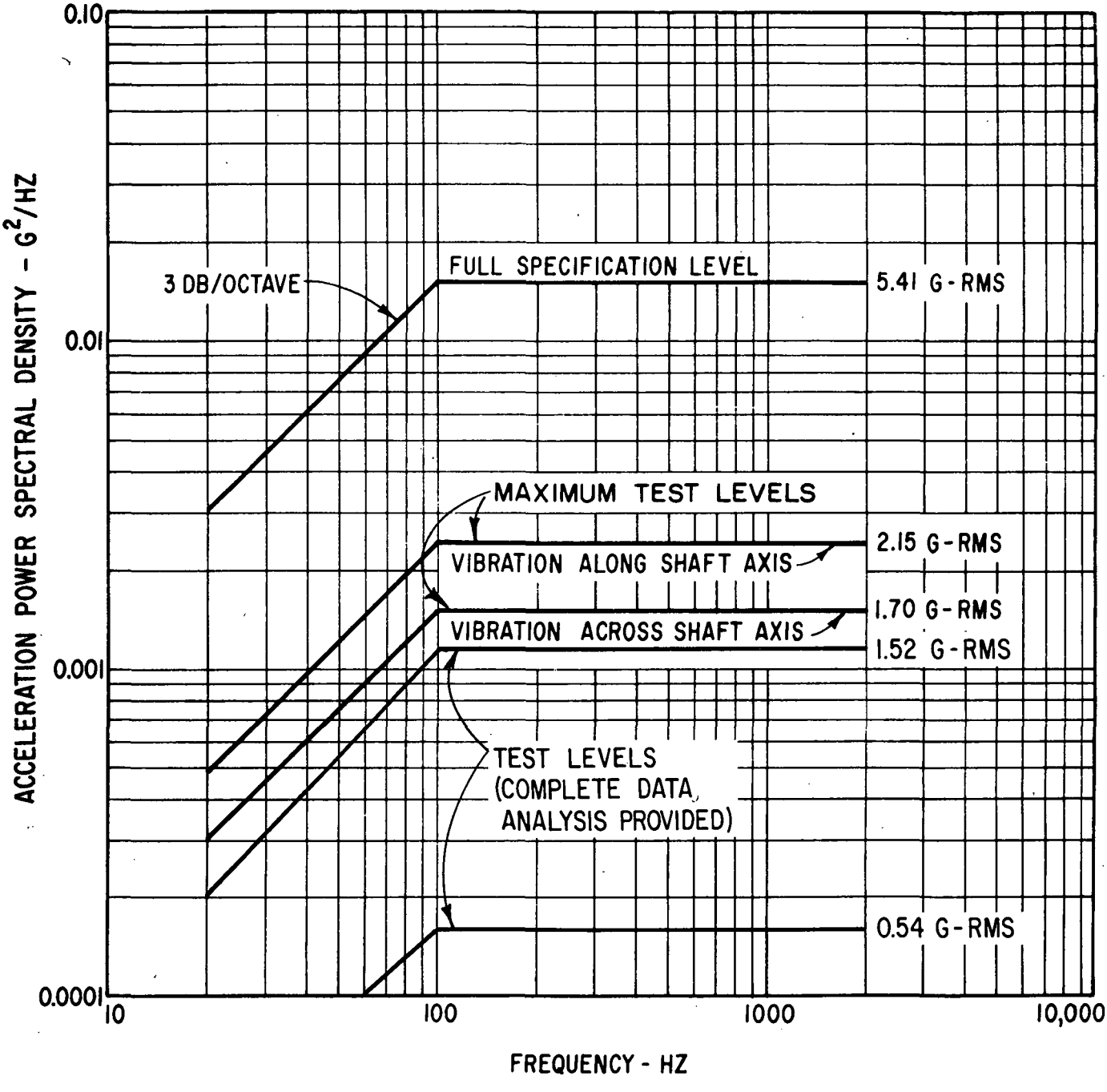

Fig. 79 Random Vibration Power Spectral Density Test Specification 417-2 (Rev. C) For Electrical Generating System Components (Operating) And Actual BRU Test Levels

DISTRIBUTION LIST

NASA-Lewis Research Center
21000 Brookpark Road
Cleveland, Ohio 44135
Attention: See List Below

G. Mervin Ault, MS 3-5
Robert E. English, MS 500-201
Donald Packe, MS 500-202
Del Drier, MS 21-4
William Wintucky, MS 500-202
Technology Utilization Office, MS 3-19
Report Control, MS 5-5
Library, MS 60-3
James H. Dunn, MS 500-202 (3 copies)
Gerald Boulanger, MS 500-206
Patent Counsel, MS 500-113

NASA Scientific and Technical Information Facility
Attention: Acquisitions Branch (10 copies)
P. O. Box 33
College Park, MD 20740

AiResearch Manufacturing Company
A Division of the Garrett Corporation
Attention: Mr. Anthony Pietsch
402 South 36th Street
Phoenix, AZ 85034